Characterisation Of The Phosphatase Control System That Prevents Premature Mitotic Entry In Mammalian Cells

Nisha Peter

A thesis submitted to the University of Sussex for the degree of Doctor of Philosophy

September 2016

Genome Damage and Stability Centre
University Of Sussex

DECLARATION

I hereby declare that thesis, whether in the same or different form, has not been previously submitted to this or any other University for the award of a degree. The work described here is my own except where otherwise stated.

Nisha Peter
September 2016

ACKNOWLEDGMENTS

First and foremost I'd like to thank God for giving me the motivation to make the most of every opportunity that came my way in my time in the UK.

I'd like to thank my supervisor and mentor, Dr. Helfrid Hochegger, for giving me the opportunity to be a PhD student in his lab at the Genome Damage and Stability Centre. I appreciate the immense effort he's put in securing funding for four years of my studentship and his continuous support during my PhD. His numerous ideas and unbeatable enthusiasm have driven me to be proficient in diverse skills in my research area. I'd like to extend my sincere gratitude to all my fellow lab mates, Dr. Nadia Hegarat (my first boss!!) in particular, for her patience with my countless annoying questions. I would also like to thank Dr. Thomas Stiff and Dr. Tony Ocasio for all their help and guidance in the lab. I thank my fellow PhDs: Stephy, Aimee and Maria (for feeding me ☺) for all the fun we had in the last four years. Also, I thank all my friends in the Genome Centre.

My heartfelt thanks to my proofreading and stress-busting team: Amruta, Sarika, Stephy and Pallavi for the sleepless nights we were working together before deadlines. Last but not the least I'd like to thank my parents for their prayers and love, my siblings (Motta, Sharu and Checha) for their surprises, love and support, and friends (Baiju and Yash) for their patience and sense of humour that kept me sane during my crazy PhD times.

This work was funded by Cancer Research UK and Doctoral School, University of Sussex, UK.

UNIVERSITY OF SUSSEX

NISHA PETER – DOCTOR OF PHILOSOPHY

CHARACTERISATION OF THE PHOSPHATASE CONTROL SYSTEM THAT PREVENTS PREMATURE MITOTIC ENTRY IN MAMMALIAN CELLS

Accurate chromosome segregation during mitosis prevents aneuploidy and cancer. The Wee1-Cdc25-Cdk1 feedback loop ensures cells enter mitosis in a timely and orderly manner. This signalling system has been proposed to work as a bistable switch that is maintained by the counterbalancing action of kinases and phosphatases. However, the phosphatases critical for this transition in mammalian cells are yet to be identified. Cdc14 is the major phosphatase antagonising CDK in yeast. But its eukaryotic homologue does not appear to play an essential role in mitotic control. Studies in *Drosophila* and *Xenopus* have shown that PP2A/B55 inhibition is crucial for MPF activation, and that this is brought about by Greatwall kinase and its substrates, the closely related 17kDa proteins Ensa and Arpp19. However, it remains unclear, if PP2A/B55 inhibition by phosphorylated Ensa/Arpp19 is a critical event in regulating mitotic entry in somatic cells.

In this thesis I have performed a cell biological, genetic and biochemical characterisation of Ensa/Arpp19. I have generated and optimised tools to study the function of these two proteins and characterised their localisation, their depletion phenotypes, the nature of their interaction with the PP2A/B55 phosphatase and their protein interactome in metaphase and anaphase in mammalian cells. In parallel I have been optimising a novel protein transfection based method to study the effects of constitutively phosphorylated Ensa/Arpp19 in cells.

The experiments described in this thesis show a surprising divergence of the functions of Ensa/Arpp19 and their upstream kinase Greatwall, suggesting a more complex signaling cascade involving these proteins. Our biochemical characterization of the Ensa/B55 interaction also suggests a novel mechanism of action for these proteins. Overall this work sheds light on how the balanced activity of the Cdk1 activation switch and its counteracting phosphatases contribute to the regulation of mitotic entry.

TABLE OF CONTENTS

ABBREVIATIONS

3D	3-dimensional
aa	Amino acid
ADP	Adenosine diphosphate
APC/C	Anaphase-promoting complex/cyclosome
APS	Ammonium persulphate
Arpp19	cAMP-regulated phosphoprotein 19
as	ATP-analogue sensitive
ATM	Ataxia telangiectasia mutated kinase
ATP	Adenosine triphosphate
ATR	Ataxia telangiectasia and Rad-3-related kinase
bp	Base pairs
BSA	Bovine serum albumin
Bub	Budding uninhibited by benzimidazole
C-lobe	Carboxy-terminal lobe
Ca2+	Calcium
CaCl2	Calcium chloride
CAK	CDK-activating kinase
cAMP	Cyclic adenosine monophosphate
Cdc	Cell division cycle
Cdh1	Cell division cycle homologue 1
CDK	Cyclin dependant kinase
CDPK1	Calcium-dependant protein kinase 1
cDNA	Complimentary DNA
cGMP	Cyclic guanosine monophosphate
Chfr	Checkpoint protein with an FHA domain and RING finger
CKI	CDK-inhibitors
cm	Centimetre
CO2	Carbon dioxide
CPC	Chromosome passenger complex
CSF	Cytostatic factor
D-box	Destruction box
DAPI	4', 6-diamidino-2-phenylindole
dCTP	Deoxy cytosine triphosphate
ddH2O	Double distilled water
DDK	Dbf4-dependant kinase
DMEM	Dulbecco's modified eagle's medium
DMSO	Dimethyl sulphoxide
DNA	Deoxyribonucleic acid
DSBs	Double strand breaks
DTT	Dithiothreitol
E.coli	Escherichia coli
ECL	Enhanced chemiluminescence
EDTA	Ethylene diamine tetraacetic acid
EGTA	Ethylene glycol tetraacetic acid

Emi2	Endogenous meiotic inhibitor 2
Ensa	α-Endosulfine
es	Electrophile-sensitive
FACS	Fluorescence-activated cell sorting
FBS	Foetal bovine serum
FCP-1	F-Cell Production 1 gene
FCS	Foetal calf serum
g	Centrifugal force constant
gm	Grams
GFP	Green fluorescent protein
GVBD	Germinal vesicle breakdown
HAT	Histone deacetylase
HBSS	HEPES-buffered saline solution
HCl	Hydrogen chloride
HEK	Human embryonic kidney cells
HRP	Horseradish peroxidase
Inc.	Incorporation
INCENP	Inner centromere protein
INK	Inhibitors of CDK
IP	Immunoprecipitation
IPTG	Isopropylthio-β-galactoside
IR	Ionising radiation
MAPK	Mitogen-activated protein kinase
MASTL	Microtubule associated serine/threonine-like
MBP	Myelin basic protein
MCM	Mini-chromosome maintenance
MEF	Mouse embryo fibroblast
Mg2+	Magnesium
MgCl2	Magnesium chloride
ml	Millilitre
mM	Millimolar
mm	Millimetre
MnCl2	Manganese chloride
Na3VO4	Sodium orthovanadate
NCBI	National centre for biotechnology information
NCMR	Non-conserved middle region
NEBD	Nuclear envelope breakdown
NF-κB	Nuclear factor-kappa B
NF-Y	Nuclear transcription factor Y
ng	Nanogram
Ni-NTA	Nickel-nitrilotriacetic acid
nM	Nanomolar
ORC	Origin recognition complex
PBS	Phosphate-buffered saline
PCAF	p300/CBP-associated factor
PCNA	Proliferating cell nuclear antigen

PCR	Polymerase chain reaction
PDK1	3-phosphoinositide-dependant kinase 1
PHYRE	Protein homology/analogy recognition engine
PI	Propidium iodide
PKA	cAMP-activated protein kinase
PKC	Protein kinase C
PLK1	Polo-like kinase 1
Plx	*Xenopus* PLK
PMSF	Phenylmethylsulphonyl fluoride
PNBM	p-nitrobenzyl mesylate
PP1	Protein phosphatase 1
PP2A	Protein phosphatase 2A
pRB	Retinoblastoma protein
pre-RC	Prereplication complex
PTM	Post-translational modification
RFP	Red fluorescent protein
RNA	Ribonucleic acid
RNAi	RNA interference
RPA	Replication protein A
RPE	Human retinal pigmented epithelium cells
rpm	revolutions per minute
RT Room temperature	Room temperature
RT-PCR	Reverse transcription PCR
s, min, h	second, minute, hour
S6K	p70 ribosomal S6 kinase
SAC	Spindle assembly checkpoint
S.cerevisiae	Saccharomyces cerevisiae
S. pombe	Schizosaccharomyces pombe
Scant	Scott of the Antarctic
Scc1-4	Sister chromatid cohesion 1-4
SDS-PAGE	Sodium dodecyl sulphate polyacrylamide gel electrophoresis
s.d.	Standard deviation
Ser	Serine
s.e.m.	Standard error of the mean
shRNA	Short hairpin RNA
siRNA	Small interfering RNA
Smc	Structural maintenance of chromosomes
STLC	S-trityl-L-cysteine
TEMED	Tetramethylethylene diamine
Thr	Threonine
Tyr	Tyrosine
U	Units
µg	Microgram
µl	Microlitre
µM	Micromolar

UK	United Kingdom
USA	United States of America
UTR	Untranslated region
UV	Ultra violet
w/v	Weight per volume
WT	Wild type
X. laevis	Xenopus laevis

LIST OF FIGURES

LIST OF TABLES

CHAPTER1 INTRODUCTION

1.1 Cell Cycle Control

1.1.1 Historical Overview

Cells are the universal building blocks of any living organism. Robert Hooke in late 1600 coined the word “cell”, meaning “unit”, while observing a sliced cork under a basic light microscope. Although he was observing the cell walls of dead plant cells, the term has been used ever since to describe the fundamental unit in all living organisms (Alberts et al. 2014).

The ancestral cells were formed 3–4 million years ago by spontaneous chemical reactions and have been passing down their characteristics to the daughter cells through cell division. The observations and work of Matthias Schleiden (1838), Theodor Schwann (1839) and Rudolf Virchow (1858) have led to the “cell theory”, which indicates that “living cells were made from division of the pre-existing ones”; this theory was later experimentally proven by Pasteur (1860) (Alberts et al. 2014; Turner 1890).

However, features of the parents and daughters were not exactly the same always. Darwin explained these differences were owing to random adaptations and natural selection in organisms for survival in different environments(Alberts et al. 2010). Over the years, numerous studies have been done to gain an in-depth understanding of cell reproduction.

Cell reproduction needs to be a robust process that occurs over generations and is common to all living organisms and a fundamental characteristic of life. However, due to the fundamentally different organisations of prokaryotic and eukaryotic cells, the reproductive processes differ dramatically between the two super-regna; in this thesis, we will only consider eukaryotic cells. The advent of sexual reproduction introduced a dramatic change in the way organisms pass on their genetic material from one

generation to the next, and this is reflected by the specific meiotic cell division as compared to the standard mitotic cell cycle, which is the major subject of this thesis. The mitotic cell cycle consists of a stepwise and well-regulated series of events. Each cell first duplicates its genetic material, distributes it evenly to its daughter cells, and then splits into two cells. This order of events maintains the genetic integrity in an organism. In unicellular organisms like amoeba, a new organism is generated, and in multicellular organisms like humans, cell division contributes to development and tissue repair.

The timely duplication and segregation of chromosomes in eukaryotic cell cycle is key to successful cell division. This regulation is achieved by a number of signalling molecules that activate or deactivate effector proteins, thus leading to a cascade of events that eventually forms two daughter cells. These regulatory mechanisms also enable the survival of cells via energy production and maintenance of the structural components of the cell (Morgan 2007; Alberts et al. 2014).

De-regulation of these mechanistic pathways and mutations in the regulatory proteins may lead to uncontrolled cell proliferations and cancer. According to the World Health Organisation, cancer has been responsible for 8.2 million deaths in the world in 2014 (Cancer Research UK 2014). Hence, it is an area of intensive research. Although the cell division machinery differs in different organisms and different cell types, there are broad similarities that allow valuable insight for cancer research even in diverse organisms like yeast, *Drosophila*, frogs and mice. In recent years, the molecular machinery that drives the cell cycle has been defined in detail. This chapter introduces the key aspects of cell cycle regulation in mammalian cells relevant to the work in this thesis.

1.1.2 Phases of the Cell Cycle

The cell cycle has been historically categorised into different phases based on the microscopic observation of dividing cells under the light microscope (Flemming 1882; Paweletz 2001) and on radiolabelling cells to measure the timing of DNA synthesis

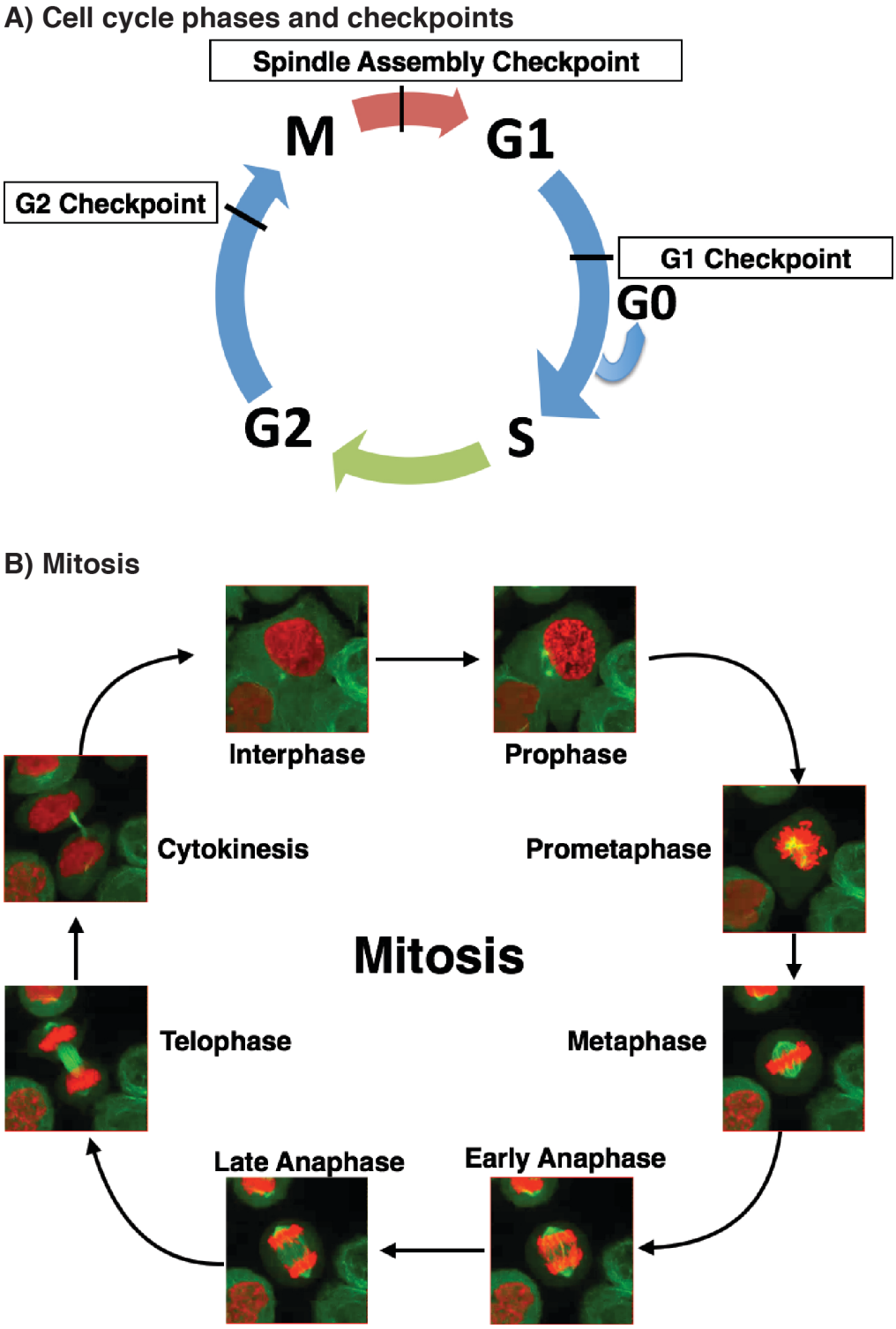

Figure 1.1 Phases of the cell cycle
A) The cell cycle has two major phases: interphase and M phase. G1: gap phase 1, G0: specialised resting state in G1, S: DNA synthesis phase, G2: gap phase 2 and M: mitotic phase. The G1-S-G2 collectively is called interphase. B) Mitotic stages in HeLa cells expressing GFP-tubulin and mCherry-H2B. Animal mitosis is divided into five main phases of nuclear division: prophase, prometaphase, metaphase, anaphase and telophase. Cytokinesis follows nuclear division to produce two identical daughter cells.

(Howard & Pelc 1953). These were further characterised based on the biochemical events occurring at the specific times. Initially, proliferating cells were either in 'mitosis', where their chromosomes were divided, or in 'interphase', the intervening phase between the divisions. The cell cycle, as we know today, comprises four distinct phases: the S phase and the Gap phases (G1 and G2) that constitute the interphase and the mitotic phases, respectively (Fig. 1.1A).

S Phase

The DNA duplicates during S phase by semi-conservative replication of its two complementary strands (Meselson & Stahl 1958), a process tightly regulated by the replication molecular machinery. Replication begins at the specific points on the DNA called "replications origins" that are scattered in large numbers on the chromosomes. The replications machinery employs a helicase that opens up the double helix at these positions, a *primase* generates a short stretch of RNA at the start of replication and the DNA *polymerase* continues replication by extending complementary nucleotides to the template strand from the 5' end of the RNA primer. This is done continuously on the leading strand and discontinuously on the lagging strand. The two strands are looped, so that a uniform single replication fork proceeds from the origin replicating both leading and lagging strands. DNA replication also requires histone synthesis, which form nucleosomes and package the DNA within the cell behind the replication fork. The duplicated chromosomes are called sister chromatids and they are held together by a ring-shaped protein complex called cohesin consisting of the structural maintenance complex proteins SMC1/3, alpha-Kleisin (SCC1) and Scc3.

The Gap Phases

The two Gap phases, G1 and G2 give the cell time to grow and prepare for their transition into S phase and M phase respectively. These phases are also essential to regulate progression of the cell to the next stage integrating intracellular and extracellular mechanisms.

During Gap phase 1 (G1), the cells coordinate molecular signals and prepare for the duplication of the DNA material. The G1 phase is also the time when the cell decides whether to enter the next cell cycle. In the event of nutrient deficiency or any such hindrances, the cell might choose to enter the G0 or the non-dividing stage. This is usually observed in highly proliferative populations such as stem cells. In budding yeast

(Rupes 2002) and possibly also higher eukaryotes (Zetterberg et al. 1984), this is also the time when most of the new cell mass is gained. Interestingly, fission yeast performs this predominantly in G2 phase. The precise coordination of cell growth and division remains poorly understood so far. G2 is the tail end of interphase, when the cell prepares to enter mitosis. During G2, the proteins essential for mitosis, such as A and B-type Cyclins, are synthesised. This is also the time when DNA damage that occurred during the S phase is repaired. Transition between the gap phases and the S and M phases is strictly monitored by cell cycle checkpoints to ensure genome integrity and to prevent aberrant cell division (Barnum & O'Connell 2014)(Fig. 1.1). G1/S and G2/M are the two main checkpoints leading from the gap phase to the next cell cycle phase. The G2/M checkpoint is discussed in detail in the later sections.

Mitosis

Once the DNA is duplicated, cell division can occur symmetrically or asymmetrically. Asymmetric divisions are usually observed during developmental stages or during production of differentiated cell types from stem cells. Symmetric divisions occur in somatic cells and leads to doubling the cell number with every division. Mitosis is the complex process of cell division comprising of four sub-phases: prophase, metaphase, anaphase and telophase (Fig. 1.1B).

1. During prophase, the replicated chromosomes condense and the mitotic apparatus starts to form. The centrosome duplicates and migrates to the poles forming the spindle poles. The nuclear envelope breaks down.
2. The condensed chromosomes then pair up as sister chromatids and align in the midzone called the metaphase plate. The microtubules attach to the sister chromatids through the kinetochore, and tension is generated.
3. In anaphase, the microtubules begin to shorten. This results in pulling apart the sister chromatids to the opposite poles.
4. Lastly, during telophase the chromosomes de-condense and the nuclear envelope reforms. With the help of the actin and microtubule cytoskeleton the cell forms the cytokinesis furrow and splits into two daughter cells with equal number of chromosomes (Morgan 2007; Alberts et al. 2010).

In addition to the distribution of the genetic material (DNA), other cellular organelles such as centrosomes, mitochondria and Golgi should also be distributed among the daughter cells. This is achieved by association of the fragmented organelles with the

components of the cytoskeleton and is not a passive process (Shima et al. 1998; Boldogh et al. 2001; Alberts et al. 2010; Morgan 2007). The biochemical components driving this process are described in detail in the following sections.

1.1.3 Cell Cycle Models and the Discovery of MPF

The cell cycle has to be tightly regulated so that DNA replication occurs 'once and once only' per cell cycle. The centrosomes, the microtubule organising centre and residence of the centrioles also undergo an analogous semi-conservative replication cycle and are evenly distributed between daughter cells. Thus, the cell cycle consists of nuclear division cycle, a centrosome cycle and cellular division (cytokinesis), ideally controlled by the same timing mechanism (Alberts et al. 2014; Morgan 2007). Two lines of work determined the molecular mechanisms that orchestrate the cell division cycle. The major initial breakthrough came from genetic studies in budding and fission yeast in the 1970s and from biochemical characterisation of cell cycle control enzymes in *Xenopus* oocytes and sea urchin eggs.

Two models were proposed for the control of the cell cycle. Yeast studies proposed the domino model: where one cell cycle event occurred after another and showed inter-dependence on each other. This was observed in experiments where a cell lacking a gene necessary for the initiation or the completion of a particular phase, prohibited the cell from progressing in the cell cycle. This eventually led to the concept of cell cycle checkpoints that ensures the sequential order of the cell cycle phases to safeguard its fidelity (Nurse et al. 1976; Weinert & Hartwell 1989; Nishimoto 1992). The 'cell division control' (cdc) mutant strains, in particular cdc2, were identified in yeast screens. These mutants were characterised by their size, once identified by their arrest in a particular stage of the cell cycle. In *Schizosaccharomyces pombe,* the cdc2 mutants fail to divide at restrictive temperatures and are elongated as compared to the wild type (Nurse & Thuriaux 1980). These findings were consistent with the budding yeast phenotypes (*Saccharomyces cerevisiae*) where the *cdc28* mutants failed to divide (Hartwell et al. 1974). These proteins were implicated to have important roles in the cell cycle, especially for the 'Start' (yeast equivalent of restriction point) and for mitotic control.

On the other hand, *Xenopus* oocytes and cytoplasmic extracts studies predicted the Clock model: a cytoplasmic clock triggered entry into mitosis and was independent of each phase. An unknown activity was found to promote meiotic entry in *Xenopus* oocytes. *Xenopus* oocytes have rapid mitotic to interphase cycles, which makes it easier to sturdy cell cycle transitions. The cytoplasm form M-phase oocytes but not interphase oocytes could induce M-phase entry in immature oocytes. This unknown activity was the named 'maturation-promoting factor' (MPF) (Masui and Markert 1971; Smith and Ecker 1971). This led to the 'clock model' where a biochemical component was responsible to drive the cell cycle, which was present in the cytoplasm. Similar biochemical component from mitotic *HeLa* cells when injected in *Xenopus* oocytes led to germinal vesicle breakdown (GVBD). Thus, the MPF activity was found to be conserved among higher eukaryotes (Sunkara et al. 1979). However, later as the molecular mechanisms underlying these cell cycle transitions were revealed, both models were reconciled (K. Hara et al. 1980; Hartwell 1978).

1.1.4 Discovery of Cyclins and the Unifying Theory of the Cell Cycle

In the meanwhile, T. Hunt and colleagues did continuous methionine labelling studies in sea urchin to observe protein synthesis in the initial few cell cycles. This led to the discovery of the 56-kDa protein that oscillates between mitosis and interphase. Due to the cyclic appearance of this protein, it was named Cyclin. On the basis of sequence comparison, they were divided into 2 classes: Cyclin A and B (Evans et al. 1983; Pines & Hunt 1987b). Cyclin A was cloned from the clam embryos and it was similar to sea urchins. Additionally, the mRNA also triggered M phase in *Xenopus* oocytes (Swenson et al. 1986). Similar results were observed with Cyclin B as well (Pines & Hunt 1987a). The fact that Cyclins are associated with MPF was shown by cell-free extracts experiments in *Xenopus*. MPF was purified from oocytes and was found to be composed of two subunits of approximately 34 kDa and 45 kDa. The kinase activity of MPF was also able to phosphorylate the endogenous 45-kDa protein as well as H1 (Lohka et al. 1988). Further studies with purified MPF and antibodies related the two subunits of MPF to be cdc2 and Cyclin B (both B1 and B2) (Gautier et al. 1988; Gautier et al. 1990). The Cdc2 protein from clams was found to form a complex with both

Cyclin A and Cyclin B. Both these protein complexes showed cell-cycle dependent kinase activity (Draetta 1993). Thus, the concept of Cyclin-dependent kinases (Cdk) was introduced in cell cycle regulation.

Moreover, protein synthesis studies in cell-free extracts by Kirschner and colleagues showed that Cyclin synthesis was important and sufficient for mitotic entry. Cell-free extracts were treated with ribonuclease to degrade endogenous Cyclin mRNA. These extracts could enter the cell cycle when exogenous Cyclin mRNA was added (Murray & Kirschner 1989a). Additionally, Minshull et al. (1989) showed that the mRNA of Cyclin B in particular induced mitotic entry in *Xenopus* extracts (Minshull et al. 1989). Thus, Cyclin synthesis is crucial for mitotic entry similar to MPF. Cdc13 was found to be crucial for G2/M entry and proper cytokinesis in fission yeast. The gene interacted closely with both yeast and human cdc2 and was similar to the sea urchin Cyclin. In addition to these experiments, a unified view of the cell cycle emerged when it was demonstrated that the critical players of the embryonic (*Xenopus*) and somatic (yeast) cell cycle are proteins encoded by homologous genes. In 1982, Beach et al. complemented *cdc* mutants in *S. pombe* with the *cd28* gene from budding yeast. This rescued the elongated phenotype in *S. pombe* thus showing that Cdc2 and Cdc28 are functional homologues of the 'cell division control' proteins and encoded a protein with kinase activity (Reed et al. 1985; Simanis & Nurse 1986). Cross-species gene complementation assays were done with purified MPF activity, the human homologue of Cdc 2, in yeast. The human Cdc2 (later named CDC2) could complement the temperature-sensitive *cdc2* mutants and a *cdc2*-deficient strain. A comparison of the amino-acid sequence of CDC2 with Cdc2 and Cdc28 revealed 63% and 58% homology, respectively (M. G. Lee & Nurse 1987). Similarly, the product of the gene *cdc13* is homologous to Cyclin. Humans were also found to have several Cdk and Cyclins that were homologous to the yeast, sea urchin and *Xenopus* equivalents.

Thus, the cell cycle as we know it today is regulated by a wide variety of Cdk-Cyclin complexes as shown in Fig. 1.3. The Cyclins bind to their Cdk partners via the 'Cyclin-box'. This is a 150 amino acid sequence and is highly conserved(Kobayashi et al. 1992).

1.2 MPF Regulation: Cdk-Cyclin Complex Regulation in Mitosis

The basic regulatory elements of the cell cycle are the Cdk-Cyclin complexes. Although around 20 ‘Cdk’ proteins and 29 ‘Cyclin’ genes were found in humans due to sequence similarity, only a few have been known to have a function linked to the cell cycle. These are Cdks 1, 2, 4, 6 and 7 and Cyclins A, B, D, E and H (Malumbres & Barbacid 2005). Among these Cyclins, Cdks characteristically bind with a particular Cyclin partner to drive different stages of the cell cycle. Cdk1 binds Cyclin A or Cyclin B, Cdk2 with Cyclin E or Cyclin A, and both Cdk4 and Cdk6 with Cyclin D (Draetta et al. 1989; Pines & Hunter 1989; Tsai et al. 1991; Koff et al. 1992; Matsushime et al. 1992; Rosenblatt et al. 1992; Meyerson & Harlow 1994).

Of these Cdk -Cyclin complexes, Cdk1-Cyclin B is known to be the master regulator of mitosis. When MPF was purified, Cdk was observed to co-purify with Cyclin (Lohka et al. 1988). Although Cyclin binding is an important part of Cdk activation, it is not sufficient to activate Cdk completely. The Cdk-activating kinase phosphorylates Cdk in the Cdk -Cyclin complex and activates it fully(Jeffrey et al. 1995). However, due to the presence of CAK throughout the cell cycle, it is not considered as one of the regulatory mechanism in Cdk -Cyclin activation. Inhibitory phosphorylations by Wee1/Myt1 and their dephosphorylation by Cdc25 maintain the on/off state of the Cdk -Cyclin complex at G2/M transition (Nurse & Thuriaux 1980; Gautier et al. 1991; Parker et al. 1992; McGowan & Russell 1993; Mueller et al. 1995). Additionally, the action of Cdk inhibitors like p21, p27 and p57 or the INK4 family, keep Cdks inhibited. They function mainly in the G1/S transition of the cell cycle (Sherr & Roberts 1999). Cyclin proteolysis at the end of mitosis is the irreversible step in MPF regulation, which occurs at the end of mitosis. Once the cell exits mitosis, they need to re-synthesise the Cyclins to initiate the next cell cycle (Evans et al. 1983; Murray & Kirschner 1989b). Thus, Cdk activation is regulated by a combination of mechanisms such as Cyclin synthesis and binding, phosphorylation of specific residues and the action of Cdk inhibitors (CdkIs). Among these, the mechanisms controlling the mitotic Cdk -Cyclin complexes are described in detail in the following sections.

1.2.1 Cyclin Synthesis and Cdk Binding

Cyclins were named based on their fluctuating concentrations throughout the cell cycle. These proteins were observed to accumulate through interphase and disappear abruptly in mitosis. Cyclin levels are mostly regulated by both transcriptional and degradative mechanisms. This, in turn, drives the cell cycle by inducing the appropriate Cdk activity. Cdk remains constant throughout the cell cycle, while the oscillations in Cyclin activity and the resulting Cdk activity is crucial in licensing cell cycle progression. The activated Cyclin A/B-Cdk1 complex phosphorylates mitotic substrates and initiates mitotic entry. However, not all cyclins alter their activities throughout the cell cycle, and some of them have also been found to function in other phases of the cell cycle at later time points. Cyclins are classified according to their Cdk binding domain, the conserved Cyclin box structure (Hochegger et al. 2008; Fung & Poon 2005). The presence of a particular Cyclin defines a period where the accompanying Cdk is competent for activation (Fig. 1.2A).

In mammalian cells, Cyclin A and Cyclin B are the mitotic Cyclins as they are synthesised and degraded around mitosis. Cyclin A binds and activates both Cdk1 and Cdk2, whereas Cyclin B only binds Cdk1. Two types of Cyclin A (A1 and A2) (Girard et al. 1991; Zindy et al. 1992; Sweeney et al. 1996; Ravnik & Wolgemuth 1999) and three types of Cyclin B (B1, B2, B3) (Pines & Hunter 1989; Chapman & Wolgemuth 1992; Gallant & Nigg 1992; Lozano et al. 2002; Nguyen et al. 2002) are present in mammalian cells. Of these A2, B1 and B2 are known to function in proliferating somatic cells. These Cyclins have similar promoters containing CCAAT-boxes. These promoters are regulated by transcriptional factors like CBP (Cyclin A) (Krämer et al. 1997) and trimeric NF-Y transcriptional activator (Cyclin A and B) (Katula et al. 1997; Bolognese et al. 1999). Additionally, the synergistic p300 co-activator that binds to the promoters activates transcription of *Cyclin B1 and B2* (Wasner, Tschöp, et al. 2003; Salsi et al. 2003). The mRNA of Cyclin A starts accumulating earlier than Cyclin B at the start of DNA replication (Henglein et al. 1994; Erlandsson et al. 2000), whereas the Cyclin B levels rise in mid-S phase (Norbury & Nurse 1992; Pines & Hunter 1989). Cyclin A protein levels peak at the beginning of mitosis whereas the Cyclin B levels peak slightly later at the metaphase-anaphase transition. During S phase the NF-Y is

further activated by Cyclin E/A-Cdk2, leading to a rise in the Cyclin B transcription (Katula et al. 1997). In *HeLa* cells, the NF-Y factor remains bound to the promoter and

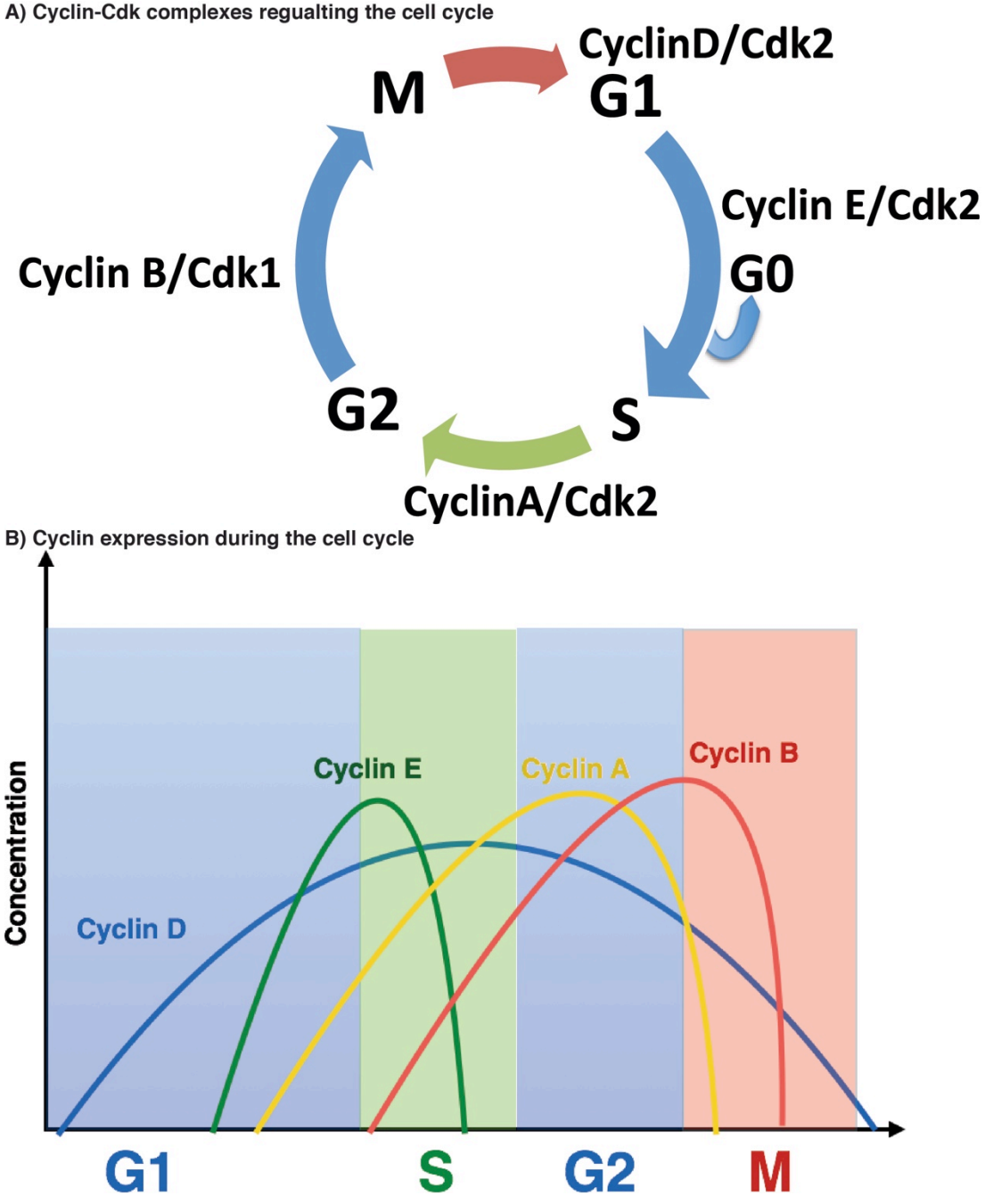

Figure 1.2 Control of the mammalian cell cycle by Cyclin-Cdks

A) Cyclin-Cdk complexes regulating the cell cycle. Schematic representation of mammalian Cyclin-Cdk complexes, involved in progression throughout different phases of the cell cycle. These are the master regulators of the cell cycle. Adapted from Malumbres et al. (Malumbres & Barbacid 2005). B) Cyclin expression during the cell cycle. D-type cyclins are relatively stable throughout the cell cycle but have an important role in early G1. E-type cyclins are expressed at G1/S to drive S-phase entry. A-type cyclins allow progression into mitosis from S phase and B-type cyclins are responsible for mitosis. Adapted from Morgan (Morgan 2007).

Cyclin B transcription continues even in mitosis. This occurs as the Cyclin B gene maintains an open chromatin configuration even in the mitotic stage (Sciortino et al. 2001). Conversely, the transcription of Cyclin B1 and B2 is repressed in response to DNA damage and this repression requires the NF-Y and CCAAT boxes (Manni et al. 2001).

Cyclin A transcription is repressed during G1 by a repressor element called cell cycle responsive element (CCRE) or cell cycle dependent element (CDE), which contains an E2F binding site. The Cyclin B1 promoter also houses both positive and negative acting E2F-promoter elements. In the S phase, Cyclin D/E-Cdk hyperphosphorylates pRb and releases E2F, leading to the transcription of Cyclin A2. This works through the CCRE/CDE elements. Moreover, Cyclin A-Cdk2 also inhibits the transcriptional activity of E2F by phosphorylating it (Zwicker et al. 1995; Huet et al. 1996; Soucek et al. 1997; Schulze et al. 1995; Zhu et al. 2004; Knudsen et al. 1999). Additional elements contributing to repression of mitotic Cyclins (Cyclin A2, Cyclin B1 and Cyclin B2) in G1 are cell cycle gene homology regions (CHRs), which are also present in many G2/M genes along with CCAAT boxes, NF-Y and B-MYB binding. B-MYB is regulated by E2F and its expression is enhanced by Cyclin a-Cdk2. This in turn regulates transcription of Cyclin A and Cyclin B positively. Additionally, FOXM1 is another transactivator of Cyclin B1 expression (Wasner, Haugwitz, et al. 2003; Wasner, Tschöp, et al. 2003; Zwicker et al. 1995; N. Liu et al. 1998; Philips et al. 1999; Joaquin & Watson 2003; Laoukili et al. 2005) (Fig. 1.2B).

Once synthesised Cyclins bind to Cdks and act as allosteric activators. The crystal structure of human Cdk2 shows that the protein-binding site is sandwiched between the small amino and large carboxyl-terminal lobes. Binding of the substrate in this cleft enables it to be closer to the γ-phosphate of the ATP. However, this substrate binding site is blocked by an alpha-helix called the ‘T’ loop, which acts as an auto-inhibitor of the kinase (De Bondt et al. 1993). This ‘T’ loop undergoes conformational changes on binding Cyclin A, due to the presence of conserved charged residues interacting with Cdk. Thus, the active site is no more blocked. However, Cdk1 structure with Cyclin B shows fewer interactions between the activation segment and Cyclin B, has a disordered region and substrate-recognition requires considerable re-arrangement (Nicholas R Brown et al. 2015; Petri et al. 2007). Cyclins themselves have no enzymatic activity but

have substrate binding sites and target Cdks to specific subcellular locations (Evans et al. 1983; Dorée & Hunt 2002).

1.2.2 Post-translational Modification of Cdk-Cyclins: CAK Phosphorylation

Once Cyclin binds to Cdk, it needs to be activated by post-translational modifications. The Cyclin-binding region on Cdk1 has the PSTAIRE motif, which contains Thr160 in humans. This residue needs to be phosphorylated by the Cdk-activating kinase (CAK) in order to fully activate the Cdk-Cyclin complex. Human Cdk2/Cyclin A is phosphorylated at Thr161 by CAK. In budding yeast, cdc2 alone is not a substrate of CAK, unlike Cdk2 in vertebrates. Structural data of unphosphorylated Cdk2/Cyclin A complex show the T-loop interfering with the putative substrate-binding site as well as the subsequent Cdk2-Cyclin A contacts. Phosphorylation of Thr160 leads to a conformational change in the T-loop. Thus, phosphorylation of Thr160 is required to activate the Cdk-Cyclin complex, which allows access to the active site and stabilises ATP binding (Draetta 1993; Endicott & Noble 2013; Russo et al. 1996; Fisher & Morgan 1994; Mäkelä et al. 1994)

CAK is very similar to MO15, a kinase protein structurally related to cdc2 in *Xenopus laevis*. Two types of CAK have been identified. Budding yeast contains monomeric CAK1p that localises in the cytoplasm, while the trimeric $p40^{MO15}$ (Cdk7)/Cyclin H/MAT complex in vertebrates localizes in the nucleus. MO15 is the catalytic subunit of CAK and Cyclin H is its prime partner.
The trimeric complex is also a subunit of TFHII (general transcription factor) and phosphorylates various components in the transcription machinery in addition to Cdks (Fisher & Morgan 1994; Mäkelä et al. 1994; Kaldis et al. 1998; Kaldis 1999). Although CAK phosphorylation fully activates the Cdk-Cyclin complex, it is not considered as a regulatory step, because CAK is not regulated in a cell-cycle dependent manner and is ubiquitously present throughout the cell cycle (Lolli & L. N. Johnson 2005).

1.2.3 Post-translational Modification of Cdk-Cyclins: Cdk Inhibitors

Another regulatory mechanism is the binding of small peptides called Cdk inhibitors (CKIs). Two types of these peptides have been identified based on sequence homology and targets of inhibition: Cdk4 (INK4) family and the Cdk-interacting protein or Kinase inhibitory protein (Cip/Kip) family (Sherr & Roberts 1999).

Cdk4/INK4 binds Cdk4/6 as monomers. The family comprises of p15(INK4b), p16(INK4a), p18(INK4c) and p19(INK4d). p16 is a prominent Cdk4 inhibitor that accumulates in cells lacking pRb. Its transcription is repressed by pRb, which in turn is phosphorylated and inhibited by active the Cyclin D-Cdk4/6 complex, which results in a negative feedback loop. Structural data indicate that these CKIs bind Cdk directly and cause distortion of both the Cyclin and ATP binding sites. The activity of Cyclin D-Cdk4/6 is important in re-entry into the cell cycle from the G0 phase. Thus, both p16 and pRb are important in cell proliferation from quiescence (Ruas & G. Peters 1998; Sherr 2001; Jeffrey et al. 2000).

The Cip/Kip family has a preference for bound Cdk-Cyclin complexes. This family comprises of p21(Cip1), p27(Kip1) and p57(Kip2). These CKIs can have activating or inhibitory effects. The N-terminal of the inhibitory domain is conserved, and this domain is essential and sufficient for Cdk2 inhibition (J. Chen 1996; Nakanishi et al. 1995; Luo et al. 1995). These CKIs negatively regulate Cyclin A-Cdk2, Cyclin E-Cdk2 and Cyclin B-Cdk1 and positively regulate Cyclin D-Cdk4/6. p21 leads to high expression of Cyclin D, which eventually leads to an increase in Cdk activity. The active Cdk-Cyclin complex phosphorylates the pocket proteins to release the EF2 transcription factors. Thus, cell cycle genes are expressed in G1 to induce S phase progression (Sherr & Roberts 1999; LaBaer et al. 1997).

1.2.4 Post-translational Modification of Cdk-Cyclins: Wee1/Myt1 Inhibitory Phosphorylations

CAK phosphorylation fully activates the mitotic Cdk -Cyclin complexes. These complexes need to be kept inert until it is required in the cell cycle. This is achieved by

phosphorylating two key residues on Cdk1 and Cdk2, Thr14/Tyr15. This layer of negative regulation contributes to the switch-like property of cells during mitotic entry (Welburn et al. 2007; Gu et al. 1992).

Wee1 was originally identified in a fission yeast screen for cell cycle regulators. The functional loss of this gene in *Schizosaccharomyces Pombe* (fission yeast) leads to the formation of smaller daughter cells after premature mitosis followed by death. These phenotypes suggest a role of this kinase in co-ordinating cell size with cell cycle to prevent smaller cells from entering mitosis. This was the first evidence suggesting a G2/M role of Wee1. In yeast Wee1 phosphorylates both T14 and Y15 residues of Cdc2, while human Wee1 only phosphorylates Tyrosine 15 residue on Cdk1 (Nurse & Thuriaux 1980; Parker & Piwnica-Worms 1992; Parker et al. 1992; McGowan & Russell 1993). This suggests the need for another kinase to phosphorylate the Thr14 residues in vertebrates. A dual-specificity kinase, Myt1, phosphorylates both Thr14 and Tyr15 residues in *Xenopus leavis* cdc2 and is conserved in humans (Mueller et al. 1995; Fattaey & Booher 1997).

Both these kinases show different localisation in interphase. While Wee1 is nuclear or associated with centrosomes, Myt1 is associated with endoplasmic reticulum and Golgi complex (Mueller et al. 1995; F. Liu 1997; Kornbluth et al. 1994; Baldin & Ducommun 1995). The differential impact of these kinases on the G2/M transition is yet to be determined. Although studies with Wee1 depletion have been documented, very little is known about Myt1. Wee1 depletion in yeast and *Drosophila* induce premature mitotic entry. Depletion of Wee1 in mice causes embryonic lethality (Tominaga et al. 2006) and in human cell lines leads to striking mitotic phenotypes (Neumann et al. 2010). Interestingly, in *HeLa* cells, treatment with Wee1 specific inhibitor (Pd0166285) at the S/G2 border causes abrupt and premature mitotic entry even in the absence of G2. This strongly suggests a critical role of this kinase in the G2/M transition (Potapova et al. 2011). Functions of Myt1 have only been characterised in DNA damage, where it contributes to checkpoint recovery independent of Wee1(Chow & Poon 2013). The importance of Myt1 in the G2/M transition is yet to be determined.

1.2.5 Cdk-Cyclin Activation: Cdc25 Phosphatases

Inhibitory phosphorylations by Wee1/Myt1 have to be removed to activate Cdk1 at the onset of mitosis(Gautier et al. 1991). Dual-specificity phosphatase called Cdc25 performs this function. They were initially identified in fission yeast. The protein encoded by cdc25+ gene was found to be antagonistic to Wee1+ and the overexpression of this protein induced mitosis in cells with reduced cell size (Russell & Nurse 1986; Galaktionov & Beach 1991). *Xenopus leavis* studies revealed these phosphatases can dephosphorylate both serine-threonine and tyrosine residues (Dunphy & Kumagai 1991). The cdc25 gene was found to be hyperphosphorylated near the onset of mitosis at the N-terminal region. Moreover, purified cdc25 could rescue and induce mitosis in *Xenopus leavis* interphase extracts arrested due to inhibition of DNA synthesis (Kumagai & Dunphy 1991; Kumagai & Dunphy 1992). Thus, the activation of cdc2 by cdc25 dephosphorylation appeared to be mandatory for mitosis. The cdc25 gene was highly conserved in all eukaryotic organisms (Sadhu et al. 1990; Draetta & Eckstein 1997; Khadaroo et al. 2004). In humans there are three different of *cdc25* located on chromosomes 3, 20 and 5, encoding the paralogues Cdc25 A, B and C, respectively (Alonso et al. 2004).

All three paralogues in humans regulate cell cycle checkpoints by activating Wee1/Myt1 inactivated Cdk -Cyclin complexes. Cdc25A is thought to activate Cdk2 and promote S-phase entry as depletion of Cdc25A in G1 phase blocks entry into S phase. Cdc25A is also expressed predominantly in G1 phase and is mostly nuclear. It accumulates in late S phase but is present in all phases in the cell cycle. It is transcriptionally controlled by c-Myc and E2F transcription factors. (Hoffmann et al. 1994; Blomberg & Hoffmann 1999; Jinno et al. 1994).

On the other hand, CDC25B and C primarily regulate G2/M transition. They are targeted to the centrosomes in G2 and activate Cdk1-CyclinB1 there. CDC25B increases in the cytoplasm, and the prophase microtubule nucleation is thought to be a consequence of this increase (M. S. Chen et al. 2001). Surprisingly, knockout mouse models of Cdc25 B and C are viable both individually and together, but Cdc25A deletion has a lethal effect. Double deletion of Cdc25 B and C was found to only cause sterility, which already occurs in Cdc25B knockout mice (M. S. Chen et al. 2001;

Ferguson et al. 2005; Lincoln et al. 2002); this suggested that Cdc25A steps in to perform mitotic functions in the absence of the other paralogues. It was later found that Cdc25A activates Cdk1-CyclinB and plays a role in chromatin condensation. Similarly, Cdc25 B and C were also shown to be involved in promoting S phase, in addition to controlling Cdk1-CyclinB activation at the G2/M transition (Hoffmann et al. 1994; Gabrielli et al. 1996; Lindqvist et al. 2005; Boutros et al. 2006).

Localisation of the Cdc25 paralogues changes during the course of the cell cycle. In G2 phase, Cdc25 A, B and C shuttle between the nucleus and the cytoplasm. The subcellular localisation is regulated by a nuclear localisation sequences and nuclear export signal located in the N-terminal regulatory domain of Cdc25 phosphatases (Kumagai & Dunphy 1999; Uchida et al. 2004). Additionally, interactions with 14-3-3 proteins also partly regulate the localisation of Cdc25 by binding to the phosphatase upon phosphorylation by CHK1 and/or C-TAK1 kinases (Dalal et al. 1999; Conklin et al. 1995; C. Y. Peng et al. 1998; M.-S. Chen et al. 2003). Dissociation of the 14-3-3 protein activates Cdc25 at the G2/M transition. The nuclear export signals and 14-3-3 binding enable the shuttling of the Cdc25 between the cytoplasm and the nucleus.

The regulation of these mitotic elements: Wee1/Myt1 and Cdc25 are discussed in detail in the next sections

1.2.6 The G2/M Checkpoint

DNA damage leads to varied response mechanisms in the cells of which some are involved in stalling the replication fork, some in repairing the damaged DNA and some in preventing entry into mitosis. Of these, G2/M checkpoint that regulates and inhibits mitotic entry in response to DNA damage is described here.

Mitotic entry is prevented by two pathways in response to DNA damage at the G2/M checkpoint: the ATM/ATR signalling pathway and the p53 pathway. CHK1 and CHK2 kinases are activated in the ATM/ATR pathway, which in turn phosphorylate specific serine residues on Cdc25 and inactivate it. CHK1, CHK2 and Plk3 phosphorylations leads to 14-3-3 binding on Cdc25, which is then sequestered into the cytoplasm and

becomes inaccessible to Cdk1-Cyclin B (Bulavin et al. 2001; Xiao et al. 2003; Q. H. Liu et al. 2000). CHK1 and CHK2 also inhibit Cdk1 by activating the p53 pathway. $p21^{Cip1}$, Gadd45 and 14-3-3σ are the transcriptional targets of p53, which inhibit Cdk1 directly or indirectly (Charrier-Savournin et al. 2004; Hermeking et al. 1997; Vairapandi et al. 2002; Stewart & Pietenpol 2001). p21 isolates inactive the Cdk1-Cyclin B complex in the nucleus and prevents its activation and recruitment to the centrosome, where it first gets activated (Charrier-Savournin et al. 2004). Gadd45 binds Cdk1 directly and prevents Cyclin association in a p53-dependent manner (Vairapandi et al. 2002; Zhan et al. 1999; X. W. Wang et al. 1999). Furthermore, 14-3-3 σ binds Cdk1-Cyclin B complexes, which leads to the retention of the kinase in the cytoplasm, and this binding is induced by p53. (Chan et al. 2000; Hermeking et al. 1997). Plk1 kinase, which promotes mitosis by activating Cdk1-Cyclin B is also downregulated to ensure G2 arrest (Shaltiel et al. 2015; Takaki et al. 2008; van Vugt & Medema 2005).

1.2.7 Mitotic Entry

Once the G2/M checkpoint is satisfied, the activation of Cdk1- Cyclin B starts and is amplified to initiate mitosis. Multiple feedback loops in addition to spatial regulation of the mitotic entry elements control the G2/M transition (Fig. 1.3). All these events eventually lead to the rapid and irreversible activation of the Cdk1-Cyclin B complex, and cells enter mitosis when the Cdk1 activity threshold is attained. In this section, the spatial reorganisation of the mitotic entry network elements and the positive and negative feedback loops of Cdk1-Cyclin B activation are discussed.

Cdk1-Cyclin B complexes are mostly cytoplasmic, although Cyclin B1 shuttles between nucleus and cytoplasm with short nuclear retention time (J. Yang & Kornbluth 1999). The first active complexes of Cdk1-Cyclin B are seen at the centrosomes. This is thought to trigger the nuclear import of Cyclin B1 and Cdc25, where more active Cdk1-Cyclin B complexes are found later(Jackman et al. 2003; Toyoshima-Morimoto et al. 2002; Yuan et al. 2002). The nuclear translocation of the Cdk1-Cyclin B complex is mediated by phosphorylation of various serine residues in the cytoplasmic retention sequence (CRS) or the nuclear export signals (NES) of Cyclin, which in turn is regulated by Plk1 and Cdk1 kinases (Toyoshima-Morimoto et al. 2001; Hagting et al.

1999). The other components of the entry switch, such as Cdc25B and C and Myt1, are also cytoplasmic, while Wee1 and Greatwall kinases (described in the later sections) are nuclear (Alvarez-Fernández & Malumbres 2014). Following the translocation of Cyclin B1, Greatwall kinase, which is involved in the phosphatase control of the entry switch, is activated in the nucleus. Active Greatwall then translocates to the cytoplasm to start the phosphatase control pathway necessary for mitotic entry (Alvarez-Fernández et al. 2013).

The continuous rise of Cdk2/Cyclin A activity contributes to the inhibition of Wee1 and a decrease in the threshold for Cdk1 activity and entry into mitosis. Cyclin A2 RNAi increases Wee1 activity and lowers Plk1 and Cdc25C in *HeLa* cells (Fung et al. 2007). Moreover, siRNA depletion experiments with Cyclin A2 suggest that it could constitute the initial trigger of Cdk1 activation (Fung et al. 2007; Gong et al. 2007; Gong & Ferrell 2010); however it is unclear if these effects of Cyclin A2 depletion are due to problems in the previous S phase. Clearly, both Wee1/Myt1 and Cdc25 are regulated by phosphorylation by Cdk1, which constitute the negative and positive feedback loops of Cdk1-Cyclin A and B activation (Perry & Kornbluth 2007). These initial feedback loops are complex and involve a number of regulatory elements.

The regulation of Cdc25 phosphatase occurs via phosphorylation of various inhibitory and activating residues. Some of the kinases involved in this regulation, Chk1/2 and cTAK1 are described before. CDC25 is hyperphosphorylated at the onset of mitosis. These activating phosphorylations of CDC25 are mediated through Plk1, Cdk1 and Cdk2. The 14-3-3 inhibitory binding is released in G2 mediated by Cdk2 and Plk1 activities (Margolis et al. 2003; Elia et al. 2003; Kumagai & Dunphy 1992). Cdk1 further activates Cdc25 via PP1 dephosphorylation of the inhibitory Ser287 (Margolis et al. 2006) and the conformational change via Pin1. Pin 1 is a *cis/trans* peptidyl-prolyl isomerase that catalytically modifies the conformation of Cdc25 in response to phosphorylation (Stukenberg & Kirschner 2001; Crenshaw et al. 1998). Thus active Cdk1-Cyclin B initiates a positive feedback loop to drive up the concentration of active Cdk1-Cyclin B (Kumagai & Dunphy 1992; Izumi & Maller 1993; Hoffmann et al. 1993). Cdc25A concentration also increases in cells since S-phase as it is protected from targeted proteolysis by Cdk1 (Busino et al. 2003).

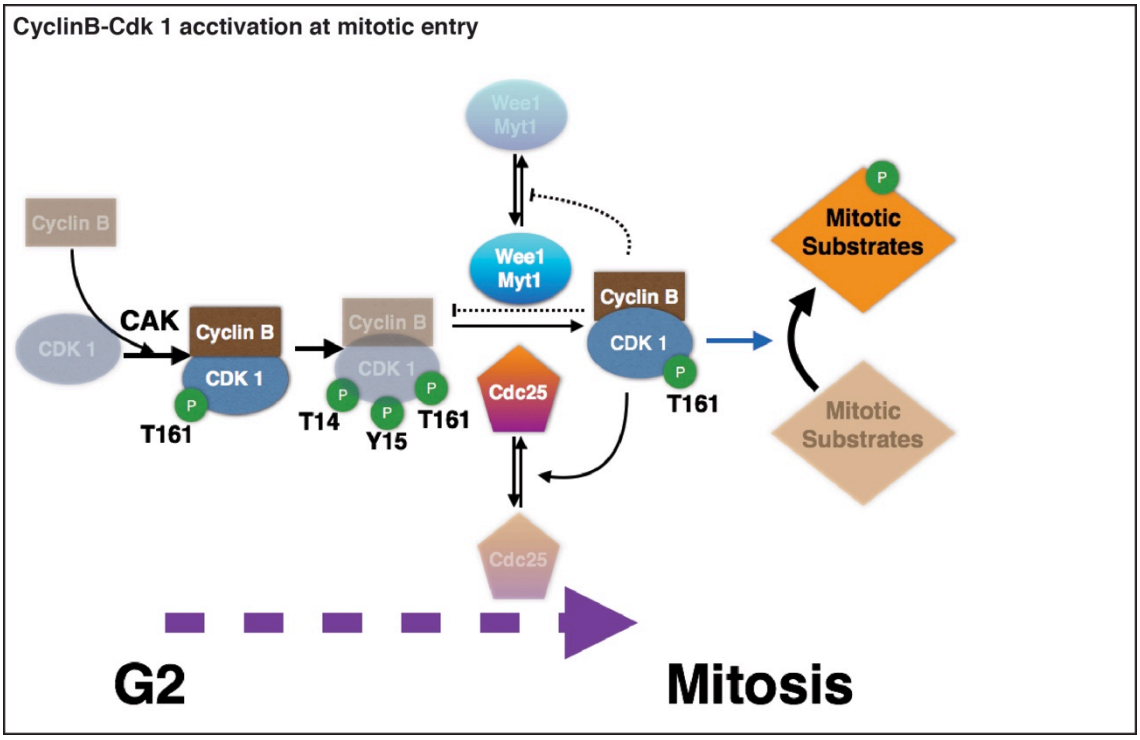

Figure 1.3 Cyclin B-Cdk1 activation at mitotic entry

Schematic representation of Cyclin b-Cdk1 activation at mitotic entry. Cyclin B binds with Cdk1 and is fully activated by CAK by phosphorylation at Thr161 (Kaldis 1999). This complex is inactivated by T14 and Y15 inhibitory phosphorylations by Wee1/Myt1 kinase (Nurse & Thuriaux 1980; Mueller et al. 1995). At G2/M transition, Cdc25 dephosphorylates the T14 and Y15 residues to activate Cyclin B-Cdk1 complex, which then phosphorylates the mitotic substrates (GAUTIER et al. 1991). Cdk1 also activates its activator, Cdc25, and inhibits its inhibitor, Wee1/Myt1. The faded colours show inactivated proteins and the brighter ones show active proteins/protein complexes.

Similar regulatory mechanism are involved in inhibiting Wee1/Myt1 kinase from phosphorylating mitotic Cdk -Cyclin complexes (Perry & Kornbluth 2007). Myt1 is hyperphosphorylated via Plk1 that eventually inhibits its kinase activity (Booher et al. 1997). Wee1 is degraded at the G2/M transition by SCF (Skp, Cullin and F-box) E3-ubiquitin ligase complex (Ayad et al. 2003; Michael & Newport 1998). Phosphorylation of Wee by Cdk1 itself and other kinases such as Plk1 and Casein kinase 1 target it for proteolysis by SCF complex, by generating a phospho-degron. This is achieved by phosphorylating the Ser53 and Ser123 residues which are then recognized by β-TrCP that binds Skp and leads to SCF mediated proteolysis (Watanabe et al. 2004; Watanabe et al. 2005; Bartholomew et al. 2001). Moreover, Cdk phosphorylates a conserved threonine in the N-terminal region of Wee1, called Wee-box that is essential for normal kinase activity. This phosphorylation enables binding of Pin1, which disrupts the active conformation of the kinase (Okamoto & Sagata 2007). Additionally, 14-3-3 binding in the presence of protein kinase inhibitor UCN-01 stimulates the Wee1 interphase kinase activity (Rothblum-Oviatt et al. 2001; J. Lee et al. 2001).

As observed above Plk1 phosphorylation is involved in activating Cdc25, inhibiting Myt1 (Nakajima et al. 2003) and inhibiting Wee1 kinase (Watanabe et al. 2005). This auxiliary kinase is activated by Aurora-A kinase by phosphorylating Thr210 via the co-factor Bora binding (Seki et al. 2008; Macůrek et al. 2008). Cdk1-Cyclin B phosphorylation (Hutterer et al. 2006) enhances this interaction, thus activating Plk1 to contribute in its positive feedback loops at G2/M transition. Additionally, Aurora-A kinase can also directly act on Cdc25B by phosphorylating it at Serine 353 at the centrosomes. This indicates that Aurora A kinase is involved in the initial activation of Cdk1-Cyclin B along with Plk1 (Cazales et al. 2005; Dutertre et al. 2004). Moreover, Plk1 and Aurora A kinases need to be activated to facilitate centrosome maturation and bipolar spindle formation in parallel to Cdk1-Cyclin B activation, to ensure well-timed mitotic entry (Lindqvist et al. 2009). However, it is noteworthy that Cdk1-Cyclin B activation can proceed without significant delays even in the absence of both Plk1 and Aurora-A (Hégarat et al. 2011).

Thus, Cdk1 phosphorylations generate a positive feedback loop via cdc25 activation and Wee1/Myt1 inhibition. Cdk1 activates its activator and inhibits its inhibitor, directly or indirectly via auxiliary kinases such as Plk1 and Aurora A. Together these positive

feedback loops rapidly drive up the concentration of active Cdk1-Cyclin B1 at G2/M transition. Once the sufficient threshold is reached, the nuclear lamina is disassembled by Cdk1 phosphorylation of the lamins (Smoyer & Jaspersen 2014). The nuclear envelope is then broken and cells are committed to enter mitosis. The fine balance of these activating and inhibitory pathways tightly controls mitotic entry (O'Farrell 2001; Boutros et al. 2006; Hochegger et al. 2008; Lindqvist et al. 2009).

1.2.8 Regulation of Kinetochore-Microtubule Attachments

Initial activation of mitotic Cdk1-Cyclin B complex occurs at the centrosomes as discussed earlier. The regulatory networks controlling Cdk1-Cyclin B activation at the centrosomes need to be tightly controlled to facilitate subsequent mitotic entry (Hagan 2008). The centrosomes are also microtubule-nucleating centres at the beginning of mitosis that are important for the formation of the spindle apparatus and thus maintaining genome stability (Abal et al. 2002; Chevrier et al. 2002). Centrosome duplication occurs at the same time as DNA synthesis in the G1/S transition (Blagden & Glover 2003). Centrosome maturation occurs during late G2/M, where Plk1 and Aurora A mitotic kinases recruit γ-ring complexes and microtubule nucleation components to initiate spindle formation (Blagden & Glover 2003). Centrosomes then migrate to the poles to form microtubule-emanating centres. Microtubules from these opposite poles of the cells connect condensed chromosomes to the spindle pole via a proteinaceous structure on the centromere of each sister chromatid called the kinetochore. Each sister chromatid is held together by cohesins, and is attached to the opposite poles ensuring bi-orientation of the chromosomes which in turn leads to faithful chromosome segregation(Miyazaki & Orr-Weaver 1994; Nicklas 1997). During the formation of bipolar spindles, erroneous sister kinetochore attachments are corrected by mechanism mediated by Aurora B kinase to prevent chromosome mis-segregation and aneuploidy(Tanaka et al. 2002; D. Liu et al. 2009).

Aurora B is at the heart of the Chromosome Passenger Complex that promotes chromosome alignment by preventing kinetochore-microtubule mis-attachments and is localised to the centromeres. Aurora B along with the non-enzymatic subunits INCENP (Inner Centromere Protein), Borealin and Survivin form the Chromosome Passenger

Complex (CPC) (ref). It is a key component in detecting aberrant kinetochore-microtubule attachments, as spindle attachments from the same pole exhibit lack of tension (Cheeseman & Desai 2008; Ruchaud et al. 2007; Vader et al. 2006). Lack of tension activates the kinase activity of Aurora B, which phosphorylates various kinetochore bound substrates such as yeast Dam 1 ring complex and the mammalian Ska complex, and the kinesis MCAK and Ndc80 complex (ref). This negatively regulates the microtubule binding as it destabilises the kinetochore-microtubule interaction (Cheeseman et al. 2006; Cheeseman et al. 2002; Deluca et al. 2006; Andrews et al. 2004; Lan et al. 2004). PP1γ is recruited in early mitosis to kinetochore by kinetochore-null1 (KNL1) and inactivates Aurora B as it comes into contact with it (Pinsky et al. 2006; Trinkle-Mulcahy et al. 2003). PP1γ at the outer kinetochore keeps Aurora B activity minimal. Thus, the kinase activity is maximal at the centromere and minimal at the outer kinetochore. Erroneous attachment cannot push the kinetochore away from the centromere, which leads to Aurora B phosphorylating Ndc80 and destabilizing the attachments. The correct attachment pushes the kinetochore away from the centromere and active Aurora B, thus stabilizing the end-to-end attachments (Cimini 2007; Kelly & Funabiki 2009; Maresca & Salmon 2009). PP1γ is thus the Aurora-B counteracting phosphatase involved in promoting end-to-end attachments (ref). Furthermore the phosphatase PP2A-B56 also contributes in regulating influencing PP1γ recruitment (Etemad & Kops 2016; Rosenberg et al. 2011).

1.2.9 Spindle Assembly Checkpoint (SAC)

To ensure the chromosomes are equally segregated to the daughter cells, eukaryotic cells have evolved the Spindle Assembly Checkpoint (SAC). The SAC proteins monitor kinetochore-microtubule attachments and proper alignment of chromosomes on the metaphase plate. SAC controls the onset of anaphase in response to tension generated by correct bipolar attachment (McIntosh et al. 2002; Musacchio & Salmon 2007). Mutation screens in *S. cerevisiae* uncovered the proteins involved in spindle assembly checkpoint. In humans, SAC comprises of serine-threonine kinases: Mps1 (monopolar spindle protein), Bub1 (budding uninhibited by benomyl), a putative pseudokinase Bub1-related (BubR1; human orthologues of yeast Mad3) and other components like mitosis arrest deficient 1 (Mad1), Mad2 and Bub3. These proteins are highly conserved

among eukaryotes and are essential for preventing mitotic progression in the presence of unattached kinetochores to ensure normal cell division (Li & Murray 1991; Hoyt et al. 2016; Weiss & Winey 1996). Loss of SAC function in higher eukaryotes leads to inaccurate chromosome segregation and aneuploidy (Wassmann & Benezra 2001; Kops et al. 2005).

The Sac proteins Mps1, Mad1, Mad 2, Bub 1, BubR1 and Bub 3 bind kinetochores prior to chromosome attachment. Additionally, the kinase Aurora B and APC/C cofactor Cdc20 are also recruited to the kinetochore along with motor proteins CENP-E (kinesin) and dynein (Musacchio & Salmon 2007; Cheeseman & Desai 2008). APC/C is an ubiquitin ligase (see Section 2.10) that mediates the ubiquitination of securin, a stoichiometric inhibitor of the protease Separase. Separase is required to cleave the cohesins that hold sister chromatids together, and enable equal distribution of chromosomes to the daughter cells (J.-M. Peters 2006). SAC negatively targets Cdc20 ability to activate APC/C-mediated poly-ubiquitination and subsequent proteosomal degradation of Cyclin and securin (Kim et al. 1998; Hwang et al. 1998). Cyclin degradation by APC/C is described in the following section. SAC catalyses the formation of this mitotic checkpoint complex (MCC) that binds APC/C and prevents it from ubiquitinating its substrates. The MCC is a heterotetramer comprising of three SAC proteins, MAD2, BUBR1/Mad3 and BUB3, as well as CDC20 itself, and is the effector of SAC. The current model of SAC focuses on conformational changes in Mad-2 from the open conformation (O-Mad2) to the closed conformation (C-Mad2). C-Mad2 binds unattached kinetochores and promotes the binding of O-Mad2 to Cdc20. Once bound to Cdc-20, Mad-2 is converted to a closed conformation in an Mps1-dependent manner. The C-Mad2-Cdc20 complex is sequestered away from APC/C by binding the BubR1-BuB3 complex (Sudakin et al. 2001; H. Yu 2002; Hagting et al. 2002; R.-H. Chen et al. 1999). On the other hand, once all the kinetochores are attached to bipolar spindles the SAC is satisfied, MCC releases the sequestered Cdc20 and APC/C is activated by mitotic Cdks. This leads to securin degradation that results in sister chromatid separation. The mechanism proposed for checkpoint inactivation includes dynein-mediated pole-ward transport of checkpoint proteins (Howell et al. 2001; Gassmann et al. 2010), capping of the Mad1-Mad2 complex using the Mad-2 inhibitor p31Comet (De Antoni et al. 2005; M. Yang et al. 2007; Fava et al. 2011; Xia et al. 2004; Mapelli et al. 2006) and finally antagonising the activity of PP2 phosphatase by

dephosphorylating substrates of checkpoint kinases like Aurora-B and Mps-1 (Shepperd et al. 2012; Qian et al. 2011; London et al. 2012). The inactivation of SAC leads to the onset of anaphase and activation of APC/C. Securin is degraded to release Separase, which cleaves cohesins, and an equal number of chromosomes migrates towards the opposite poles (Hauf et al. 2001). Kinesin and dynein motors as well as microtubule dynamics facilitate the poleward movement of chromatin (Brust-Mascher et al. 2004).

Even minor alterations in the microtubule dynamics causes errors in chromosome attachment and lack of tension, which in turn activates SAC (Zhou et al. 2002). Thus, onset of anaphase is delayed which allows for chromosome re-alignment and spindle tension corrections.

1.2.10 APC/C Activation and Cyclin Degradation

In contrast to Cdk1 activation, which is mainly regulated by dephosphorylation of Thr14/Tyr15, inactivation of Cdk1 during mitotic exit is achieved by Cyclin degradation. As mentioned earlier, many key cell cycle regulators like Wee1 and CKIs are targeted for 26S proteosomal degradation by ubiquitination. Basic cell cycle control involves two ubiquitination complexes: the SCF complex (Skp-cullin-F-box) and the APC/C complex (Anaphase promoting complex/ Cyclosome). The SCF plays pivotal roles in G1/S and G2/M transition. The role of SCF in Wee1 regulation at the G2/M transition has been described earlier (Section 2.7). Conversely, APC/C is the major driver of the metaphase-anaphase transition and the establishment of G1 phase following mitotic exit.

Protein degradation by 26S proteasome following poly-ubiquitination is a system to target misfolded and damaged proteins, also proven to have essential role in signal transductions mechanisms (Hershko & Ciechanover 1998; Alberts et al. 2014). The ubiquitination process is mediates by three enzymes: an activating enzyme (E1), a conjugating enzyme (E2) and an ubiquitin ligase (E3). These enzymes act in a stepwise manner to covalently attach multiple ubiquitin chains to the target protein, which is subsequently recognised and degraded by the proteosomal complex (Harper et al. 2002; J.-M. Peters 2002).

APC/C is a RING finger family E3 ubiquitin ligase and comprises of 14 subunits in humans (Schreiber et al. 2011). It targets specific substrates for degradation at the metaphase-anaphase transition (Pines 2011). APC/C is activated via two co-factors: Cdc20 and Cdh1. APC/A recognises substrates containing degradation motifs like D-box and KEN-box. APC/C-Cdc20 prefers D-box containing substrates while APC/C-Cdh1 can target both D-box and KEN box containing substrates (Pfleger & Kirschner 2000).

Cdc20 is expressed during S phase, G2 and mitosis. However, its binding to APC/C is dependent on phosphorylation of several subunits of the complex by mitotic kinases such as Plk1 and Cdk1. Thus, cdc20-mediated activation of APC/C only occurs in mitosis from prophase to anaphase (Shteinberg et al. 1999; Kramer et al. 2000; Acquaviva & Pines 2006; J.-M. Peters 2006). Additionally, in G2, APC binds to inhibitor Emi1 (early mitotic), thus preventing its interaction with Cdc20. Plk1 phosphorylation of Emi1 in prophase directs it for SCF-mediated degradation and activates APC/C (Hansen et al. 2004). The APC subunit, APC15 is responsible for Cdc20 turnover and MCC release when the SAC is satisfied. If this subunit is absent, MCC and ubiquitylated Cdc20 remains attached to APC even when the SAC is satisfied (Mansfeld et al. 2011).

Active APC/C-Cdc20 mediates degradation of Cyclin A and Nek2 in prometaphase (Sedgwick et al. 2013; Geley et al. 2001; Elzen & Pines 2001)and Cyclin B and Securin (See Section 2.9) at metaphase-anaphase transition. Cyclin degradation is mediated by two motifs within the N-terminal region: the D-box (sufficient for degradation in *Xenopus*) and the KEN-box (Evans et al. 1983; Murray & Kirschner 1989a). These sequences correspond to a two-part degron or degradation signal, which is a disordered region where polyubiquitin chains are attached.

APC/C-Cdc20 triggers the onset of anaphase by degrading Securin. This causes the release of Separase and cleavage of Kleisin subunit Scc1 in the cohesion ring resulting in the separation of sister chromatids (Thornton & Toczyski 2003; J.-M. Peters 2006; Acquaviva & Pines 2006). Moreover, APC/C-Cdc20 initiates degradation of mitotic Cyclins which results in downregulation of Cdk1 activity (Kramer et al. 2000; J.-M. Peters 2006). Due to low Cdk1 activity, the key mitotic substrates are dephosphorylates

which leads to decondensation of chromosomes and reformation of the nucleus. Moreover, the cytokinesis regulator ECT2 is relieved from its inhibition, allowing the cytokinetic ring to constrict (Niiya et al. 2005).

At anaphase, since the Cdk1 activity is low due to Cyclin degradation, Cdh1 is activated and can replace Cdc20 on APC/C to maintain high APC/C activity (Castro et al. 2005). Unlike Cdc20, Cdh1 (also called FZR1) binds APC/C irrespective of its phosphorylation state. However, from late G1 to anaphase, Cdk1 activity is high, and the kinase phosphorylates and prevents the binding of Cdh1 to APC/C. APC/C-Cdh1 is active in late mitosis and during anaphase and telophase and stays active until late G1. It is involved in the degradation of Cyclins, residual Securin, Plk1, Aurora kinases and various proteins involved in DNA replication, as well as in the degradation of Cdc20, which inactivates APC/C-Cdc20. Eventually, APC/C-Cdh1 degrades its E2 enzyme, leading to self-inactivation. This promotes the accumulation of S-phase Cyclins and the subsequent entry of the cells into the S phase (J.-M. Peters 2006; Pfleger & Kirschner 2000). In yeast, following anaphase the phosphatase Cdc14 dephosphorylates Cdh1 and promotes the interaction and subsequent activation of Cdh1-APC/C (Hatano et al. 2016). RNAi and gene deletion studies with Cdh1 show that it is not essential for mitotic exit but G1 phase is shortened and S phase is prolonged in its absence. Thus, Cdk1 activation switches APC/C-Cdh1 off, while high APC/C-Cdh1 activity prevents Cyclin accumulation and leads to establishment of stable G1-phase (Sigl et al. 2009).

Thus, in addition to reversible post-translational modifications such as phosphorylation by mitotic kinases, SCF- and APC/C-mediated proteolysis provides an irreversible mechanism that ensures a strict unidirectional progression of the cell cycle.

1.3 Greatwall Kinase and the Phosphatase Control System

1.3.1 Phosphatases and Cell Cycle Control

Kinases have been at the centre of attention in cell cycle control research for decades. Following the discovery of Cdc2- Cyclin, it was believed that the cell cycle is controlled by the activation and downregulation of kinases. However, it was only recently that a

prominent role of phosphatases in the regulation of mitotic entry and exit control was recognised. Protein phosphatases have counteracting functions to mitotic kinases. These enzymes were thought to be ubiquitously present and the dephosphorylation of substrates was assumed to be a result of broad-acting phosphatase activity (Trinkle-Mulcahy & Lamond 2006). However, this view of phosphatases as silent kinase partners in regulation is changing. Recent mounting evidence shows that mitotic protein dephosphorylation requires involvement of specific phosphatases that are tightly regulated in time and space. For example, a large scale RNAi screen of human kinases and phosphatases, identified 32% of the total phosphatases to promote survival while only 11% of the kinases appeared to be essential (MacKeigan et al. 2005).

Phosphatases have been implicated to play crucial roles for the timely dephosphorylation of substrates in events such as spindle assembly, SAC activation, anaphase onset and mitotic exit (Bollen et al. 2009). Thus, a delicate interplay of kinases and phosphatases is essential for controlling mitotic events (Domingo-Sananes et al. 2011; De Wulf et al. 2009). Two important classes of phosphatases have been the focus of research: the dual specificity phosphatases Cdc25 and Cdc14 and the serine-threonine phosphatases PP1 and PP2A. Recently, FCP-1 phosphatase that belongs to the Asp family of serine-threonine phosphatases has been implicated to have a regulatory role in the mitotic exit network(Visconti et al. 2012; Monica et al. 2015; Hégarat, Vesely, Vinod, Ocasio, Peter, Gannon, Oliver, Novák & Hochegger 2014a).

Cdc25 is responsible for Cdk1-Cyclin B activation by dephosphorylating the inhibitory phosphorylations by Wee1/Myt1 kinase at the G2/M transition (Kumagai & Dunphy 1992; Lindqvist et al. 2005; Domingo-Sananes et al. 2011). Cdc25 functions and regulation has been described in detail in the earlier sections (See section 2.5 and 2.6).

1.3.2 Phosphatases and Cell Cycle Control: Cdc14

Cdc14 is one of the mitotic dual-specificity phosphatases that controls mitotic exit in budding yeast. Cdc14 is sequestered in the nucleus from the G1 phase until metaphase by its inhibitor Cif1 (also known as Net1). In anaphase, it is released into the cytoplasm in a Cdk1 phosphorylation-dependent manner (Stegmeier & Amon 2004; Queralt et al.

2006). This results in dephosphorylation of the Cdk1 substrates, eventually leading to mitotic exit (Visintin et al. 1998). In addition to Cdk1 inactivation, Cdc14 also triggers localization of chromosomal passenger proteins to the spindle midzone in anaphase, regulates spindle dynamics, inhibits rDNA transcription during anaphase (Clemente-Blanco et al. 2009), and contributes to rDNA decondensation and segregation (Varela et al. 2009) as well as to cytokinesis (Stegmeier & Amon 2004; D'Amours & Amon 2004). Cdc14 inactivates Cdk1 via two mechanisms: mitotic Cyclin degradation by APC/C-Cdh1 and dephosphorylating Sic1 (Clb-Cdk inhibitor) and Swi5 (Sic1 transcription factor) (Stegmeier & Amon 2004). However, the orthologues of Cdc14 are dispensable for mitotic exit in *S. pombe* (Cueille et al. 2001; Trautmann et al. 2001) and *Caenorhabditis elegans* (Roy et al. 2011). Likewise gene deletions of vertebrate Cdc14A and B do not display mitotic exit defects (Mocciaro & Schiebel 2010).

The human homologs Cdc14A, B and C are suggested to be involved in various mitotic and non-mitotic processes, but are not required to dephosphorylate Cdk substrates. Centrosomal Cdc14A counteracts Plk1 function and antagonizes Cdc25C (Krasinska et al. 2007). It is also suggested to contribute in centrosome separation, spindle assembly and chromosome segregation (Kaiser et al. 2002; Mailand et al. 2002). Cdc14B has been implicated in the removal of activating phosphorylations on Cdc25 in anaphase, thereby negatively regulating Cdk indirectly to promote mitotic progression (Mocciaro & Schiebel 2010; Vázquez-Novelle et al. 2010; Tumurbaatar et al. 2011). Human Cdc14 B is also sequestered in the nucleolus and is translocated to the cytoplasm in response to DNA damage prior to mitotic entry. Here it dephosphorylates and activates Cdh1, which in turn leads to APC/C-Cdh1 dependent degradation of Plk1 that blocks mitotic entry (Bassermann et al. 2008). Moreover, Cdc14B also stabilizes microtubules by mediating dephosphorylation of the tubulin deacetylase SIRT2. However, Cdc14B was also observed to stabilize and bundle microtubules independent of its phosphatase activity (Dryden et al. 2003; H. P. Cho et al. 2005; Rodier et al. 2008). Overall, a final triple knockout of Cdc14A, B and C has not been reported yet, making it difficult to exclude the possibility that this phosphatase might plays a role in mitotic exit in mammalian cells.

1.3.3 Phosphatases and Cell Cycle Control: PP1 and PP2A

PP1 and PP2A are serine threonine phosphatases that are implicated in mitotic exit. However, their precise mode of action remains to be determined. These phosphatases are multimeric complexes to build up holoenzymes comprising of a catalytic subunit (α, β/δ or γ), a regulatory subunit and a scaffolding subunit. Substrate specificity and localisations are determined by the catalytic subunit in association with over 200 PP1 interacting proteins (PIPs) (Bollen et al. 2010). The mitotic functions of PP1 and PP2A are briefly described in this section.

Nuclear lamin dephosphorylation is essential for nuclear envelope reassembly at mitotic exit. PP1 was implicated in lamin dephosphorylation as this phosphatase activity was inhibited by the PP1 inhibitor, Inhibitor-1 and high nanomolar concentration of okadaic acid. PP1 was observed to promote timely dephosphorylation and reassembly of the nuclear envelope in partnership with PP2A at mitotic exit (Thompson et al. 1997). PP1 also contributes to kinetochore reassembly and cytokinesis, though its substrates and mechanisms in these roles still remain elusive (Barr et al. 2011; Bollen et al. 2009). The characteristic architecture of chromosome is preserved by activation of RepoMan-PP1 activity at anaphase following Repo Man dephosphorylation in co-operation with condensin (Vagnarelli et al. 2006). Roles of PP1 in counteracting Aurora B kinase at the kinetochore in metaphase and spindle assemble checkpoint have been described earlier (See Section 2.7 and 2.8). Studies with the nuclear inhibitor of PP1 (NIPP1) in *HeLa* cells suggest the main function of PP1 in SAC signalling can be rescued by simultaneous inhibition of its counteracting kinase, Aurora B. However, these observations argue against the role of PP1 as the major Cdk-counteracting phosphatase (Winkler et al. 2015).

In *Xenopus* egg extracts PP1 is reported to be the main catalyst to initiate the dephosphorylation cascade at mitotic exit. PP1 is suppressed via two mechanisms: Thr 320 phosphorylation by Cdc2 (Kwon et al. 1997; Dohadwala et al. 1994) and binding of its inhibitor, Inhibitor-1. The binding of Inhibitor-1 is mediated by protein kinase A (PKA) –dependent phosphorylation site and is analogous to Ensa/Arpp19-PP2A B55 interaction explained in the later sections. At mitotic exit, once Cdc2 is inactivated by

Cyclin degradation, PP2 auto-dephosphorylates at the Cdc2 site (Thr320) and partially activates itself. Full activation of PP1 is achieved by dephosphorylating the activating site on Inhibitor-1 (Thr32), leading to its dissociation from the phosphatase(Wu et al. 2009). PP1 is also shown to initiate Greatwall dephosphorylation (described in the later section) as well. This places PP1 at the top of cascade in mitotic exit dephosphorylation (Heim et al. 2015; Ma et al. 2016; Rogers et al. 2016). Similar cross talk was observed among the serine-threonine phosphatases in fission yeast where PP1 activates PP2A-B55 and PP2A-B56, suggesting PP1 as the initiator of the relay of mitotic exit phosphatases. PP1 was found to bind the regulatory subunits B55 and B56 via the PP1 docking site. At mitotic exit, once PP1 is activated fully following Cdk inactivation, it first activates PP2A-B55. PP2A-B55 in turn activate PP2A-B56 by dephosphorylating the PP1 docking site on the B56 subunit (Grallert et al. 2015). However, this function of PP1 needs to be verified in mammalian cells as the existing experimental evidence with siRNA depletion of PP1 catalytic subunits fails to inhibit Greatwall dephosphorylation(Rogers et al. 2016). Moreover, inhibition of PP1 using tautomycetin also does not affect Greatwall inactivation and Ensa/Arpp19 dephosphorylation in somatic cells (Hégarat, Vesely, Vinod, Ocasio, Peter, Gannon, Oliver, Novák & Hochegger 2014b).

PP2A is another mitotic phosphatase and is ubiquitously present in the cell cycle. PP2A is also a holoenzyme comprising of a scaffold subunit (PP2AA), catalytic subunits (PP2Ac) and regulatory subunits (PP2AB). PP2Ac exists as two isoforms: Cα and Cβ. The scaffold subunit has two isoforms: Aα and Aβ. There are four isoforms of the regulatory subunit: B55/B, B56/B', PR72/B'' and PR93/B'''. Of these B55 and B56 have been identified to play important roles in cell cycle control (Seshacharyulu et al. 2013). PP2A holoenzymes of the B55 family have been proposed to have Cdk1-counteracting roles at mitotic entry and exit (Lorca & Castro 2012). These functions of PP2A-B55 are described in further detail in the following sections. There are four B55 paralogues, alpha to delta, of which alpha and delta are the dominant forms in proliferating cells. PP2A-B55α is involved in post-mitotic assembly of the nuclear envelope, Golgi apparatus and condensed chromosome. It co-operates with the nuclear transport factor Importin β1 to execute these functions (Schmitz et al. 2010).

1.3.4 Phosphatases and Cell Cycle Control: FCP1

FCP-1 belongs to the Asp-based group of serine-threonine phosphatases. FCP-1 shows the presence of the Asp-based signature catalytic sequence DXDXT/V, in the N-terminus (FCPH). It was initially thought to be a regulatory subunit of the phosphatase, as it had no homology to the known serine-threonine phosphatases. FCP-1 consists of a BRCT (BRCA1 C-terminus domain) domain in the mid-region. It is the only phosphatase in the transcription machinery to show the presence of this domain and was initially identified in the tumour suppressor gene BRCA1 in breast cancer cell lines.

FCP-1 was the first phosphatase shown to dephosphorylate the CTD (C-terminal repeat domain) of the largest subunit of RNA polymerase II (Pol II). FCP-1 was first purified from HeLa extracts and showed two isoforms: the predominant one of 205 kDa and the less abundant one of 150 kDa. It requires magnesium ions for its phosphatase activity, a characteristic feature of type 2C phosphatases (Chambers & Dahmus 1994). In 1996, yeast CTD phosphatase was seen to exhibit identical properties of mammalian FCP-1. Although the human and yeast CTD are almost identical, both phosphatases failed to dephosphorylate the polymerase molecule from the other species(Chambers & Kane 1996).

CTD is observed in various phosphorylation states during transcription. It is a 7-amino acid (heptapeptide) repeats, with as many as 52 copies in the mammalian genome. In human and mouse, it is phosphorylated at Ser2 and Ser5. These phosphorylation states contribute to the recruitment of various nuclear factors involved in mRNA maturation. Although various stages of phosphorylation of CTD is required for recruitment of the processing factors, docking of Pol II and elongation (Y. Zhang et al. 2006; Meinhart et al. 2005), CTD need to be dephosphorylated during the termination phase of transcription. This dephosphorylation is crucial for the employment of a new-pre-initiation complex to continue to the second round of transcription. Thus, FCP-1 is important for recycling Pol II (Meinhart et al. 2005). Smaller CTD phosphatases such as SCP-1 are present in higher eukaryotes. SCP-1 contains the FCPH domain but lacks the BRCT domain (Yeo et al. 2003).

Mutating the *fcp-1* gene in yeast revealed that it dephosphorylates Ser2 on the CTD repeat. (E. J. Cho et al. 2001). Partially purified FCP-1 identified general transcription factors such as TFIIF and TFIIB to have roles in is regulation. While TFIIF was seen to stimulate FCP-1 activity, TFIIB had an inhibitory effect on the function of TFIIF. However, TFIIB on its own did not have any effect on the phosphatase activity (chambers 1995). Concurrently, yeast FCP-1 activity was inhibited by TFIIF, purified from cellular extracts(Chambers & Kane 1996). TFIIF is a general transcription factor comprising of two subunits RAP30 and RAP74 and plays important part in both initiation and elongation. Later in 1998, FCP-1 cDNA was isolates in two-hybrid screen for RAP74 (largest subunit of TFIIF) interacting proteins(J. Archambault et al. 1998). FCP-1 docks on phosphorylated CTD via the BRCT domain in its C-terminal domain (X. Yu et al. 2003).

Although the phosphatase function of FCP-1 in the transcriptional machinery was well known, it was only recently that the mitotic role of FCP-1 was discovered. FCP-1 contributes to the mitotic network by dephosphorylating Greatwall kinase at mitotic exit(Monica et al. 2015; Visconti et al. 2012). These observations are discussed in detail in the following sections (Section 1.3.10).

1.3.5 Greatwall Kinase: Mitotic Functions of a Novel AGC Kinase

Greatwall (Greatwall) kinase was discovered during the last decade due to its mitotic phenotypes in *Drosophila* embryos (J. Yu et al. 2004) and has proven to be a major mitotic kinase. The discovery of Greatwall changed the way G2/M transition was perceived in cell cycle control. In 1996, *greatwall (gwl)* was initially discovered in *Drosophila* as *scant* (Scott of the Antartic). Mutants of *scant* in female syncytial embryos were sterile and when homozygous caused mitotic defects (White-Cooper et al. 1996). This gene was later mapped to *greatwall* gene in *Drosophila* and found to express a hyperactive form of the kinase (K97M) (V. Archambault et al. 2007). The first recessive allele of *greatwall* was identified in *Drosophila* by Yu et al (J. Yu et al. 2004), where it was found to encode a nuclear protein belonging to the AGC kinase family. This paper was the first to describe mitotic functions of the kinase in larval neuroblasts.

They named this gene ‘Greatwall’ as the mutant phenotype indicated an important role for this protein in protecting chromosome structure (J. Yu et al. 2004).

Greatwall is conserved across species from insects to vertebrates. *Drosophila* and human greatwall have 59% sequence identity. The homology extends beyond the bifurcated kinase domain into the flanking amino acids. It belongs to the family of serine-threonine kinases called AGC kinases, which target amino acids flanked by basic residues for phosphorylation (Tamaskovic et al. 2003). Greatwall is an unusual kinase as its kinase domain is bifurcated by an unrelated stretch of ~ 500 amino acids separating the sub-domains VII and VIII (Hanks & Quinn 1991; J. Yu et al. 2004). Greatwall is sequestered in the nucleus due to the presence of two nuclear localization signals in the uncharacterized loop region in both *Drosophila* and mammalian Greatwall kinase (P. Wang et al. 2013; Alvarez-Fernández et al. 2013). Greatwall re-localizes partly to the centrosomes but is present universally in the cytoplasm during mitosis (J. Yu et al. 2004; Voets & Wolthuis 2010).

The initial mitotic phenotypes of Greatwall were characterised by the Goldberg lab in *Drosophila* larval neuroblasts. The most striking phenotype of the mutant *gwl* allele was under-condensed chromosomes and delayed mitotic progression from the late G2 phase until nuclear envelope breakdown (NEBD), which was accompanied by chromosome segregation defects. Despite the presence of aberrant chromosomes, phospho-histone H3 and condensin component Barren was recruited, which is indicative of normal chromosome condensation apparatus. However, later it was shown with RNAi treatment in *Drosophila* S2 cells that Greatwall contributes to chromosome congression and segregation but not to chromosome condensation (J. Yu et al. 2004; Bettencourt-Dias et al. 2004). Greatwall appeared to arrest or delay anaphase onset and the mutants that progressed into anaphase or telophase displayed lagging chromosomes or chromosome bridges. This was not due to defective spindle apparatus as the spindles in all stages of mitosis were morphologically normal. Mutations in gwl also lead to activation of spindle assembly checkpoint as the sister chromatids never separated and high levels of Cyclin were observed. This was not a consequence of DNA replication problems or activation of caffeine-sensitive checkpoint (J. Yu et al. 2004).

Similar phenotypes were observed on depletion of the mammalian orthologue of Greatwall, MASTL (microtubule-associated serine/threonine kinase-like) using siRNA in human cells. Cells strongly depleted of Greatwall exhibited a prolonged delay in G2, but eventually entered mitosis. Chromosome condensation and mitotic progression is delayed with segregation defects at anaphase. This in turn leads to the trapping of chromatin in the cleavage furrow and cytokinesis failure as well as aneuploidy (Voets & Wolthuis 2010; Burgess et al. 2010). Genetic ablation of Greatwall in mice is lethal in the embryonic stage. Although Greatwall-depleted cells enter mitosis with normal kinetics, they display condensation defects with prometaphase arrest. This is accompanied by reductions in Cdk1-substrate phosphorylation, which is comparable to the mitotic collapse phenotype observed upon on co-depletion of Wee1/Myt1 and Cdc25, which was characterised by Potapova et al. (Alvarez-Fernández et al. 2013; Potapova et al. 2011). Depletion of Greatwall in *Xenopus* egg extracts prevents mitotic entry (Castilho et al. 2009), while the addition of purified Greatwall to immature oocytes initiates meiosis even in the absence of progesterone (Zhao et al. 2008).

Yu et al. suggested that Greatwall is required to maintain high Cdk1-Cyclin B activity at mitotic entry and this was further supported by Greatwall depletion in *Xenopus* extracts, where Cdk1-Cyclin B activation and mitotic entry was prevented (J. Yu et al. 2006). Activate Greatwall in egg extracts was also observed to promote meiotic and mitotic entry. Additionally, Greatwall-depletion in CSF extracts results in mitotic exit and reversion of MPF activity to interphase levels concurrent with loss of phosphorylation of mitotic proteins Wee1, Myt1, Cdc25, Plx (*Xenopus* Plk1) and MAP kinase. This drop in MPF activity occurred due to the accumulation of inhibitory phosphorylation (Try15) on Cdk1. Moreover, Cdk1AF mutant (constitutively active Cdk1 (Pomerening, Ubersax & Ferrell 2008a)) rescue G2-arrested Greatwall phenotype, suggesting that Greatwall is a part of the MPF auto-amplification loop (Zhao et al. 2008; J. Yu et al. 2006). Activated Greatwall induces CDC25C phosphorylation in the absence of Cdk1, Plx and MAP kinase or activator of protein kinase A (PKA) that usually blocks mitotic entry. G2 arrest induced by Greatwall depletion can be rescued by the phosphatase inhibitor, Okadaic acid. Thus, Greatwall might negatively regulate an Okadaic acid–sensitive phosphatase to ensure increased concentration of MPF activity in order to maintain M phase–specific phosphorylations of mitotic proteins Cdc25 and Wee1/Myt1 (Vigneron et al. 2009; Zhao et al. 2008; Lorca et al. 2010). This

phosphatase was later identified to be PP2A-B55delta in *Xenopus* studies (Mochida et al. 2009; Castilho et al. 2009). The PP2A-B55 regulation by Greatwall kinase is described in detail in the following section.

1.3.6 Regulation of PP2A-B55 by its Antagonising Kinase, Greatwall

The existence of an MPF-counteracting phosphatase has been hypothesised since a long time. Studies in *Xenopus* extracts by Cyert and Kirschner identified an inhibitor of the MPF activity and proposed it to be phosphatase called INH. INH was shown to control the nuclear Cyclin accumulation thresholds in *Xenopus* oocytes. Moreover, protein phosphatase -1 (PP1) was thought to regulate the activity of INH either directly or indirectly(Cyert & Kirschner 1988; Solomon et al. 1990). These findings were later demonstrated using microinjection or incubation with specific phosphatase inhibitor of types 1 and 2A protein phosphatases in cytoplasm of G2 arrested starfish oocytes and in G2 arrested *Xenopus* that led to MFP activation. Treatment of okadaic acid in mammalian cells also initiated mitotic entry even when Cdk1 was inhibited using specific inhibitors, implying that phosphatase activity is crucial for G2/M transition (Gowdy et al. 1998). INH was postulated to be type 2A protein phosphatase as only okadaic acid treatment but not inhibitor-1 triggered germinal vesicle breakdown in *Xenopus* oocytes. Interestingly, the presence of a nuclear component was prerequisite to inhibit the phosphatase in the cytoplasm, which was later discovered to be the unusual AGC kinase, Greatwall (Goris et al. 1989; Picard et al. 1989; Picard et al. 1991; J. Yu et al. 2004; Castilho et al. 2009; Vigneron et al. 2009; Mochida et al. 2009).

PP2A, with the B55 regulatory subunit, dephosphorylates artificial peptides pre-phosphorylated with Cdk1 *in vitro* and Cdk1 substrates in vertebrate cell extracts (Agostinis et al. 1992; Ferrigno et al. 1993). Meanwhile, a loss-of-function mutation in the gene encoding the PRC55 (B55) subunit of PP2A leads to defective chromosome condensation and the subsequent anaphase. These phenotypes were due to the strong depletion of PP2A-B55 in embryos, which inhibited dephosphorylation of Cdk1 substrates at mitotic exit (Mayer-Jaekel et al. 1994). Thus, PP2A-B55 was found to be a promising candidate as the Cdk1-counteracting phosphatase in cell cycle control.

Mochida and Hunt (2007) observed the regulation of anti-Cdk1 activity in a cyclic fashion, where it appeared at mitotic entry and disappeared at mitotic exit and was targeted at mitotic phospho-proteins. This phosphatase was later identified as PP2A-B55δ in *Xenopus* extracts, inhibiting Cdk1 peptide phosphorylations (Mochida et al. 2009). Two papers in 2009 by Vigneron et al. and Castilho et al. described the Greatwall regulation of anti-Cdk1 phosphatase in mitotic entry. Greatwall depletion in *Xenopus* CSF (Cytostatic factor) extracts caused MPF inactivation by Try-15 phosphorylation and rapid dephosphorylation of Cdk substrates. This was accompanied by DNA decondensation. Co-depletion of Greatwall, Wee1 and Myt1 triggered exit form mitosis. This was unusual as MPF activity was highly indicated by the lack of Tyr15 phosphorylation. These observations suggests that the principal function of Greatwall is phosphatase inhibition and not auto-amplification of MPF (Vigneron et al. 2009). Furthermore, peptides phosphorylated at Cdk1 phospho-sites were dephosphorylated by Greatwall-depleted extracts but not the control or untreated extracts. This indicated phosphatase activation in the absence of Greatwall is directed towards Cdk1 phospho-sites. The activation of this phosphatase was independent of MPF activity as supplementing the depleted extracts with Cdk1AF (Constitutively active Cdk1) still led to phosphatase activation(Castilho et al. 2009).

Null mutations of *gwl* caused significant delay or cell cycle arrest at the G2/M transition in *Drosophila* (J. Yu et al. 2004). Similar phenotypes were observed in 'Cycling' *Xenopus* extracts, where Greatwall immunodepletion arrested them in G2 phase(Castilho et al. 2009). However, a dual inhibitor of PP1 and PP2A, microcystin as well as 500 nM of okadaic acid (inhibits 70% of PP2A (Félix et al. 1990; Favre et al. 1997; Vigneron et al. 2009)) reversed the Greatwall phenotype. However, Inhibitor-1, the specific PP1 inhibitor did not. Additionally, immunodepletion of the B55δ subunit of PP2A also rescued Greatwall phenotypes. The inhibition of PP2A–B55δ in Cycling extracts (interphase) using specific inhibitors or immunodepletion leads to premature mitotic entry and arrests them in mitosis. Thus, Greatwall antagonises PP2A–B55δ, as depletion of the phosphatase rescues Greatwall-induced phenotypes (Mochida et al. 2009).

To investigate if Greatwall influences the phosphatase activity of PP2A in-vitro phosphatase assays were performed. The dephosphorylation of Cdk phosphosites on synthetic peptides was reduced significantly in the presence of greatwall in comparison

to exogenous PP2A- B55δ (Castilho et al. 2009). Similarly, cMos was phosphorylated *in vitro* using radiolabelled ATP by its known kinase, Cdk1- Cyclin B IP. Phosphorylated substrates were then assayed for release of phosphates with immunoprecipitated PP2A/C from control and Greatwall-depleted CSF extracts. A three-fold increase in the phosphatase activity was observed with PP2A/C from Greatwall-depleted extracts, despite adding equal amounts of substrate and phosphatase in the assays (Vigneron et al. 2009). These data convincingly show that Greatwall inhibits PP2A dephosphorylation of Cdk1- Cyclin B substrates.

In agreement with these observations, Lorca et al. reported that the Greatwall-PP2A B55 pathway functions are important along with the MPF amplification pathway for *Xenopus* first embryonic cycle. In metaphase II-arrested oocytes, inhibition of Greatwall before the activation of Cdk1- Cyclin B activation induced premature mitotic entry with incomplete mitotic substrate phosphorylation by Cdk1-Cyclin A. This eventually led to rapid degradation of the Cyclins A and B and abrupt exit from mitosis. Thus, Greatwall functions as an inhibitor of the phosphatase targeting mitotic substrates and is involved in controlling mitotic entry as well as maintenance of the mitotic state (Lorca et al. 2010).

Direct interaction of the kinase and phosphatase was demonstrated by expressing exogenous YFP-Greatwall in Hek293 cells. Transiently expressed PP2A/A (scaffold) and PP2A/C (catalytic subunits of the phosphatase) immunoprecipitates with the exogenous kinase in mammalian cells. This also occurs when these subunits are used as bait by over-expressing HA-tagged PP2A/C, as Greatwall is present in the immunoprecipitate. However, Greatwall does not seem to interact with the scaffold subunit in the absence of exogenous PP2A/C. Thus, the catalytic subunit of PP2A appears to be important for the kinase-phosphatase interaction, although Greatwall interacts with both PP2A/A and PP2A/C subunits. These pull-downs were performed with overexpression of both the kinase and the phosphatase. Therefore, the observation that Greatwall shows very little enrichment of PP2A indicates that either the kinase interacts with only a few subunits of PP2A complex or the direct interactions of these proteins is mediated by unknown interactors. In agreement with these observations, Castilho et al. (2009) reported that no indication of Greatwall phosphorylation of any of the PP2A-B55 δ subunits was observed in the in vitro kinase assays (Vigneron et al. 2009).

1.3.7 The Endosulphine Family: Endosulphine-alpha (Ensa) and Arpp19

As observed in the previous *Xenopus* work (Castilho et al. 2009), Greatwall does not directly phosphorylate PP2A subunits. Work in *Xenopus* extracts by the Mochida and Castro labs identified two unstructured small proteins, Endosulphine-alpha (ENSA) and cyclic adenosine monophosphate–regulated phosphoprotein 19 (Arpp19) as Greatwall substrates that mediated its action on the PP2A-B55 (Fig. 1.4) (Mochida et al. 2010; Gharbi-Ayachi et al. 2010)(Fig. 1.8).

Arpp19 was first discovered in the mammalian nervous tissue, enriched in dopamine – receptive neurons coupled to adenylate cyclase (Ivar Walaas et al. 1983). Its distribution was varied in all adult vertebrate tissues and malignant cells, while concentrations decreased with embryonic development towards pre-natal and post-natal periods (Girault et al. 1990). Arpp19 is a phosphoprotein found to be regulated by cyclic-AMP signalling pathway with an increase in phosphorylation at Ser104 in response to PKA activation (Dulubova et al. 2001). Arpp19 was found to be similar to another protein named Endosulphine-alpha involved in the endogenous regulation of sulfonylurea-sensitive potassium channels. Endosulphines are described as endogenous ligands that bind sulphonylurea receptor and inhibit the coupled potassium channels in the presence of ATP. This, in turn, increases the secretion of insulin in the β-cells of the pancreas thus mimicking sulphonylurea drugs used to manage non-insulin dependent diabetes mellitus. They are ubiquitously present in the muscle, nervous and endocrine tissues (Virsolvy-Vergine et al. 1992; Peyrollier et al. 1996; Heron et al. 1998). Structural studies displayed similarities of this protein to Arpp19 in mammalian tissues (Peyrollier et al. 1996). Endosulphine-alpha comprises of four helices when bound to lipid mimetics, while is intrinsically unstructured in solution. Mutating the PKA phosphorylation site (S109E) disrupts the fourth helix as well as its interaction with its binding partner α-synuclein (Parkinson's disease associated membrane protein) (Boettcher et al. 2008).

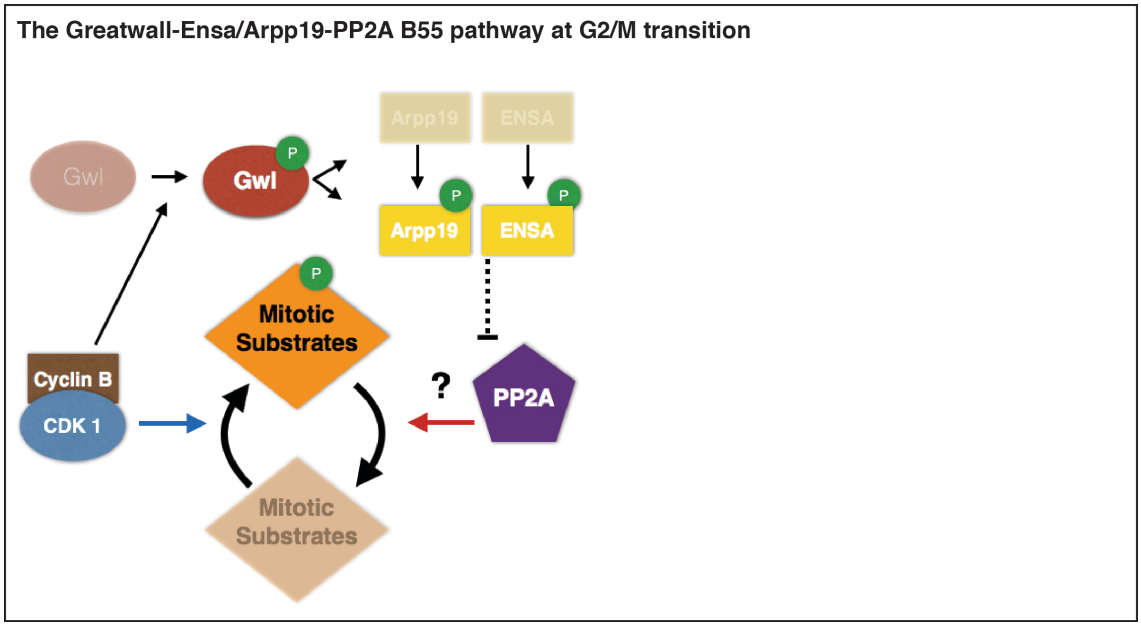

Figure 1.4 The Greatwall-Ensa/Arpp19-PP2A B55 pathway at G2/M transition

Schematic representation of the Greatwall-Ensa/Arpp19-PP2A B55 pathway at G2/M transition. Cdk1 activates Gwl by phosphorylating various Cdk phosphosites. Phosphorylated Greatwall activates Ensa/Arpp19 by phosphorylating Ser67 residue. Activated Ensa/Arpp19 are potent inhibitors of PP2A-B55 to prevent Cdk substrate dephosphorylation. The faded colours show inactivated proteins and the brighter ones show active proteins/protein complexes. Adapted from T Lorca and A Castro (Lorca & Castro 2012).

Cell cycle phenotypes of the Ensa (Endosulphine alpha) homologue, Endos, were identified initially in Drosophila oocytes. Mutating the endos gene in oocytes displays phenotypes analogous to that conferred by cdc2 and cdc25, such as an extended prophase I and inability to progress after metaphase I, which is also reminiscent with the Greatwall-depletion phenotypes observed in Xenopus extracts (Vigneron et al. 2009); moreover, protein levels of Polo and Twin (PP2A meiotic homologue) are reduced. These meiotic maturation phenotypes could rescued by exogenous human-Ensa, which showed that these proteins are conserved functionally in higher eukaryotes. A novel binding partner of Endos called Early girl (Elgi), which is known to be an E3 ubiquitin ligase, has also been identified (Stetina et al. 2008).

Two papers in 2010 identified Ensa and Arpp19 as Greatwall substrates. Mochida et al. identified Greatwall substrates using KESTREL (kinase substrate tracking and elucidation) method in which the potential substrates containing extracts were phosphorylated *in vitro* by active Greatwall, while endogenous kinase was inhibited. The phosphorylated bands were analysed by proteomic screening, and Arpp19 and Ensa were found to be the potential Greatwall substrates(Mochida et al. 2010). Interestingly, biochemical fractionation of meiotic-arrested CSF extracts and subsequent mass spectrometry only identified Arpp19 as Greatwall substrate in the proteomic screen (Gharbi-Ayachi et al. 2010).

As mentioned earlier, Greatwall depletion in interphase extracts inhibits mitotic entry and triggers premature mitotic exit in mitotic extracts (Castilho et al. 2009; Mochida et al. 2009; Vigneron et al. 2009). Immunodepletion of Ensa (Mochida et al. 2010) and Arpp19 (Gharbi-Ayachi et al. 2010) in Cycling extracts prevents mitotic entry, similar to that observed with Greatwall depletion. Adding back the wild type or recombinant S67 thiophosphorylated Ensa and Arpp19, but not the S67 mutant, can rescue these phenotypes. The mitotic phosphorylations were minimal in the depleted extracts while the inhibitory Tyr 15 phosphorylation remained on Cdk1. This implies that Ensa/Arpp19 control mitotic entry by inhibiting the phosphatase activity towards mitotic substrates, in a S67 dependent manner(Mochida et al. 2010; Gharbi-Ayachi et al. 2010). Subsequently, the depletion of Arpp19 from mitotic extracts triggers premature mitotic exit. PP2A appeared to mediate this abrupt exit, as the inhibition of the phosphatase with okadaic acid triggered mitotic re-entry(Gharbi-Ayachi et al. 2010).

Mutating the various serine and threonine sites in these small proteins identified S67 in Ensa and S62 in Arpp19 as the Greatwall phosphorylation sites. Four distinct phosphorylation sites were mapped in these proteins. Of these the FDSGDY motif contains the Greatwall site, and is conserved among the Endosulphine family (Gharbi-Ayachi et al. 2010; Mochida et al. 2010; Labandera et al. 2015). Phosphorylation of Ensa/Arpp19 by Greatwall generates a potent inhibitor of PP2A-B55δ, inhibiting its phosphatase activity against radiolabelled MBP-Fizzy-Ser50 substrate (Mochida et al. 2010). Similar inhibition was observed when thiophosphorylated Arpp19 was incubated with PP2A purified from CSF extracts and radiolabelled c-Mos (Cyclin-Cdk substrate) (Gharbi-Ayachi et al. 2010). This reduction in substrate phosphorylations is key in mitotic regulation, as addition of thiophosphorylated Ensa/Arpp19 into Greatwall-depleted interphase extracts triggered mitotic entry rescuing the Greatwall phenotype. Interestingly, phosphorylated forms of Ensa /Arpp19 could not rescue Greatwall phenotype as they were actively dephosphorylated in the absence of the kinase. This shows that the presence of active Greatwall kinase is essential for Ensa/arpp19 to counterbalance their dephosphorylation and induce mitotic entry. Conversely, addition of thiophosphorylated Ensa/Arpp19 to CSF *Xenopus* extracts also inhibited mitotic exit, implying that PP2A-B55 could be the Cdk-counteracting phosphatase at mitotic exit (Mochida et al. 2010; Gharbi-Ayachi et al. 2010)

Similarly, Arpp19 was found to contribute towards meiotic resumption by promoting Cdk auto-amplification (Dupré et al. 2013). Immature oocytes are arrested in prophase 1 by high PKA activity (Frank-Vaillant et al. 1999). Greatwall (K72M) promotes meiotic resumption by activating Cdk1, irrespective of the presence of progesterone (Yamamoto et al. 2011). In 2013, Dupre et al. reported that this activity of Greatwall is executed via Arpp19 and is S67 dependent (Dupré et al. 2013). This was demonstrated when the addition of S67 phosphomutant of Arpp19 (S67A) reversed Cdk1 activation, induced by hyperactive K72M Greatwall. Thus, Arpp19 is a downstream effector of Greatwall. Additionally, Arpp19 (S67A) prevented meiotic resumption in response to progesterone as well as transfer of metaphase II arrested cytoplasm. Moreover, Arpp19 inhibits PP2A on Greatwall phosphorylation thereby enhancing Cdk activation. Greatwall phosphorylation of Arpp19 appears to be controlled by Cdk activity. Addition of thiophosphorylated Arpp19 into prophase oocytes accelerated GVBD in the presence of

progesterone. However, this mechanism was dependent on protein synthesis of Cyclin B and c-Mos.

A direct interaction of PP2A-B55δ with Ensa/arpp19 was first demonstrated in *Xenopus* extracts. PP2A/C, PP2A/A and PP2A/B55δ were immunoprecipitated using recombinant Ensa and Arpp19. Structural data showed that the conserved middle region of Ensa surrounding the S67 site physically interacts with the catalytic and regulatory subunits of the phosphatase. Greatwall phosphorylation of Ensa/Arpp19 is indispensable for its interaction with PP2A-B55, while the T28 and S109 on Ensa might influence the binding of the middle region in a stepwise manner (Mochida 2014). Weak interaction of PP2A-B55 with Ensa was detected in both interphase and mitosis, but was enhanced significantly in mitotic extracts (Mochida et al. 2010; Gharbi-Ayachi et al. 2010), while Arpp19 was observed to pull down PP2A-B55 only from CSF extracts (Gharbi-Ayachi et al. 2010). Similarly, in *Xenopus oocytes*, once Greatwall activates Arpp19 it continuously inhibits PP2A to activate the Cyclin-Cdk complex at prophase, even in the absence of protein synthesis, presence of Cdk inhibitors or fully active PKA (Dupré et al. 2013). The D66A mutation in Ensa was found to inhibit the interactions of Ensa-PP2A B55 and prevent mitotic entry despite being phosphorylated at S67 (Gharbi-Ayachi et al. 2010). Taken together, these data indicated that Greatwall inhibits PP2A by promoting Ensa and Arpp19 binding.

Proline-directed phosphosites in Ensa/Arpp19 can be targeted either by Cdk or by MAPK kinases. One such motif containing S28 in Arpp19 and Thr28 in Ensa is phosphorylated by Cdk 2-Cyclin A in *Xenopus* CSF extracts, while T99 is phosphorylated *in vitro*. The Thr28 site is highly phosphorylated in *Xenopus* oocytes and cell-free metaphase-II extracts and results in 14-fold more PP2A inhibition than that achieved with the non-phosphorylated version of Ensa; in contrast, no additive effect has been observed with S67. Furthermore, PKA phosphorylation antagonises the inhibitory function of Thr28 but not that of S67. (Mochida et al. 2010; Mochida 2014). It was later demonstrated in starfish oocytes that the Cdk phosphorylation of Arpp19 (Ser69) also potentiated it to be a PP2A-B55 inhibitor, independent of Greatwall phosphorylation. This phosphorylation appeared to be critical for starfish oocyte maturations but had only moderate inhibitory effects in *Xenopus* (Okumura et al. 2014).

Finally, S109 in *Xenopus* Ensa (S107 human) was phosphorylated by PKA kinase and thought to contribute towards structural integrity of the protein when bound to lipid membrane (Boettcher et al. 2008). However, further structural data is required to determine the significance of this phosphorylation in cell cycle control. The PKA site is conserved in higher eukaryotes but is not found in lower organisms. Taken together the phosphorylation of Ensa/Arpp19 by three distinct kinases contributes differently to its cellular functions.

In budding yeast, PP2A-Cdc55 (homologue of mitotic PP2A) was found to interact with Igo1/2 (homologue of Ensa/Arpp19) (Bontron et al. 2013; Juanes et al. 2013) and Zds1/2 (Wicky et al. 2011; Rossio & Yoshida 2011). Zds1/2 is only present in fungi and is cytoplasmic while Igo1/2 were nuclear. Rim15-dependent phosphorylation of Igo1/2 inhibits PP2A-Cdc55 activity and promotes mitotic entry, while Zds1/2 stoichiometric binding to the phosphatase sequesters it in the cytoplasm facilitating closed mitosis in yeast (Rossio et al. 2014). Binding of Zds1/2 to the phosphatase also targets it to Cdc25 (Wicky et al. 2011). Surprisingly, the deletion of *zds1/2* impairs mitosis more severely than that of *igo1/2*. These observations, along with the different spatial arrangements of these interacting proteins, suggest that their action on PP2A-Cdc55 is distinct from each other (Rossio et al. 2014).

These observations from *Xenopus*, Starfish, *Drosophila* and yeast studies ultimately propose a novel phosphatase inhibition pathway (Greatwall-Ensa/Arpp19-PP2A B55) that functions at the mitotic and meiotic entry points to facilitate amplification of the Cyclin-Cdk complexes as well as mitotic phosphorylations.

1.3.8 Other Function of Greatwall in the Cell Cycle

Greatwall also performs non-mitotic functions in such as DNA checkpoint recovery, cellular adaptation in response to nutrient deprivation in yeast and embryonic development in *Drosophila* and *Xenopus*.

DNA Checkpoint Recovery

DNA damage response (DDR) at G2/M transition has been described in section 2.6. Once the DNA is repaired, this signalling pathway must be turned off. This process is called checkpoint recovery and it involves deactivation of checkpoint elements followed by activation of the proteins promoting G2/M transition. Checkpoint effectors are inactivated by dephosphorylation and proteolysis. Wip1 (p53-induced phosphatase) has been shown to bind and dephosphorylate key DDR factors such as ATM, γ-H2AX, Chk1, Chk2, and p53 (Lu et al. 2008). Additionally, the phosphorylation of Claspin (required for Chk1 activation) and Wee-1 (inhibitor of Cdk1) by Plk-1 targets them to SCF for proteolysis and inactivation of DDR (van Vugt et al. 2004; van Vugt & Medema 2004; Mailand et al. 2006; Peschiaroli et al. 2006; Mamely et al. 2006). In addition, Plk-1–mediated phosphorylation of 53BP1 (required for Chk1 and Chk2 activation) may disrupt its function. These data indicating that Plk-1 acts as a key regulator in *Xenopus* egg extracts (A. Peng et al. 2010) suggest a novel role for Greatwall in checkpoint recovery.

Immunodepletion of Greatwall in DDR egg extracts amplifies the response to DNA damage, while addition of wild-type Greatwall inhibits the DDR speeding recovery (A. Peng et al. 2010). A functional relationship between Plx and Greatwall in checkpoint recovery was also proposed based on studies in *Xenopus* extracts (A. Peng et al. 2011). Depletion of Greatwall and Plx individually delays checkpoint deactivation significantly but not synergistically. Purified Greatwall and Plx interact directly and Greatwall phosphorylation by Plx1 at the N-terminal increases during checkpoint recovery. However, an indirect regulation was seen when purified Aurora-A kinase restored Plx activation in Greatwall-depleted extracts. Thus, activation of Aurora-a might mediate Plx activation by Greatwall, representing a specific pathway for cell cycle entry following checkpoint recovery(A. Peng et al. 2011).

Similar studies in human cells, using IR-induced DNA damage suggest that hyperactive MASTL (K72M) and its substrates Ensa/Arpp19 control the timing of mitotic entry following checkpoint recovery. Although MASTL (K72M) was expressed at very low levels (consistent with *Drosophila* and *Xenopus* data), it strongly stimulated mitotic entry after DNA damage. MASTL does not affect DDR initiation or DNA repair, as the 53BP1 foci formation were similar after IR with overexpressed K72M Greatwall or siMASTL. However, the timing of mitotic entry is accelerated by the K72M MASTL in

HeLa cells and while mitotic entry is delayed on silencing MASTL. Similar phenotypes were observed with the Greatwall substrates Ensa and Arpp19 individually, while both together were cytotoxic. Both these phenotypes are independent of DNA repair. However, acceleration of mitotic entry after DNA damage led to number of mitotic defects such as lagging chromosomes and DNA bridges during anaphase. This work also suggested that the Greatwall functions in checkpoint recovery by regulating the kinetics of Cdk1 inhibition, as Try15 phosphorylation of Cdk1 reduces in the presence of MASTL (K72M) (Wong et al. 2016).

Cellular Adaptation in Response to Growth Factors and/or Nutrients

Preliminary work on Rim-15 (Greatwall homologue in *Saccharomyces cerevisiae*) indicated its interaction with three nutrient sensory kinases (TOR, PKA and Sch9). In response to nutrient deficiency, budding yeast cells arrest growth in G1 and enter G0 by unknown mechanisms or trigger gametogenesis. TORC1 (Target of Rapamycin) pathway responds to nitrogen deficiency and the PKA/Ras pathway responds to glucose-deficiency signals (Gray et al. 2004; De Virgilio 2012). Both these pathways are highly conserved from yeast to mammals. Both TORC1 and PKA (main controllers of the cell growth) negatively regulate Rim-15 (downstream effector) and inhibit G0 entry. Nutrient deficiency leads to dephosphorylation of the PKA sites and Thr 1075 (TORC1-mediated site) on Rim-15 and its subsequent nuclear accumulation. Ultimately this release of inhibition of Rim-15 kinase activity contributes towards G0 entry (Pedruzzi et al. 2003; Swinnen et al. 2006). The activated kinase induces expression of the genes controlled by transcription factors Msn2, Msn4, Gi1 and Hsf1. Rim-15 directly phosphorylates, zinc finger transcription factor Msn2/4 and heat-shock transcription factor Hsf but not Gis1, indicating different activation mechanisms (P. Lee et al. 2013). The Rim-15 substrates Igo1/2 (Endosulphine homologues in yeast) were also found to be crucial for mRNA stabilization and have a proposed role in initiating entry into G0 and gametogenesis by regulating PP2A-Cdc55 phosphatase activity (Talarek et al. 2010; Sarkar et al. 2014). This was demonstrated in fission yeast where the nutritional response pathway is linked to mitotic progression by the Ppk18-Igo1 (PP2A-B55-Ensa) pathway. Nutrient deprivation permitted smaller cells (adaptation for survival) to enter mitosis, due to the inhibition of PP2A by active Greatwall kinase via Ensa. This leads to prolonged G1 phase that subsequently leads to quiescence or

gametogenesis under starvation conditions. Greatwall kinase is phosphorylated by S6 kinases that are downstream of TORC1 and PKA in rich medium and these phosphorylations inhibit Greatwall activity and to allow the cells to grow larger before mitosis (Chica et al. 2016; Pérez-Hidalgo & Moreno 2016). However, this mechanism of survival mediated by Greatwall in higher eukaryotes is yet to be determined.

Embryonic Development

As mentioned earlier, the *scant* allele encodes a hyperactive version of Greatwall kinase with a K97M mutation. Expression of this hyperactive kinase causes developmental failure in *Drosophila* larval neuroblasts. However, a recessive allele that functions as a revertant of *scant* specifically disrupts this isoform. Female larvae containing only one copy of this allele (hemizygotic) produce embryos with reduced viability. Oocytes from these females do not display secondary meiotic arrest in metaphase 1, and progression in meiosis is accompanied with little or no segregation of sister chromatids and homologous chromosome pairs on the elongated meiotic spindles. Thus, Greatwall is implicated in sister-chromatid cohesion during female meiosis I (V. Archambault et al. 2007). Surprisingly, the kinase activity of related K71M Greatwall (Scant) is sufficient to trigger M-phase entry in *Xenopus* oocytes despite its low expression levels and high rate of proteolysis. Greatwall binds and inactivates PP2A/B55 via Endosulphine phosphorylation in G2. When these oocytes are treated with progesterone to induce maturation, Greatwall dissociates from PP2A in the M phase, independent of kinase activity or T748 phosphorylation (Yamamoto et al. 2011). Preliminary analysis of Greatwall function using an RNAi-mediated approach in mouse oocytes also indicated a vital role of the kinase in chromosome segregation and in the prevention of exit after anaphase 1. Greatwall-depleted oocytes show the presence of the second polar body, indicating failure to arrest in metaphase II. However, Greatwall is dispensable for resuming meiosis, prometaphase 1 progression, condensation of chromosomes and cytokinesis (Adhikari et al. 2014; Pfender et al. 2015). Together, these data suggest a yet undiscovered role for Greatwall in oocyte maturation.

Work from Archambault, Wang and Rangone indicate coordination between Polo (Plk1) kinase and Greatwall kinase in performing developmental functions in *Drosophila.* Spindle aberrations and developmental failure due to the *scant* mutation of

Greatwall increased proportionally with decrease in Polo function (V. Archambault et al. 2007). This coordination was later identified due to the interdependent function of Polo and PP2A-B (regulatory) subunit. Depletion of Polo and PP2A-Twins together was embryonic lethal, while they ensured proper centrosome attachment to the nucleus in early prophase and mitotic exit respectively. Greatwall was found to antagonise PP2A-Twins function in metaphase 1 and early mitotic cycles. (P. Wang et al. 2011). Heterozygous Endos (*Drosophila* homologue of Ensa/Arpp19) mutants were found to suppress *scant* phenotypes with reduced Polo. However, homozygous Endos mutations or depletion and *scant* dominant mutation have similar phenotypes, which were rescued by depletion of catalytic or regulatory subunit of PP2A-Twins in cultured cells(Rangone et al. 2011). This shows that Greatwall interacts with Endos and activates it. Additionally, when PP2A catalytic subunit is mutated it acts with *scant* Greatwall synergistically, when maternal Polo level are reduced. Based on these genetic interactions, Rangone proposed that Greatwall supresses PP2A-Twins via Endos and allows Cdk activation. This in turn leads to activation of Polo and execution of its mitotic functions via phosphorylated partners. When Cdk activity decreases in anaphase, Polo executes its function via partners dephosphorylated by PP2A-B55. Thus, when hyperactive Greatwall inhibits PP2A with reduced Polo activity, the interphase partners are not dephosphorylated and their association with Polo is prevented (Rangone et al. 2011). This proposes precise control of meiotic entry and exit by Greatwall, Polo and PP2A-Twins, where Greatwall is shown to play multiple roles in meiotic and mitotic progression (V. Archambault et al. 2007).

1.3.9 Regulation of Greatwall Kinase

The regulation of Greatwall kinase has only been studied in detail in the recent years. Greatwall is an unconventional AGC kinase due to the presence of a 540 amino acid-long insertion loop between the N-terminal and C-terminal domains, which separates the sub-domains VII and VIII (Hanks & Quinn 1991; J. Yu et al. 2004). Findings in recent years advocate that the activation-inactivation of Greatwall is controlled by phosphorylation by Cdk1 (Fig. 1.5) (Yamamoto et al. 2011; J. Yu et al. 2004; J. Yu et al. 2006; Zhao et al. 2008; Vigneron et al. 2011) and Polo kinase (P. Wang et al. 2013). However, mitotic functions also require Greatwall to be spatially regulated in a

phosphorylation-dependent manner (P. Wang et al. 2013; Alvarez-Fernández et al. 2013; P. Wang et al. 2016; Pedruzzi et al. 2003).

The structure of Greatwall comprises of the N-terminal and C-terminal domain separated by a long insertion of amino acids called the non-conserved middle region (NCMR) and a C-terminal-tail/linker region. The length of the NCMR is conserved in all orthologues of Greatwall but the amino acid sequence is very poorly conserved between species. Moreover, this region is dispensable for the kinase activity of Greatwall(Blake-Hodek et al. 2012). A minimal kinase where the NCMR is substituted for conventional AGC kinase activation segment, is functional *in vitro* and readily phosphorylates Ensa in radioactive kinase assays (Ocasio et al. 2016). In *Xenopus* S3 cells, Greatwall was found to bind chaperones like Hsp90 (Heat shock protein) that influences the stability of the kinase and its mitotic entry function. The glycine rich loop on the N-terminal was seen to be important for Hsp90 binding along with its co-chaperone Cdc37 (Yamamoto et al. 2014).

Two models have been proposed for the activation of the Greatwall. In 2011, Vigneron et al. proposed that Greatwall is first phosphorylated at Serine 883, a C-terminal linker residue. This phosphorylation causes a conformational change and allows the C-terminal tail to interact with N-terminal domain via the tail-linker binding site, stabilising the partially activated kinase. Further, full activation of Greatwall occurs as a result of its interaction with another AGC kinase via the N-terminal hydrophobic motif (Vigneron et al. 2011). This is to compensate for the lack of the C-terminal hydrophobic motif in Greatwall, that usually contributes to the intramolecular interaction with the N-terminal hydrophobic patch and subsequent stabilization in conventional AGC kinases (Biondi et al. 2000).Conversely, an alternate model suggested that Greatwall is initially phosphorylated by Cyclin-Cdk at the presumptive activation segment residues (T193 and T206 in *Xenopus*). This activates Greatwall to enable autophosphorylation of Ser883 and subsequent interaction between hydrophobic motifs at the N- and C- termini to stabilise the active kinase. The second model suggested multimerisation of Greatwall

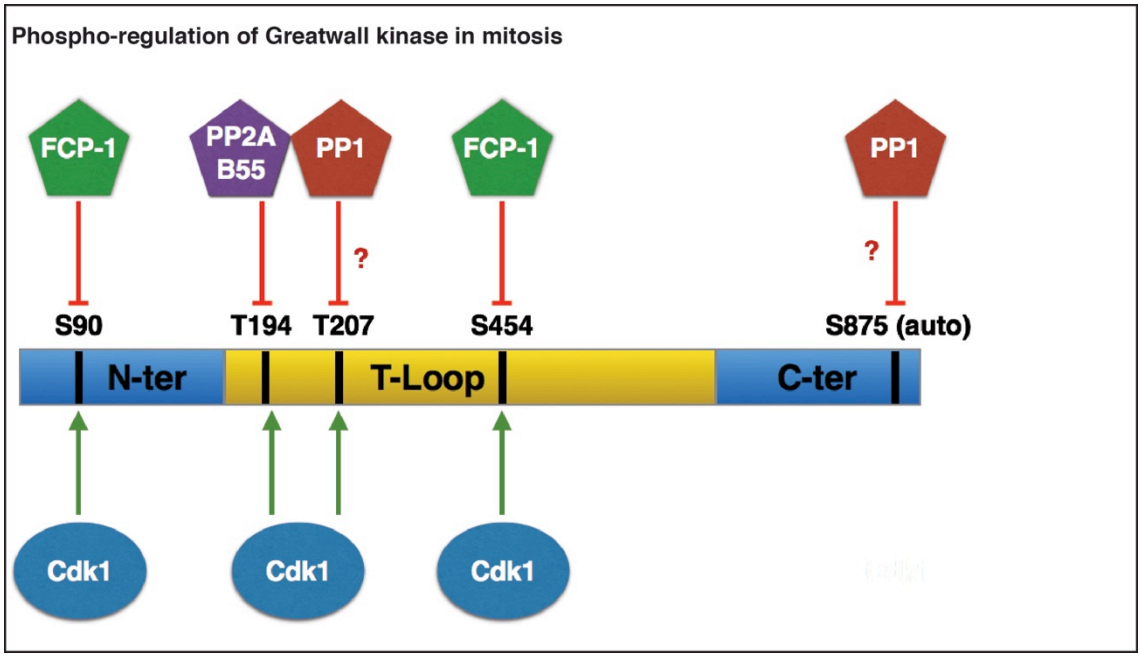

Figure 1.5 Phospho-regulation of Greatwall kinase

Schematic representation of activation (green arrows) and inactivation (red arrows) of Greatwall kinase in mitosis. Cdk1 phosphorylates and activates Gwl kinase at the indicated residues at mitotic entry. Ser875 is the auto-phosphorylation site in human Greatwall. At mitotic exit PP2A targets Thr194 (Hégarat et al. 2014), PP1 is thought to dephosphorylate other Cdk sites such as T207 and/or Ser875 (Heim et al. 2015; Ma et al. 2016; Rogers et al. 2016) while FCP-1 targets Ser90 and Ser454 (Monica et al. 2015). The N-terminus and C-terminus of the kinase are shown in blue and the long mid-region thought to be the T-loop is shown is yellow.

molecules to compensate for the lack of C-terminal hydrophobic motif (Blake-Hodek et al. 2012).

Although both models contradict each other, the influence of Cdk1 dependent phosphorylation on Greatwall activation is generally well supported. Cdk1 phosphorylates purified Greatwall in-vitro (J. Yu et al. 2006) while Greatwall is specifically phosphorylated in mitosis both in cell extracts and oocytes of *Xenopus* and starfish (Zhao et al. 2008; Yamamoto et al. 2011; M. Hara et al. 2012). Similarly, Greatwall activity was required to induce mitotic (J. Yu et al. 2006; Zhao et al. 2008) and meiotic entry (Yamamoto et al. 2011), as kinase dead Greatwall could not perform this function. Greatwall was found to function downstream of Cdk1-Cyclin B in starfish oocytes (K. Hara et al. 1980). Finally, Cdk1 inhibition by Roscovitine or p21/Cip1 reduces Greatwall phosphorylation both in CSF extracts and oocytes (Zhao et al. 2008). However, Cdk1 phosphorylation of Greatwall was not equivalent to endogenous Greatwall phosphorylations in *Xenopus*. This indicates the occurrence of additional phosphorylations either by the kinase itself or by other kinases that act on greatwall to phosphorylate it completely (J. Yu et al. 2006). Greatwall autophosphorylation has been observed in *Xenopus* extracts (J. Yu et al. 2006) and has also been reported in previous papers as essential for its complete activation (Blake-Hodek et al. 2012; Vigneron et al. 2011).

In *Drosophila*, Polo kinase interacts with Greatwall specifically and this interactions does not require phospho-priming the Polo-box domain(P. Wang et al. 2013). Although Plx1 (*Xenopus* Plk1) was observed to phosphorylate Greatwall *in vitro*, it showed no functional significance, as Plx1-treated Greatwall did not phosphorylate myelin basic protein in *in vitro* kinase assay or autophosphorylate itself. Additionally, this kinase was unable to induce mitosis in Greatwall-depleted CSF extracts (J. Yu et al. 2006). However, if this binding controls the localisation of Greatwall as observed in *Drosophila* (Yamamoto et al. 2014) is not known.

In addition to phosphorylation, the mitotic functions of Greatwall also depend on its cellular localization. Two papers demonstrated that the nucleo-cytoplasmic shuttling of Greatwall is phosphorylations dependent in *Drosophila* and mammalian cells (P. Wang et al. 2013; Alvarez-Fernández et al. 2013). Both *Drosophila* and mammalian Greatwall

have two nuclear localization sequences and one nuclear export sequence in the NCMR region (P. Wang et al. 2013; Alvarez-Fernández et al. 2013; P. Wang et al. 2016). The NES motif is not conserved among vertebrates and is required to control the dynamics of Greatwall nuclear export along with NLS sequences (P. Wang et al. 2016). However, they are regulated differently. In *Drosophila*, NCMR contains multiple phosphorylation sites for the Polo kinase, which when phosphorylated is thought to promote Greatwall association with 14-3-3ε to be sequestered into the cytoplasm. In addition to Polo kinase, Cdk1 phosphorylations of Greatwall on the consensus sites in NCMR were observed to be important for nuclear exclusion. However, Greatwall localisation is controlled by Cdk1 in a Polo/14-3-3ε independent manner (P. Wang et al. 2013). In *Xenopus* S3 cells one NLS motif was identified in the N-terminal region of the kinase. This NLS was located around KR456/457 and is conserved in human cell line (KR444/445 (Alvarez-Fernández et al. 2013)). Nuclear retention of Greatwall during interphase is attributed to its association with importin α and importin β via the NLS (Yamamoto et al. 2014). In mammalian cells, Greatwall was translocated just before nuclear envelope breakdown (NEBD) in a CRM1-exportin–dependent manner. This translocation depends on Cdk1 phosphorylation of Greatwall and the proposed sites are T194, T107 and the ATP-binding site D156. The role of Plk1 in gwl translocation is not preserved in mammalian cells, probably due to the high sequence dissimilarities in the NCMR region across species (Alvarez-Fernández et al. 2013).

Subcellular localisation of Greatwall is necessary to execute its mitotic functions. Inhibition or delay of nucleo-cytoplasmic shuttling of the kinase causes mitotic defects similar to those observed on Greatwall depletion (P. Wang et al. 2013; Alvarez-Fernández et al. 2013; P. Wang et al. 2016). While Greatwall was discovered to be highly nuclear (J. Yu et al. 2004), PP2A is majorly cytoplasmic during the interphase (Schmitz et al. 2010; Mayer-Jaekel et al. 1994; P. Wang et al. 2013; Alvarez-Fernández et al. 2013). At the G2/M transition, PP2A activity is high in the cytoplasm, inhibiting phosphorylation of initial Cdk substrates at the cell cortex such as membrane proteins involved in cell rounding (Gavet & Pines 2010). Alvarez-Fernandez (2013) observed that Cyclin B is transported into the nucleus prior to the nuclear export of Greatwall. This suggests that the active Cyclin B-Cdk1 complex activates Greatwall and induces its nuclear export prior to NEBD (P. Wang et al. 2013; P. Wang et al. 2016). This in turn inhibits PP2A activity in the cytoplasm, so that the mitotic substrates can be readily

phosphorylated to facilitate mitotic progression. Conversely, PP2A-Tws dephosphorylates Greatwall at NLS2 and Cdk sites to regulate the return of the kinase to its nuclear location at cytokinesis (P. Wang et al. 2016). Although some of the factors contributing to nucleo-cytoplasmic shuttling of Greatwall have been uncovered, the exact mechanism regulating this process remains elusive.

1.3.10 Inactivation of Greatwall-Ensa/Arpp19 and Reactivation of Phosphatases during Mitotic Exit

Similar to kinase activation during mitotic entry, phosphatases that remove Cdk1 site phosphorylations have to be reactivated during mitotic exit. This will, in parallel, require the inactivation of Greatwall and dephosphorylation of Ensa/Arpp19. Analogous to the G2/M switch, this phosphatase reactivation step is likely to constitute a major element of the mitotic exit switch. PP2A-B55 has been implicated as one of the major Cdk-counteracting phosphatases in the recent years. However, whether it is the only phosphatase at mitotic exit remains a matter of debate. A major question in this transition is thus the nature of the phosphatases that inactivate Greatwall and EnsaArpp19 in anaphase. As Cdk1 phosphorylates Greatwall and PP2A-B55 dephosphorylates Cdk substrates at mitotic exit, Greatwall might also be dephosphorylated by PP2A-B55.

PP2A/A and PP2A/C subunits have been shown to interact with Greatwall in immunoprecipitation experiments in both human cells and *Xenopus* cell extracts. Greatwall-induced phenotypes could also be rescued by the removal of PP2A using inhibitors like okadaic acid and immunodepletion using monoclonal antibodies. Greatwall depletion enhances the phosphatase activity of PP2A against Cyclin B-Cdk 1 substrates (Vigneron et al. 2009). Our lab showed that PP2A-B55 αδ acts on the Thr194 site in Greatwall, based on the observation that siRNA depletion of these subunits blocked Greatwall dephosphorylation in *HeLa* cells during mitotic exit (Hégarat, Vesely, Vinod, Ocasio, Peter, Gannon, Oliver, Novák & Hochegger 2014b). Moreover, depletion of Arpp19, which is an established substrate of Greatwall, leads to a rapid decrease in Greatwall phosphorylation and causes mitotic exit. This could be due to the reactivation of the phosphatase (Gharbi-Ayachi et al. 2010). However, at mitotic exit,

PP2A-B55 is bound and inhibited by Ensa/Arpp19, which suggests the presence of another phosphatase that initiates Greatwall dephosphorylation, as postulated by a recent mathematical study(Vinod & Novák 2015).

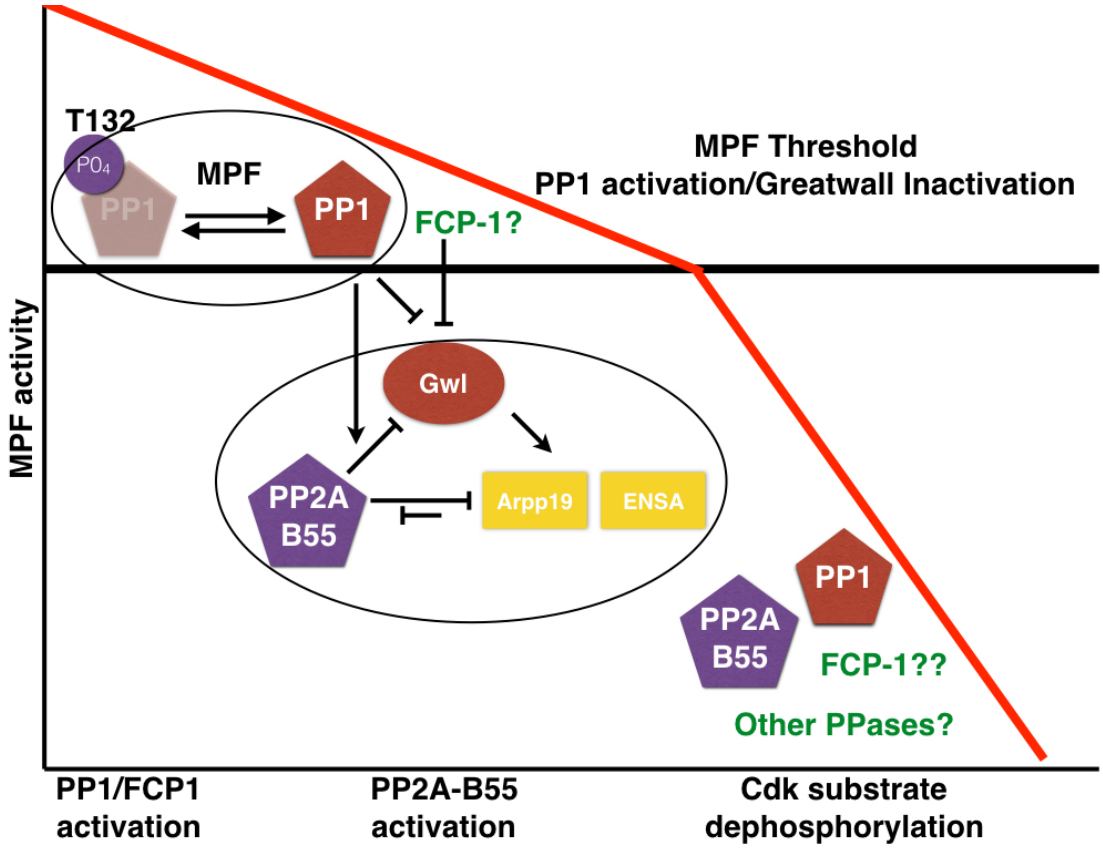

Figure 1.6 Dephosphorylation cascade at mitotic exit

Cyclin B results in a drop in Cdk1 activity and activates the Cdk-counteracting phosphatases in a stepwise manner. Cdk1 (MPF) directly inhibits PP1 by T320 phosphorylation. The drop in Cyclin B levels below a critical threshold can lead to PP1 reactivation by auto-dephosphorylation at T320. PP1 then inactivates Greatwall, which allows PP2A-B55 activation, but this remains to be confirmed in mammalian cells (Heim et al. 2015; Ma et al. 2016; Rogers et al. 2016). FCP-1 has also been implicated in this mechanism by directly contributing to Greatwall dephosphorylation (Monica et al. 2015). These phosphatases would possibly also participate in the exit reaction (Barr et al. 2011; Bollen et al. 2009; Schmitz et al. 2010; Cundell et al. 2013). This figure was adapted from Hegarat et al. (2016) with permission from the authors(Hégarat et al. 2016).

One of these phosphatases was found to be PP1 in *Xenopus* (Heim et al. 2015) as well as human cells (Rogers et al. 2016). *Xenopus* studies proposed a model where the inactivation of Cdk1 leads to PP1 auto-activation and subsequent dephosphorylation of Greatwall at its autophosphorylation site Ser883. In *Xenopus* extracts, two intermediate states of phosphorylated Greatwall were observed. In the presence of Roscovitine, thio-Arpp19 only blocked the dephosphorylation partially, while Inhibitor-2 blocked Greatwall dephosphorylation completely. This confirmed that PP1 is the initial phosphatase acting on Greatwall when Cdk1 is inactivated. PP1 was also found to be required to keep Greatwall inactivated and prevent rephosphorylation of the kinase at the autophosphorylation site (Heim et al. 2015). In human cells, SILAC and subsequent mass spectrometry showed that PP1 interacted with MASTL (human homologue of Greatwall). Moreover, a simulated mitotic exit network showed that PP1 is associated with MASTL in the early phases of mitotic exit and could potentially be the molecule that initiates Greatwall dephosphorylation at mitotic exit. PP1α and PP1β were found to only partially dephosphorylate Greatwall in an *in vitro* phosphatase assay, where MASTL was purified from cells treated with okadaic acid and PP1 siRNA oligos to maintain maximal Greatwall phosphorylation. Although the direct effects of PP1 dephosphorylation could not be observed using PP1 siRNA in vivo, a simulated mitotic exit network was used to confirm the association with Greatwall at mitotic exit. Interestingly, the autophosphorylated residue of Greatwall remained stable throughout mitosis and was proposed not to contribute to the inactivation of the kinase.

Recent studies have also implicated Greatwall dephosphorylation by FCP-1 phosphatase at mitotic exit. FCP-1 was observed to bind and dephosphorylate serine residues at position 90 and 453, which are phosphorylated by Cdk1 (Monica et al. 2015). Although PP1 is suspected to initiate Greatwall dephosphorylation and activate PP2A at mitotic exit, how FCP-1 fits in in the dephosphorylation cascade is yet to be determined(Hégarat et al. 2016)(Fig. 1.6).

Two papers in 2014 explored PP2A reactivation by studying Ensa/Arpp19 dephosphorylation as well at mitotic exit (Williams et al. 2014; Hégarat, Vesely, Vinod, Ocasio, Peter, Gannon, Oliver, Novák & Hochegger 2014b). While the Goldberg lab claimed that PP2A-B55 itself is the Ensa/Arpp19 phosphatase, our lab found FCP-1 to influence Ensa/Arpp19 dephosphorylation indirectly.

Williams et al. (2014) proposed a simple model of 'unfair competition' for PP2A-B55 reactivation. Careful measurements of the binding constant (Km) and catalytic activity (Kcat) of the phosphatase against pEndos (*Drosophila* Ensa/Arpp19) suggested that phospho-Ensa/Arpp19 is a potent inhibitor of the phosphatase as it binds strongly to the active site, but that it is a bad substrate as the dephosphorylation kinetics were very slow. The authors proposed that as long as Greatwall is active, Ensa/Arpp19 that is dephosphorylated and released from the Ensa/Arpp19-PP2A B55 complex is rephosphorylated and captures the phosphatase repeatedly. However, at mitotic exit on Cyclin B-Cdk1 inactivation, Greatwall activity drops (Zhao et al. 2008), thus shifting the balance towards the dephosphorylation of Ensa/Arpp19 (anti-Endos activity) and subsequent disruption of the Ensa/Arpp19-PP2A B55 complex and releasing PP2A-B55 to execute mitotic dephosphorylations. The authors additionally observed that other serine-threonine phosphatases such as PP4 and PP6 do not contribute to anti-Endos activity. Although depletion or mutation of PP2A-B55 reduced majority of anti-Endos activity, PP1 was also observed to decrease it by ≈ 15%-20% (Williams et al. 2014). The 'unfair competition' model also proposes that Okadaic acid outcompetes Ensa/Arpp19 for the active site on PP2A-B55. In this scenario, Ensa/Arpp19 should remain phosphorylated but the complex should fall apart when okadaic acid is present, as observed *in vitro* (Williams et al. 2014).

In the meanwhile, our lab investigated dephosphorylation of Ensa/Arpp19 in human cells artificially synchronised at mitotic exit. Cells were synchronised in mitosis using the Eg5 inhibitor, STLC and then inhibiting Cdk1 using the potent inhibitor RO336 triggered mitotic exit. Under these conditions, Ensa/Arpp19 dephosphorylation was blocked only in the presence of okadaic acid and tautomycetin together but not individually. This suggests the influence of more than one phosphatase on this dephosphorylation process. Additionally, the depletion of FCP-1 (RNA Polymerase II carboxy terminal domain phosphatase) blocked Ensa/Arpp19 dephosphorylation but Greatwall appeared to be dephosphorylated at Thr194 (Hégarat, Vesely, Vinod, Ocasio, Peter, Gannon, Oliver, Novák & Hochegger 2014b). This proposed that PP2A-B55 dephosphorylates Greatwall at Thr194, while FCP-1 contributes to Ensa/Arpp19 dephosphorylation indirectly as direct interaction was not demonstrated (Williams et al. 2014; Hégarat, Vesely, Vinod, Ocasio, Peter, Gannon, Oliver, Novák & Hochegger

2014b). The later findings that both PP1 and FCP1 act on Greatwall dephosphorylation could reconcile the findings of these two studies.

The unfair competition model appears counter-intuitive. How can a phosphorylated residue be both an inhibitor and a substrate of a phosphatase at the same time? The measurements of the binding affinity and the dephosphorylation dynamics of Ensa (pEndos) give a compelling answer to this question. Phosphorylated Ensa is a very potent binder of the active site, but is dephosphorylated only very slowly (Km = 0.0009–0.0017 μM, Kcat = 0.021–0.035 s^{-1}). One pitfall of this model is that at the rate of dephosphorylation observed *in vitro*, a small amount of Greatwall activity would always push the equilibrium in favour of re-phosphorylation. Thus, Greatwall would have to be completely inactivated by another phosphatase before Ensa can start to be dephosphorylated. Conversely, Hegarat et al. showed that Ensa could still be dephosphorylated even when Greatwall maintains 60% of its activity. However, this data may represent an overestimation of Greatwall activity, since it is performed after purification of the kinase. It is possible that the kinase can reactivate itself once removed from counteracting phosphatases such as PP1. Overall, a model is taking shape whereby; PP1 and FCP1 trigger Greatwall inactivation early during mitotic exit allowing Ensa dephosphorylation and PP2A-B55 re-activation. Crosstalk of these phosphatases and their regulation as well as additional regulation of pEnsa dephosphorylation can, however, not be ruled out.

1.3.11 Greatwall and Ensa/Arpp19 in Mammalian Cells

Greatwall has been well characterised in lower organisms as well as higher eukaryotes, though its downstream effectors Ensa and Arpp19 need further investigation. Although Greatwall appears to contribute to mitosis among all species, some differences are observed between the lower organisms and mammalian studies.

Greatwall is indispensable for mitotic and meiotic entry in lower organisms. However, the same phenotypes are not recapitulated in mammalian mouse and human cells. Greatwall depletion does not inhibit mitotic entry in mouse embryos and only slows down G2/M transition in human cells. Similarly, during mitotic exit, the major

phenotypes documented are chromosome segregation and cytokinesis defects. In this thesis, I have performed biochemical and cytological analysis of Ensa and Arpp19 to characterise the mitotic functions of these small proteins in order to reconfirm the mitotic regulation of Greatwall kinase.

The phospho-regulation of Ensa and Arpp19 at mitotic exit is yet to be understood clearly. While *Xenopus* data propose an essential role for PP1 in PP2A-B55 activation, this is not completely recapitulated in the mammalian system. Additionally, the influence of FCP-1 adds to the complexity of Greatwall dephosphorylation and subsequent reactivation of PP2A-B55. In this thesis, I have attempted to analyse mitotic exit dephosphorylations by testing the 'unfair competition' model in intact mammalian cells and by examining the effects of dominant active Ensa/Arpp19 in mammalian mitotic entry. I also attempted to identify novel phosphatases interacting with Ensa/Arpp19 by performing a proteomic screen.

1.4 Molecular Mechanisms Underlying a Phosphorylation Reaction: Thiophosphorylation

Protein phosphorylation is the most common post-translational modification in cell cycle regulation and signal transduction. The following section provides a detailed explanation of the molecular interactions between kinases and phosphatases with their substrates.

1.4.1 Phosphorylation reaction

Protein groups called kinases exert their effect by transferring the terminal γ-phosphate of the ATP to the phosphoryl group acceptor on the substrate such as a serine, threonine or tyrosine residue. This molecular mechanism is a two-substrate reaction: while a phosphate moiety is introduced into a polypeptide substrate, ATP is also converted to ADP (Fig 1.7). In addition to exogenous substrates, many kinases undergo auto-phosphorylation reactions. These auto-phosphorylations could be either intermolecular or intramolecular (DeLange et al. 1968).

The phosphorylated substrates could elicit a cascade of molecular reactions or carry out its own bonafide functions. Phosphorylated proteins are known to exhibit specific localisation (Obsil & Obsilova 2008), active enzymatic action (Agius 2008) or protein-

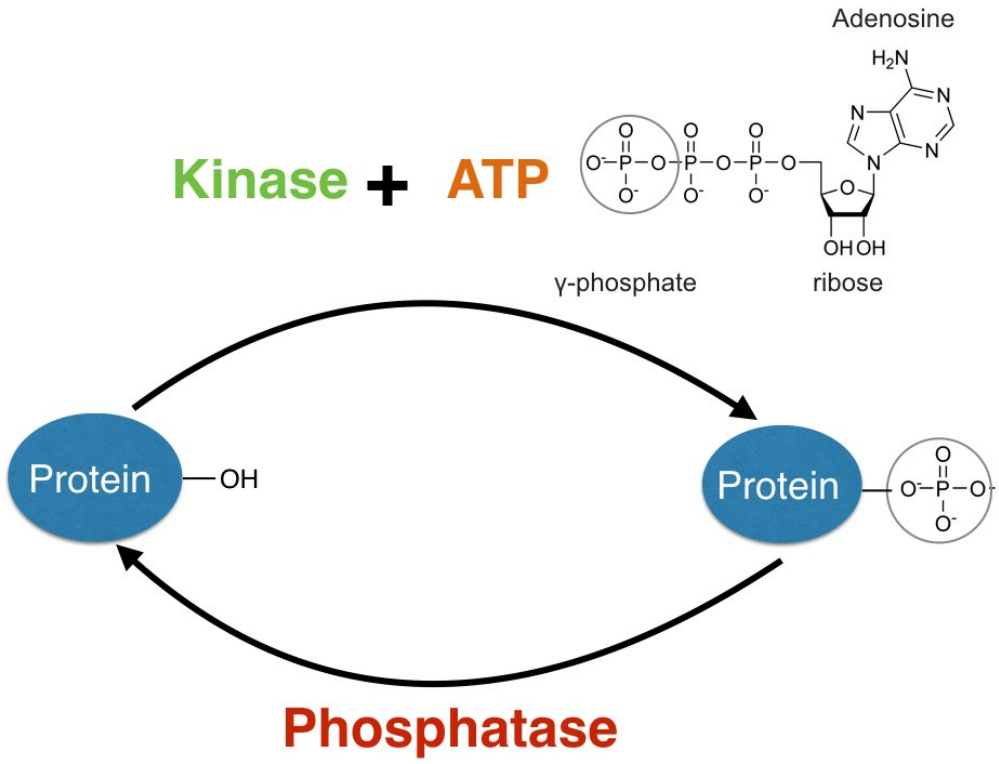

Figure 1.7 Phosphorylation Reaction
Schematic representation of a phosphorylation reaction

protein interactions (Pieroni et al. 2008). On the contrary, phosphatases hydrolyse the bond between the acceptor residues and the phosphoryl group and reverse the effect, enabling switch-like transitions in cellular regulation.

1.4.2 Structural similarities among protein kinases

Every kinase defined follows the same molecular reaction of phosphate transfer. Every kinase has a catalytic domain and regulatory domain. In eukaryotes, the kinase domain extends from 250 to 300 amino acids. The kinase domain in turn is divided into 12 sub-domains that fold into a common catalytic core (Hanks & Hunter 1995). Conserved

residues essential for substrate recognition were also found among these sub-domains: consensus motifs in the catalytic loops region in subdomain VIB and the activation loop in subdomain VIII (Taylor et al. 1995; L. N. Johnson et al. 1998). Eukaryotic kinases have a conserved catalytic kinase domain with an array of glycine-rich residues at the N-terminus close to the lysine-residue involved in ATP-binding and hydrophobic residues at the C-terminus (Knighton, Zheng, Teneyck, Ashford, et al. 1991; Knighton, Zheng, Teneyck, Xuong, et al. 1991). Following the sequencing of the human genome, considerable effort has been put towards mapping the superfamily of eukaryotic protein kinases (Kostich et al. 2002; Manning et al. 2002).

1.4.3 Challenges in studying phosphorylation reactions

Phosphorylation reactions at the cellular level are ubiquitous and hence there are many challenges in studying these reactions. The kinase-substrate network is very complex as the human kinome itself consists of around 520 genes (Manning et al. 2002). Additionally, other post-translational modifications such as methylation, glycosylation and ubiquitylation can also influence phosphorylation levels (Garcia et al. 2005). Owing to the ubiquitous nature of these reactions, it is difficult to distinguish between the phospho-receptor substrates of every kinase. Moreover, the low abundance of these kinases and substrates at the cellular level also make it difficult to study phosphorylation stoichiometrically.

The reversal of these reactions is brought about by protein phosphatases, by hydrolysing phosphorylated residues back to their native state (Jiang & Z.-Y. Zhang 2008). These are also important protein modifications that contribute to signalling pathways and cell proliferation. Most kinase and phosphatase reactions are transient and cannot be purified unless they form tight complexes. Cell cycle regulation comprises of many such transient reactions that enable switch-like responses in mitosis (Rudolph 2007).

1.4.4 Thiophosphorylation reaction and its advantages

Thiophosphorylation reactions involve ATP with a thiol on the γ-phosphate group. This is a non-hydrolysable, or at least very slow to hydrolyse, analogue of ATP. Thiophosphorylation results in the transfer of the thio- γ-phosphate group to the substrate, which in turn stays constitutively phosphorylated as the rate of dephosphorylation is comparatively slower for this moiety(Shimizu et al. 2002). The sulphur atom of the thiol group is both larger and less electronegative than the oxygen atom that is replaces and results in a decrease in electrophilicity of the central phosphorous atom, making it difficult for the phosphatase to hydrolyse it. As the phosphorylated form of the substrate binds with higher affinity to the phosphatase, the phosphatase-substrate complex would be slow to disassociate (Fig 1.8), essentially trapping the substrate-bound phosphatase. This technique has been used in the past to

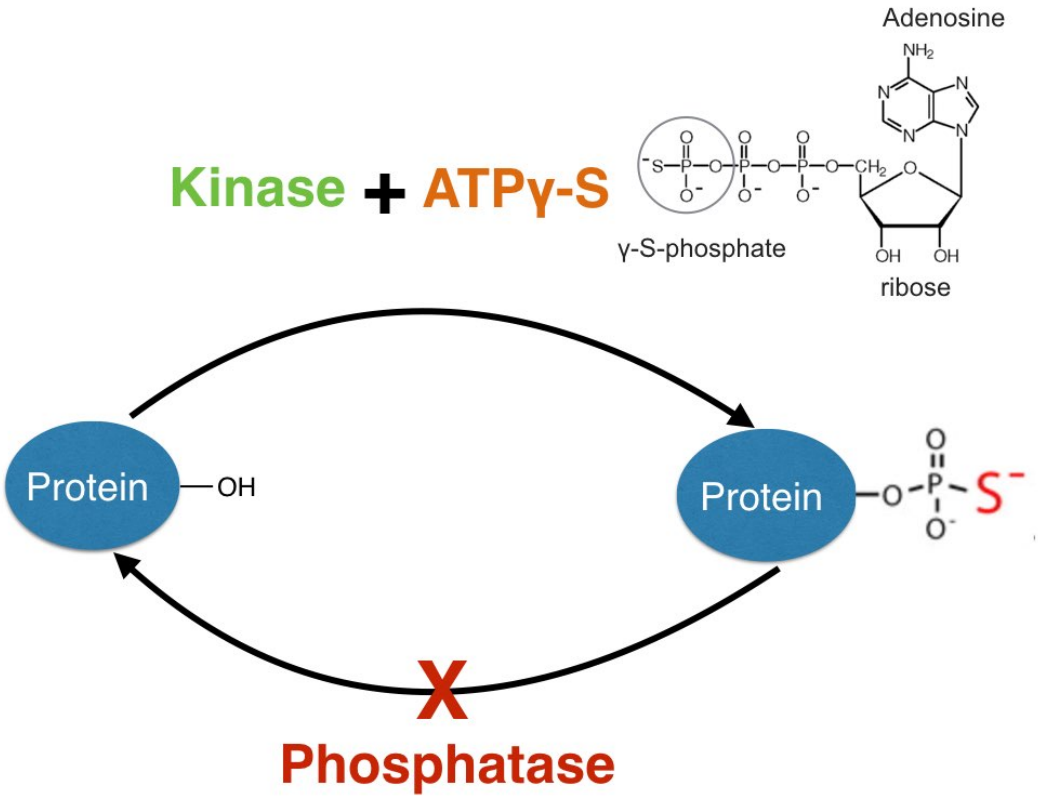

Figure 1.8: Thiophosphorylation reaction
Schematic representation of phosphorylation and dephosphorylation of a protein in the presence of ATP-γ-S

purify tyrosine phosphatases (Mei & Huganir 1991).

Initial studies were done with tyrosine phosphatases purified from post-synaptic membrane lysates using unhydrolysable thiophosphorylated substrates in a species of

electric ray called *Torpedo californica* (Mei & Huganir 1991). Conversely, mutations in the catalytic site of phosphatases led to substrate-trapping of associated proteins (Flint et al. 1997). However, these techniques have not been used to study serine-threonine phosphatases.

Another way of studying the effects of protein phosphorylation is generating phospho-mimetic mutants. The serine residues in the substrate can be replaced with aspartate or glutamate to impart the negative charge associated with phosphorylation. In some cases, this might generate a constitutively phosphorylated protein. However, these amino acids are much smaller and carry a single negative charge as opposed to the double negative charge in a phosphate group. Thus, they fail to recapitulate the steric nature of a phosphate moiety. On the other hand, thiophosphorylation does not have these shortcomings.

Therefore, thiophosphorylation was used to generate constitutively active Ensa and Arpp19. In this thesis, I have attempted to transfect the purified active protein to study its effects in mitotic entry. I have also attempted to purify interacting phosphatases from cell lysate using the thio-phosphorylated protein as a bait.

AIMS OF THE THESIS

At the beginning of this project, only preliminary data about Ensa and Arpp19 in mammalian cells was available. The aim of this project was to generate tools to characterise the mitotic function of Ensa and Arpp19 and to compare them to that of Greatwall as well as to determine if Ensa and Arpp19 are redundant in mammalian mitosis. This involved generating specific antibodies to study subcellular localisation and depletion phenotypes of Ensa and Arpp19 in human cells.

Moreover, the phospho-regulation of Ensa and Arpp19 was not explored when this project began. To initiate understanding of the biochemical interaction of Ensa/Arpp19, I investigated the formation of its complex with PP2A-B55 in the presence and absence of phosphatase inhibitors. In the meanwhile, data from our lab and the Goldberg lab describing Ensa/Arpp19 phosphorylation led us to test the 'unfair competition' model in intact mammalian cells and to perform a proteomic screen to identify novel phosphatases acting in the Ensa/Arpp19 dephosphorylation network.

Finally, I also generated dominant active Ensa/Arpp19 and attempted various approaches of protein transfection to analyse the effect of the constitutively active Ensa and Arpp19 in mammalian mitotic entry and exit.

Overall, this dissertation provides insights into the functions and phospho-regulations of Ensa and Arpp19 in mammalian mitosis.

CHAPTER2 MATERIALS AND METHODS

2.1 Materials

2.1.1 Chemicals, Biochemicals and Kits

All chemicals were obtained from Fisher Scientific (Leicestershire, UK) or Sigma-Aldrich (Missouri, USA) unless otherwise stated. Complete Protease Inhibitor Cocktails were from Roche Diagnostics (West Sussex, UK). The Eg5 inhibitor, S-trityl-L-cysteine (STLC) was purchased from Tocris Bioscience (Bristol, UK). All restriction enzymes used were from New England Biolabs (Beverly, USA).

2.1.2 Buffers

All buffers were prepared in ddH_2O, unless indicated otherwise. Buffers were frozen at –20°C and thawed soon before use.

a. Mitotic Lysis Buffer (Table 1.1)

The mitotic lysis buffer was prepared as previously described in by Cundell et al. (2013)

	Working Concentration	**Stock Concentration**
Tris HCl	50 mM	2 M
DTT	1 mM	1 M
$MgCl_2$	1 mM	1 M
$MnCl_2$	0.1 mM	500 mM
NaCl	50 mM	5 M
NP-40	1%	-
Protease inhibitor	1 tablet/50 ml	-

b. Immunoprecipitation Buffers (Table 1.2)

Flag-IP buffer

	Lysis Buffer	**Wash Buffer**	**Elution buffer**
Tris pH 7.5	20 mM	20 mM	20 mM
NaCl	137 mM	250 mM/500 mM	137 mM
Glycerol	10%	10%	10%
NP-40	0.5%	0.5%	0.5%
EDTA	2 mM	2 mM	2 mM
Flag peptide solution	-	-	0.5 µg/µl
Protease Inhibitor	1 tablet/50 ml	-	1 tablet/50 ml

GFP-IP buffer

	Lysis Buffer	**Wash Buffer**
Tris pH 7.5	20 mM	20 mM
NaCl	137 mM	250 mM/500 mM
Glycerol	10%	10%
NP-40	0.5%	0.5%
EDTA	2 mM	2 mM
Protease Inhibitor	1 tablet/50 ml	-

c. Bacterial protein purification buffers (Table 1.3)

His purification buffers

	Lysis Buffer	**Wash Buffer**	**Elution buffer**	**Stock**
Hepes	50 mM	50 mM	50 mM	2 M
NaCl	250 mM	250 mM	250 mM	5 M
TCEP	0.2 mM	0.2 mM	0.2 mM	0.5 M
Imidazole	20 mM	20 mM	250 mM	
Protease Inhibitor	1 tablet/50 ml	-	1 tablet/50 ml	-

GST purification buffers

	Lysis Buffer	**Wash Buffer**	**Elution buffer**	**Stock**
Tris pH 7.5	50 mM	50 mM	50 mM	2 M
NaCl	250 mM	500 mM	500 mM	5 M
EDTA	0.5 mM	0.5 mM	0.5 mM	0.5 M
DTT	1 mM	1 mM	1 mM	1 M
Glutathione	-	-	40 mM	0.5 M
Protease Inhibitor	1 tablet/50 ml	-	1 tablet/50 ml	-

Kinase Assay Buffer

	Lysis Buffer	**Wash Buffer**	**Elution buffer**	**Stock**
Tris pH 7.5	50 mM	50 mM	50 mM	2 M
EGTA	1 mM	1 mM	1 mM	0.5 M
$MgCl_2$	10 mM	10 mM	10 mM	1 M
Protease Inhibitor	1 tablet/50 ml	-	1 tablet/50 ml	-

d. Silver staining buffers (Table 1.4)

	Composition
Fix solution	50% MeOH, 12% acetic acid, 100 µl 37% paraformaldehyde solution/200 ml
Wash Solution	50% MeOH
Pre-treatment Solution	0.02% (w/v) $Na_2S_2O_3$
Silver Solution	0.2% (w/v) $AgNO_3$
Develop Solution	6% Na_2CO_3. 4 ml 0.02% $Na_2S_2O_3$, 100 µl 37% paraformaldehyde solution/200 ml
Stop Solution	50% MeOH, 12% acetic acid
Drying Solution	30% MeOH, 5% glycerol

2.1.3 Cell Culture

Transformed human cervical epithelial cancer cells (HeLa), human osteosarcoma cell line U2OS, Human embryonic Epithelial Kidney (HEK) 293T cells were used.
The HeLa derivatives, HeLa Kyoto cells, a kind gift from Dr. Mark Petronczki and HeLa CDK1_as cells, from Dr. W.C. Earnshaw's lab, University of Edinburgh.
The HeLa Kyoto cells stably expressing EGFP-alpha-tubulin and H2B-mCherry were a gift from the Dr. Eva Hoffmann. Dr. Thomas Stiff generated U2OS cells stably expressing *Xenopus laevis* CDK1_as and Stephy Joseph generated HeLa CDK1_as cells stably expressing RFP-H2B in the lab.

Cell culture reagents like DMEM and Foetal Bovine Serum were purchased from Invitrogen. Cell culture vessels and plates were from Corning (New York, USA)

2.1.4 Antibodies

Primary antibodies used for this study are enlisted in the Table 1.5.
Secondary antibodies used were HRP-conjugated (Horseradish peroxidase) rabbit, mouse or goat polyclonal antibodies from Dakocytomation (Cambridge, UK). For Immunoprecipitation blots, Mouse TrueBlot® ULTRA: Anti-Mouse IgG HRP from Rockland, USA was also used.
Alexa-flour® conjugated secondary antibodies for Immunostaining; Alexa488 anti-rabbit, Alexa488 anti-mouse, Alexa594 anti-rabbit, Alexa594 anti-mouse, Alexa647 anti-mouse were purchased form Invitrogen.

Primary Antibody	Raised in	Dilution for IB	Dilution for IF	Catalogue Number	Source
Anti-Ensa/Arpp19 EPR8008 (2)	Rabbit	1:200	1:100	ab180513	Abcam Ltd
Anti Greatwall	Rabbit	1:200		HPA027175	Sigma-Aldrich Company UK
Anti- α tubulin	Mouse	1:2000	1:1000	ab7291	Abcam Ltd

Anti- Actin	Mouse	1:1000		ab40864	Abcam Ltd
Anti-B55 alpha (2G9)	Mouse	1:100	1:200	sc-365282	Santa Cruz Biotechnology, Inc
Anti-B55 PAN (D10)	Mouse	1:100	1:200	sc-81606	Santa Cruz Biotechnology, Inc
Anti- PP1 (E9)	Mouse	1:100		sc-7482	Santa Cruz Biotechnology, Inc
Anti-Flag M2	Mouse	1:1000	1:500	F3165	Sigma-Aldrich Company UK
Anti-GFP	Rabbit	1:1000	1:500	A6455	Invitrogen
Anti-His	Mouse	1:1000		27-4710-01	GE Healthcare UK
Anti-GST	Mouse	1:1000		G7781	Sigma-Aldrich Company UK
Anti-phospho-Ensa	Rabbit	1:100	1:100	Clone 73	Eurogentec
Anti-phospho-Gwl	Rabbit	1:100	1:100		Hochegger Lab
Anti-Ensa	Rabbit	1:100			Eurogentec
Anti-Arpp19	Rabbit	1:100			Eurogentec
Anti-Thiophosphate Ester	Rabbit	1:1000		ab92570	Abcam Ltd.
Anti phospho-histone H3	Rabbit	1:500 (FACS)		06-570	Merck Millipore (UK) Ltd.

2.2.2 Primers

cDNA and genomic DNA sequences were obtained from the National Centre for Biotechnology Information website (NCBI; http://www.ncbi.nlm.nih.gov/). Primers were designed according to cloning requirements using Lasergene SequBuilder 10.1 DNASTAR (Madison, USA) and Serial Cloner 2.5, http://serialbasics.free.fr. Primers were ordered from Eurofins MWG Operon (Ebersberg, Germany) or GATC Biotech (London, UK). The primers used in this study are listed in the Table 1.6.

Primers	Sequence (5'-3')
att Arpp19 F+R Gateway cloning primers	GGGGACAAGTTTGTACAAAAAAGCAGGCTTAatgtct gcggaagtccccga GGGGACCACTTTGTACAAGAAAGCTGGGTCtcagcca gccagcttgctagcaac
att ENSA F+R Gateway cloning primers	GGGGACAAGTTTGTACAAAAAAGCAGGCTTAtcccag aaacgagaagaagag GGGGACCACTTTGTACAAGAAAGCTGGGTCtcattcaa cttggccacccgcaagc
FlaghENSANde1F hENSA EcoRV rev For cloning Flag Ensa into pthreeE and ptwoE vectors	catatggattacaaggatgacgacga gatatcTCATTCAACTTGGCCACCCG
Nde1 Flagarpp1F Arpp19 BamH1R For cloning Flag Ensa into pthreeE and ptwoE vectors	GGTGGTCATATGgattacaaggatgacg TATATAGGATCCtcagccagccagcttgc
GFP ensa_fwd gb	gacgagctgtacaagtccggaGGCGCCTCAGCGGCATCA

GFPensa_rev gb For GFP Linker Ensa construct in pEGFP C1	agctcgagatctgagtccggaTCATTCAACTTGGCCACCCGC
Ensa_Linker_fwd Ensa_Linker_rev For Ensa Linker GFP construct in pEGFP N1	cgggcccgggatccaccggtATGTCCCAGAAACAAGAAGAA GAGAACCCTG tcaccatggtggcgaccGGTGCGGCCGCTGAGCCA
PP2AB55alpha F+R	tatatagggaattcgATGGCAGGAGCTGGAGGAGGG tatataggatccCTAATTCACTTTGTCTTGAAA

2.1.5 Vectors

Vectors used in this work are listed in the Table 1.7.

Vector	Source	Features	Notes
pDONR™221	Invitrogen	Att sites P1, P2	For cloning of Ensa and Arpp19 full-length cDNA and use with the Multisite Gateway®system from Invitrogen
pDEST17		T7 promoter	Bacterial expression vector for N-terminal HIS tagging of Ensa and Arpp19
deltaT-FLAG-DEST	A kind gift from Stephan Geley (Biocenter,	EFIa promoter; tet-repressible	Mammalian expression vector for N-terminal flag-tagged Ensa and Arpp19.
pGEX-SG-DEST		Tac promoter, Prescission	Bacterial expression vector for N-terminal GST tagging of

	Innsbruck Medial University, Austria)	cleavage	Ensa and Arpp19
pEGFP-C-DEST		CMV promoter	Mammalian expression vector for N-terminal GFP-tagged Ensa and Arpp19.
pEGFP-C1	Clontech	CMV promoter	Mammalian expression vector for N-terminal GFP-tagged Linker-Ensa construct.
pEGFP-N1		CMV promoter	Mammalian expression vector for C-terminal GFP-tagged Ensa-Linker construct.
p2E -3	A kind gift from Dr. Tony Oliver (GDSC, University of Sussex, UK)		Bacterial expression vector for N-terminal His tagging of Flag-Ensa and Flag-Arpp19
p3E- 7			Bacterial expression vector for N-terminal GST tagging of Flag-Ensa and Flag-Arpp19
Flag B55 alpha	Addgene		Flag-B55alpha was cloned into the mammalian expression vector pMIG using the BglII and EcoRI sites
Linker-Ensa		cDNA was synthesised by Addgene	Linker-Ensa gene was cloned into pUC57 vector using XbaI and BamHI sites
Ensa-Linker			Ensa-Linker gene was cloned into pUC57 vector using XbaI and BamHI sites

2.1.6 siRNA sequences

siRNA oligonucleotides were ordered from Qiagen or from Dharmacon, GE Healthcare as smart pools (Table 1.8).

Name	Catalogue number	Source	siRNA sequence
ARPP19	J-015338-05	Dharmacon smart pools, GE Healthcare	CAAGCUGGCUGGCUGAUUA
ARPP19	J-015338-06		CAACAUGGCUAAAGCAAAA
ARPP19	J-015338-07		GUUCAGAUUUCUUAAGGAA
ARPP19	J-015338-08		GCACAAGAGUUCCUACACA
ENSA	J-011852-05		GCUAAAGGCCAAAUACCCA
ENSA	J-011852-06		AGAGAGCUGAAGAGGCAAA
ENSA	J-011852-07		UGAAGAGACUCCAGAAAGG
ENSA	J-011852-08		AGGACACGCAGGAGAAAGA
Non Targeting siRNA pool	D-001810-10		UGGUUUACAUGUCGACUAA UGGUUUACAUGUUGUGUGA, UGGUUUACAUGUUUUCUGA, UGGUUUACAUGUUUUCCUA
PPP2CA	J-003598-09		CCGGAAUGUAGUAACGAUU

	J-003598-10		ACAUUAACACCUCGUGAAU
	J-003598-11		UCAUGGAACUUGACGAUAC
	J-003598-12		CAGGUAGAGCUUAAACUAA
PPP2CB	J-003599-07		CACGAAAGCCGACAAAUUA
	J-003599-08		UUUAGUAGAUGGACAGAUA
	J-003599-09		CCAGAACGCAUUACAAUAU
	J-003599-10		GAACCAGGCUGCUAUCAUG
Hs_MASTL_6	SI02653014	Qiagen	ACGCCTTATTCTAGCAAATTA
Hs_PPP2R2A_5	SI0222582		CTGCAGATGGATTTGCGGATTA
Hs_PPP2R2D_5	SI02759148		TTCATCCATATCCGATGTAAA

2.2 Methods

2.2.1 Molecular Biology

a. Bacterial Culture and Plasmid preparation

Individual colonies were picked from LB (Luria Bertani medium; 0.5% yeast extract, 1% tryptone and 171 mM sodium chloride (NaCl)) agar plate containing appropriate selective antibiotics (kanamycin was used at 50 μg/ml and ampicillin was used at 100 μg/ml). To prepare small amounts of plasmid deoxyribonucleic acid (DNA), 3 ml LB cultures containing the appropriate selective antibiotics were incubated overnight at 225 revolutions per minute (rpm) and at 37°C. Cells were harvested by centrifugation at 4000 rpm for 5 min. The plasmid DNA was then purified from the cells using the alkaline lysis method following the manufacturer's protocol with the QIAprep Spin Miniprep Kit using microcentrifuge from QIAGEN (West Sussex, UK). Plasmid DNA was eluted in 50 μl ddH2O and the concentration was analysed by measuring the absorbance at 260 nm on a spectrophotometer and confirmed by restriction digestion and sequencing. Restriction digests were performed according to manufacturer's instructions and as recommended by the New England Biolabs website (https://www.neb.com/) and analysed by agarose gel electrophoresis. DNA was sent to GATC Biotech for sequencing and then analysed using Lasergene SequBuilder 10.1 DNASTAR.

For preparation of larger quantities of plasmid DNA for transfection into human cells, 5-ml starter cultures were grown for 8 h at 225 rpm/37°C. Then, 100 μl of the starter cultures were used to inoculate 100 ml LB containing appropriate selective antibiotics, which were incubated at 225 rpm and at 37°C overnight. Cells were harvested by centrifugation at 4000 rpm and at 4°C for 20 min. The plasmid DNA was then purified from the pelleted cells again using the alkaline lysis method following the manufacturer's protocol with the QIAFilter Plasmid Midi Kit from QIAGEN. The concentration of the purified plasmid DNA was then measured and the presence of the expected plasmid DNA confirmed by restriction digestion and sequencing.

b. Transformation of Recombinant Plasmids in Bacteria

Competent DH5α *Escherichia coli* were thawed on ice for a few minutes. Fifty-microliter aliquots were used per transformation; 50–100 ng of plasmid DNA was used and the bacteria were added to the DNA and mixed gently, followed by incubation on ice for 20 min. The tubes were then heat-shocked at 42°C for 45 s and incubated on ice for 2 min to help the cells to recover. Two hundred microliters of warm SOC media was added to the cells and mixed gently. The tubes were incubated for further 1 h in at 37°C in a water bath. After this, 50–200 µl of the cell culture were plated onto LB agar plates with appropriate selection antibiotics and placed at 37°C overnight. For transformation of the Gibson, Gateway and traditionally ligated plasmids, the entire suspension was spun down and the supernatant was removed to leave a 50 µl concentrated suspension, which was then plated onto LB plates.

c. Cloning, PCR and RT-PCR

All DNA extractions were performed using QIAprep Spin Miniprep from QIAGEN and all restriction digests were performed using restriction endonucleases and buffers from New England Biolabs (NEB). All ribonucleic acid (RNA) extractions were performed using the Phusion High-Fidelity PCR Kit from Finnzymes (Waltham, USA). Reverse – transcriptase PCRs (RT-PCRs) were performed using the SuperScript™III One-Step RT-PCR System from Invitrogen. Ensa and Arpp19 cDNA was amplified from HeLa messenger RNA (mRNA) using the *att* Ensa19 F+R and *att* Arpp19 F+R respectively. They were then cloned into the entry vector pDONR™221 using the Gateway cloning method. The entry clone was then used to generate tagged Ensa and Arpp19 using different destination vectors.

The Flag-Ensa and Flag-Arpp19 constructs were used as templates to PCR the Flag-tagged cDNA with different enzymes. The PCR products were then ligated using the Quick Ligation™ Kit from NEB into the p3E and p2E vectors used for bacterial purification.

PP2A B55-alpha was amplified from the pMIG-B55alpha plasmid and ligated into pEGFP-C1 with EcoRI and BamHI sites using Quick Ligation™ Kit from NEB. The

Linker-Ensa and Ensa Linker cDNA were cloned into pEGFP-C1 and pEGFP-N1 respectively using the Gibson Assembly® Master Mix from NEB.

d. Agarose Gel Electrophoresis and Gel Extraction

DNA was separated using 1% Agarose gels by electrophoresis in TAE (40 mM Tris base, 1 mM ethylene diamine tetraacetic acid (EDTA) and 20 mM acetic acid) for bands ≥ 1000 kB and TBE (45 mM Tris borate and 1 mM ethylene diamine tetraacetic acid (EDTA) for bands <1000 kB. The gels were visualized using the gel imaging system InGenius LHR from Syngene (Cambridge, UK). The 1 kB/+ DNA ladder from NEB was used to confirm the size of the DNA fragments. The manufacturer's protocol was used to purify DNA using the QIAquick Gel Extraction Kit from Qiagen. The DNA fragments were eluted in ddH_2O.

e. Gateway Cloning

In this work, MultiSite Gateway® technology from Invitrogen was used to manipulate the cDNA of Ensa and Arpp19 to generate various tagged versions of the protein. This technology takes advantage of the lambda phage recombination system to allow transfer of cloned DNA between site-specific *att* recombination sequences on different vectors. Recombination is conservative and does not require any DNA synthesis. Once the cDNA has been cloned into the entry vector in this system, it can be transferred to several other destination vectors, i.e. expression vectors, for protein purification or protein tagging.

In order to create an entry clone with the Ensa or Arpp19 cDNA, the appropriate *att* recombination sequences were added to the cDNA by RT-PCR using the primers *att* Ensa F+R and *att* Arpp19 F+R respectively (listed in section). A BP reaction was then performed following the manufacturers' recommended protocol using Gateway® BP Clonase II Enzyme Mix to move the cDNA into the pDONR™221 vector (Invitrogen), creating the entry clones. This was then subsequently used for further cloning step by performing an LR reaction using the Gateway® LR Clonase II Enzyme Mix (Invitrogen) with various destination vectors to yield the different constructs detailed throughout this work. Details of all reactions can be found in the Gateway®

Technology with Clonase II Manual available on the Invitrogen website (www.invitrogen.com).

f. Gibson Assembly

For this work, the Gibson Assembly Cloning Technology from NEB was also used to generate GFP-tagged versions of Ensa and Arpp19 with a linker separating the tag and the cDNA. Dr. Daniel Gibson and his colleagues developed Gibson Assembly, which method allows efficient joining of multiple overlapping DNA fragments in a rapid single tube isothermal reaction at 50°C. The reaction Master Mix includes three different enzymes for three different enzymatic reactions in one buffer. First, the *5' exonuclease* chews the 5' end sequences to create single stranded 3' end complementary sequence to facilitate annealing. Then the *DNA polymerase* with the 3' extension activity fills the gaps between the complementary annealed fragments. The DNA ligase then seals the nicks and covalently links the DNA fragments together. The PCR fragments for Linker-Ensa were amplified using the GFP ensa_fwd gb and GFPensa_rev gb and for Ensa-Linker using the Ensa_Linker F+R primers (Listed in Table 1.6). The Linker-Ensa and Ensa-Linker plasmids created by Addgene were used as templates for the PCR reaction. The PCR products and the linearized destination vectors (pEGFP-C1 and pEGFP-N1) were mixed in the appropriate ratio and the Gibson Assembly reaction was done as per the manufacturers' protocol Listed in Table.

g. Sequence Alignments

All sequence alignments were carried out using CLUSTAL Omega Version 1.2.1 using the Multiple Sequence Alignment Tool on the European Bioinformatics Institute website (http://www.ebi.ac.uk/).

2.2.2 Biochemical methods

a. Western Blotting

Cells were lysed in Mitotic Lysis Buffer (50 mM Tris-HCl [pH 7.35], 150 mM NaCl, 1% [vol/vol] IGEPAL, 1 mM dithiothreitol, and protease inhibitor cocktail [Sigma-Aldrich, P8340]) and 1X SDS sample buffer was added to it. The samples were then sonicated at high power with 0.5-s intervals using a Bioruptor (Diagenode, Cambridge, UK) for about 10–20 s. Samples were then boiled at 95°C for 5 min and run on SDS-polyacrylamide gels by electrophoresis using Bio-Rad Mini Protean III System from Bio-Rad in running buffer along with a ColorPlus Prestained Protein Marker (Broad-Range, New England Biolabs). The samples were allowed to run through the stacking gel to the resolving gel at 200 V for about 35–40 min. The protein was then transferred by electro-blotting onto a nitrocellulose PVDF membrane (Amersham Hyperfilm ECL 18 × 24 cm 100 sheets, Scientific Laboratory supplies Ltd.) using the semi-dry system Trans-Blot® TurboTM Blotting System, BioRad. Stacks of filter papers were immersed in Anode 1, anode 2 and Cathode solution and the PVDF membrane was activated with methanol before making the transfer sandwich with the gel. Protein bands were then visualized using Ponceau S solution. The membranes were washed in PBS with 0.1% NP40 and blocked with 5% milk (Marvel with PBS-0.1% NP40) for about an hour at room temperature. Antibodies were diluted in 5% milk or 3% BSA (BSA; with PBS-0.1% NP40), and secondary HRP-conjugates rabbit, mouse or goat polyclonal secondary antibodies were used at recommended concentrations. Proteins were then visualized with the homemade Luminol, Enhancer and Hydrogen peroxide mix as per the protocol. For antibodies with reduced or faint signal, Super sensitive ECL (SUPERSIGNAL WEST FEMTO MAX, Thermo Scientific, UK) was used by diluting in the homemade ECL mix as per requirement. The membrane was exposed to Hyperfilm ECL (Amersham) and processed using an automatic X-ray film processor (ECOMAX, PROTEC GmbH & Co. KG).

b. Antibody Generation

Ensa and Arpp19 specific antibodies were custom made by Eurogentec for this study. The N-terminal bit of the protein has significant dissimilarities, which were exploited to

map a peptide with minimal sequence cross-alignment. This peptide sequence was sent to Eurogentec. They provided us with the initial and final bleeds and the affinity-purified antibodies. The purified antibodies were used in this study to analyse their specificity towards these similar small proteins.

c. Immunostaining

Cells were seeded on glass coverslips (18 mm), prior to fixation. For immuno-staining of over-expressed proteins, the transfection was done on cells seeded on coverslips. Post-transfection or once the cells reached 60%-80% confluency, the media was aspirated and cells were washed with warm PBS. The cells were then fixed with 3.7% freshly made Paraformaldehyde (F1635 Formaldehyde solution, Sigma) for 10 min at room temperature. The fixed cells were next washed with PBS three times for 5 min. For some antibodies, the cells were then treated with ice-cold methanol at -20°C for 30 s to 1 min. the cells were then washed with PBS three times and then permeabilised using PBS 0.1% NP40 for 15–20 min. After this, the cells were blocked for 30 min at room temperature in 3% BSA-PBS and incubated for 1 h with primary antibodies made up in 3% BSA-PBS. The cells were then washed with PBS three to five times and incubated in secondary antibodies diluted in 3% BSA-PBS for 1 h at room temperature. The cells were washed again with PBS before being mounted onto standard laboratory slides faced down with 5-µl Prolong® Gold mounting solution with DAPI with (ProLong® Diamond Antifade Mountant, Thermo Fisher, UK) and allowed to set for at least 16 h at 4°C.

d. FACS Analysis

Flow cytometry was used to analyse and sort cells stained with fluorescent antibodies or expressing fluorescent proteins. Sorting was done to determine the cell cycle profile according to DNA content by Propidium iodide (PI staining) and the expression of various proteins stained with different antibodies.

Cells were fixed in 70% methanol for at least 16 h at 4°C. Cells were then centrifuged at 1500 rpm for 5 min and rinsed in 0.5 ml of 3% BSA-PBS. For staining mitotic cells, the cells were incubated with anti-phospho-histone H3 antibody made in 3% BSA-PBS for 1 h at room temperature. The cells were then washed with 3% BSA-PBS two times and

resuspended in secondary FITC-labelled anti-rabbit antibody at 1:2000 for 1 h in the dark. The cells were again washed with 3% BSA-PBS two times. After this, they were re-centrifuged and resuspended in 3% BSA-PBS with 5 µg/ml Propidium iodide to stain the DNA and 1 µg/ml RNAse. These were analysed on a BD Accuri machine from BD Biosciences (Oxford, UK). The BD Accuri software (BD Biosciences) was used to plot PI -intensity (FL-2) versus cell count and FITC-phospho-histone H3 intensity (FL-1) versus PI-intensity (FL-2) to determine mitotic index.

e. Immunoprecipitation

i) Immunoprecipitation from overexpressed proteins

Cells were harvested by trypsinisation after transfection of Flag tagged constructs in Hek293 or HeLa cells. The cells were resuspended in 25 µl of chilled IP lysis buffer and incubated on ice for 20 min. The cell lysates were then clarified by spinning them at 1300 rpm for 30 min at 4°C and the supernatant was transferred to new tubes. Total protein was equalised using the Bio-Rad Protein Assay Reagent (Bio-Rad) and measuring absorbance at 600 nm. A 50-µl sample of the whole cell equalised lysate was kept and SDS-sample buffer was added for evaluation by immuno-blotting. The Anti Flag M2 Magnetic beads were prepared by washing two times with IP buffer on a chilled magnetic stand. The equalised whole cell lysate was then incubated with 20 µl of equilibrated beads, resuspended in IP buffer for 1 h with end over end rotation at 4°C to capture the Flag-Ensa/Arpp19 protein. After this, the supernatant was removed from the beads using chilled magnetic stand and the beads were then washed two times with High Salt IP buffer. Next, the beads were resuspended in 20 µl of the Elution IP buffer and incubated at 4°C in a Falcon tube on a roller for 30 min. The elution was done twice with 20 µl of Elution Buffer each time. The eluates were then pooled in a new tube and either used for immuno-blotting with SDS-sample buffer or for Size-exclusion chromatography.

ii) Immunoprecipitation using recombinant proteins and cell lysates

Cells were seeded in 10 cm dish until they were 50% confluent. Cells were then treated with 5 µM STLC for 16–18 h to arrest them in mitosis (metaphase). The following day, the cells were collected by mitotic shake-off and counted. Half of the cells were

resuspended in media containing 5 µM 1NMPP1 and 5 µM STLC to induce mitotic exit and were incubated at 37°C for 30 min. The mitotic and mitotic exit samples were used for immunoprecipitation at 7 x 10^6 per condition. The respective cells were centrifuged at 1500 rpm for 5 min and lysed with 200 µl of Mitotic lysis buffer for 20 min on ice. The protein concentration was measured using Bio-Rad Protein Assay Reagent (Bio-Rad) and measuring absorbance at 600 nm. The protein concentration was maintained between 10 mg/ml to 20 mg/ml using this method. The cell lysates were clarified by centrifuging at 13000 rpm for 30 min. Two hundred nanograms of recombinant protein, Flag Ensa/Arpp19 (non-phosphorylated or thio-phosphorylated) was added to the whole cell lysates and incubated at 37°C for 30 min to allow protein-protein interaction with the recombinant protein. During this time, 20 µl of Anti-Flag M2 Magnetic beads were equilibrated, by washing once with High Salt Mitotic lysis buffer and once with Mitotic lysis buffer for 5 min using a chilled magnetic stand. They were then resuspended in 300 µl of mitotic lysis buffer. The protein-lysate mixture was added to the equilibrated beads and incubated for 1 h at 4°C with end over end rotation to re-capture the Flag Ensa/Arpp19 protein. The supernatant was then removed from the beads using chilled magnetic stand. The beads were washed with High Salt Mitotic lysis buffer twice for 5 min. They were then resuspended in 25 µl of Mitotic Elution buffer and incubated at 4°C in a Falcon tube over a roller.

f. Size Exclusion Chromatography

Analytical size-exclusion chromatography experiments were performed on a calibrated Superose 6 3.2/300 (GE Healthcare Cat: 29-0915-98) Column in the presence of the IP buffer run at a flow of 0.04 ml/min at 4°C in a cold cabinet. Sample injection volume was 50 µl for all runs (samples + controls). Elution of proteins was monitored at $A_{280\ nm}$. To detect complex formation, the elutions from immunoprecipitation were injected through the column. Fraction collection was 50 µl each and analysed by SDS-PAGE, Coomassie staining and western blotting.

Calibration standards were run using the same settings as with the samples. The proteins used for calibration were Thyroglobulin (669 kDa), Ferritin (440 kDa), Aldolase (158 kDa), Conalbumin (75 kDa) and Carbonic Anhydrase (29 kDa), all from Gel Filtration Calibration Kit (GE Healthcare). Void volume of the column was determined using

dextran blue (GE Healthcare). Calibration curve plot, formula and statistics are shown in the figure.

g. Silver Staining

The SDS-PAGE gels were first incubated in the Fix solution for at least 1 h. After fixing, gel was washed with 50% methanol (Wash solution) thrice for 8 min. The gel was then sensitized with 0.02% sodium thiosulphate for exactly 1 min. Following sensitisation, the gel was washed three times with MilliQ water for 20 s each time and then stained with silver staining solution for 20 min. Before developing, the gel was washed two times with distilled water for 20 s. The bands were developed with developing solution. Development was stopped with stop solution once the bands were clearly visible and staining was stopped, by treating with Stop solution for 10 min. To preserve the gel between sheets of porous plastic, wash the gel with Wash Solution for 2 x 10 min. Then incubate the gel with Drying Solution for a maximum of 1 h (the glycerol will begin to leach out the silver after 1–2 h).

h. In-gel Trypsinisation and Mass Spectrometry

The elutions form IP were run on SDS-PAGE and stained with InstantBlue-Protein Stain (Expedeon). The gel band of interest was excised using a surgical razor blade and transferred to a 0.6 mL low retention Eppendorf microcentrifuge tube. Staining was removed by two consecutive washes with 50% acetonitrile and 25 mM ammonium bicarbonate solution for 5 min with shaking. The sample was then dried to completeness for 5 min in a speed vac. The gel pieces were rehydrated with 10 mM DTT solution for 45 min at 50°C. Once the gel pieces return to room temperature, the liquid was replaced with 50 mM iodoacetamide in 25 mM NH_4HCO_3. The gel pieces were dehydrated as before with 50% acetonitrile and 25 mM ammonium bicarbonate solution for 5 min with shaking. The sample was then dried to completeness for 5 min in a speed vac. Then, 20 µl of trypsin reaction buffer (12.5 ng/µl trypsin in 25 mM NH_4HCO_3 was added and incubated on ice for 5 min. The solution was then replaced with 25 mM NH_4HCO_3 and incubated at 37°C overnight (or for 4 h at least). Formic acid was added for a final concentration ~5%. The peptides in the solution were removed into a clean tube after vortexing. Next, 1X volume of acetonitrile, i.e. equal to the volume of gel

pieces, was added and shaken for 5 min. The supernatant was then removed and added to the peptides. The process was repeated if gel pieces did not look dehydrated. When the entire sample needed to be loaded in one go, the volume of peptide eluates were reduced to ~8 µl using speed vac, with low or medium heat setting. This takes at least 30 min depending on volume and heat setting. Next, 0.1% FA was added to get a volume of ~8 µl when necessary. Storage was done at -20 or -80°C.

i. Protein identification and quantification

Peptide samples were analysed by Nano-LC-MS (Thermo Fisher U3000 nanoLC and Orbitrap XL mass spectrometer). Data were acquired using the Xcalibar v2.1 software. The raw data files were processed and quantified using MaxQuant version 1.5.5.1 and searched against the SwissProt human proteome database. The proteingroups.txt file from MaxQuant was loaded to Perseus version 1.5.5.3. The protein list was filtered on categorical and text annotations to remove reverse hits, proteins only identified by site, and contaminants. Log_2 transformation of LFQ Intensity values was performed before comparison between the mentioned data sets by two-sample *t*-test using permutation-based FDR ($P < 0.05$) and fold-difference (S0 > 2).

2.2.3 Cell Culture

a. Thawing Cells

Cells frozen at -80°C or -170°C (Liquid nitrogen stocks) were allowed to thaw at 37°C in a water bath. These cells were then added to 10 ml of warm media in falcon tubes and centrifuged for 5 min at 1500 rpm. The media was aspirated and cell pellet was resuspended in 10 ml of fresh warm media. The cells were then plated onto a T75 flask and incubated at 37°C and under 5% CO_2 for 1 or 2 days before passaging them.

b. Cultivating Cells

Cells were cultured in DMEM supplemented with 2 mM L-glutamine, 10% Foetal Calf Serum (FCS) and 1% Penicillin G (sodium-salt)-Streptomycin in saline solution. The cells were plated in their respective culture vessels and incubated in 37°C and 5% CO_2 incubators. Trypsin-EDTA (Gibco™) was used to trypsinise and passage cells.

c. Counting Cells

Cells were trypsinised using 0.5 mg/ml of trypsin, to detach them from the cell culture vessels for 5 min at 37°C. They were then resuspended in appropriate volume of warm media to stop the enzymatic action of trypsin and mixed by pipetting. Eight microliters of the cell culture was placed on Neubauer's chamber and cells were counted under a bright-field/phase-contrast microscope. The 'Neubauer' chamber is a glass slide with an etched grid, defining a specific volume. Four large squares (of 1 mm^2 each) further divided into 16 smaller squares of equal dimension can be observed when seen under a light microscope. The chamber is cleaned, dried and placed on a flat surface and covered with a coverslip. Next, 8–10 µl of the cell suspension is carefully introduced by placing the tip closer to the edge of coverslip at the centre of the chamber. Care should be taken to avoid air bubbles. Cells in the four large squares were counted and cell counts per ml were calculated using the formula below

Total cells per ml = (Total cells counted/4) X dilution factor X 10^4

d. Freezing Cells

Cell stocks were prepared by centrifuging trypsinised cell cultures at 1500 rpm for 5 min. The cell pellets were then resuspended in 0.5 ml of freezing media (FCS, 10% DMSO) and added in cryo-vial. To achieve -1°C/min cooling rate, the cryo vials were placed in "Nalgene ^{TM} 1°C cryo freezing container" filled with isopropanol at -80°C overnight. The cells were then transferred to the -80°C stock or liquid nitrogen shelves for long-term storage.

e. Inhibitor Treatment

Cells were treated with different inhibitor to arrest them in different cell cycle phases. Cells were treated with 100 ng/ml of Nocodazole or 5 µM of STLC (S-trityl-l-cysteine) for 16–18 h for a mitotic arrest. Cells were treated with varying concentrations of phosphatase inhibitors like Okadaic Acid. Cells stably expressing the CDK1_as gene were arrested in G2 using 1NMPP1 inhibitor in varying concentrations for 18–20 h. For these treatments, the media was aspirated and replaced with the drug containing media and mixed thoroughly by pipetting.

f. Plasmid Transfection

i) $CaCl_2$ transfection in Hek293 cells

Cells were seeded into 10 cm^3 culture dishes at 0.75 x 10^6 in 10 ml media. Cells were transfected the next day using calcium phosphate precipitation method. For this, 5 µg of plasmid DNA was added to 61 µl of 2 M calcium chloride ($CaCl_2$) and sterile water was added up to 500 µl. This solution was added drop wise to 500 µl of 2X HEPES-Buffered Saline Solution (HBSS) (12 mM dextrose, 50 mM HEPES, 10 mM KCl, 280 mM NaCl, 1.5 mM disodium hydrogen phosphate dihydrate (Na2HPO4. 2H2O)) while bubbling gently using a glass Pasteur pipette and electronic pipette to mix. The 1-ml solution was then immediately added drop wise to the cells and swirled to mix. The next day the precipitate-containing medium was removed, the cells washed with PBS and fresh medium added back. Samples were collected 48 h following the transfection.

ii) Jet-Pie transfection in HeLa_CDK1_as cells

Cells were seeded into 10 cm^3 culture dishes at 1.5 x 10^6 in 10 ml media. Cells were then transfected the following day using the Jet-Pie (Polyethylenimine, Linear, MW 2,500 (PEI 2500)) method. For this, 15 µl of Pie reagent was added to 250 µl of 150 mM sterile NaCl in a tube. Similarly, 5 µg of DNA plasmid was added to 250 µl of 150 mM sterile NaCl in another tube. The contents in both the tubes were mixed well by vortexing and the DNA mix was then added to the transfectant tube and mixed. The DNA-PIE mixture was then incubated at room temperature for 15–20 min. During this time media was aspirated from the cells and 5 ml of fresh media was added. After

incubation, the DNA-PIE mixture was added drop-wise to the cells and incubated at 37°C for 4–6 h. The media was then aspirated, and fresh 10 ml warm media was added, followed by incubation of the cells for 24 h. The transfection was performed again after 24 h of incubation and the cell lysates were collected after 48 h of the second transfection.

iii) Lipofectamine™ 2000 transfection

Cells were trypsinised and diluted to a concentration of 3.5 x 10^5 cells /ml. Two millilitres of the cell suspension was plated into a well of 6-well plate. The DNA-transfectant mixture was prepared as follows

	Lipofectamine™ 2000	Plasmid DNA	Serum Free-Media
Tube 1	2.5 µl		200 µl
Tube 2		2 µg	200 µl

Tube 1 was added to tube 2 and mixed well by pipetting. The DNA-Lipofectamine complex was incubated for 15–20 min at room temperature. The complex was then added drop-wise on the cells. The cells were incubated for 24–48 h and then used for further analysis.

g. siRNA Transfection

siRNA transfection was done by a technique called Reverse transfection. For this technique, trypsinised cells at the concentration of 1 x 10^5 cells /ml were used. The siRNA mixture with Lipofectamine™ RNAiMAX was prepared as follows:

siRNA concentration	Lipofectamine™ RNAiMAX	Serum Free-Media
40–50 nM (total)	5 µl	Up to 500 µl

This mixture was incubated at room temperature for 20 min and then mixed with 2 ml of the cell culture. The cells-siRNA mix was then plated into 6-well dish. Cells were then grown at 37°C for 48 to 72 h before the lysates were collected for immunoblotting. (Table 1.8) enlists the sequences of siRNA oligos used in this study.

2.2.4 Microscopy

a. Time Lapse Imaging

Time-lapse imaging was done using the IX71_Olympus or the IX73_Olympus microscope. The microscopes were equipped for differential interference contrast imaging and with different filter units for epifluorescence microscopy. For live imaging, the microscope was further equipped with a CO_2 incubator and a heating plate (temperature control 37°C). Micromanager software enabled full-control of the microscope, allowing acquisition of time-lapse movies, Z-series, as well as image manipulation, 3D reconstructions or quantitative analysis.

b. Quantification of Mitotic cells and Phenotypes

Mitotic index was calculated by counting cells on ImageJ. Time in mitosis was quantified from nuclear envelope breakdown (NEBD) until telophase. Online tool at http://boxplot.tyerslab.com was used to generate boxplots to depict mitotic time. Images were cropped an adjusted for brightness and contrast using Omero WebClient and appropriate scale bars were added.

2.2.5 Protein Expression, Purification and Transfection

a. Protein Purification from Bacteria

His-Ensa/Arpp19 and GST-Ensa/Arpp19 were cloned using the Gateway technology. GST-Flag Ensa and GST-Flag Arpp19 were traditionally cloned into the p3E vector. These vectors were transformed in *E.coli* Rosette strains. Transformed colonies were used to inoculate 20 ml culture of LB medium supplemented with appropriate

antibiotics overnight. This culture was used to inoculate a 1-L flask of LB broth supplemented with appropriate antibiotics. Cultures were grown in an orbital shaking incubator until the optical density at 600 nm reached ~0.8, and then induced with 1 mM isopropyl-thio-β-galactoside (IPTG) at 18°C overnight. Fifty-microliter aliquots were kept and SDS-sample buffer was added to them to analyse the over-expression of the protein before and after induction. They were then harvested with 25 ml Bacterial lysis buffer per litre of culture and sonicated at 30% amplitude for 1 min with a 5-s on-off cycle. The lysates were then clarified at 20,000 rpm for 1 h by centrifugation. Aliquots of the lysates were kept and SDS-sample buffer was added to them to analyse the effect of sonication on the over-expressed proteins. His-tagged proteins were purified using Nickel-NTA Agarose beads (Qiagen) and were eluted using 1 M Imidazole. The GST-Tagged proteins were purified using the Glutathione Sepharose Beads (GE Healthcare) and eluted using 10 mM Glutathione. One-millilitre beads per litre of culture was equilibrated, by washing them twice with 20 volumes bacterial lysis and centrifuging them at 400*g* for 5 min. The clarified lysates were added to the equilibrated beads and incubated for 1–2 h on a roller at 4°C. After the binding, the unbound fraction was separated from the beads and they were washed with 20 volumes of Bacterial wash buffer with high salt. The bound protein was eluted by adding 1 ml at a time of the respective elution buffers and incubated at room temperature for 10 min. The beads were then centrifuged at 400*g* for 5 min and the elutions were collected. Aliquots were kept from each elution and SDS-page sample buffer was added to identify the elution containing the protein of interest. Elutes containing the protein of interest in high amounts were pooled and dialyzed into the Kinase buffer for *in vitro* thiophosphorylation.

b. *In vitro* Thiophosphorylation of Recombinant Ensa and Arpp19

The ratio between substrate and kinase is of key importance in an in-vitro phosphorylation reaction. At a given time, 0.5 mg of purified Ensa/Arpp19 was successfully thio-phosphorylated using 2 µg Gwl-E2. Maximum phosphorylation was obtained in 5 h. Reaction was carried out in kinase buffer in the presence of 50 µM gamma-S-ATP at 37°C. The condition were adapted from (Allen et al. 2007) and used to thio-phosphorylate recombinant Ensa/Arpp19 *in vitro*.

c. Protein Transfection with Xfect™ Protein Transfection Reagent

Xfect kit from Clontech, USA was used for the protein transfection initially. Five micrograms of protein was transfected using manufacturer's recommended protocol and the cells were harvested 2 h post-transfection. For mitotic entry studies, transfection was done on PP2A-B55-alpha and delta depleted cells that were arrested in G2 with INMPP1 overnight. In these experiments, the cells were washed with warm PBS 3–5 times and media-containing 25 μM of MG132 was added. This was done to prevent cells from going out of mitosis, which makes it easier to count cells entering mitosis from G2 after 1NMPP1 is washed off.

d. Neon Transfection of Proteins

Purified proteins were transfected into 5 x 10^5 U2OS_CDK1_as cells using Neon® Transfection System 10 μl Kit (Invitrogen UK). Two micrograms of protein was incubated in resuspension buffer for 10 min at RT before mixing it with cell pellet. Meanwhile, 0.5×10^6 cells were transferred to a sterile test tube and centrifuged at 500*g* for 5 min. Supernatant was aspirated and the cell pellet was resuspended in 1 ml of PBS without Ca^{2+} and Mg^{2+}. Upon centrifugation, the supernatant was carefully aspirated so that almost all the PBS buffer was removed with no or minimum loss of cells. The Resuspension Buffer R containing the purified Ensa/Arpp19 was then used to resuspend the cell pellets. A 10-μl cell suspension was electroporated at a given time using 1400 V/15 ms/4 pulses. Cells were plated in warm media and incubated for varying time-points.

e. Electroporation of Proteins

Cells were detached from the culture flasks using trypsin/EDTA (0.05%/0.02%), centrifuged at 130 × g for 5 min at 25°C, washed once in PBS and counted on a haemocytometer. Recombinant Ensa or Arpp19 was added to freshly prepared and sterile filtered electroporation buffer (EPB: 100 mM sodium phosphate, 5 mM KCl, 15 mM $MgCl_2$, 15 mM HEPES, 2 mM ATP (Thermo Fisher), 2 mM reduced glutathione (Sigma) at pH 7.2) to final concentrations of 20 μM or 40 μM. Next, the cells were pelleted again and mixed with protein solution in EPB. One hundred-microliter aliquots

(4 x 10^6 cells) were then transferred into 2 mm cuvettes and electroporated on an Amaxa Nucleofector I (Lonza). Pulse programs were #B28 or #A28 for HeLa cells. Cells were pulsed twice with gentle mixing in between the pulses. For control experiments, cells were mock electroporated with EPB alone. Directly after electroporation, 0.3 mL of pre-warmed (37 °C) CO_2-adjusted and cell line-matched growth medium was added to each cuvette and samples were transferred to cell culture dishes. For small-scale experiments (i.e. immunofluorescence microscopy, western blotting, flow cytometry) aliquots of 4 x 10^6 cells were added to separate wells of a 6-well plate (3.5 cm diameter), filled with 2 mL/well of pre-warmed cell line-specific growth medium. Cells were returned to the incubator and allowed to recover for 5 h. During this period, cell viability and morphology was monitored by bright-field microscopy. Once cells regained their adherent morphologies, dishes were washed three times with pre-warmed PBS and cells were harvested by trypsinisation. Cells were washed twice with pre-warmed PBS before further analyses.

f. Pro-DeliverIN™ Transfection

Transfection using Pro-DeliverIN™ Transfection Reagent was optimised using the manufacturer's recommended protocol (http://www.ozbiosciences.com/transfection-protein/35-pro-deliverin-transfection-reagent-protein-delivery.html), in a 24-well plate. The positive control (R-Phycoerythrin) provided was also used as per the manufacturer's protocol.

CHAPTER3 PRELIMINARY CHARACTERISATION OF ENSA AND ARPP19

Greatwall kinase has been implicated to play a major role in the mitotic entry network in higher eukaryotes. Greatwall performs its functions by phosphorylating two small phospho-proteins, Endosulphine-alpha (Ensa) and Arpp19. The phosphorylated substrates then bind to PP2A-B55, to inhibit the dephosphorylation of Cdk substrates and hence maintain the mitotic state.

Ensa and Arpp19 have not been extensively studied in human cells and their precise contributions to mitotic entry as well as their mode of action and regulation remain to be investigated. Although these proteins are highly similar, we do not know if they share individual or overlapping functions. We lack information on their subcellular localisation throughout the cell cycle. We also know little about their precise structural interaction with the B55/PP2A phosphatase and do not have a good understanding of interaction with other proteins. To embark on a study on the cellular function of these two proteins we decided to generate the necessary tools for cell-biological and biochemical analysis of these two closely related proteins. This includes specific antibodies, potent and validated siRNAs and tagged expression constructs that have been functionally characterised. In this chapter, we describe the generation of these tools and a basic characterisation of Ensa and Arpp19 localisation in interphase and mitotic cells.

3.1 Generating Antibodies and Analysing Their Specificity

Ensa and Arpp19 are two small regulatory proteins that are Greatwall kinase substrates. They are ~70% identical in their amino acid sequences making it difficult to study them individually. This thesis focuses on exploring the proteins Ensa and Arpp19 in the mitotic entry network. When I started this study, the functions of these proteins were roughly mapped using antibodies raised against full-length cDNA or the dissimilar

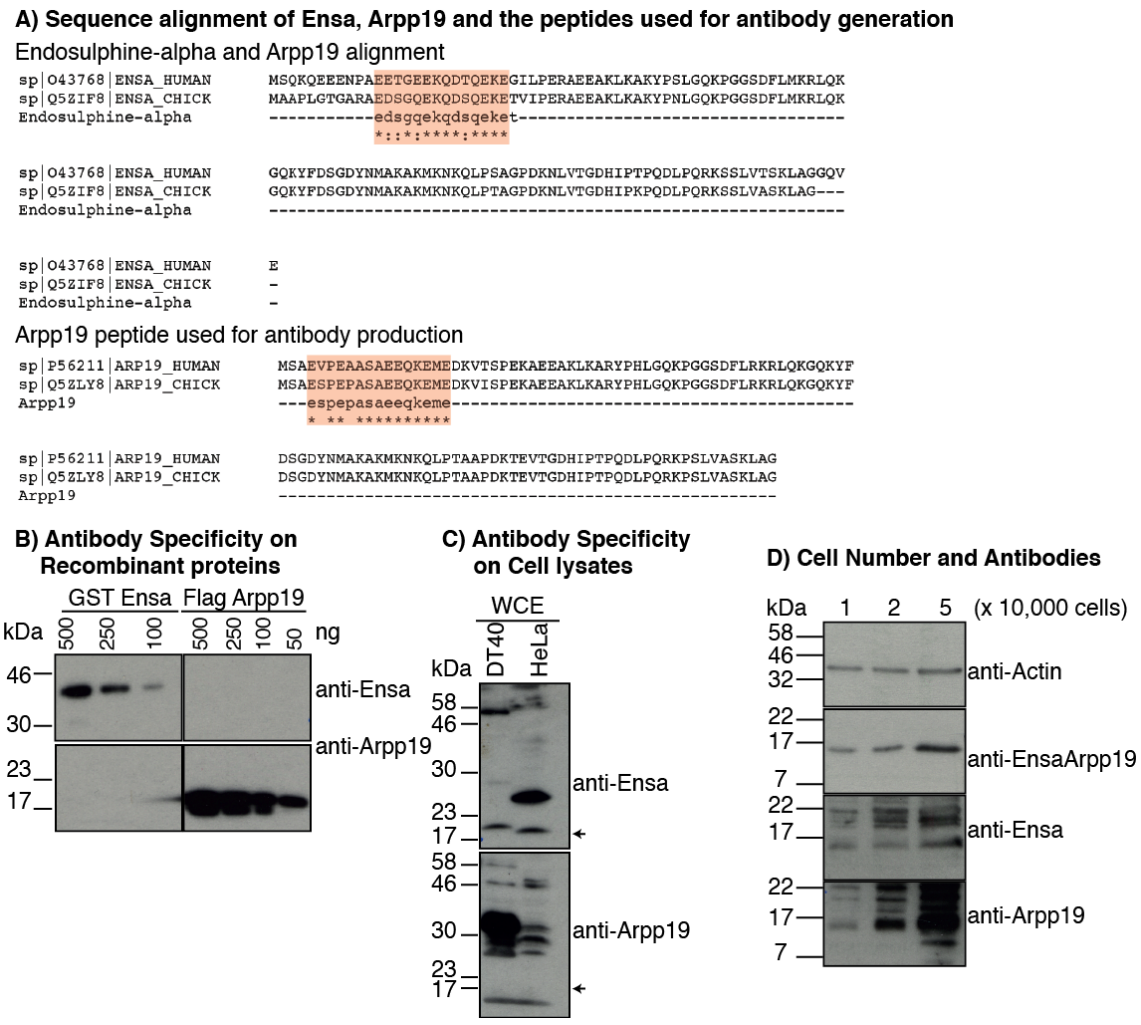

Figure 3.1 Specificity analyses of antibodies generated against Ensa and Arpp19 for this study

A) Multiple sequence alignment of Ensa and Arpp19 peptides with Clustal Omega used for rabbit polyclonal antibody generation. The sequences marked in red show the similarity of the peptides to the chicken and human protein sequences. B) Purified antibody was used to test specificity using recombinant proteins purified from E.coli Defined amounts of GST-Ensa and Flag-Arpp19 were probed to test antibody affinity. C) Purified antibodies were used to probe for endogenous Ensa and Arpp19 in total cell lysates from *HeLa* and chicken DT40 cells. D) Defined number of cells was used to test antibody affinity. Total cells lysates were prepared from *HeLa* cells. Purified antibodies were used for immunoblotting.

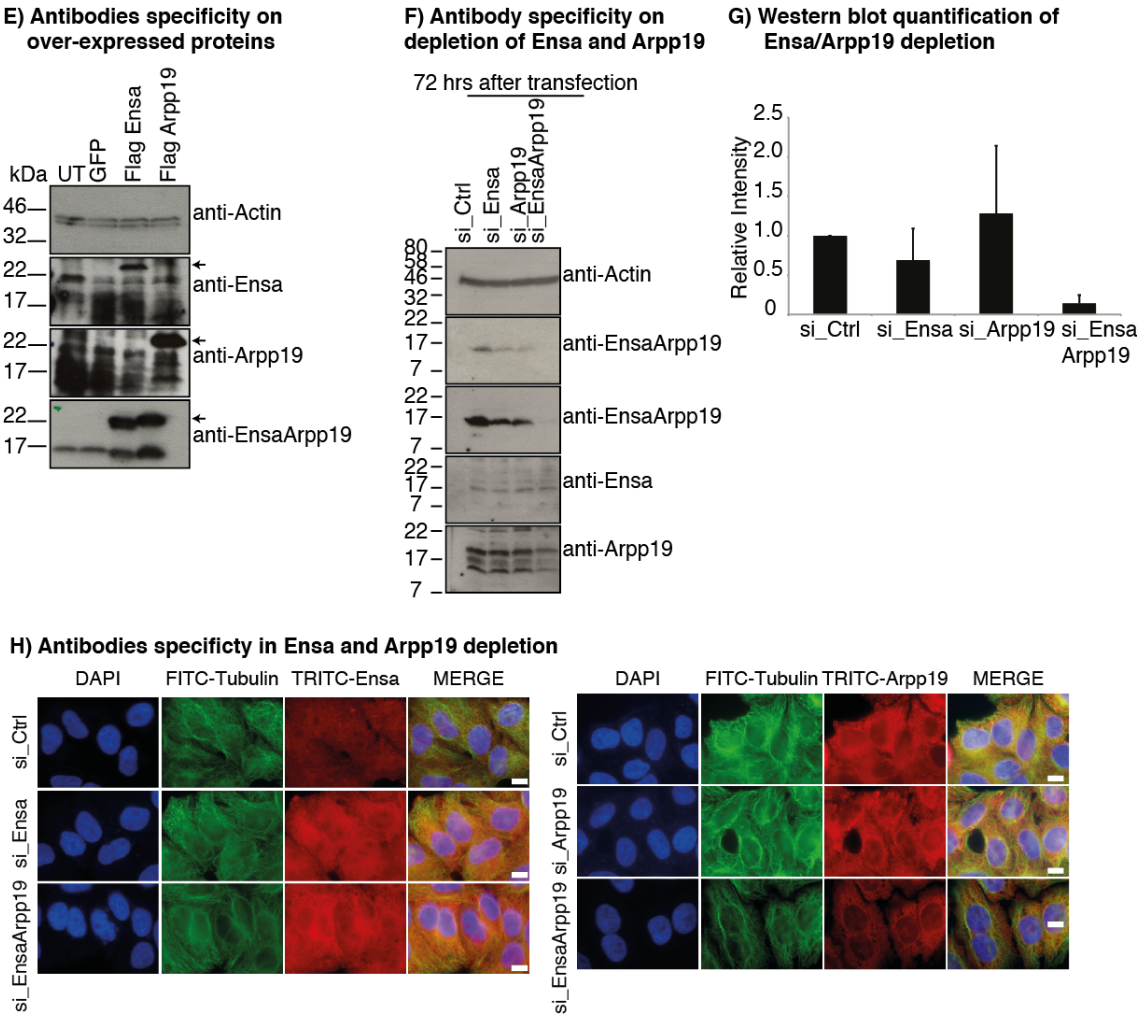

Figure 3.1 Specificity analyses of antibodies generated against Ensa and Arpp19 for this study

E) Hek293 were transfected with expression constructs encoding full length human Ensa and Arpp19. After 48 h of incubation, total cell lysates were prepared and immuno-blotted with purified antibodies. F) siRNA knockdowns were performed using Dharmacon siRNA smart pools at 50 nM concentration for 72 h. Total lysates were probed with newly purified and commercial antibodies. G) Western blots of siRNA depletion were quantified using ImageJ software and relative intensities were plotted. Data expressed as mean (±S.D) and a representative western (F). Immunofluorescence staining of endogenous Ensa and Arpp19 using purified antibodies after siRNA treatment for 72 hrs. The cells were fixed and co-stained with antibodies against α-tubulin (green) and EnsaArpp19 (red). The nuclei was visualised with DAPI (blue). Images were taken on the Olympus IX70 microscope with a 60X, oil –immersion lens, N.A 1.42. Scale bar: 10 µM

C-terminal residues in *Xenopus* (Mochida et al. 2010; Gharbi-Ayachi et al. 2010). For studies in other vertebrates like starfish and mammalians; the full-length cDNA was used to raise polyclonal antibodies (Cundell et al. 2013; Okumura et al. 2014; Dulubova et al. 2001; Mochida et al. 2010; Gharbi-Ayachi et al. 2010). However, these antisera were not tested for cross-reactivity in cellular extracts. Therefore, it was difficult to differentiate between specific roles and distributions of Arpp19 and Ensa and to determine their relative importance as B55/PP2A inhibitors.

To initiate this study I attempted to generate specific antibodies for Ensa and Arpp19 in vertebrate cell lines cells. I started this project before the onset of CrispR technology with the plan to perform genetic studies in chicken DT40 lymphocytes. Thus, I raised the peptides used for specific antibody generation matching the divergent N-termini of Gallus Arpp19 and Ensa. The chicken and human proteins share a significant homology and polyclonal antibodies are likely to be cross-reactive between chicken and mammalian species. With the help of Eurogentec, we generated peptides mapping 14 residues at the Arpp19 and Ensa N-terminal (Fig. 3.1A) that showed considerable sequence differences between the paralogues. Rabbits were injected with these peptides coupled to KLH carrier and we obtained purified antibodies following a standard immunisation and purification protocol provided by Eurogentec. To test these antibodies I performed immuno-blotting using recombinant human Arpp19 and Ensa that were expressed and purified from *E.coli*. Ensa was tagged with GST (46 kDa) and purified with glutathione sepharose beads, while Arpp19 was his-tagged and purified with Nickel-agarose-affinity columns (Materials and Methods 2.2.5). Using this method, I confirmed that these antibodies could specifically detect recombinant human Ensa and Arpp19 and that they showed no sign of cross-reactivity (Fig. 3.1B). I then used DT40 and *HeLa* extracts to probe endogenous expression of Arpp19 and Ensa. The antibodies showed a weak signal at the expected size (17 kDa), but also showed a number of non-specific bands (Fig. 3.1C). Given this non-specific background, it is unlikely that these antisera can be used for immuno-fluorescence studies to assess the localisation of Ensa and Arpp19.

The weak signal for the supposedly specific bands in the cell extract blots may be due to the limited sensitivity of the antibodies, or due to low abundance of Ensa and Arpp19. To improve the signal in the immuno-blots, I prepared highly concentrated cell lysates

of *HeLa* cells and probed them with the newly made antibodies. The signal for the expected size band increased proportionally with the increasing cell number, and so did the non-specific signal (Fig. 3.1D). However, a band at the expected molecular weight was clearly visible, so that these antibodies could be useful to detect the endogenous expression of Ensa and Arpp19.

To further confirm that our antisera can specifically detect Ensa and Arpp19 in cell extracts, I decided to express Ensa and Arpp19 exogenously in mammalian cells. To differentiate between the endogenous and exogenous proteins, I tagged them with a Flag-tag. Flag-tag (1 kDa) being negatively charged migrates slower than the endogenous protein, even though the molecular weight is approximately the same. The constructs were expressed transiently in Hek293 cells, known for their high transfection efficiency, using the Calcium chloride method (Materials and Methods 2.2.3). Forty-eight hours post-transfection, I collected the cells and prepared concentrated lysates. Although, the antibodies recognised the exogenous proteins (~22 kDa) specifically (Fig. 3.1E), they also showed a lot of background along with the endogenous protein (17 kDa).

The commercial Abcam antibody recognised both the Flag-tagged proteins as well as the endogenous ones very strongly. The 17-kDa band also corresponds to the endogenous band observed with the homemade antibodies. To assess if these bands were the endogenous proteins or background signal, I performed siRNA depletion studies in *HeLa* cells. The depletion of the individual proteins did show a mild reduction in their corresponding antibody signal with the commercial antibody, and this signal was significantly decreased in the double knockdown cells (Fig. 3.1 F-G). Our homemade antisera did not show a significant decrease in the signal at the expected molecular weight, suggesting that this was non-specific background staining. From these observations (Fig. 3.1 F-H), I concluded that these antibodies could not be used for further studies due to their non-specific nature. Further, in this study, only the Abcam antibody that recognises both Ensa and Arpp19 is used for analysis.

3.2 Localisation of Ensa and Arpp19 in Mammalian Somatic Cells

Localisation of proteins in the cell cycle usually relates to their cellular function. For example, the nuclear import of Cyclin B is indicative of mitotic entry. Similarly, Greatwall's nuclear export preceding nuclear envelope breakdown, is important for its mitotic function (Alvarez-Fernández et al. 2013). Likewise, identifying the localisation of Arpp19 and Ensa in mammalian cells might lead to better understanding of their roles in the cell cycle.

Initially when Arpp19 was discovered, Girault observed it in all vertebrate species at various levels in all tissues. The highest concentration of Arpp19 was seen in malignant tissues and early embryos (Girault et al. 1990). Similarly, Ensa was identified as sulfonylurea receptor ligand in brain tissues. It is implicated in dopamine regulation, as endogenous regulators of potassium channels. Ensa was classified as an intrinsic unstructured protein due to lack of tertiary structure. It formed distinct secondary structures only when bound to lipid membrane. Hence, it was speculated to be present near the cytosolic phase of the cell membrane (Virsolvy-Vergine et al. 1992). It was also thought that the presence of these proteins in tissues with no or less dividing tissues (brain, pancreas) may attribute to its role in cell proliferation (Girault et al. 1990). Thus, it is important to study the localisation of these small proteins to understand their mitotic role.

It might also be useful to compare the subcellular localisation of Ensa and Arpp19 with Greatwall and PP2A-B55 to better understand the interaction between these proteins. Although, Greatwall was identified as a nuclear protein in *Drosophila* larvae, in human cells it also localises at the centrosomes in the gap phases (G1 and G2) and S-phase (Burgess et al. 2010; Voets & Wolthuis 2010). Additionally, Greatwall is concentrated at the centrosomes during mitosis in mammalians cells. At mitotic exit it is observed in the cytoplasmic cleavage furrow on the midzone microtubules (Burgess et al. 2010; Voets & Wolthuis 2010; J. Yu et al. 2004; H. J. Johnson et al. 2009). On the contrary, the phosphatase PP2A-Tws or PP2A-B55 is largely localised in the cytoplasm in *Drosophila* (Mayer-Jaekel et al. 1994) and humans (Santos et al. 2012). B55-alpha, the

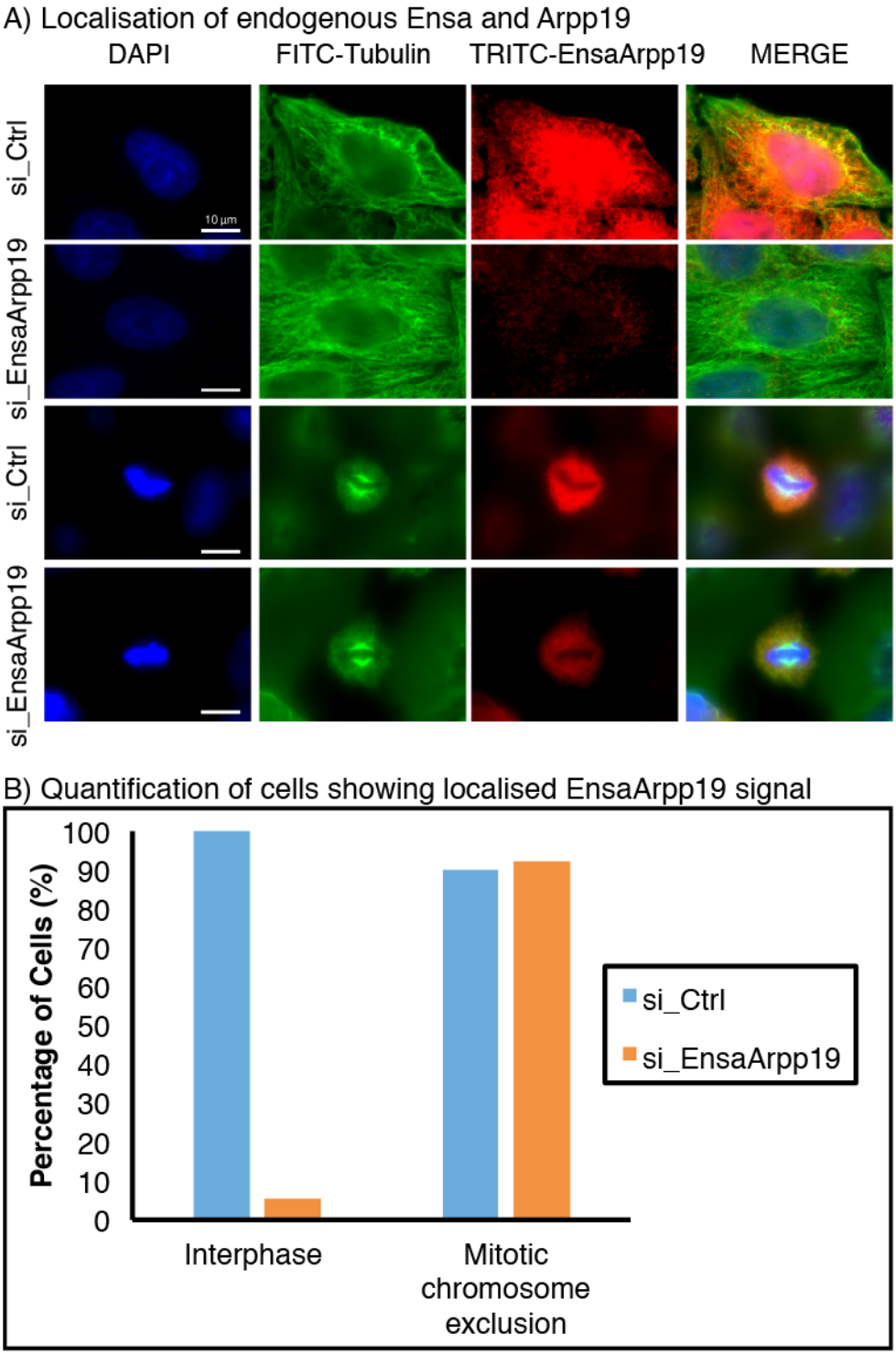

Figure3.2 Localisation of endogenous Ensa and Arpp19

A) Probing localisation of endogenous Ensa and Arpp19 in interphase (top panels) and mitotic phase (bottom panel) using a commercial antibody and immunofluorescence. To control for unspecific signal of the antiserum, we compared Ensa/ARPP siRNA transfected and control siRNA transfected cells. After 48 h post-transfection, the cells were fixed and co-stained with antibodies against α-tubulin (green) and EnsaArpp19 (red). The nuclei was visualised with DAPI (blue). Images were taken on the Olympus IX70 microscope with a 60X, oil –immersion lens, N.A 1.42. Scale bar: 10 µM. B) Quantification of the number of cells the show localisation in A).

regulatory subunit of the phosphatase that interacts with Ensa/Arpp19 in mammalian cells, is also majorly cytoplasmic (Alvarez-Fernández et al. 2013).

According to Alvarez-Fernández (2013), Greatwall (Gwl) shuttles from the nucleus to the cytoplasm just before mitotic entry. This nucleo-cytoplasmic shuttling of Greatwall is followed by Cyclin B import and nuclear envelope breakdown. Alvarez proposes that this shuttling occurs to inhibit the premature dephosphorylation of Cdk substrates by B55-alpha during mitotic entry. If this is true, Ensa and Arpp19 could either localize in the nucleus and be exported similar to Greatwall or be present in the cytoplasm and be activated following the nuclear export of Greatwall to inhibit B55-alpha.

Thus, the study of localization of these proteins might shed light on the mechanisms of the mitotic entry network.

3.3 Localization of Endogenous Ensa and Arpp19 in Mammalian Cells

I began the localisation studies by observing endogenous Ensa and Arpp19 in *HeLa* cells. To control for non-specific signal from the polyclonal antibody we compared cell before and after siRNA depletion of Ensa and Arpp19 for 72 h (Fig. 3.2). We used the same dharmacon smartpools siRNA against Ensa and Arpp19 that showed a good depletion of both the proteins in the western blots shown in Fig. 3-1. The Abcam antibody showed a significant decrease in the immuno-fluorescence signal in the siRNA-treated interphase cells, confirming that is specific to the phosphoproteins in interphase cells. However, in the mitotic cells although the signal reduced some background was observed. This suggests that either the knockdown was not complete or the antibody shows non-specific signal of mitotically enriched proteins.

The immunofluorescence images shown in Fig. 3.2 A indicate that Ensa and Arpp19 are enriched in the nucleus, but are also present in the cytoplasm in interphase cells. The cytoplasmic staining does not show a significant overlap with tubulin, but shows a distinct granular staining, which could be pointing to a more specific sub-cellular localisation, but could also be an artefact due to fixation. Further, 90% of the interphase

cells showed a considerable (<5%) reduction in the Ensa/Arpp19 signal (Fig 3.2B). The antibody showed an even staining throughout mitotic cells but a clear exclusion from mitotic chromosomes. However, this signal was only slightly reduced (25-30%) in siRNA treated cells (Fig 3.2B), suggesting that this staining could at least partially be non-specific. These initial observations need to be confirmed further by using alternative methods to study the subcellular localisation of these proteins.

3.4 Localisation of Overexpressed Ensa and Arpp19 in Mammalian Cells using Live-cell Imaging

Another way to study localisation was expressing Ensa and Arpp19 as tagged fusion proteins and following them in live cells using fluorescent proteins, or in fixed cells using tag-specific antibodies. I generated Flag and GFP-Ensa expression constructs to allow over-expression of the tagged protein in mammalian cells. Before the localisation study, I analysed the impact of the tag on the function of the protein by immunoprecipitation. Flag-Ensa and GFP-Ensa were transiently expressed in Hek293 cells and the interaction with B55-alpha was investigated using immune-precipitation. Both fusion proteins were well expressed in the whole cell lysates and enriched by immunoprecipitation. However, GFP-Ensa did not appear to co-immunoprecipitate with B55-alpha, suggesting that the tag renders Ensa inactive, while the shorter Flag-tag still appeared to be functional and co-precipitated with B55 (Fig. 3.3A). It is also noteworthy that the GFP fusion protein showed a smear of apparent degradation products in the Ensa immune-blot, suggesting that this protein may be unstable and has problem to achieve a stable confirmation.

This discrepancy could be due to the large size of the GFP tag that makes Ensa inaccessible to the phosphatase. This hinders their physical interaction and hence the pull-down. Therefore, to allow some flexibility and accessibility to Ensa in the presence of GFP tag, I integrated a glycine-alanine-serine linker between the GFP tag and the protein. These fusion proteins were also overexpressed in Hek293 cells and enriched using GFP-Trap beads (Chapter 2.2.2e). However, as observed in Fig. 3.3 B-C, tagging Ensa with the linker-GFP on N- or C-terminal did not pull down B55. This implies that the presence of large tags really affects the Ensa-B55 interaction and is therefore its primary known function. This was further confirmed when GST-Ensa/Arpp19 fusion

proteins also failed to interact with B55-alpha (Discussed in Chapter 6.2 and (Williams et al. 2014)).

Having made the effort to generate the GFP fusion proteins we decided to nevertheless analyse their localisation in live cells and compare it to an available GFP-B55alpha expression construct. We expressed the fusion proteins in *HeLa-cdk1as* cells (see Chapter 2.2.3c and f) stably expressing RFP-H2B. The transfected cells were imaged over time, to observe the localisation of these fusion proteins during mitosis and the impact of the over expression on mitosis (Fig. 3.3D).

We first imaged GFP-B55-alpha in this experiment. As expected, GFP-B55 was enriched in the cytoplasm (Fig. 3.3D top panel). GFP-B55 was distributed evenly throughout the mitotic cell upon NEBD and did not appear to be excluded from the chromosomes during mitosis. It was exported from the nucleus during its reformation in telophase. No striking mitotic phenotypes were observed and GFP-B55 positive cells went through mitosis in an average of 60–100 min (Fig. 3.3E).

In case of both N and C-terminal GFP-tagged Ensa, the protein did not significantly change its localisation during the G2/M transition, but was excluded from metaphase mitotic chromosomes, similar to the endogenous proteins. In addition, these proteins were enriched in the midzone region during mitotic exit, similar to Greatwall localisation (Burgess et al. 2010; Voets & Wolthuis 2010).

Surprisingly, GFP-linker versions of Ensa delayed the exit from mitosis significantly. The cells displayed prolonged metaphase and hence, a delayed mitosis (Fig. 3.3D bottom panel and 3.3E). In addition, the N-terminal tagging of Ensa seems to have stronger mitotic phenotype in comparison to the C-terminal fusion protein, suggesting that this protein could exert a specific dominant negative function. However, neither C, nor N-terminal fused Ensa can interact with B55. This makes it unlikely that the dominant negative effect is exerted via the known function of Ensa as a PP2A-B55 inhibitor. A possible explanation for the mitotic delay might be a novel uncharacterised function of the protein. These functions may require the N-terminal of the protein and be

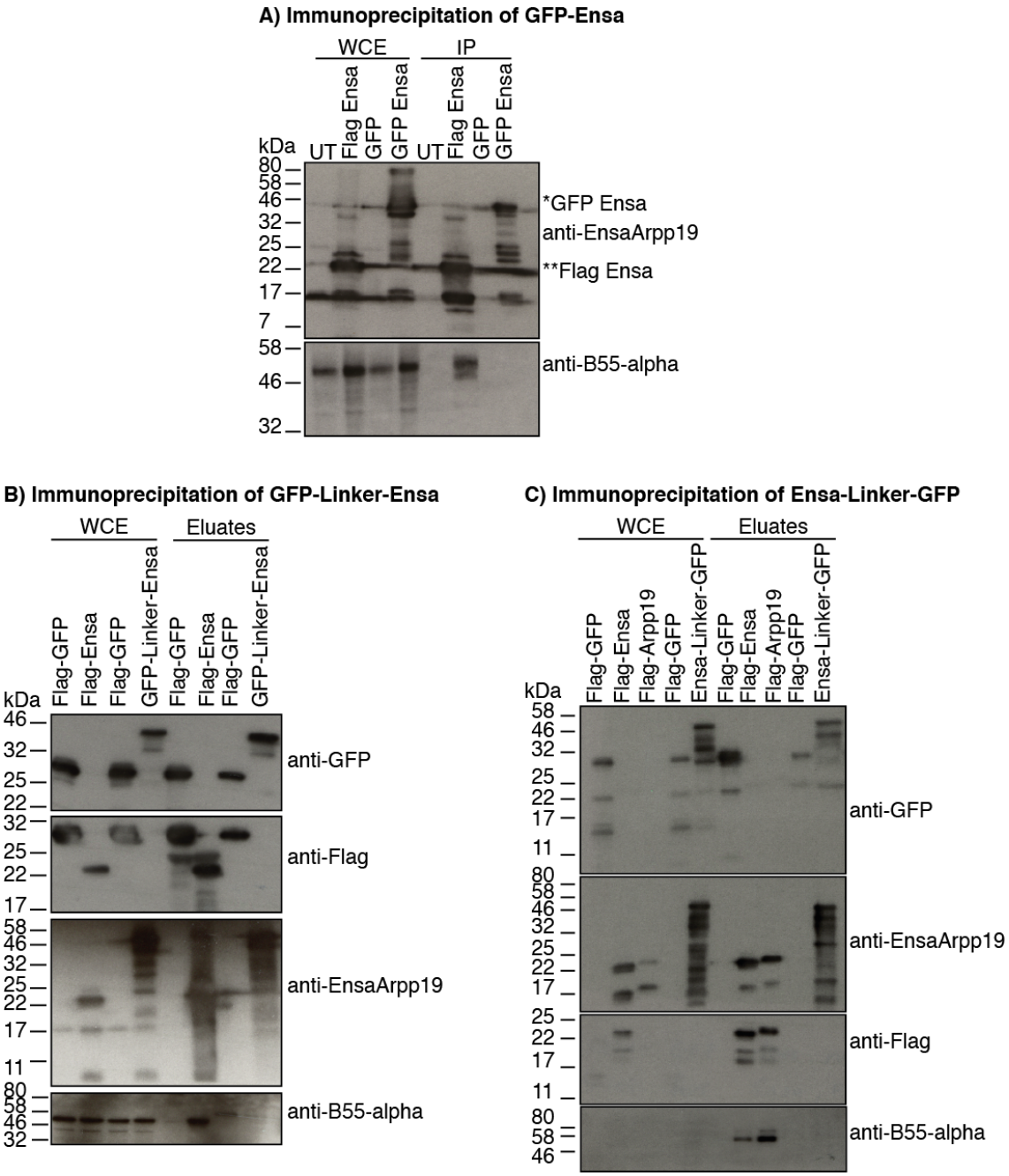

Figure 3.3 GFP-Tagging for Ensa and Arpp19 for localisation studies

Hek293 cells were transfected with the indicated vectors A) Flag Ensa (positive control), GFP (negative control), GFP Ensa, B) Flag GFP, Flag Ensa (positive control), GFP-Linker-Ensa and C) Flag GFP (negative control), Flag Ensa (positive control) and Ensa-Linker-GFP. Forty-eight hours post-transfection, the cells were lysed and subjected to co-IP using either anti-Flag M2 resin or GFP-Trap®_M beads. The elutions after the IP were analysed by western blotting for interaction with PP2A-B55-alpha.

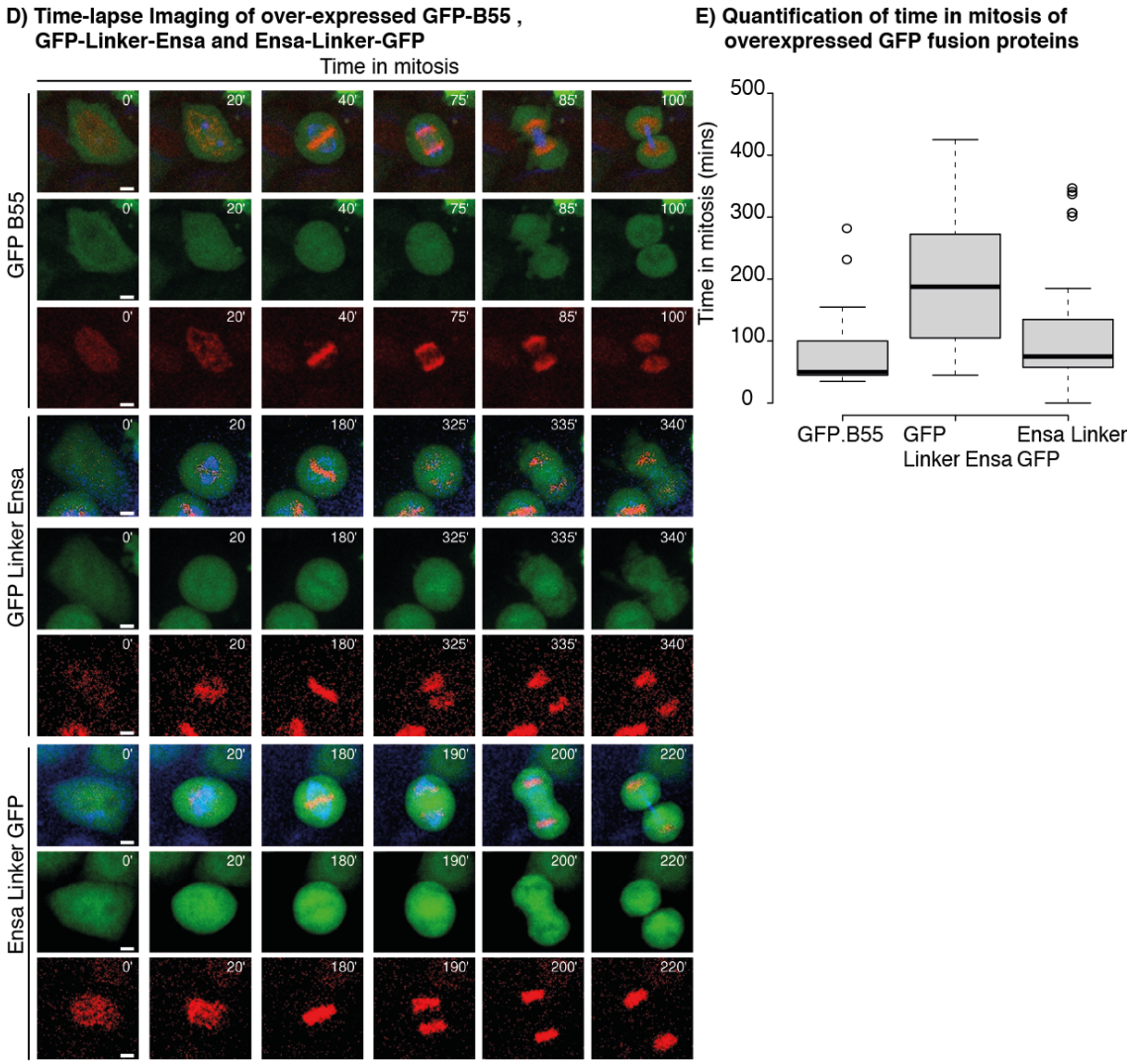

Figure 3.3 GFP-Tagging for Ensa and Arpp19 for localisation studies

D) Time lapse imaging of the GFP-fusion proteins using confocal microscopy to study localization. *HeLa* cells expressing H2B-mCherry (red) were transfected with GFP-fusion proteins were imaged overnight using the 3i-Confocal microscope with a 40X lens, N.A 0.60. Time from the onset to exit of mitosis was recorded and plotted using http://boxplot.tyerslab.com. Centre lines show the medians; box limits indicate the 25th and 75th percentiles as determined by R software; whiskers extend 1.5 times the interquartile range from the 25th and 75th percentiles, outliers are represented by dots. Scale bar: 10 µM

independent of their interaction with B55-alpha. These phenotypes will need to be investigated in detail to understand the mitotic roles of Ensa and Arpp19.

3.5 Localisation of Overexpressed Ensa and Arpp19 in Fixed Cells

Although the GFP-fusion proteins localise similar to the endogenous proteins, their inability to interact with B55 make these observations doubtful. Therefore, I examined the localisation of Ensa and Arpp19 in fixed cells using smaller Flag-tags to detect them with well-characterised and specific antisera raised against the tags. As discussed above (Fig. 3.3A-C), Flag tagged Ensa and Arpp19 interact with B55-alpha successfully and should therefore be functional as PP2A-B55 inhibitors.

Thus, Flag-Ensa and Flag-Arpp19 were overexpressed transiently in *HeLa* Kyoto cells. A truncated version of Greatwall protein (E2), generated in the lab for other studies (Ocasio et al. 2016) was used as a positive control and a non-transfected negative controlled was used to exclude background due to Flag tag localisation and non-specific staining. Flag E2 like full-length Greatwall localised strongly in the nucleus. Flag Ensa and Arpp19 were distributed evenly in the interphase cells (Fig. 3.4 A-B), similar to the endogenous staining and GFP-Ensa. I next co-expressed GFP-B55 and Flag-Ensa/Arpp19 exogenously to visualise the co-localisation of the phosphatase and the inhibitor. The transfected cells were fixed and stained 48-h post-transfection. Again, Flag Ensa and Arpp19 appeared to be localised both in the cytoplasmic and in the nucleus, while B55 appeared to be more concentrated in the cytoplasm and excluded from the nucleus (Fig. 3.5 top panel and 3.5 B). On co-expressing both the proteins, we observed an overlap in the cytoplasm in interphase cells. In mitotic cells, Flag Ensa and Arpp19 appeared to be excluded from the chromosomes co-localising with GFP-B55 alpha (Fig. 3.5 bottom panel and 3.5 B). An interesting difference became apparent in this experiment, because Flag-Arpp19 appeared to be specifically enriched in the outer cell periphery, revealing an area that does not co-localise with B55 (compare the yellow and red staining in the merged bottom panel in Fig. 3.5A and 3.5 B.

In conclusion, Ensa and Arpp19 are localised both in the cytoplasm and in nucleus during interphase and are evenly distributed throughout mitotic cells, but remain

excluded from chromosomes during mitosis. The enrichment of Arpp19 at the cell periphery could be interesting, especially in the light of the phenotypes described later in this thesis. However, we only observed this distinct localisation pattern after overexpression, so these data could be artefactual and need to be further confirmed by following the endogenous protein

Lastly, the preliminary characterisation in this chapter confirmed that the antibodies generated could not be used to study the individual functions of Ensa and Arpp19, as they were non-specific on the cellular level. Thus, further in this study both the protein have been characterised together, using the commercial antibody recognising both the homologues. Alternative approaches with smaller tags have to be used to study the localisation of the protein *in-vivo*, as the fluorescent tags seem to deter some key functions of the proteins. From my observations so far, Ensa and Arpp19 appear to be present ubiquitously in cells but seem to be excluded from the chromosomes during mitosis. The peripheral localisation of Arpp19 needs to be investigated more carefully to draw detailed conclusions.

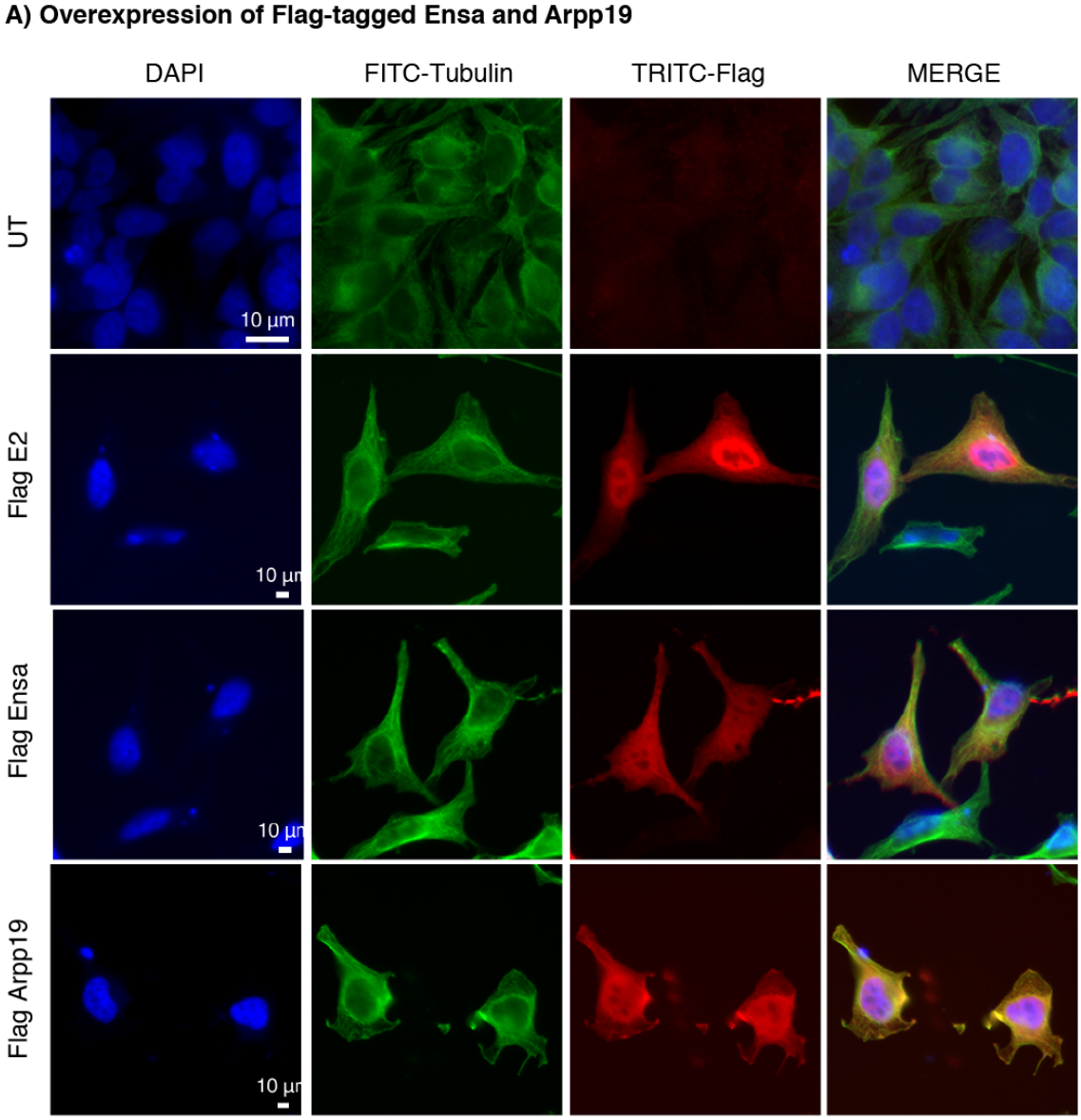

Figure 3.4 Overexpression of Flag-Ensa, Flag-Arpp19 and GFP-B55

A) *HeLa* Kyoto cells were transiently transfected with Flag-Ensa, Flag-Arpp19 and Flag-E2 (truncated Gwl protein). Cells were fixed and immuno-stained 48 h post-transfection. DNA was stained with DAPI (blue). Flag tagged proteins were visualised with anti-Flag antibody and a TRITC-labelled secondary antibody. Endogenous tubulin was visualised using an anti-Tubulin antibody and FITC-labelled secondary antibody. B) *HeLa*-cdk1as cells stably expressing RFP-H2B were transiently transfected with GFP-B55alpha plasmid. Twenty-four hours post-transfection images were taken on the Olympus IX73 microscope with a 60X, oil -immersion lens, N.A 1.42. Scale bar: 10 µM.

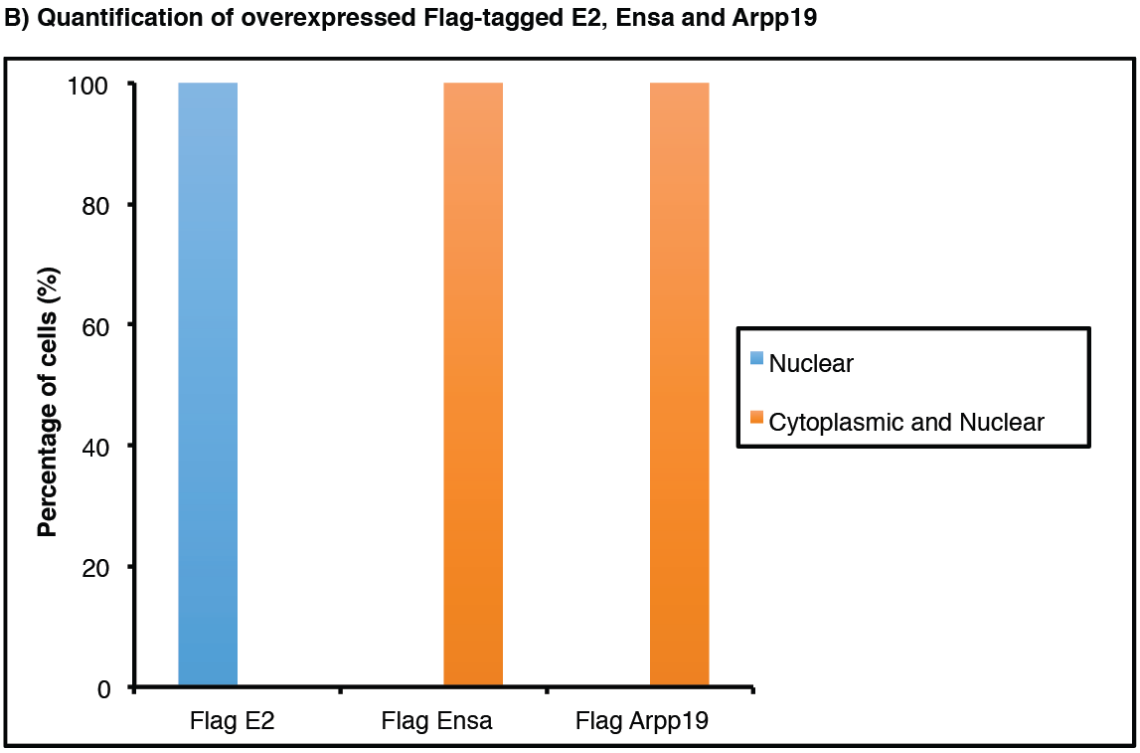

Figure 3.4 Overexpression of Flag-Ensa, Flag-Arpp19 and GFP-B55

B) Quantification of number of cells showing nuclear and cytoplasmic localisation in A).

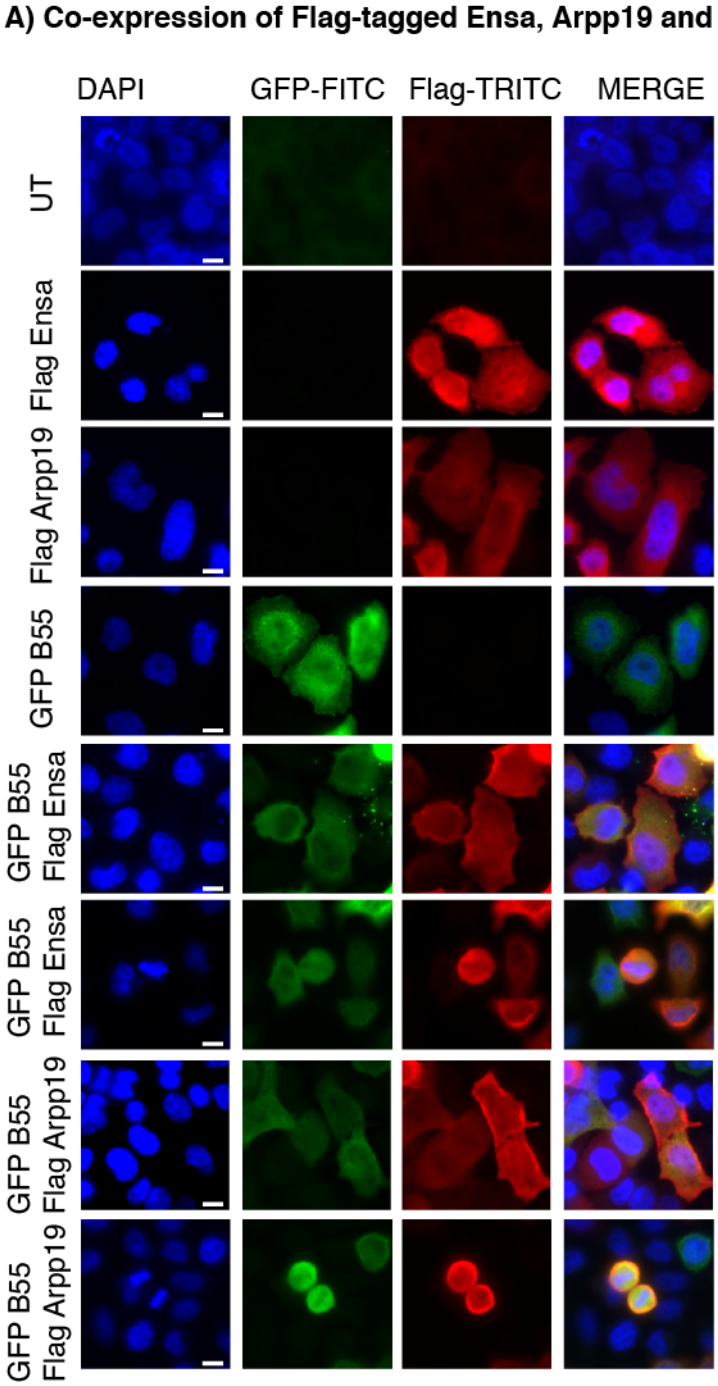

Figure 3.5 Co-Expression of B55 and Ensa/Arpp19 to study co-localisation

A) Flag-tagged Ensa and Arpp19 and GFP-B55 were co-expressed exogenously in *HeLa* cells and immuno-stained 48 h post-transfection. GFP-B55 appears to be cytoplasmic and was visualised using anti-GFP antibody and FITC-conjugated anti-rabbit secondary antibody (green). Both Ensa and Arpp19 were observed mostly in the cytoplasm. Ensa and Arpp19 were visualised using anti-Flag antibody and TRITC-conjugated anti-mouse antibody (red). Nucleus was stained with DAPI (blue). Images were taken on the Olympus IX73 microscope with a 60X, oil-immersion lens, N.A 1.42. Scale bar: 10 µM

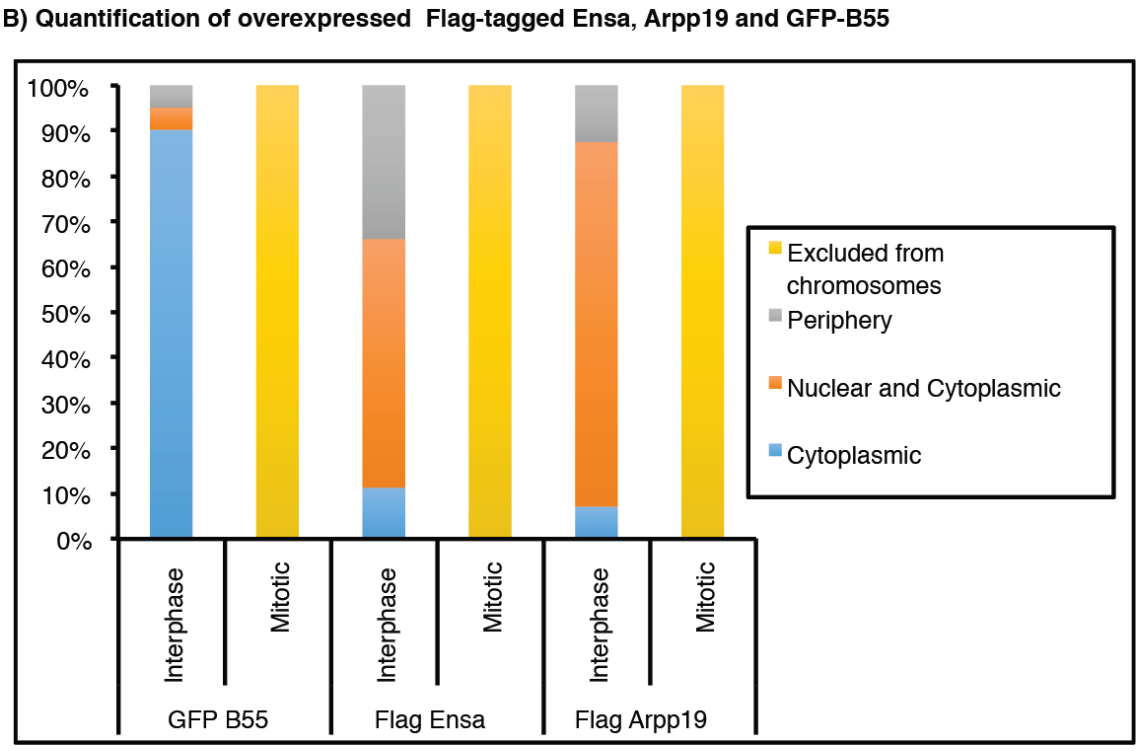

Figure 3.5 Co-Expression of B55 and Ensa/Arpp19 to study co-localisation

B) Quantification of cells showing different subcellular localisation post-transfection as done in A).

CHAPTER4 CHARACTERISATION OF MITOTIC PHENOTYPES OF ENSA/ARPP19 IN MAMMALIAN MITOSIS

In order to understand the mitotic role of Ensa and Arpp19, I decided to observe the effect on mitosis when these proteins are depleted. During the initial studies about the role of Ensa and Arpp19, they were described as substrates of Greatwall that act as phosphorylation dependent inhibitors of PP2A-B55 δ in *Xenopus laevis* egg extracts (Gharbi-Ayachi et al. 2010; Mochida et al. 2010). They were also implicated in mitotic progression in *Drosophila* (Glover 2012; Lorca & Castro 2013). Given that Greatwall phosphorylation is thought to be essential for Ensa and Arpp19 activity, it is not surprising that the reported phenotypes are very similar to the ones observed after Greatwall depletion in these organisms. While Greatwall depletion prevents mitotic entry in *X. laevis* extracts (J. Yu et al. 2006; Zhao et al. 2008) and human cells (Burgess et al. 2010; Voets & Wolthuis 2010), Greatwall is also implicated in promoting entry in *Drosophila* (Bettencourt-Dias et al. 2004; J. Yu et al. 2004). Likewise, Gharbi-Ayachi showed that RNAi-mediated Arpp19 depletion affects the mitotic index in *HeLa* cells. However, the cytological phenotypes of Ensa and Arpp19 in mammalian mitosis are not characterised in detail.

Similarly, the mitotic exit phenotypes of Greatwall are well characterized in *Drosophila* and human cells. In *Drosophila*, Greatwall depletion leads to delay in progression to anaphase. Also, the characteristic phenotype observed is elongated sister chromatids scattered on the mitotic spindle in neuroblasts (J. Yu et al. 2004; Bettencourt-Dias et al. 2004). Chromosome segregation failure was observed in Greatwall/Scant mutants in *Drosophila* (J. Yu et al. 2004; V. Archambault et al. 2007) and on Greatwall depletion in human cells. In human cells cytokinesis failure was also a prominent phenotype (Burgess et al. 2010; Voets & Wolthuis 2010; Cundell et al. 2013). Still, the Ensa and Arpp19 depletion phenotypes have not been identified or studied in mammalian cells.

Several important questions remain to be answered about the function of these two proteins. Firstly, characterising Ensa/Arpp19 depletion phenotypes should provide proof of principle that these proteins act in the same pathway as Greatwall kinase. Secondly,

the relative importance of each paralogue needs to be firmly established. Do these highly related proteins have specific functions, or are they entirely redundant? Finally, one cannot rule out that these two small proteins have additional Greatwall independent functions that remain to be explored. The impact of Ensa and Arpp19 on different phases of mitosis can be investigated in detail using time-lapse imaging. This enables meticulous classification of the cytological effect Ensa/Arpp19 depletion on mitotic entry and exit.

Thus, in this chapter I have characterised the mitotic phenotypes of Ensa/Arpp19 in comparison with Greatwall depletion and further explored the mitotic entry role of Greatwall and Ensa/Arpp19.

4.1 Depletion Phenotypes of Greatwall and Ensa/Arpp19 in Mammalian Cells

Greatwall localisation and mitotic phenotypes have been extensively studied and documented. In 2010, Burgess published a detailed characterisation of the Greatwall mitotic phenotypes in *HeLa* cells. Cells were synchronised using thymidine and the entry into mitosis and phenotypes in mitosis were documented. Complete Greatwall depletion showed an increase in 4n population in FACS and multinucleate cells in immunofluorescence. This could be due to improper cytokinesis in these cells (Burgess et al. 2010). Similarly, Voets and Wolthuis observed a slower increase in mitotic index in 2010, following Greatwall depletion, when thymidine blocked cells were released into Nocodazole. Studies in mouse mammalian cells revealed that Greatwall does not prevent mitotic entry(Alvarez-Fernández et al. 2013). Taken together these results suggest that Greatwall delays mitotic entry in mammalian cells but do not prevent it.

The major phenotypes documented in (Burgess et al. 2010) were non-congressed metaphase plate, scattered chromosomes along the spindle, prolonged metaphase or metaphase arrest, segregation defects and lagging chromosomes in cells that proceed to anaphase. A subpopulation of cells showed DNA bridges and mitotic death in metaphase-arrested cells. The metaphase delayed/arrested cells also showed a longer transit time in mitosis. Similarly, Voets and Wolthuis observed majority of the cells

showing DNA bridges indicative of cytokinesis failure and chromosome segregation defects. (Burgess et al. 2010; Voets & Wolthuis 2010). Moreover, prolonged prometaphase/metaphase arrest and segregation problems were the major defects reported in mouse mammalian cells (Alvarez-Fernández et al. 2013). All these defects indicate a prominent role of Greatwall in mitotic progression and exit.

According to the current models, Greatwall functions in mitosis via Ensa/Arpp19 by inhibiting PP2A/B55 phosphatase to allow elevated levels of Cdk1 substrate phosphorylation in mitosis. In 2010, Burgess et al quantified cells entering mitosis on Greatwall-depletion by measuring the percent of Cdk substrate phosphorylation by 2D-FACS. He observed 22% signal of Cdk substrates following complete depletion of Greatwall and a delayed mitotic entry (using time-lapse imaging after release from thymidine block). This data shows mammalian cells exhibit delayed mitotic entry with ~22% Cdk phosphorylated substrates. Following that Arpp19 depletion showed a 50% reduction in the mitotic index, in cells released from a thymidine block into nocodazole (Gharbi-Ayachi et al. 2010). However, most of these experiments were done using a single time point measurement that cannot distinguish between delay in entry or problems with maintaining mitotic arrest.

In this work, I wanted to explore the mitotic functions of Ensa/Arpp19 together and to compare them to the Greatwall phenotypes. For this, I began by studying the Greatwall phenotypes in the *HeLa* cells stably expressing RFP-H2B and GFP-Tubulin to confirm the published phenotypes and have set of data using our cell lines and experimental procedures for accurate comparison. This cell line was used as chromosome and tubulin dynamics are ideal visual markers of mitosis in mammalian cells. In these experiments, I used asynchronous cells to study the mitotic effects of Greatwall and to set an internal reference to analyse Ensa/Arpp19 phenotypes.

Greatwall knockdown was induced using Qiagen siRNA oligos for 48 h. The knockdown was analysed using western blot. The levels of Greatwall decrease significantly to as low as ~10% after 48 h treatment with 40 nM dose of the siRNA (Fig. 4.1A-B). I used the 4-well and 8-well microscopic plates for these experiments; hence, these plates were also used for quantifying the extent of depletion. After transfection, I performed time-lapse imaging on these cells for 16 h on a spinning disc

confocal microscope to observe mitotic cells in physiological conditions. As seen in Fig. 4.1C, the reduction in the mitotic population is ~10%.

When analysing the time-lapse movies, I observed only a slight decrease in mitotic entry in the Greatwall depleted cells, but found a number of mitotic defects reminiscent of the published phenotypes mentioned above. Firstly, about 50% of the cells showed delayed progression through prometaphase and metaphase and often fail to form a compact metaphase plate arrangement of the chromosomes (Fig. 4D-F). Nevertheless, most of these cells initiate anaphase within 100 min from NEBD albeit often with lagging chromosomes (Fig. 4E). About 15% of cells going through mitosis displayed a clear cytokinesis defect resulting in a single binucleate daughter cell, a hallmark Greatwall phenotype that was previously characterized (Cundell et al. 2013). In addition, around 10% of the cells with cytokinesis defect, showed chromosome segregation defects, where the cell divided into 3 daughters of which 2 fused to form a single binucleate cell (not quantified separately). A representation of the imaged cells is shown in Fig. 4.1F. The top panel for Greatwall knockdown shows a cell with prolonged metaphase arrest and the bottom panel shows a cell with cytokinesis defect.

The phenotypes I observed are in support of the previous studies where the prometaphase/metaphase delay and cytokinesis defects were documented. It is currently unclear why Greatwall depletion in mammalian cells does not cause a more significant delay in G2, as would be expected from the *X. laevis* results. One possibility could be that this kinase is highly processive, so that only a complete depletion results in a significant loss of Ensa/Arpp19 phosphorylation. The phenotypes we observe could thus be simple hypomorphic due to partial activity of PP2A/B55 in mitosis.

Now that the Greatwall phenotypes were reconfirmed, I went ahead and transfected *HeLa* cells with 50 nM (25 nM Ensa and 25 nM Arpp19) Ensa/Arpp19 siRNA smartpools. Smartpools are a mixture of four siRNA oligos that have been carefully selected and pre-optimized to minimize off-target effects. Ensa/Arpp19 were depleted significantly in 72 h and the protein level decreased to ~10–15% (Fig. 4.2A-B). I also depleted individual proteins using the smartpools, but the precise extent of knockdown could not be measured, as specific antibodies are unavailable (Fig. 4.2C and Chapter 3.1). However, since the double knockdown has a significant effect on total

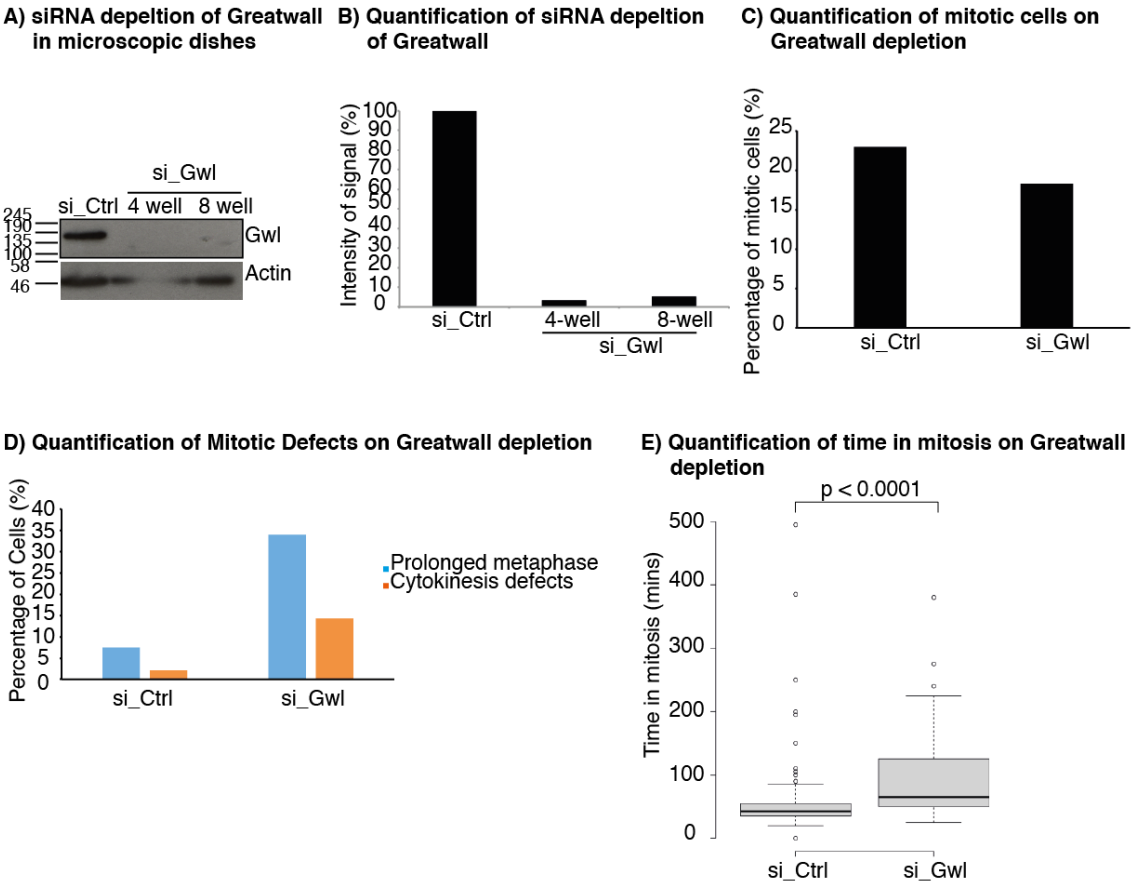

Figure 4.1 siRNA mediated depletion of Greatwall

A) Western blot analyses of Control (si_ctrl) and Greatwall (si_Gwl) siRNA transfected *HeLa* cells. The depletion experiments were done in 4-well and 8-well microscopic dishes. Actin is used as the loading control. B) Western blot quantification using ImageJ to show depletion of Greatwall protein. C) Mitotic indices were calculated for asynchronous *HeLa* cells transfected with control and Gwl siRNA and stably expressing RFP-H2B and GFP-tubulin. D) The percentage of *HeLa* cells exhibiting mitotic defects (prolonged metaphase/cytokinesis defects) were scored over total mitotic cells and plotted graphically. E) A box-and- whisker-plot showing the duration from NEB to cytokinesis with control and Gwl knockdown in *HeLa* cells stably expressing RFP-H2B and GFP-Tubulin. Centre lines show the medians; box limits indicate the 25th and 75th percentiles as determined by R software; whiskers extend 1.5 times the interquartile range from the 25th and 75th percentiles, outliers are represented by circles. n = 94, 57 sample points. Analysis between samples was performed by the Mann-Whitney Rank Sum test, and p-values are presented above the box-plots.

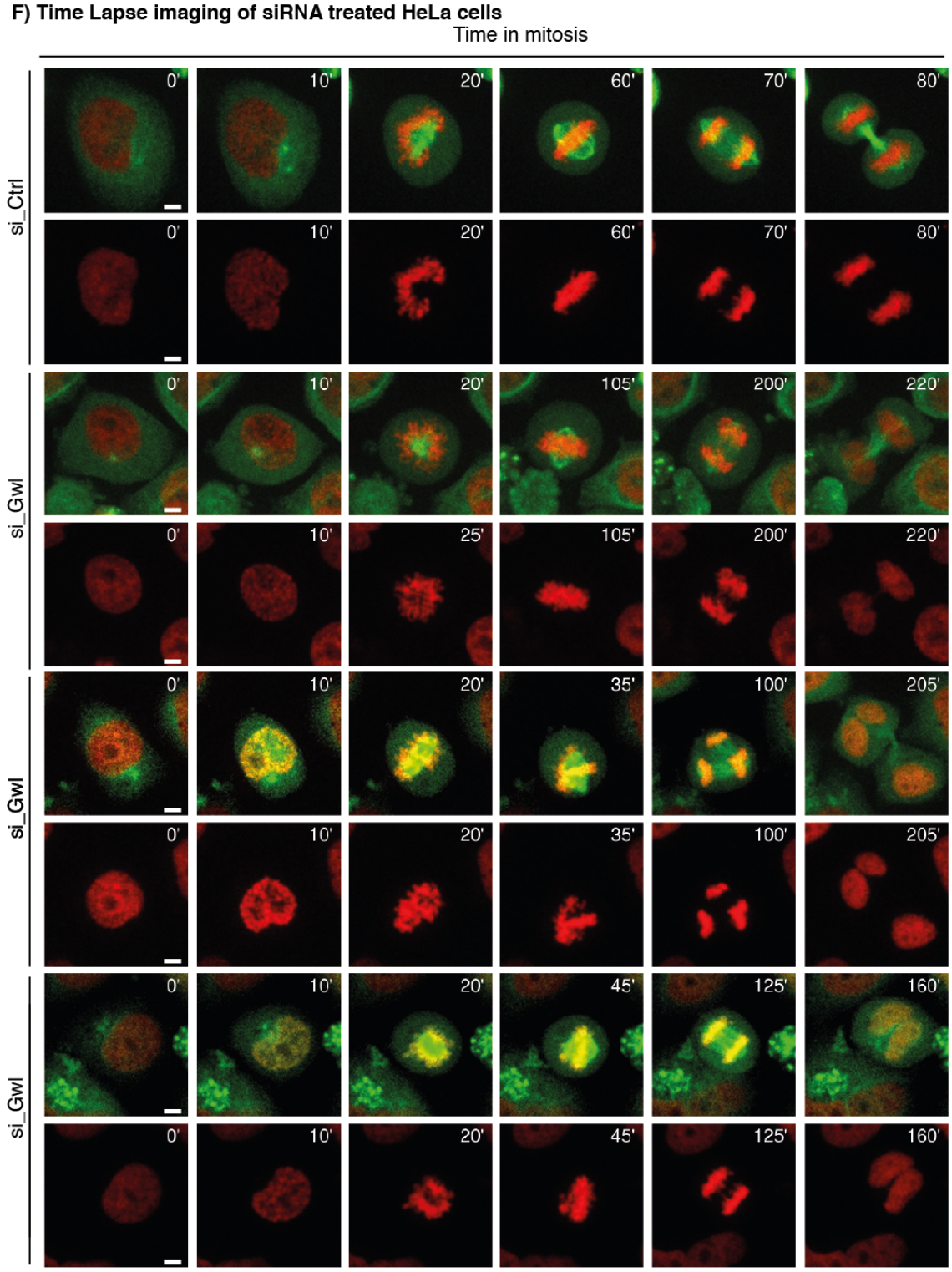

Figure 4.1 siRNA mediated depletion of Greatwall

F) Confocal time-lapse imaging of a *HeLa* cells stably expressing RFP-H2B and GFP-tubulin with control and Gwl knockdown. The Gwl siRNA kymographs represent both the defects (prolonged metaphase and cytokinesis defect) in mitotic cells. Time is in minutes; maximum intensity projection of seven-z dimension slices. Images were taken using the 40X lens, N.A 0.60. Scale bars, 10 μM.

Ensa/Arpp19 levels one can deduce that the smartpools are effective against the individual proteins. After these preliminary experiments, I could now use the smartpools to knockdown Ensa and Arpp19, both individually and together to analyse the mitotic profile of the cells. Similar to Greatwall knockdown experiments, I imaged the cells transfected with Ensa and Arpp19 for 16 h using time-lapse imaging on a spinning disc confocal microscope. When these cells were scored for mitotic index, the double knockdown showed a ~10% decrease in mitotic population, similar to Greatwall. Ensa seems to affect mitotic entry more than Arpp19 (Fig. 4.2C). Similar to Greatwall, Ensa/Arpp19 knockdown does not arrest the cells in G2 but the cells entering mitosis exhibit a variety of mitotic defects (Fig. 4.2D). Majority of the cells were arrested in metaphase for longer periods (mitotic time >100 min) with chromosomes moving towards and from the metaphase plat suggestive of alignment/attachment problems. Interestingly, we did not observe an increase in cytokinesis defects as compared to the Greatwall depleted cells, even in the case of double Ensa/Arpp19 depletion. Thus, the major phenotype of Ensa/Arpp19 knockdown is metaphase arrest and sister chromatid alignment defect, although the cells do eventually exit mitosis with lagging chromosomes. In addition, it is seen that the mitotic defects increase two-fold after double knockdown as compared to the individual proteins. Thus, the Ensa and Arpp19 have an additive effect with significantly more pronounced metaphase delays in the double knockdown cells.

There are two interesting points to be made from the comparison of Ensa/Arpp19 and Greatwall depletion phenotypes. First, the argument that partial Greatwall depletion is not sufficient for a G2 arrest cannot be maintained for Ensa/Arpp19 since they are thought to be tightly binding stoichiometric inhibitors of PP2A/B55. This strongly suggests that unlike *X. laevis* eggs and oocytes, mammalian cells can enter mitosis in the presence of active PP2A/B55.

The mitotic defects of Greatwall- and Ensa/Arpp19-depleted cells are almost identical and are very likely due to decreased Cdk1 substrate phosphorylation because of persistent PP2A/B55 activation. However, the hallmark phenotype of Greatwall depletion, namely the cytokinesis defect that led Cundell et al. to propose a novel BEG pathway during mitotic exit, seems to be specific to the Greatwall siRNA, and does not

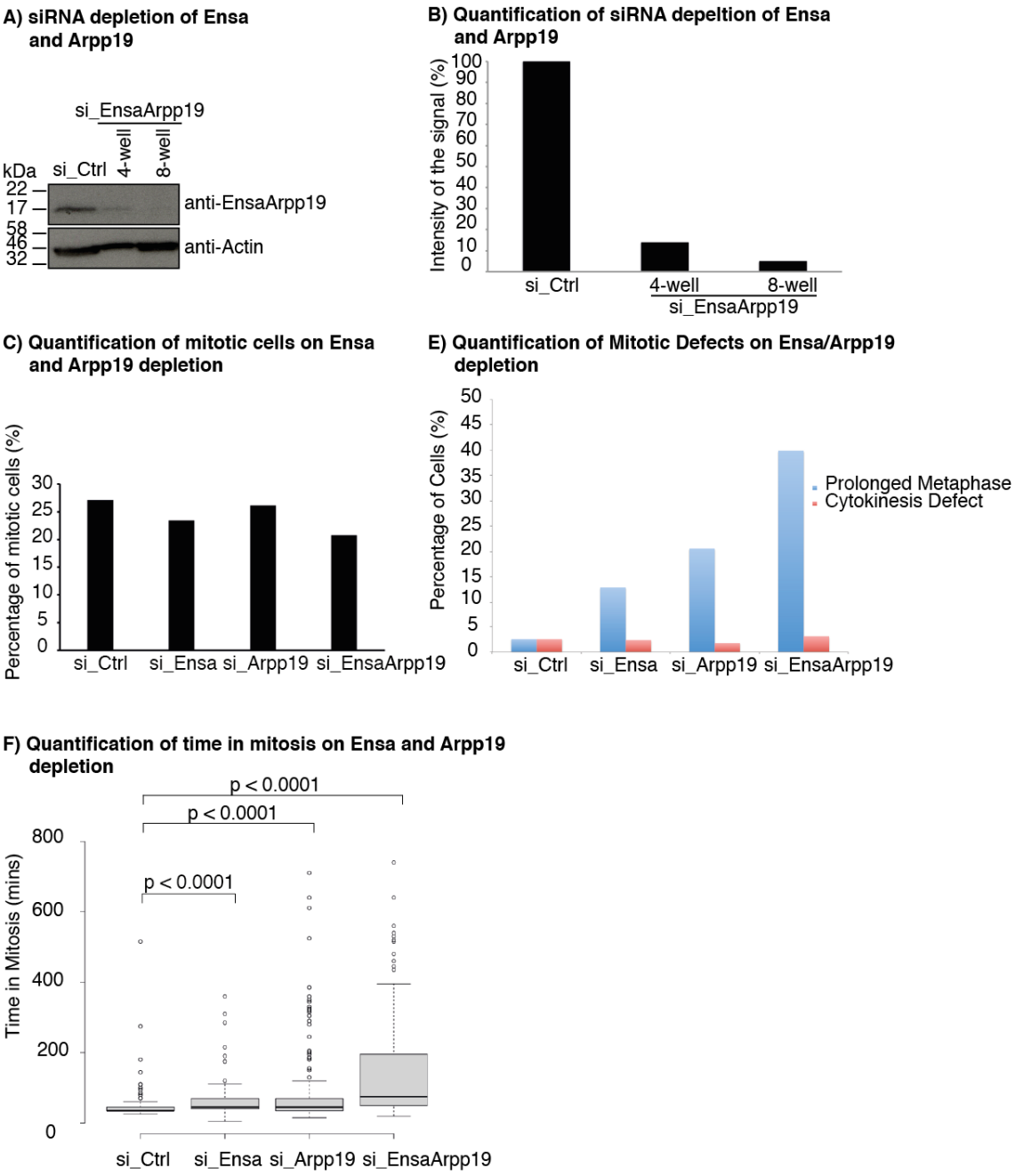

Figure 4.2 siRNA mediated depletion of Ensa and Arpp19

A) Western blot analyses of Control (si_ctrl), Ensa and Arpp19 (si_EnsaArpp19) siRNA-transfected *HeLa* cells. The depletion experiments were performed in 4-well and 8-well microscopic dishes. The lower panel shows actin as the loading control. B) Western blot quantification using ImageJ to show depletion of Ensa and Arpp19 protein levels. C) Mitotic indices were calculated for asynchronous *HeLa* cells transfected with control and EnsaArpp19 siRNA and stably expressing RFP-H2B and GFP-tubulin. D) The percentage of *HeLa* cells exhibiting mitotic defects (prolonged metaphase/cytokinesis defects) were scored over total mitotic cells and plotted graphically. E) A box-and-whisker plot showing the duration from NEB to cytokinesis with control and EnsaArpp19 knockdown in *HeLa* cells stably expressing RFP-H2B and GFP-Tubulin. Centre lines show the medians; box limits indicate the 25th and 75th percentiles as determined by R software; whiskers extend 1.5 times the interquartile range from the 25th and 75th percentiles, and outliers are represented by dots. n = 153, 85, 169, and 125 sample points. Analysis between samples was performed using the Mann-Whitney Rank Sum test, and p-values are presented above the box-plots.

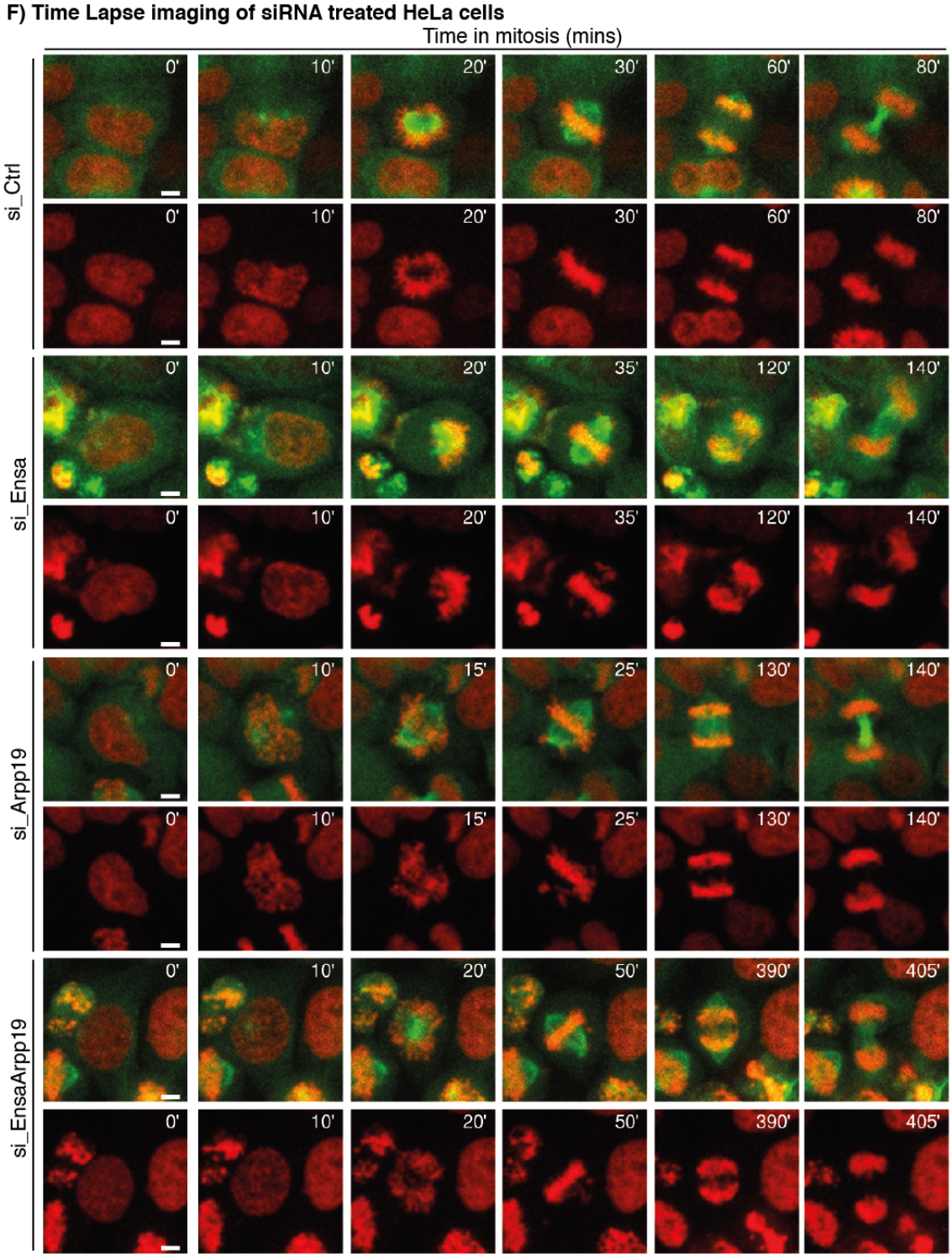

Figure 4.2 siRNA-mediated depletion of Ensa and Arpp19

F) Confocal time-lapse imaging of *HeLa* cells stably expressing RFP-H2B and GFP-tubulin with control and EnsaArpp19 knockdown. Time is in minutes; maximum intensity projection of seven-z dimension slices. Images were taken using the 40X lens, N.A 0.60. Scale bars, 10 μM.

occur in Ensa/Arpp19-depleted cells. This could suggest a specific function for Greatwall or an off target effect of these siRNAs.

4.2 Detailed Analysis of Mitotic Entry Roles of Greatwall and Ensa/Arpp19 on Cdk1 Inhibition

Historically, Cyclin B-Cdk1 is known to be the master controller of entry into mitosis. It was shown mathematically in *X. laevis* extracts that once the Cdk1-cyclin B complex reaches its activation threshold, a cell could enter into mitosis. They further showed that the G2/M switch is bistable with low Cdk1 in interphase and high Cdk1 activity in mitosis. The bistable switch causes a shift between 2 stable states, interphase and mitosis in case of G2/M transition, with no intermediate state. This was later proven experimentally in *X. laevis* egg extracts (Pomerening et al. 2003; Sha et al. 2003). Recent work in mammalian cells has shown that this cycle of Cdk1 activation/inactivation is conserved evolutionarily in the mammalian system (Yuan et al. 2002; Lindqvist et al. 2007; Pomerening, Ubersax & Ferrell 2008b). All these studies were based on the Cdk1-CyclinB1 activation levels and the resulting entry into mitosis. Initially it was thought that the phosphatases remain stable throughout the cell cycle. However, in the past few years it has been shown that even the phosphatase activity oscillates counterbalancing the Cdk1 activity. (Mochida et al. 2009; Castilho et al. 2009; Vigneron et al. 2009).

In this work, I wanted to clarify if Greatwall and Ensa/Arpp19 affect the Cdk1 threshold for mitotic entry in a similar manner, which could help elucidate the specific mitotic entry functions of Greatwall that may or may not be independent of Ensa/Arpp19.

Greatwall is activated by Cdk1 and initiates the BEG pathway to inhibit PP2A via Ensa and Arpp19. Hence, when Greatwall is depleted, it is expected that the cells would arrest in G2. Although this is true for *X. laevis* and *Drosophila*, only a delay in mitotic entry is seen in human cells (J. Yu et al. 2006; Zhao et al. 2008; Burgess et al. 2010; Voets & Wolthuis 2015). These phenotypes could be rescued even by Cdk1 depletion, hence proving that Greatwall participates in the auto-regulatory loop of Cdk1 (J. Yu et

al. 2006; Zhao et al. 2008). Active Greatwall and consequent PP2A inhibition is required both to promote the Cdk1-Cyclin B activation loop and to prevent mitotic substrates dephosphorylation. Greatwall achieves this by phosphorylating Ensa and Arpp19, which are potent inhibitors of PP2A. However, in addition to that Cdk1 also directly phosphorylates Arpp19 in starfish oocytes, promoting mitotic entry in the absence of Greatwall (Okumura et al. 2014).Hence, Ensa/Arpp19 promotes mitotic entry independent of Greatwall, once they're phosphorylated by Cdk1.

In the initial experiments with asynchronous cells, both Greatwall and Ensa/Arpp19 depletion did not affect mitotic entry significantly. This could be because the Cdk1 activation threshold could overcome the activity of partially active phosphatases. As an all or none response was observed on inhibiting of Greatwall in lower organisms, it was intriguing to analyse the mitotic entry in a bit more detail when Cdk1 was inhibited in Greatwall depleted cells. Subsequently, I could study if these effects on mitotic entry were similar or different to the ones seen on Ensa/Arpp19 depletion. For this purpose, I used *HeLa* cells stably expressing the *X. laevis* analogue sensitive Cdk1 mutant and RFP-H2B. Hereafter, in this work, these cells are mentioned as *HeLa-Cdk1as* cells. These cells can be synchronized in G2 when treated with ATP analogue, 1NMPP1 for at least 16 h. The *X. laevis Cdk1as* construct has been tested for varying concentrations of 1NMPP1 in in-vitro kinase assays and DT40 cell lines; 10 μM 1NMPP1 was used in DT40 to synchronise them in G2 (Hochegger et al. 2007). However, when a HeLa cell line stably expressing *X. laevis Cdk1as* was generated, 1 μM 1NMPP1 was sufficient to synchronise the cells in G2 (data not shown).

One micromole of 1NMPP1 was used to synchronize the cells in G2, following Greatwall and Ensa/Arpp19 knockdown respectively. 1NMPP1 is a reversible drug and can be removed by washing the cells with warm media a few times. In my assay, I washed the arrested cells five times with warm media to maintain consistency. In order to maintain different concentrations of Cdk1, I added different concentrations of 1NMPP1 and imaged the cells using time-lapse imaging. This assay was to study mitotic entry only, hence MG132 (APC/C inhibitor) was used to prevent mitotic exit. After 4 h of imaging, 70–75% of control cells were in mitosis and the count did not increase further. Hence, the Greatwall and Ensa/Arpp19 knockdown cells were also

quantified after 4 h of imaging. Cells with intact nuclear envelope were scored as G2 and cells without it were scored as mitotic cells.

Surprisingly, Greatwall and Ensa/Arpp19 cells were arrested in G2 at different Cdk1 concentrations (Fig. 4.3-4.4). While Greatwall-depleted cells could be arrested with 0.25 μM 1NMPP1 (Fig. 4.3A-B), Ensa/Arpp19-depleted cells required 0.5 μM 1NMPP1 to be arrested in G2 (Fig. 4.3C-D). This means that Greatwall-depleted cells remain in G2 even with high Cdk1 activity as compared to Ensa/Arpp19. Thus, this indirectly shows Ensa/Arpp19 and Greatwall perform different functions at mitotic entry. In addition, somatic cells can enter mitosis with suboptimal Cdk1 activity even when PP2A is active. This, has been indirectly shown when mitotic cells were quantified using phospho-Ser antibody in Greatwall-depleted cells (Burgess et al. 2010). The Cdk1 threshold decreases in the absence of Ensa/Arpp19, despite the fact that PP2A would be active (Fig. 4.3C-D). Ensa/Arpp19 are a stoichiometric inhibitor of PP2A and are present in almost equal molar concentration as compared to the phosphatase (M. Wang et al. 2015). On siRNA depletion, this concentration is reduced, decreasing the number of molecules available to interact with and thus inhibit PP2A. However, as Greatwall is active, it can phosphorylate and activate the residual Ensa/Arpp19 with higher processivity and inhibit PP2A partially. Moreover, similar to *X. laevis* cells presence of PP2A may inactivate Cdk1, owing to Wee1-dependent phosphorylation of Cdk1 (Mochida et al. 2009). Thus, active Greatwall may be potentially promoting M-phase entry on Ensa/Arpp19 depletion. Additionally, I observed peculiar surface blebbing specific to Ensa/Arpp19 depletion, when G2 arrested cell were released from the 1NMPP1 block (Fig. 4.3D). This could be owing to the presence of Arpp19 as potassium channels on the cell surface. However, how it relates to the mitotic entry and Cdk1 activation needs to be explored.

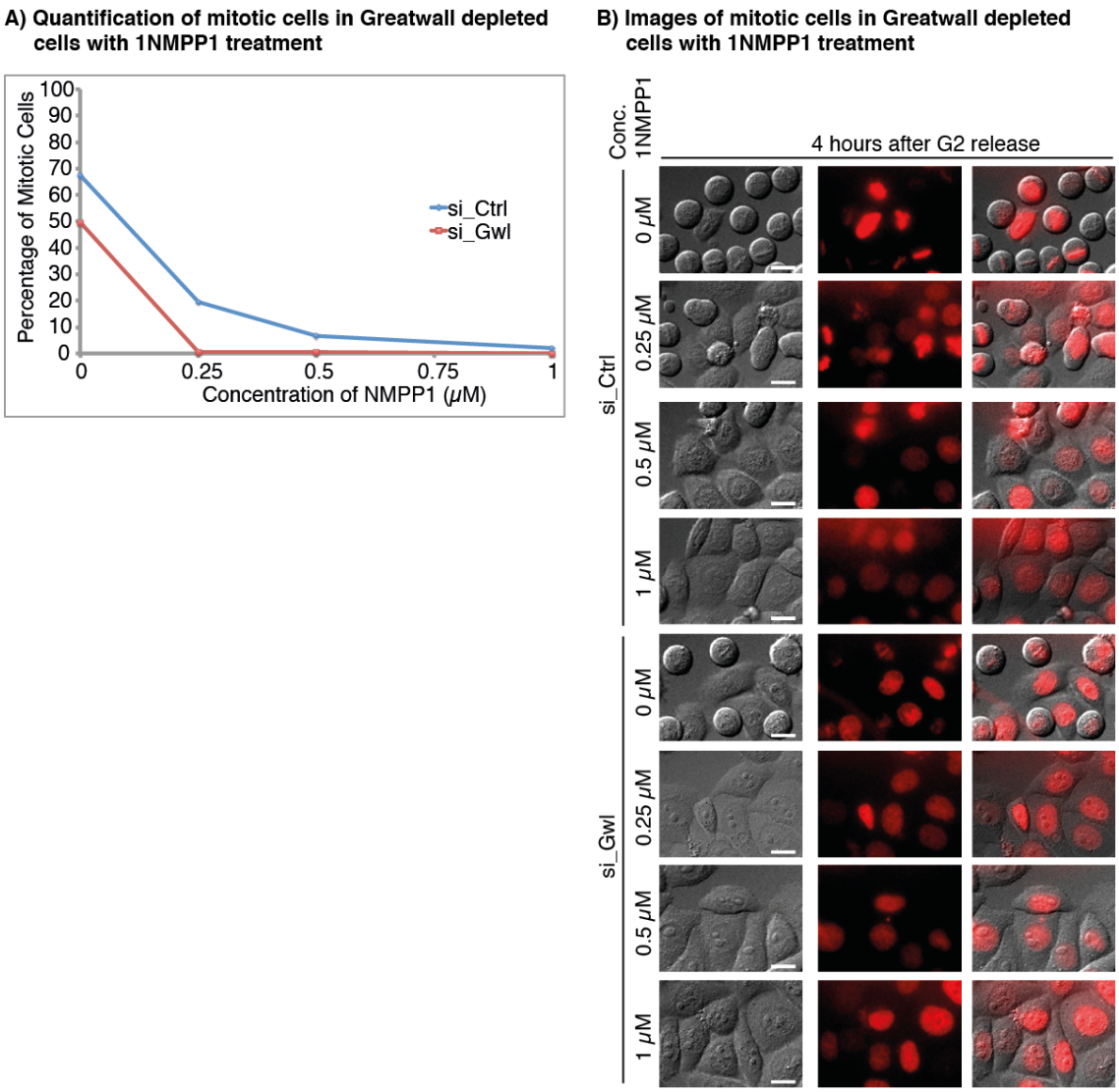

Figure 4.3 Mitotic entry on Greatwall and EnsaArpp19 depletion

A) Quantification of cells that entered mitosis with varying concentrations of 1NMPP1 (0–1 μM) on Gwl depletion. *HeLa-cdk1as* cells stably expressing RFP-H2B were released from 16 h G2 arrest following control and Gwl knockdowns. Cells were treated with MG132 (25 μM) to prevent mitotic exit and were quantified 4 h post-G2 release. B) Images of mitotic cells 4 h post-G2 release into varying concentrations of 1NMPP1, following control and Gwl knockdowns. Images were taken on the IX71_Olympus microscope using the 40X lens, N.A 0.60. Scale bars, 10 μM.

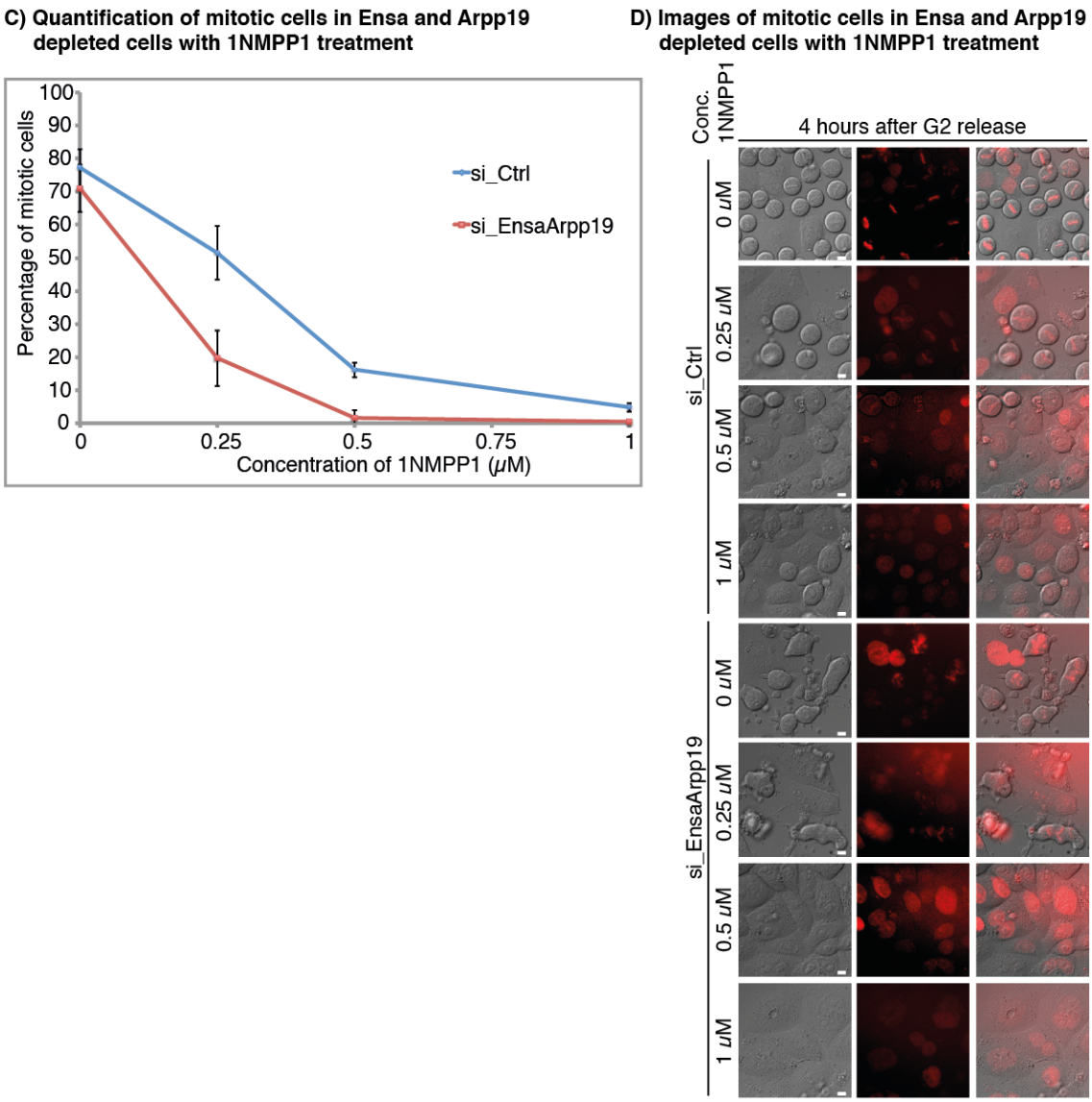

Figure 4.3 Mitotic entry on Greatwall and EnsaArpp19 depletion

C) Quantification of cells that entered mitosis with varying concentrations of 1NMPP1 (0–1 μM) on EnsaArpp19 depletion. *HeLa-cdk1as* cells stably expressing RFP-H2B were released from 16 h G2 arrest following control and EnsaArpp19 knockdowns. Cells were treated with MG132 (25 μM) to prevent mitotic exit and were quantified 4 h post-G2 release. D) Images of mitotic cells 4 h post-G2 release into varying concentrations of 1NMPP1, following control and EnsaArpp19 knockdowns. Images were taken on the IX71_Olympus microscope using the 40X lens, N.A 0.60. Scale bars, 10 μM.

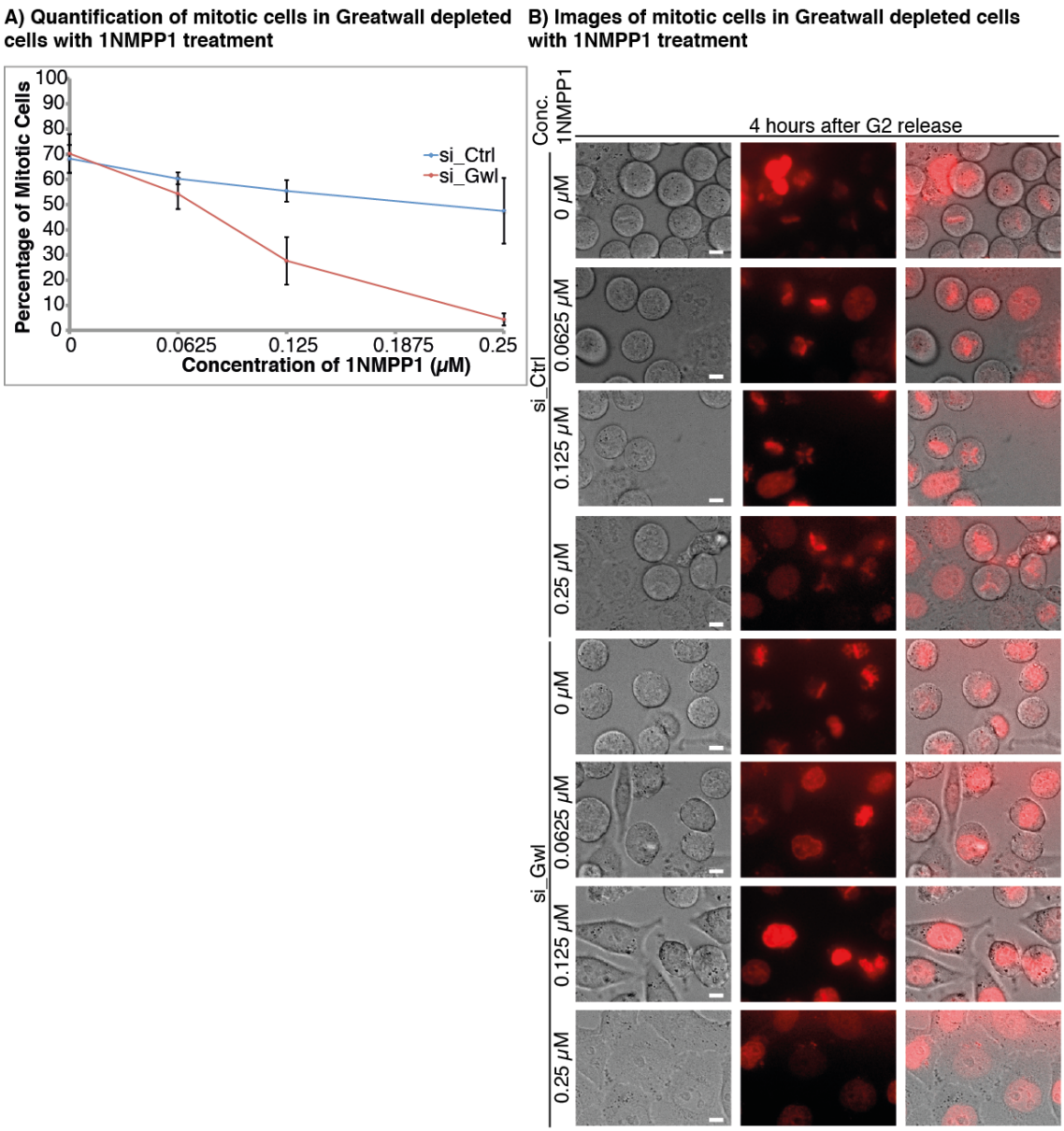

Figure 4.4 Mitotic entry on Greatwall depletion

A) Quantification of cells that entered mitosis with varying concentrations of 1NMPP1 (0-0.25 μM) on Greatwall depletion. *HeLa-cdk1as* cells stably expressing RFP-H2B were released from 16 h G2 arrest following control and Greatwall knockdowns. Cells were treated with MG132 (25 μM) to prevent mitotic exit and were quantified 4 h post-G2 release. B) Images of mitotic cells 4 h post-G2 release into varying concentrations of 1NMPP1, following control and Greatwall knockdowns. Images were taken on the IX71_Olympus microscope using the 40X lens, N.A 0.60. Scale bars, 10 μM.

It has been shown previously that Greatwall-depleted cells induce mitotic exit even with high Cdk1 activity (Vigneron et al. 2009). Here we see that Greatwall arrests cells in G2 even with Cdk1 activity comparable to 0.25 μM 1NMPP1 (Fig. 4.3A-B). This leads us to make a few hypotheses. Firstly, in the absence of Greatwall, the BEG pathway is not activated and hence PP2A is highly active. Thus, PP2A could act either on the Cdk-Cyclin B auto-regulatory loop or on mitotic substrates. Similar to *X. laevis*, PP2A could inactivate Cdk1 and prevent mitotic entry. Additionally, as Greatwall is absent, the higher amount of Cdk1 is required to overcome the substrate dephosphorylation by PP2A that was earlier inhibited. As mitotic entry phenotypes are not observed on B55 depletion, it would be interesting to check if in *HeLa-Cdk1as* cells B55 knockdown rescues the Greatwall and Ensa/Arpp19 entry phenotype.

To investigate the exact amount of 1NMPP1 inhibition that the Greatwall cells can tolerate, I analysed their mitotic entry with a smaller range of 1NMPP1 concentrations (Fig. 4.4A-B). Although, ~5% cells enter mitosis with 0.25 μM 1NMPP1, its 10 times less than the control cells. These cells could be the un-transfected population, which was observed across three independent experiments. With lower concentrations of 1NMPP1, cells entered mitosis. Thus, Cdk1 activity any higher than that seen in Fig. 4.3A-B is able to overcome the phosphatase activity and induce mitotic entry.

Finally, in this chapter, I characterised the major phenotypes of Ensa/Arpp19 in somatic cells using RNAi-mediated knockdown. However, as these cells were only imaged using fluorescence and no surface markers were present, the characteristic blebbing phenotype could not be identified. Majority of the Ensa/Arpp19 cells arrest in metaphase for longer duration but exit mitosis eventually with lagging chromosomes. Defects like chromosome accumulation at the poles and lagging chromosome are seen, indicative of premature mitotic exit. I also confirmed that Greatwall depletion prevents mitotic entry with higher Cdk activity as compared to Ensa/Arpp19. The most probable reason for this observation could be a highly processive Greatwall kinase that activates even low amounts of Ensa/Arpp19 to partially inactivate PP2A. This is not possible when Greatwall is inhibited and leads to higher activation threshold. However, further experiments quantifying the cellular processivity of Greatwall are required to confirm this observation.

It can also be speculated that an unknown phosphatase downstream of Greatwall and independent of Ensa/Arpp19 is opposing the Cdk1 activity at mitotic entry. This could lead to higher Cdk1 thresholds in the absence of Greatwall, as both PP2A and the unknown phosphatase are highly active against the mitotic substrates. However, this possibility needs to be investigated in detail to understand the role of Greatwall and Ensa/Arpp19 in mitotic entry better.

CHAPTER5 ANALYSIS OF ENSA/ARPP19 DEPHOSPHORYLATION IN MAMMALIAN CELLS.

Entry into mitosis is preceded by substrate phosphorylation on multiple mitotic proteins (Dephoure et al. 2008; McCloy et al. 2014). The active complex Cdk1-Cyclin B carries out majority of these phosphorylations. Although there is no strict Cdk consensus recognition element, preferred residues are on a proline–directed serine threonine sites, which means serine and threonine is followed by a proline (Nick R Brown et al. 1999). Mitotic entry also relies on the inactivation of phosphatases, to prevent the premature dephosphorylation of these mitotic proteins and futile phosphorylation and dephosphorylation cycles. This is reversed in mitotic exit where Cdk1 is inactivated and the counteracting phosphatases become active (Barr et al. 2011; Bollen et al. 2009). It is experimentally shown in *Xenopus*, that the activity of phosphatases fluctuates in the cell cycle being high in interphase and low in mitosis, contrary to the Cdk-Cyclin oscillations (Mochida & Hunt 2007; Virshup & Shenolikar 2009).

It was discovered in *Xenopus* that Cdk dynamics were controlled by a phosphatase of the type 2A that was named INH (Cyert & Kirschner 1988; Solomon et al. 1990). Later in 2009, Mochida et al. identified PP2A-B55δ as the major Cdk-counteracting phosphatase in *Xenopus* (Mochida et al. 2009). Similarly in mammalian cells, inhibition of an okadaic acid sensitive phosphatase initiated mitotic entry even when Cdk1 is inhibited (Gowdy et al. 1998). In recent years an unusual AGC kinase, Greatwall was found to control this phosphatase. Greatwall works on PP2A via its substrates Ensa and Arpp19, which are small proteins and potent inhibitors of the phosphatase (Zhao et al. 2008; Castilho et al. 2009; Vigneron et al. 2009; Mochida et al. 2009; Mochida et al. 2010; Gharbi-Ayachi et al. 2010). Greatwall kinase is phosphorylated and activated by Cdk1, which further leads to inactivation of phosphatase PP2A-B55, to prevent premature dephosphorylation of mitotic substrates at G2/M transition. Thus, Cdk1 inhibits its counter-acting phosphatase via the Greatwall-Ensa/Arpp19/B55 pathway (Blake-Hodek et al. 2012; Vigneron et al. 2011). Cdk1 also phosphorylates Arpp19 directly in starfish oocytes, thus inhibiting the phosphatase in a Greatwall independent manner. However, this does not have a significant impact on *Xenopus* Ensa (Okumura et al. 2014; Mochida 2014).

PP2A is a hetero-trimeric complex. It consists of the catalytic subunit CA or CB, the scaffolding subunit A and the regulatory subunit B, which is variable. The different regulatory subunits are responsible for substrate specificity of the phosphatase. The different regulatory subunits are B55 (B), B56 (B'), B'', B'''. PP2A-B55 has been suggested to be the major Cdk1 countering phosphatase, based on the observation that the B55 δ depleted cycling extracts advance into mitosis faster, whereas the mitotic exit is compromised. Conversely, addition of purified PP2A-B55 δ complex delays and blocks Cdk1 activation and mitotic entry (Mochida et al. 2009).

Direct interactions of purified Ensa and Arpp19 with B55 and C subunits of PP2A were also shown in *Xenopus* extracts. Mochida et al. showed that Ensa interacts with the active site of the phosphatase in *Xenopus* (Mochida 2014), while Williams et al. showed Okadaic acid competes with Ensa for the active site in *HeLa* extracts (Williams et al. 2014). Greatwall phosphorylation of Ensa and Arpp19 is important for this interaction to occur. Also the binding of the inhibitor reduces the phosphatase activity towards Cdk substrates significantly (Gharbi-Ayachi et al. 2010). These interactions lead to the somewhat counter-intuitive model that a phosphorylated residue becomes an inhibitor of a phosphatase by directly binding its active site. Williams et al. (2014) confirmed this model by carefully measuring the binding rates (Km) of pEnsa to PP2A-B55 and the catalytic activity of PP2A/B55 to dephosphorylate pEnsa. The results led to the "unfair competition model" of action. Ensa is a very strong binder (Km = 0.009–0.0017 μM) but a very poor substrate of PP2A-B55 (Kcat = 0.021–0.035 s^{-1}) thereby blocking the active site for access to other substrates.

In parallel, our lab reported (Hégarat, Vesely, Vinod, Ocasio, Peter, Gannon, Oliver, Novák & Hochegger 2014b) that the phosphatase inhibitor okadaic acid did not inhibit pEnsa dephosphorylation, but maintained Greatwall phosphorylation on its Cdk1 site Thr194. Ensa phosphorylation was only blocked either when both PP2A and PP1 were inhibited using a combination of okadaic acid and tautomycetin or when the phosphatase FCP1 was depleted by siRNA. Interestingly, FCP1 had previously been implicated in mitotic regulation besides its role as a RNA-polymerase phosphatase(Visconti et al. 2012)and also in Greatwall kinase regulation later (Monica et al. 2015).This led us to propose that FCP1 and PP2A-B55 were the major

contributors of Greatwall Ensa dephosphorylation during mitotic exit, with a potential additional role for PP1.

Subsequently, Heim et al. found that PP1 does indeed target the C-terminal autophosphorylation sites of Greatwall (Heim et al. 2015). Moreover, FCP1 was also shown to regulate Greatwall kinase rather than Ensa. These results could be summarised in a model whereby PP1 and FCP1 collaborate during early mitotic exit to deactivate Greatwall. This deactivation of Greatwall causes a shift in the balance of pEnsa/Ensa ratio and triggers dephosphorylation of Ensa by PP2A/B55. Subsequently, PP2A/B55 could also further contribute to completely inactive Greatwall kinase.

One particular problem with this model is that the activity of PP2A/B55 towards pEnsa is so poor that it would only ever work directly as a phosphatase, if the counteracting Greatwall kinase activity were completely removed. This does not to appear to be the situation in cells. Thus, our lab found that pEnsa dephosphorylation could still occur when Greatwall inactivation is blocked by okadaic acid and that it retains at least 50% of its mitotic activity. This could imply that another phosphatase directly contributes to pEnsa dephosphorylation in anaphase and captures that protein when it is not bound to PP2A/B55.

In this chapter, I set out to test the “unfair competition” model, to analyse the interaction between Ensa/Arpp19 and PP2A-B55 in human cells and to identify novel phosphatases acting on Ensa/Arpp19 using purified thio-phosphorylated protein as a bait in a proteomic screen.

5.1 Testing the “Unfair Competition” Model of Ensa/PP2A-B55 Interaction

Work form Williams et al. predicted the unfair competition model shown in Fig. 5.1A. According to this model, phosphorylated Ensa/Arpp19 act as both inhibitors and substrates of PP2A-B55. As long as Greatwall kinase activity remains high, the balance will be on the inhibitor side. Once Greatwall kinase is inactivated, the balance will shift to the phosphatase and dephosphorylation of Ensa and Arpp19 will occur.

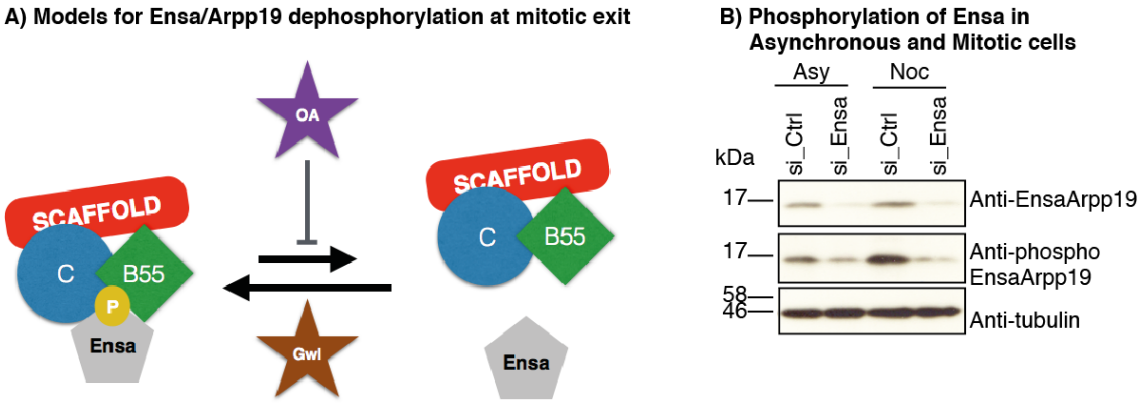

Figure 5.1 Model for PP2A-B55-Ensa/Arpp19 interaction in mammalian cells

A) Schematic representation of model proposed for Ensa/Arpp19 dephosphorylation at mitotic exit by Williams et al. (2014) B) Phosphorylation of Ensa/Arpp19 in asynchronous and nocodazole-treated mitotic cells, after Ensa and Arpp19 siRNA (20 nM each) for 48 h in *HeLa* cells. Cell lysates were probed with the indicated antibodies and alpha-tubulin was used as a loading control.

C) Phosphorylation of Greatwall and Ensa/Arpp19 in diferent phases of mitosis

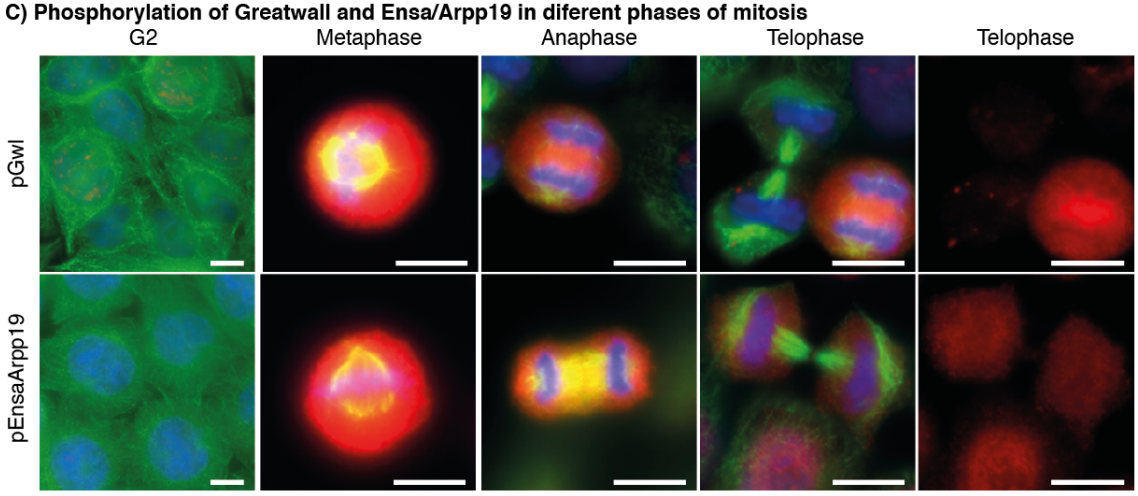

D) Quantification of phosphorylation of Greatwall and Ensa/Arpp19 in diferent phases of mitosis

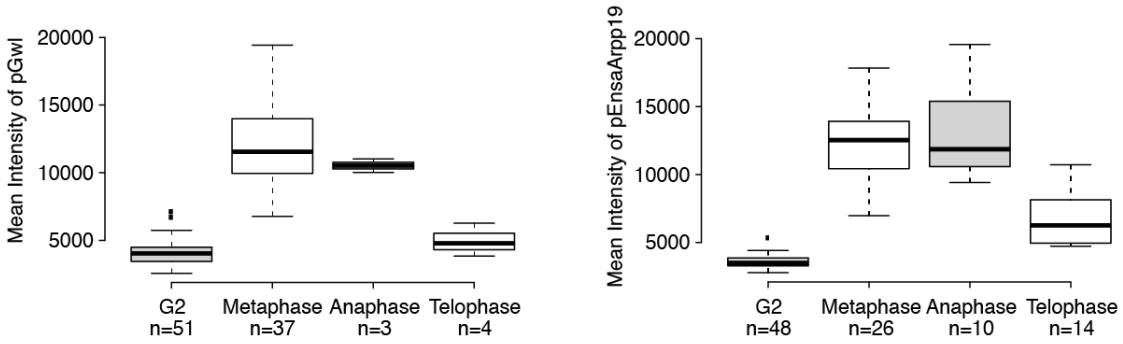

E) Protein abundance in cell lines from PaxdB database

Protein	H.sapiens - Cell line, HEK293, SC (Geiger,MCP,2012)	H.sapiens - Cell line, HEK293 (Geiger,MCP,2012)	H.sapiens - Cell line, Hela, SC (Nagaraj,MSB,2011)	H.sapiens - Cell line, Hela (Geiger,MCP,2012)	H.sapiens - Cell line, U2OS (Beck,MSB,2011)
ARPP19	1383 ppm	160 ppm	272 ppm	112 ppm	21.8 ppm
ENSA	952 ppm	183 ppm	173 ppm	187 ppm	215 ppm
PPP2R2A	38.3 ppm	176 ppm	190 ppm	189 ppm	44.4 ppm
PPP2R2D	42.8 ppm	68.7 ppm	61.8 ppm	69.8 ppm	NA

Figure 5.1 Model for PP2A-B55-Ensa/Arpp19 interaction in mammalian cells

C) Immunofluorescence of *HeLa*_as cells released from G2 arrest. Cells were synchronised in G2 for 16 h with 1 µM 1NMPP1 and samples were taken 0, 1 and 3 h after wash-off. Cells in different phases of mitosis were fixed with PFA and visualised with FITC-Tubulin (green) and TRITC-phospho-Ensa/Arpp19 or TRITC-phospho-Gwl (red). DNA was visualised using DAPI (blue). Images were taken on the IX73_Olympus microscope using the 40X lens, N.A 0.60. Scale bars, 10 µm. D) A box-and- whisker-plot showing quantification of phosphorylation signal of Greatwall and Ensa/Arpp19 in different phases of mitosis. Centre lines show the medians; box limits indicate the 25th and 75th percentiles as determined by R software; whiskers extend 1.5 times the interquartile range from the 25th and 75th percentiles, outliers are represented by dots. Greatwall: n = 51, 37, 3, 4 sample points. Ensa/Arpp19: n = 48, 26, 14, 10 sample points. E) Mass spectrometry data from PaxDB database (http://pax-db.org) showing the abundance of PP2A-B55 regulatory subunits α and δ, Ensa and Arpp19 in human cells lines.

This model makes two testable predictions. First Greatwall needs to be inactivated before Ensa is dephosphorylated. The Kcat of PP2A/B55 on Ensa is so low that in the presence of residual kinase activity, dephosphorylation would never proceed. Secondly, since pEnsa acts as a substrate and binds the phosphatase directly in the active site, okadaic acid should be a competitor of this interaction and disrupt the complex.

To test the first prediction we decided to measure the dephosphorylation of Ensa/Arpp19 and Greatwall kinase using immunofluorescence with phospho-specific antibodies (Hégarat, Vesely, Vinod, Ocasio, Peter, Gannon, Oliver, Novák & Hochegger 2014b). Nocodazole-treated cells exhibit an increase in phosphorylation of Ensa/Arpp19 at S67 (Fig. 5.1B). This signal appears to be specific since there is a significant decrease following Ensa/Arpp19 siRNA depletion. To observe the mitotic exit and dephosphorylation of Ensa/Arpp19 and Greatwall, *HeLa-cdk1as* cells were arrested in the G2 phase using 5 μM 1NMPP1, and samples were collected 1 and 3 h after release from 1NMPP1. Cells were fixed and visualised using phospho antibodies against T194 for Greatwall and S67 for Ensa/Arpp19. Cells in distinct phases of mitosis were identified to observe the dephosphorylation profile of these proteins during mitosis and at mitotic exit. The Greatwall phospho-signal disappears completely at telophase, while Ensa/Arpp19 stays phosphorylated until late telophase (Fig. 5.1C-D). This is in agreement with the Goldberg model, as Greatwall needs to be inactivated first, to prevent futile phosphorylation and dephosphorylation cycle of Ensa/Arpp19. This observation is also in agreement with the findings that PP1 initiates Greatwall dephosphorylation, while PP2A-B55 is still inactivated by phosphorylated Ensa/Arpp19 in *Xenopus* (Heim et al. 2015) and challenges the notion that T194 is dephosphorylated by PP2A/B55 (Hégarat, Vesely, Vinod, Ocasio, Peter, Gannon, Oliver, Novák & Hochegger 2014b). However, measuring the dynamics of phosphorylation of both residues directly side by side is necessary to firmly conclude that one site is dephosphorylated before the other. This is currently not possible because both antisera were raised in rabbit and cannot be used in a single immune-fluorescence experiment.

The Goldberg model also demonstrates that PP2A dephosphorylates Ensa/Arpp19 with very slow kinetics while being bound to the protein. However, the molar concentration of Ensa and Arpp19 is more than twice the amount of PP2A-B55δ and more than a few parts per millions for PP2A-B55-alpha in most mammalian cell lines (Fig. 5.1E). This

calls for a highly processive PP2A to dephosphorylate the molar excess of Ensa and Arpp19 in the short frame of time at mitotic exit. The switch-like transition of mitotic-exit does not seem possible if Ensa/Arpp19 remain phosphorylated and keep inhibiting PP2A until telophase. Thus, it is not unreasonable to speculate that a separate phosphatase assists PP2A-B55 in inactivating Ensa/Arpp19 in telophase.

5.2 Immunoprecipitation using Transient Ensa/Arpp19 Expression in *Hek293* Cells

To test the second prediction of the "unfair competition" model, i.e. that okadaic acid competes with Ensa/Arpp19 for binding the phosphatase, I transiently over-expressed Flag-tagged Ensa and Arpp19 and analysed the co-immuno-precipitation of PP2A-B55. It was previously shown in *Xenopus* using interphase and CSF extracts, that Ensa/Arpp19 interacts with the catalytic subunit of PP2A-B55 specifically in mitotic extracts (Gharbi-Ayachi et al. 2010). Surprisingly, when this experiment was done in asynchronous (~10% mitotic cells) *Hek293* cells, I observed a strong interaction Flag Ensa and Flag Arpp19 with the B55-alpha subunit, despite the minor fraction of mitotic cells. This interaction was indicated both by the B55-alpha and by PAN antibodies for all the subunits of PP2A-B55. The increasing salt concentration does not affect the complex; hence proving Ensa/Arpp19 binds strongly to the phosphatase in asynchronous extracts. To analyse if this interaction is independent of the mitotic phosphorylation of Ensa/Arpp19, it was essential to check if the exogenous Flag Ensa and Arpp19 are phosphorylated in-vivo at Serine 67, specifically in mitosis. The IP eluates also show exogenous Ensa/Arpp19 to be phosphorylated in asynchronous extracts in both high and low salt conditions (Fig. 5.2A). This could reflect specifically the mitotic population in the cells, or point to cell cycle independent phosphorylation of the two PP2A-B55 inhibitors.

According to the Goldberg model, okadaic acid will compete with Ensa/Arpp19 for binding to PP2A-B55 (Williams et al. 2014). To observe the effect of okadaic acid on Ensa/Arpp19-B55 interaction, the pull downs were also performed in the presence of Okadaic acid. As seen in Fig. 5.2 B, the binding affinity is significantly reduced in the presence of 100 nM Okadaic acid, but it does not disappear completely. This

observation is compatible with the predicted model. Interestingly, we could not detect phospho-

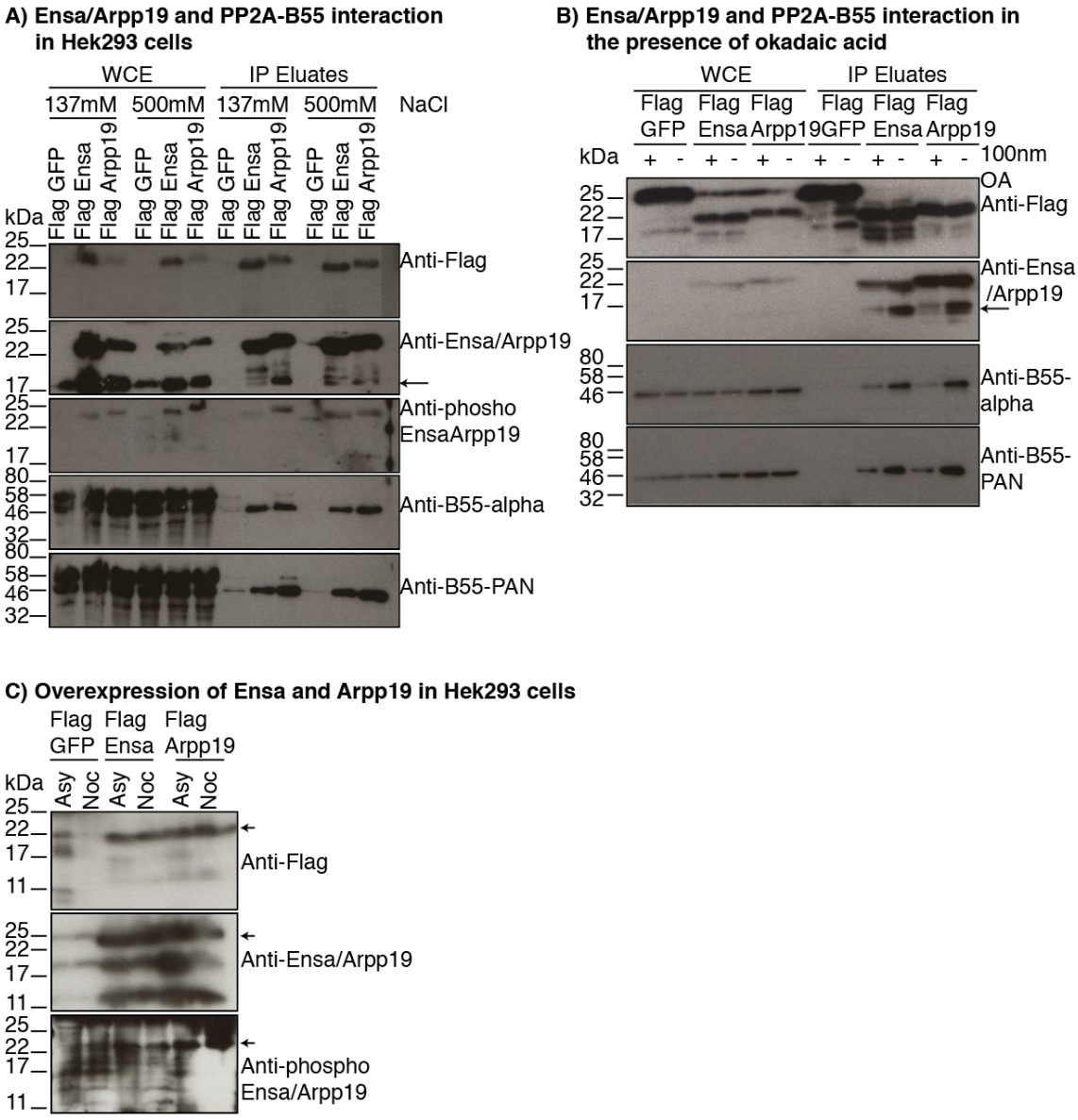

Figure 5.2 Co-immunoprecipitation with exogenously expressed Flag-Ensa/Arpp19 in *Hek293* cells

A) Immunoprecipitation assays with transiently expressed Flag-Ensa and Arpp19 in *Hek293* cells in the presence of high (500 mM) and low (137 mM) salt buffers. Aliquots of whole cell extracts (WCE) and IP elutions (IP Eluates) were analysed with the indicated antibodies. Flag-GFP was used as a negative control. Arrow indicates endogenous Ensa/Arpp19 observed in the eluted fractions. B) Immunoprecipitation assays with transiently expressed Flag-Ensa and Arpp19 in *Hek293* cells. Lysis buffer with and without 100 nM Okadaic acid was used to prepare Whole cell lysate (WCE). Aliquots of WCE and IP elutions (IP Eluates) were analysed with the indicated antibodies. Arrow shows endogenous Ensa/Arpp19 observed in the eluted fractions. C) Flag GFP, Flag Ensa and Flag Arpp19 were transiently overexpressed using CaCl2 transfection in *Hek293* cells for 48 h. Cells were either untreated or nocodazole-treated for 16 h and cells lysates were probed with the indicated antibodies. Arrows indicate the Flag-tagged
Ensa and Arpp19.

Ensa/Arpp19 in the immune-precipitates. This could suggest that complex does fall apart after it has been captured on the beads and Ensa/Arpp19 become dephosphorylated.

We also observed that exogenous Ensa and Arpp19 were seen to interact with a smaller protein that is identified by the Ensa/Arpp19 antibody but not the Flag-antibody (indicated by arrows in Fig. 5.2A-B). This co-purifying protein was also reduced after okadaic acid treatment. It is tempting to speculate that this band could represent endogenous Ensa/Arpp19 that forms a dimer with the exogenous protein to bind with PP2A-B55. However, before we proceeded to study the Ensa/Arpp19-B55 interaction in *Hek293* cells line, I decided to check if the exogenous protein behaved similarly to the endogenous one and if it was highly phosphorylated specifically in mitosis. The strong interaction between B55 and Ensa in asynchronous cells that we observed was somewhat surprising, as this should only be specific for the small pool of mitotic cells. Accordingly, both the Flag-tagged Ensa and Arpp19 are highly phosphorylated in asynchronous population (Fig. 5.2C). This constitutive phosphorylation of exogenous protein could mean that high overexpression of Ensa/Arpp19 in the *Hek293* triggers a feedback resulting in B55 inhibition and Greatwall activation. This makes this cell system unsuitable to study the dynamics of Ensa/Arpp19 interaction with PP2A/B55. Thus, further studies were done in *HeLa* cells after the necessary preliminary investigations.

5.3 Immunoprecipitation and Size-Exclusion Chromatography using Transient Ensa/Arpp19 Expression in *Hela-Cdk1as* Cells

Preliminary examination of the phosphorylation profile of exogenous Flag-Ensa and Arpp19 show that over-expressed Flag-Ensa and Arpp19 are highly phosphorylated only in STLC arrested mitotic cells (Fig. 5.3A-B). To examine if B55 interaction with Ensa/Arpp19 is enriched in mitosis, I performed Flag-pull-downs from asynchronous and STLC-treated mitotic cells. Surprisingly, B55 subunits co-precipitated equally well from interphase and mitotic extracts (Fig. 5.3C). It is possible that during the extraction process mixing of mitotic and interphase cells cause phosphorylation of the exogenous proteins. To observe an all-or-none binding of B55 to exogenous Ensa/Arpp19, I

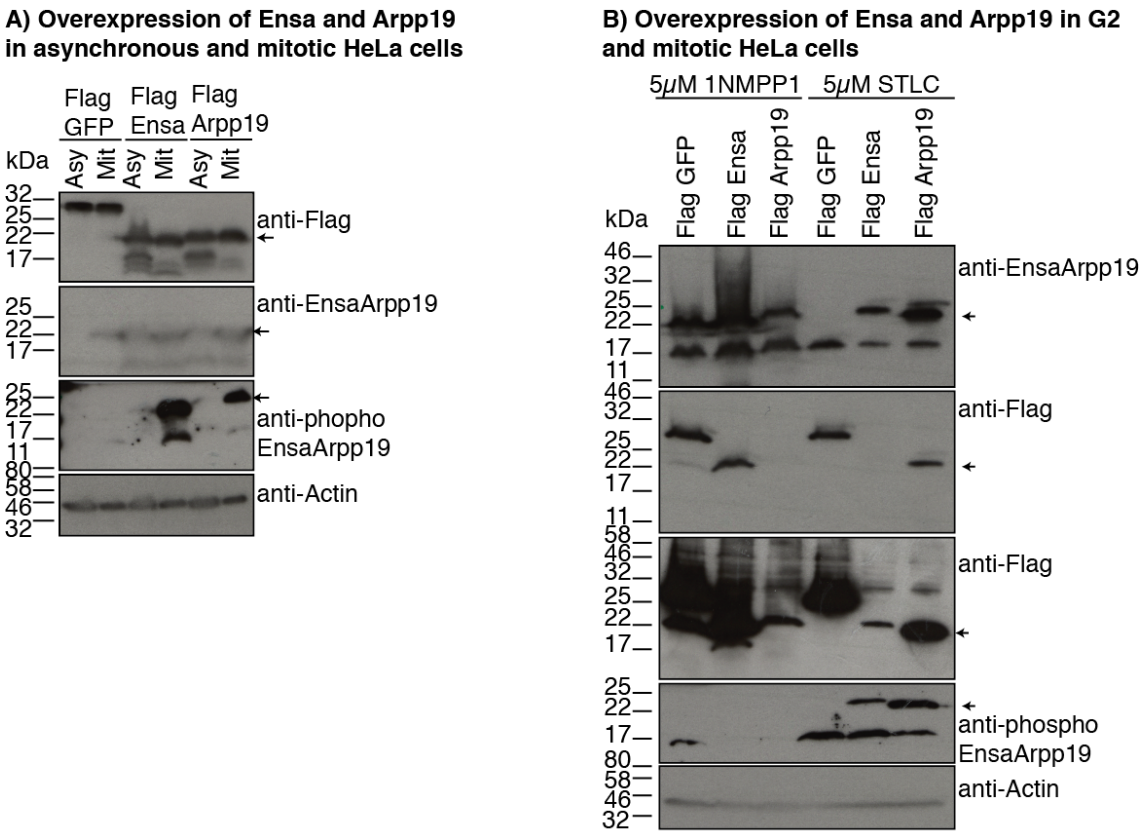

Figure 5.3 Co-immunoprecipitation with exogenously expressed Flag-Ensa/Arpp19 in *HeLa*-cdk1as cells

A) Flag GFP, Flag Ensa and Flag Arpp19 were transiently overexpressed using Jet-Pie reagent in *HeLa-cdk1as* cells for 48 h. Cells were either untreated or treated with STLC for 16 h and cells lysates were probed with the indicated antibodies. Arrows indicate the Flag-tagged Ensa and Arpp19. B) Immunoprecipitation assays with transiently expressed Flag-Ensa and Arpp19 in *HeLa-cdk1as* cells for 48 h. Transfected cells were either untreated or arrested in mitosis with 5 μM STLC for 16 h. Aliquots of Whole cell extracts (WCE) and IP elutions (IP Eluates) were analysed with the indicated antibodies. Flag-GFP was used as a negative control. Arrow indicates endogenous Ensa/Arpp19 observed in the eluted fractions.

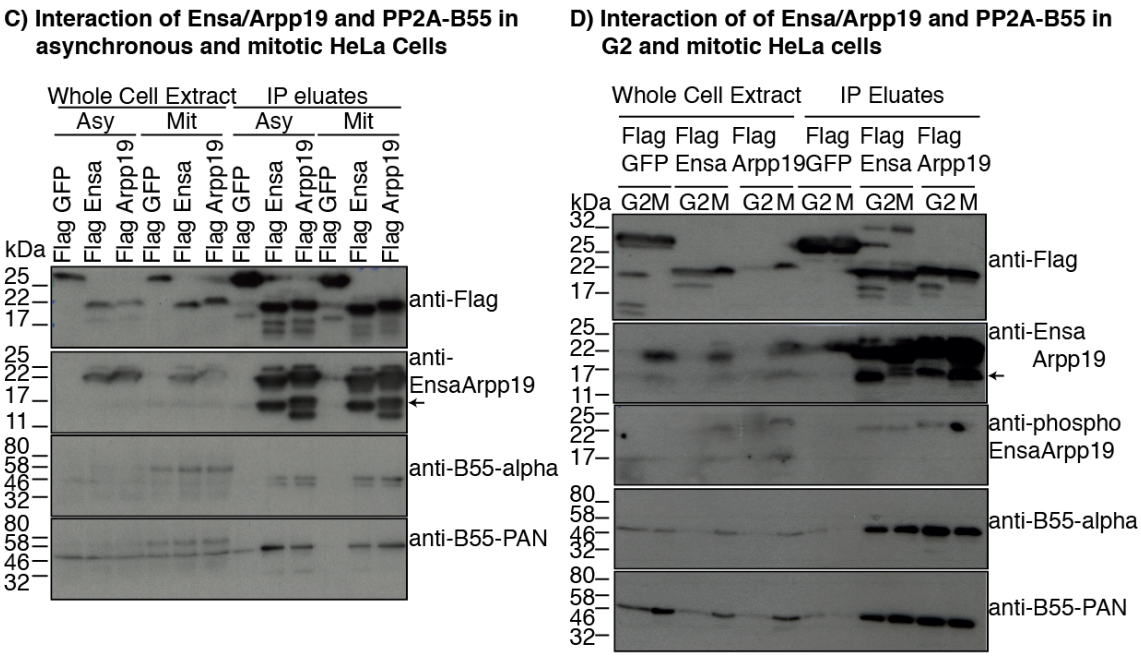

Figure 5.3 Co-immunoprecipitation with exogenously expressed Flag-Ensa/Arpp19 in *HeLa*-cdk1as cells

C) Flag GFP, Flag Ensa and Flag Arpp19 were transiently overexpressed using Jet-Pie reagent in *HeLa*-cdk1as cells for 48 h. Cells were treated with either 5 μM 1NMPP1 or 5 μM STLC for 16 h and cells lysates were probed with the indicated antibodies. Arrows indicate the Flag-tagged Ensa and Arpp19. D) Immunoprecipitation assays with transiently expressed Flag-Ensa and Arpp19 in *HeLa-cdk1as* cells for 48 h. Transfected cells were either treated with 5 μM 1NMPP1 or 5 μM STLC for 16 h. Aliquots of whole cell extracts (WCE) and IP elutions (IP Eluates) were analysed with the indicated antibodies. Flag-GFP was used as a negative control. Arrow indicates endogenous Ensa/Arpp19 observed in the eluted fractions.

performed co-immunoprecipitation assays in *HeLa-cdk1as* cells. These cells were synchronised either in G2 with 5 μM 1NMPP1 or in mitosis with the Eg5 inhibitor, 5 μM STLC, for 16 h. Surprisingly, even in these pull downs, equal binding of B55 was observed in the G2 and M phases. In addition, exogenous Ensa and Arpp19 showed similar phosphorylation level in the G2 and M phase IP fractions (Fig. 5.3D), unlike the marked increase in mitotic phosphorylation that was observed directly in the total cell extracts (Fig. 5.1B). It is possible that Ensa/Arpp19 are phosphorylated during immunoprecipitation, either during lysis or during the binding procedure.
Interestingly, even in the *HeLa-cdk1as* IPs, a specific small protein around the size of endogenous Ensa/Arpp19 was observed in the IP fractions with Flag Ensa and Flag Arpp19 (indicated by arrows in Fig. 5.3B and D). This protein was not identified by the Flag-antibody, suggesting that they could be N-terminal truncations of the exogenous proteins. However, if this is the case the truncated proteins should also be seen in the negative control pull-downs or be washed away by high-salt buffer. Moreover, this second Ensa/Arpp19 band disappears from the IP fraction after okadaic acid treatment (Fig. 5.5B), suggesting that it is involved in PP2A-B55 complex formation. This could mean that more than one Ensa/Arpp19 proteins bind PP2A-B55, either as a complex or at separate sites, or that the entire phosphatase/inhibitor complex forms a large heterodimer.

To test these possibilities, we fractionated the elution from the co-immunoprecipitation experiments using a size-exclusion chromatography column (Superose 6 3.2/300). Flag-GFP elution was used as a negative control to identify any background proteins binding to the beads. As expected, PP2A-B55 co-purified with Flag-Ensa and Flag-Arpp19 confirming that they form a complex. As seen in the profile the complex elutes approximately around 140 kDa (141.2 kDa for Flag Ensa-PP2A B55 and 138.4 kDa for Flag Arpp19-PP2A B55), determined by the standards and calibration curve-plot (Fig. 5.4A). The approximate calculations are based on the elution volumes and depend on the shape of the interacting proteins. This is the expected molecular weight when a single PP2A-B55 heterotrimer, comprising of the catalytic subunit (36 kDa), the scaffolding subunit (65 kDa) and the regulatory subunit B55-alpha (46 kDa) binds to the exogenous Ensa/Arpp19 (22 kDa), and rules out the possibility of a phosphatase heterodimer that separately binds two Ensa/Arpp19 inhibitors. However, the complex

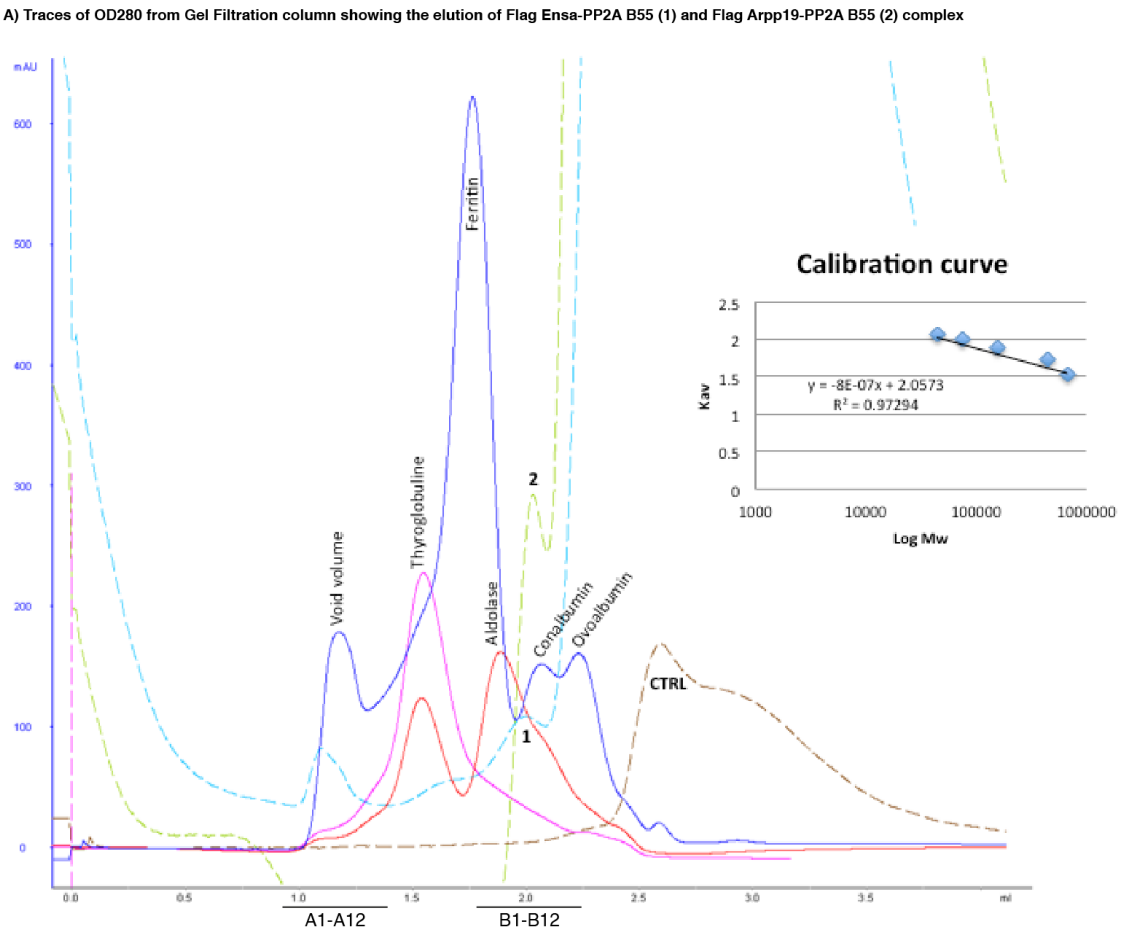

Figure 5.4 Analytical size exclusion chromatography of the Co-immunoprecipitated complex.

A) Elution profiles from Superose 6 3.2/300 column for calibration standards Thyroglobulin (669 kDa), Ferritin (440 kDa), Aldolase (158 kDa), Conalbumin (75 kDa) and Carbonic Anhydrase (29 kDa, Dextran blue (void volume) as absorption at 280 nm (mAU) versus elution volume (ml). The elution profile of Flag-Ensa co-immunoprecipitation is labelled as 1 and Flag Arpp19 co-immunoprecipitation is labelled as 2. Flag GFP (negative control) IP elution profile is labelled as CTRL. The calibrations curve was plotted the gel-phase distribution co-efficient (Kav) versus log of the molecular weighs. Kav = (Ve - Vo) / (Vc - Vo) where Ve = elution volume, Vo = column void volume, Vc = geometric column volume. Straight line is the calibration curve calculated from the data for the molecular weight standards (inset). The molecular weight of the complexes was determined to be approximately 141.2 for Flag Ensa complex (2.172 ml elution volume) and 138.4 kDa for Flag Arpp19 complex (2.28 ml elution volume).

co-purifies with a 17-kDa protein co-eluting with the complex (Fig. 5.4B) that is recognized by the Pan-ENSA/Arpp19 antiserum. This protein does not cross react with

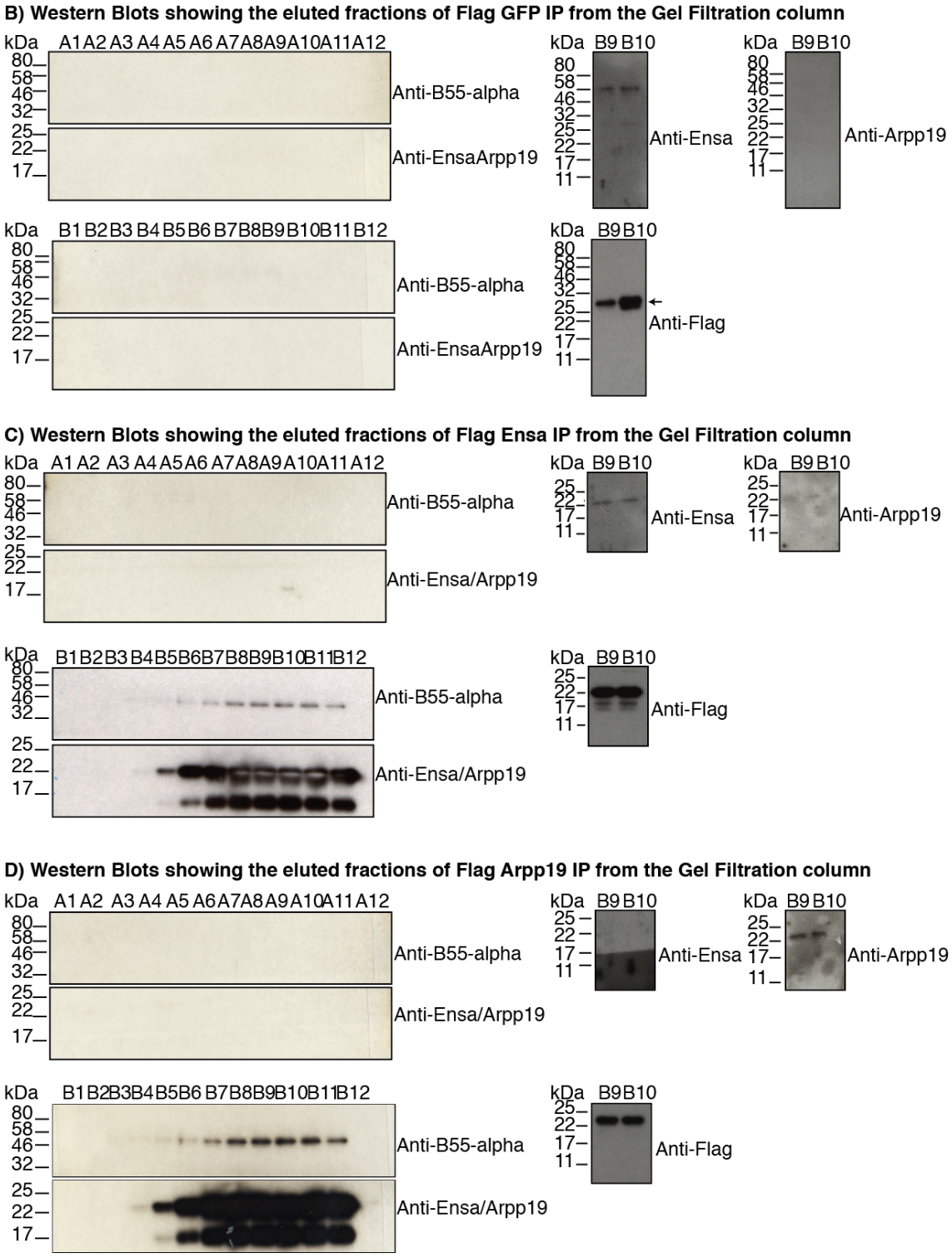

Figure 5.4 Analytical size exclusion chromatography of the Co-immunoprecipitated complex.

B) Flag-GFP Co-IP eluted fractions from the Superose 6 3.2/300 column were run on a SDS-PAGE and analyzed on a western blot using the indicated antibodies. C) Flag-Ensa Co-IP eluted fractions from the Superose 6 3.2/300 column were run on a SDS-PAGE and analyzed on a western blot using the indicated antibodies. D) Flag-Arpp19 Co-IP eluted fractions from the Superose 6 3.2/300 column were run on a SDS-PAGE and analyzed on a western blot using the indicated antibodies.

E) Alignment of Ensa isoforms in Homo Sapiens

```
sp|O43768-8|ENSA_HUMAN      MSQKQEEENPAEETGEEKQDTQEKEGILPERAEEAKLKAKYPSLGQKPGGSDFLMKRLQK
sp|O43768-4|ENSA_HUMAN      MSQKQEEENPAEETGEEKQDTQEKEGILPERAEEAKLKAKYPSLGQKPGGSDFLMKRLQK
sp|O43768|ENSA_HUMAN        MSQKQEEENPAEETGEEKQDTQEKEGILPERAEEAKLKAKYPSLGQKPGGSDFLMKRLQK
sp|O43768-2|ENSA_HUMAN      MSQKQEEENPAEETGEEKQDTQEKEGILPERAEEAKLKAKYPSLGQKPGGSDFLMKRLQK
sp|O43768-3|ENSA_HUMAN      MSQKQEEENPAEETGEEKQDTQEKEGILPERAEEAKLKAKYPSLGQKPGGSDFLMKRLQK
sp|O43768-9|ENSA_HUMAN      MSQKQEEENPAEETGEEKQDTQEKEGILPERAEEAKLKAKYPSLGQKPGGSDFLMKRLQK
sp|O43768-7|ENSA_HUMAN      ----MAGGLGCDVCYWFVEDTQEKEGILPERAEEAKLKAKYPSLGQKPGGSDFLMKRLQK
sp|O43768-5|ENSA_HUMAN      ----MAGGLGCDVCYWFVEDTQEKEGILPERAEEAKLKAKYPSLGQKPGGSDFLMKRLQK
sp|O43768-6|ENSA_HUMAN      ----MAGGLGCDVCYWFVEDTQEKEGILPERAEEAKLKAKYPSLGQKPGGSDFLMKRLQK
                                       .:      :****************************************

sp|O43768-8|ENSA_HUMAN      GVWGIVSYPLSLELKEVLRMKSVEVLLDPFLEVLLLNRSRGEFEI---------------
sp|O43768-4|ENSA_HUMAN      GVWGIASYPLSLGLKEVLRMKSVEQKY---F-------DSGDYNMAKAKMKNKQLPSAGP
sp|O43768|ENSA_HUMAN        G----------------------QKY---F-------DSGDYNMAKAKMKNKQLPSAGP
sp|O43768-2|ENSA_HUMAN      G----------------------QKY---F-------DSGDYNMAKAKMKNKQLPSAGP
sp|O43768-3|ENSA_HUMAN      GDYKSLHWSVLLC--------ADEMQKY---F-------DSGDYNMAKAKMKNKQLPSAGP
sp|O43768-9|ENSA_HUMAN      GDYKSLHWSVLLC--------ADEMQKY---F-------DSGDYNMAKAKMKNKQLPSAGP
sp|O43768-7|ENSA_HUMAN      GDYKSLHWSVLLC-------ADEMQKY---F-------DSGDYNMAKAKMKNKQLPSAGP
sp|O43768-5|ENSA_HUMAN      G----------------------QKY---F-------DSGDYNMAKAKMKNKQLPSAGP
sp|O43768-6|ENSA_HUMAN      G----------------------QKY---F-------DSGDYNMAKAKMKNKQLPSAGP
                            *                              :       . *::::

sp|O43768-8|ENSA_HUMAN      ----------------------------------
sp|O43768-4|ENSA_HUMAN      DKNLVTGDHIPTPQDLPQRKSSLVTSKLAG----
sp|O43768|ENSA_HUMAN        DKNLVTGDHIPTPQDLPQRKSSLVTSKLAGGQVE
sp|O43768-2|ENSA_HUMAN      DKNLVTGDHIPTPQDLPQRKSSLVTSKLAG----
sp|O43768-3|ENSA_HUMAN      DKNLVTGDHIPTPQDLPQRKSSLVTSKLAGGQVE
sp|O43768-9|ENSA_HUMAN      DKNLVTGDHIPTPQDLPQRKSSLVTSKLAG----
sp|O43768-7|ENSA_HUMAN      DKNLVTGDHIPTPQDLPQRKSSLVTSKLAGGQVE
sp|O43768-5|ENSA_HUMAN      DKNLVTGDHIPTPQDLPQRKSSLVTSKLAGGQVE
sp|O43768-6|ENSA_HUMAN      DKNLVTGDHIPTPQDLPQRKSSLVTSKLAG----
```

F) Alignment of Arpp19 isoforms in Homo Sapiens

```
sp|P56211|ARP19_HUMAN       MSAEVPEAASAEEQKEMEDKVTSPEKAEEAKLKARYPHLGQKPGGSDFLRKRLQKGQKYF
sp|P56211-2|ARP19_HUMAN     ----------------MEDKVTSPEKAEEAKLKARYPHLGQKPGGSDFLRKRLQKGQKYF
                                            ****************************************

sp|P56211|ARP19_HUMAN       DSGDYNMAKAKMKNKQLPTAAPDKTEVTGDHIPTPQDLPQRKPSLVASKLAG
sp|P56211-2|ARP19_HUMAN     DSGDYNMAKAKMKNKQLPTAAPDKTEVTGDHIPTPQDLPQRKPSLVASKLAG
                            ***************************************************
```

Figure 5.4 Analytical size exclusion chromatography of the Co-immunoprecipitated complex.

E) and F) Multiple sequence alignment of Ensa and Arpp19 isoforms respectively with Clustal Omega. The FASTA sequences were obtained from Uniprot database. The peptide sequences marked in red indicated the motif interacting with the Ensa and Arpp19 antibody respectively.

Flag antibody or the specific Ensa and Arpp19 antibodies generated in the lab (see Chapter 3.1). This could be because the specific Ensa-Arpp19 antibodies identify peptides around the N-terminal of the protein, whereas the Abcam Ensa/Arpp19 antibody spans 50 aa to the C-terminus. One possibility is that the complex co-purifies an N-terminal degradation product of the exogenous Flag-Ensa/Arpp19 proteins.

Alternatively, this protein could constitute a specific isoform of Ensa/Arpp19 that has a separate N-terminus. Upon searching the relevant databases, we discovered that Ensa has nine isoforms, of which three have distinguished N-terminal sequences. As shown in Fig. 5.4C and D, these isoforms do not cross-react with our ENSA specific antiserum due to high sequence dissimilarities. Likewise, the only splice variant reported for Arpp19 differs in the N-terminal sequence to the over-expressed cDNA and cannot cross-react with our N-terminal antiserum.

In summary, we found that the Flag-Ensa and Flag-Arpp19 PP2A-B55 complex co-purifies with a protein that is recognized by the Pan Ensa/Arpp19 but not the Flag, or the N-terminal ENSA and Arpp19 antisera. The binding of this protein to PP2A-B55 is inhibited by okadaic acid, suggesting that it is associated with the active site and does not bind independently at another site of the phosphatase complex. It could either constitute an N-terminal degradation product of the exogenously expressed protein that co-purifies for artefactual reasons. Alternatively, this could be biological meaningful data and the co-purifying protein could constitute an endogenous isoform of Ensa/Arpp19 that contains a distinct N-terminus.

5.4 Proteomic Screening for Ensa/Arpp19 Phosphatases at the Metaphase-Anaphase Transition

Due to the constitutive phosphorylation of exogenously expressed Ensa and Arpp19 in *Hek293* cells and the phosphorylation of G2 Ensa/Arpp19 in *HeLa* cell extracts, these cells lines and methodologies were not suitable to further study Ensa/Arpp19 dephosphorylation. Thus, we resorted to recombinant proteins to identify phosphatases interacting with Ensa/Arpp19 in mitosis. Phosphatase and substrate interactions are transient; hence, it is challenging to identify phosphatases by co-

A) Quantification of purified Flag Ensa and Flag Arpp19

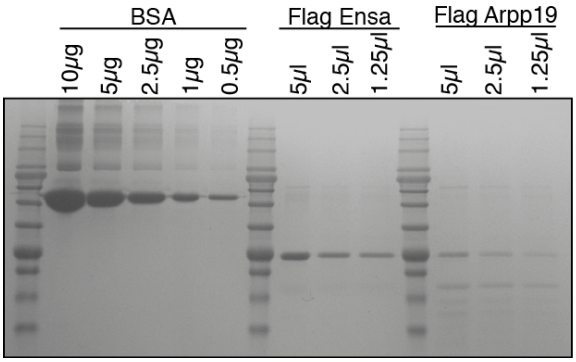

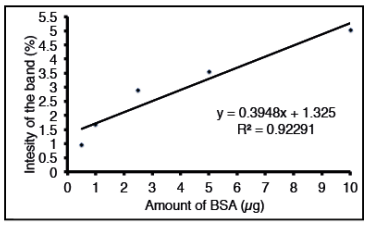

	Conc. of Protein (μg/μl)
Flag-Ensa	0.47
Flag-Arpp19	1.01

Figure 5.5 Co-immunoprecipitation with recombinant Flag-Ensa/Arpp19 from metaphase and anaphase *HeLa-cdk1as* extracts.

A) Flag Ensa and Flag Arpp19 were purified from *E. coli* were quantified by SDS-PAGE against bovine serum albumin (BSA) standards.

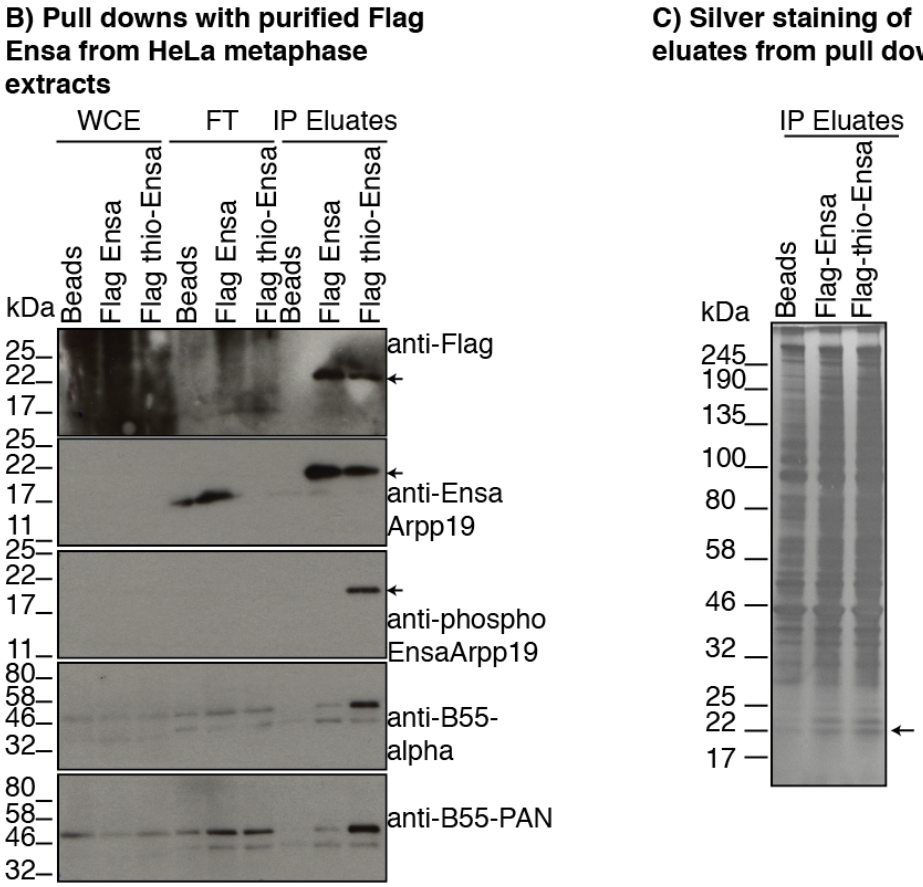

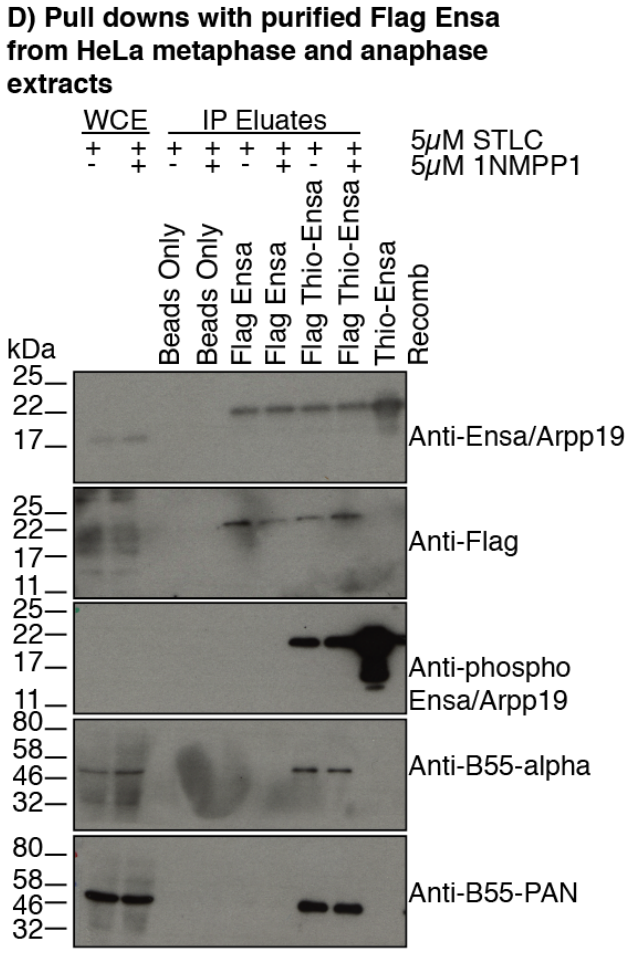

Figure 5.5 Co-immunoprecipitation with recombinant Flag-Ensa/Arpp19 from metaphase and anaphase *HeLa-cdk1as* extracts.

B) Immunoprecipitation assays using purified 100 ng Flag Ensa and Flag-thio-Ensa from STLC-treated mitotic cell lysate. Aliquots of whole cell extract (WCE), unbound fraction (FT) and eluted fractions (IP Eluates) were analysed with the indicated antibodies. Arrows show the Flag-tagged proteins. C) Elutions from (B) were run on SDS-PAGE and subjected to silver staining. Beads only were used as a negative control for the IP. Arrow indicates the bait; Flag tagged Ensa and thio-Ensa in the elutions. D) Immunoprecipitation assays using purified 100 ng Flag Ensa and Flag-thio-Ensa from STLC-treated mitotic cell lysate (metaphase extracts) and STLC + 1NMPP1 treated (anaphase extracts) mitotic exit extracts. Aliquots of whole cell extract (WCE) and IP eluted fractions (IP Eluates) were analysed with the indicated antibodies.

immunoprecipitation with phosphorylated recombinant proteins. The phospho-group placed on the substrates by kinases is easily hydrolysable by endogenous phosphatases and it is difficult to trap these interactions. In the recent years, *in-vitro* thio-phosphorylation has been used to overcome these problems. The thio-phospho group is non-hydrolysable due to the electronegativity and spatial arrangement of the thio-phospho group and thus traps any interacting phosphatase when incubated with the cell lysates. Thus, in this study we used recombinant thio-phosphorylated Ensa to pull-down interacting phosphatases in mitosis and at mitotic exit.

Flag-Ensa and Flag-Arpp19 were overexpressed from a GST vector and purified from *E.coli* using standard GST purification protocols (See Materials and Methods 2.2.5). The purified GST proteins were thio-phosphorylated by hyperactive truncated Greatwall (E2), *in vitro* at 37°C for 5 h as described in more detail below in chapter 6.2. E2 and residual thio-ATP were removed by re-purification of the GST proteins. The GST-tag was cleaved using prescission protease (Fig. 6.4), and the concentration of purified Flag Ensa and Flag Arpp19 was quantified using a BSA standard (Fig. 5.5A). *HeLa-cdk1as* cells were synchronised in metaphase using the Eg5 inhibitor, 5 µM STLC. Mitotic lysate was prepared using optimised conditions for phosphatase assays (Cundell et al. 2013). The cell lysate was then incubated with 100 ng of the thio-phosphorylated protein at 37°C for 30 min to allow binding of the phosphatases to the recombinant bait. As the thio-phospho group is non-hydrolysable, the phosphatases or any other proteins interacting with it could be co-immunoprecipitated and identified by proteomic screening. As expected, PP2A-B55 is enriched specifically with thio-Ensa (Fig. 5.5B). Interestingly, in this immuno-precipitation of the recombinant protein we could not observe the usual co-purifying 17-kDa protein. This could mean that the recombinant protein already formed a dimer or multimer and did not co-purify endogenous protein, or that post-translational modification in the recombinant protein that are necessary for complex formation were lacking.

The silver staining of the IP elution showed a number of non-specific proteins binding with the negative control. Stringent washes with 1 M NaCl and 1% detergent were unable to reduce these background proteins. However, as the bait is seen specifically in the Ensa and thio-Ensa fraction we hoped to identify some specific targets binding to thio-Ensa specifically even if they were unidentifiable on a silver stain (Fig. 5.5C).

Following the preliminary optimisation of the IPs, to gain further insight into the dephosphorylation dynamics at mitotic exit, I synchronised the cells in mitosis and triggered mitotic exit by inhibiting Cdk1. As in the previous experiment, I synchronised the cells in mitosis with STLC and triggered exit by using 5 µM 1NMPP1 to inhibit Cdk1 for 30 min at 37°C. The mitotic extracts are referred as metaphase extracts and the STLC+NMPP1 extracts are referred as anaphase extracts in this work. Due to the non-hydrolysable nature of thio-Ensa, PP2A-B55 interaction was observed in IP elution from both metaphase and anaphase extracts. These elutions were subjected to SDS-PAGE and Coomassie staining before in-gel trypsinisation.

5.5 Mass Spectrometry and Identification of Peptides Interacting with Thiophosphorylated Ensa

In-gel digestion of the protein bands stained with Coomassie was carried out (See Materials and Methods 2.2.2). Quantitative label-free LC/MS was used which allows peptides present in a complex protein mixture to be identified and the abundance of proteins quantified across different samples. The peak areas of the peptide ions from different peptides were measured and compared to their respective signals in other samples, thus generating relative, quantitative data (Bantscheff et al. 2007).

MaxQuant was used to process the raw mass spectrometric data with subsequent data analysis using Perseus. The data were analysed in sets of two to identify proteins interacting specifically with Ensa and the thio-phospho group in metaphase and anaphase. The groups used for comparison are shown on either sides of the curve.

As seen in Fig. 5.5A, Lamin B1, DKC1 and Matrin 3 were enriched with Ensa pull-downs from metaphase extracts, versus anaphase extracts. Lamin B1 belongs to the family of proteins (Lamins) that provide a framework for the nuclear envelope and may also interact with chromatin. DKC1 is a part of the ribonucleoprotein complex subunit 4 and has been proven to have roles in cell to cell or substratum adhesion and increase cell proliferation when overexpressed in *HeLa* cells (Angrisani et al. 2011). Matrin 3 is a nucleoplasmic protein and co-immunoprecipitates with Lamin A (Depreux et al. 2015). Recent studies have shown its association with microtubule-associated protein

RNAs and their regulation in triple-negative breast cancer cell lines (Subbarayalu et al. 2016). Interestingly, Ensa shows more than 2-fold enrichment but does not pass the estimated 5% FDR when compared with the bead sample (Fig 5.6B). No purified protein was added in the beads sample and hence significant enrichment is expected with the Ensa sample. This could probably be due to non-specific binding of endogenous Ensa to the Beads, as the silver staining of the IP eluates did not show a clear distinction between the negative and the Ensa/Thio Ensa samples. In addition, no proteins were significantly enriched in the Ensa samples compared to the bead-only controls. This would be consistent with the three identified nucleoplasmic proteins discussed above being bound non-specifically to the beads in the metaphase at higher levels than in anaphase. Therefore, although, these proteins might point towards an unknown nuclear function of Ensa, optimising the IP to reduce non-specific binding is required to identify and analyse them thoroughly.

Surprisingly, Lamin B1 also showed more than 2-fold enrichment with un-phosphorylated Ensa when compared with Thio-Ensa in metaphase extracts pull-downs (Fig. 5.6D). This could be biologically significant and point towards the association of Ensa with the nuclear membrane protein that might contribute to the blebbing observed in Chapter 4.2 (Fig. 4.4). However, the reduced signal in thio-Ensa can also be due to the specific binding and enrichment of the PP2A-B55 subunits to the Thio-Ensa that makes it unavailable for any non-specific binding, or simply stochastic variation in non-specific binding between samples. As seen in Fig. 5.6D-E, the PP2A-B55 subunits are enriched more than 2-fold with thio-phosphorylated Ensa. This is in agreement with the previous studies where Greatwall phosphorylation of Ensa is necessary for PP2A binding (Gharbi-Ayachi et al. 2010; Mochida 2014). The binding of the phosphatase to phospho-Ensa is also seen in anaphase due to the unhydrolysable nature of the thio-group. When pull-downs from anaphase and metaphase extracts with thio-Ensa were compared, no new interactors were found. Ensa and PP2A-B55 subunits show a slight preference towards metaphase, but this does not approach statistical significance (Fig. 5.6F). As seen in Fig. 5.6F, VDAC3 was found at the edge of the curve showing enrichment in anaphase extracts. Five unique peptides were identified for this protein, which accounts for 25% of the sequence coverage. However, it is not clear if this protein is significant, as it is not far from the other insignificant hits on the plot.

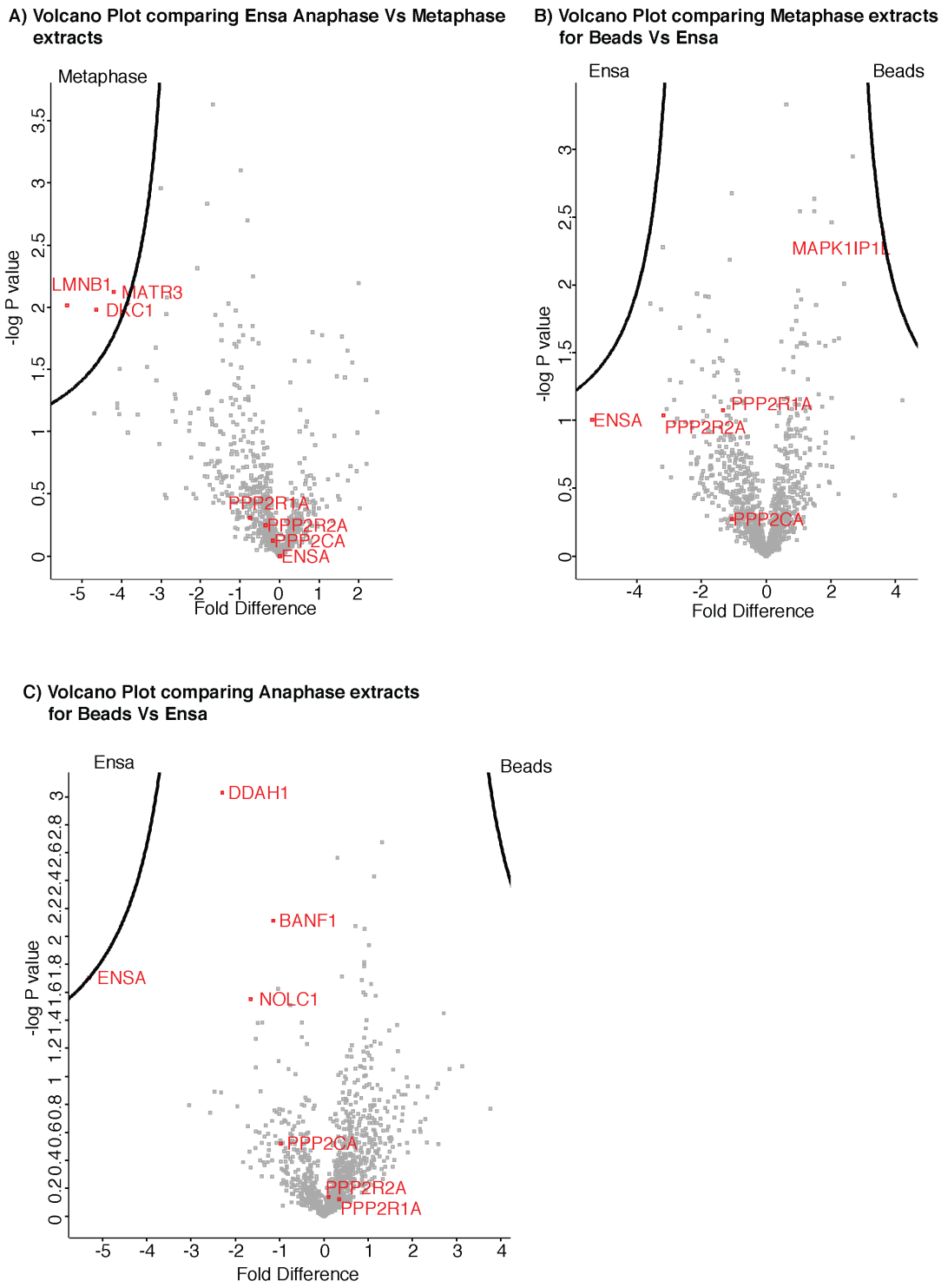

Figure 5.6 Proteomic screening for Ensa/Arpp19 phosphatases at the metaphase-anaphase transition

A) - F) 'Volcano plot' illustrating statistical significance against fold-change of the proteomic data set. The x-axis reflects the difference in protein abundance in the groups mentioned on the right side of the curve compared to the sample mentioned on the left side. The y-axis shows the -log10 of the p value of the Student's t-test. The proteins groups of PP2A-B55 subunits, Ensa (positive controls) and the significantly enriched protein groups are indicated by red dots (FDR = 0.05, S0 = 2, indicated by black line). Each dot represents a protein group. A) The data indicates the distribution of protein groups interacting with Ensa in metaphase and anaphase. B)- C) The data indicates the distribution of protein groups interacting specifically with Ensa in comparison to the Beads (negative control).

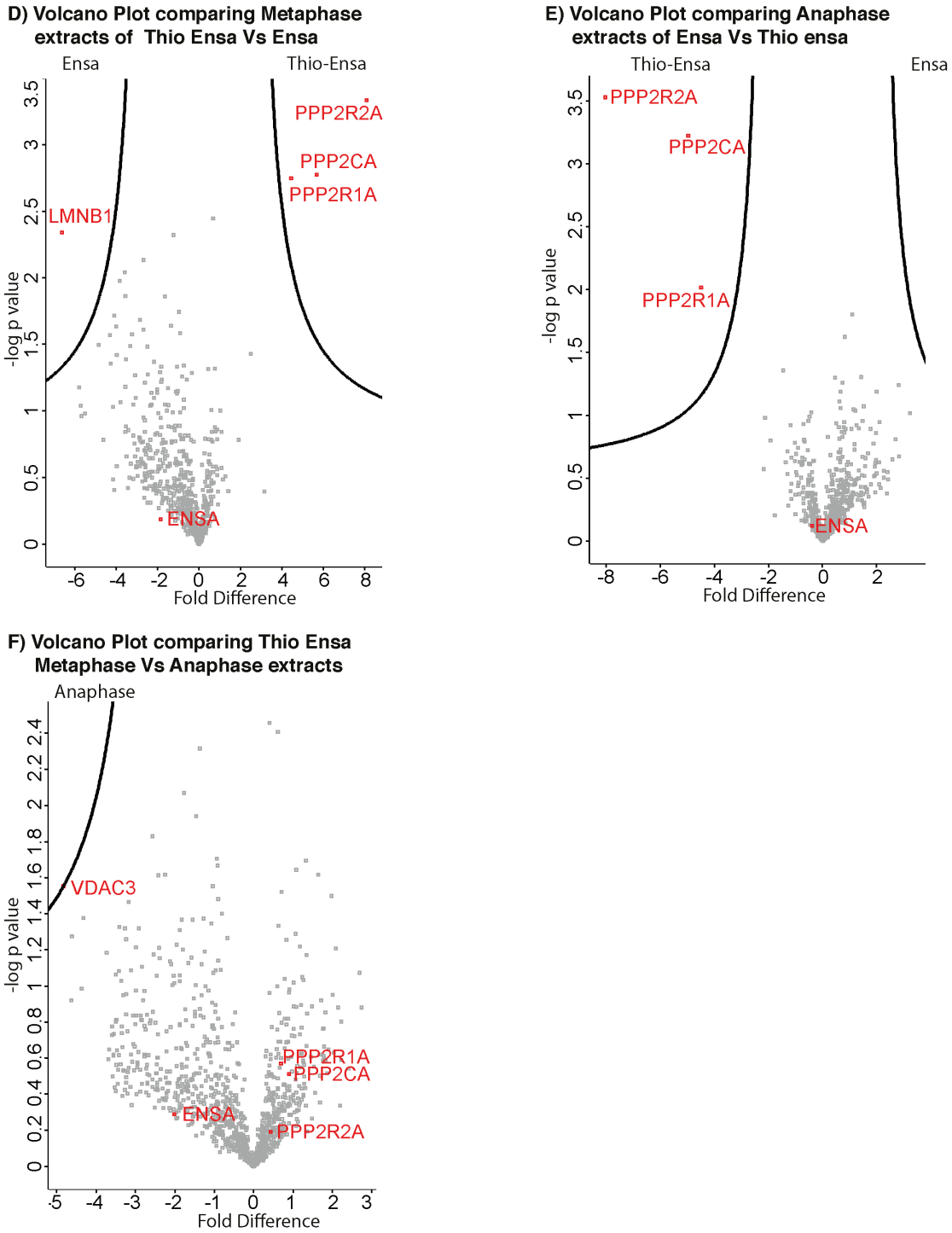

Figure 5.6 Proteomic screening for Ensa/Arpp19 phosphatases at the metaphase-anaphase transition

D)- E) The data indicates the distribution of protein groups interacting specifically with Thio-Ensa in comparison with the unphosphorylated Ensa in metaphase and anaphase. F) The data indicates the distribution of protein groups interacting with Thio-Ensa in metaphase and anaphase extracts.

H)Table showing the number of peptides identified for each protein group in the experiment

Gene Name	Full name	Total peptides	No. of unique peptides	Sequence coverage	Mol weight
ENSA	Alpha-Endosulphine	13	13	62.8	13.389
PPP2CA	Serine/threonine-protein phosphatase 2A catalytic	21	3	73.1	35.59
PPP2R1A	Serine/threonine-protein phosphatase 2A 65kDA regulatory subunit A alpha isoform	45	45	68.8	65.3
PPP2R2A	Serine/threonine-protein phosphatase 2A 55kDA regulatory subunit B alpha isoform	30	21	78.3	51.69
MATR3	Matrin-3	11	11	18.3	94.622
LMNB1	Lamin B1	39	32	62.3	66.408
DKC1	H/ACA ribonucleoprotein complex subunit 4	10	10	27.8	57.673
VDAC3	Voltage-dependent anion-selective channel protein 3	6	5	25.1	30.658
MAPK1IP1I	MAPK-interacting and spindle-stabilising protein-like	1	1	6.9	24.269

Figure 5.6 Proteomic screening for Ensa/Arpp19 phosphatases at the metaphase-anaphase transition

G) Tabular representation of the number of unique peptides (peptide that occurs in only one protein in the proteome of interest), sequence coverage and molecular weight of the protein groups marked in the volcano plots.

Phosphatase subunits of PPP1, PPP5 and PPP6 were detected but not enriched in Enso or thio-Ensa over the beads, which indicated non-specific binding.

As no other phosphatases were identified in anaphase with thio-Ensa in these preliminary analyses, it seems that PP2A-B55 is the dominant phosphatase it interacts with. These results are in agreement with the observations from Williams et al. that Ensa acts both as an inhibitor and as a substrate of PP2A-B55. However, as phosphatases like PPP1, PPP5 and PPP6 are expressed in such low amounts in the cells cycle, it might be worth analysing the spectral data with a much-relaxed FDR of 5%. This could also identify low-level interactors of Ensa and shed light on new function the protein might be involved in and out of the cell cycle. However, due to time constraints these analyses could not be carried out at the time of writing this work. Overall, the large contamination of the beads only sample probably masked meaningful interaction data. Thus, the purification and elution method will need to be further optimised to allow this method to be successfully applied to thio-phospho interactor analysis.

In conclusion, this chapter probed the interaction of Ensa/Arpp19 with PP2A-B55. We have identified a potential dimer of different Ensa/Arpp19 isoforms in the PP2A/B55 complex but this has to be further investigated using differentially tagged Ensa/Arpp19 and their isoforms. The preliminary proteomic screen did not identify any novel phosphatase interacting with phosphorylated Ensa at mitotic exit, but it is likely that the high background in the sample preparation did mask potential novel interactors.

CHAPTER6 GENERATING A DOMINANT ACTIVE ENSA AND ARPP19 FOR FUNCTIONAL ANALYSIS OF THE ENSA/ARPP19-B55 PATHWAY

The precise role of the Gwl/Ensa/B55-PP2A axis in the mammalian G2/M switch remains to be determined. Depletion of either Ensa/Arpp19 or Gwl does not appear to have a significant impact on the dynamics of mitotic entry when Cdk1 is fully active (see Chapter 4.2). This suggests that cells can trigger Cdk1 activation and mitotic phosphorylation even in the presence of high phosphatase activity. On the other hand, inhibition of phosphatases by okadaic acid (OA) triggers rapid and premature mitotic entry even when Cdk1 is inhibited, suggesting that it is indeed a phosphatase that constitutes the major obstacle to enter mitosis. A critical question that remains to be addressed is whether the major target of OA that prevents premature mitotic entry is indeed B55-PP2A. It also remains unclear what the consequences of prolonged B55-PP2A inhibition on mitotic exit will be. Artificially activating and maintaining Ensa/Arpp19 phosphorylation could be used to investigate this question. This can be achieved by activating either Greatwall or Ensa/Arpp19 constitutively. However, attempts to generate phospho-mimicking mutants of human Greatwall have failed in the past (Vesely 2013). Another attractive approach would be to generate dominant active Ensa or Arpp19. Unfortunately, phospho-mimicking mutants of Ensa/Arpp19 that express negatively charged amino acids such as aspartate or glutamate instead of S67 are unlikely to be functional. The negative charge on an aspartate or a glutamate might not be enough to execute the function of Ensa/Arpp19, as this phospho-site has to interact directly with the catalytic domain of the phosphatase to exert its inhibitory effect.

Dominant active thio-phosphorylated recombinant Ensa/Arpp19 has been used in the past in *Xenopus* to study its effects on mitotic entry and exit. In *Xenopus* interphase extracts, previously depleted of Gwl, the addition of thio-phosphorylated Ensa or Arpp19 rescues Gwl phenotype and induces mitotic entry (Gharbi-Ayachi et al. 2010). Thus, cell cycle mechanisms can be easily analysed by adding recombinant effector proteins in cell extracts. In addition, recombinant proteins can be injected easily into *Xenopus* oocytes to observe their effects. One such example was microinjection of Cdk

inhibitor, p21, into oocytes that prevent Gwl phosphorylation (Zhao et al. 2008). Although very few similar experiments have been done with human cells, protein delivery techniques in mammalian cells need to be improved to study cell cycle functions.

Thio-phosphorylated Ensa/Arpp19 have been generated and either added into cell-free extracts or injected in *Xenopus*. However, this cannot be exploited in the human system, as cell-free mammalian extracts do not mimic in-vivo cellular transitions like frog extracts. In addition, the few existent protein delivery methods in mammalian cells take a long time to display the effect and cannot be used to study the mitotic entry and exit switch-like transitions.

Hence, we are engineering a technique to produce constitutively active Ensa and Arpp19 that can be directly transfected into mammalian cells in-vivo. This will enable us to have a replica of the *Xenopus* technique in mammals to investigate the effects of dominant active Ensa/Arpp19.

6.1 Analysing the Effects of PP2A/B55 Depletion on Mitotic Entry

To begin determining if PP2A-B55 is the okadaic acid (OA)-sensitive Cdk-counteracting phosphatase, I decided to first reproduce the okadaic acid experiment using the *HeLa-cdk1as* cells to analyse the effects of a general phosphatase inhibitor in these cells. OA is a chemical inhibitor of various protein phosphatases. It inhibits PP2A at lower concentrations (0.5–1 μM), while PP1 is only inhibited at 5–10 fold higher concentrations (M. Hara et al. 2012). I synchronised the *HeLa-cdk1as* cells in G2 with 5 μM 1NMPP1 and added varying concentrations of OA to inhibit the phosphatases. The cells were imaged every 30 min for 4 h to see the effect of phosphatase inhibition on mitotic entry. Fig. 6.1A shows that OA overrides Cdk1 inhibition and promotes mitotic entry even at 125 nM concentration. This agrees with the previous studies that indicate that OA triggers mitosis even in Cdk1 inhibited cells (Gowdy et al. 1998). To verify if B55-PP2A is the target of OA in this experiment, I used siRNA depletion in the *HeLa-cdk1as* cell line. The cells were treated with B55 siRNA (α+δ: 20 nM each and PP2A

catalytic subunit siRNA (CA/CB: 25 nM each) for 72 h and synchronised in G2 with 0.5 µM 1NMPP1 for 18 h. The samples were collected and analysed using

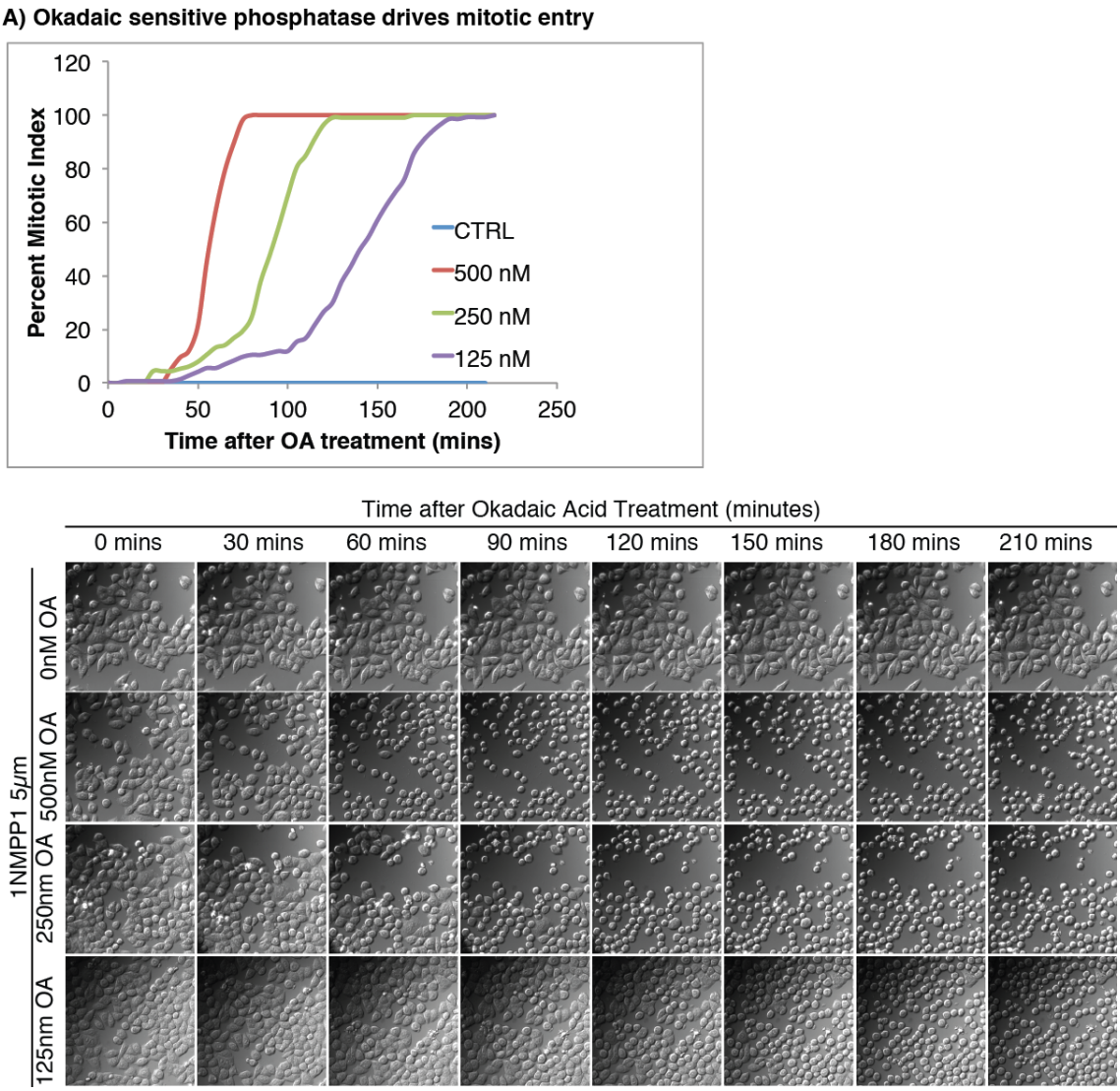

Figure 6.1 Analysing the effect of Okadaic acid and PP2A-B55 depletion on mitotic entry.
A) *HeLa-cdk1as* cells were arrested in G2 with 5 µM 1NMPP1 for 20 h and then treated with varying amounts of Okadaic acid. Time-lapse imaging was done for 4 h post-treatment. The cells were quantified and mitotic index was plotted. Images were taken using DIC on the IX71_Olympus microscope, using the 40X lens, N.A 0.60. Scale bars, 10 µm.

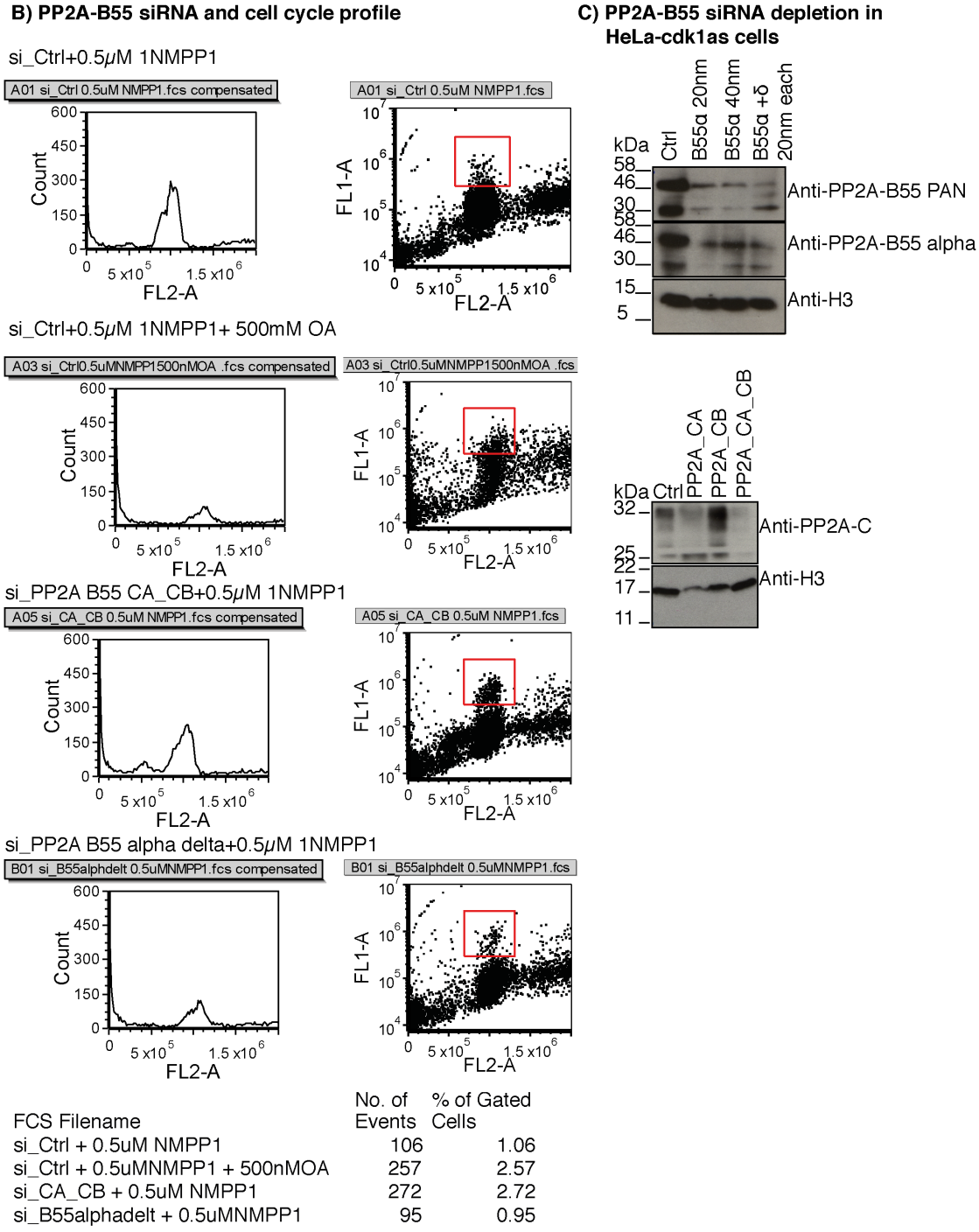

FCS Filename	No. of Events	% of Gated Cells
si_Ctrl + 0.5uM NMPP1	106	1.06
si_Ctrl + 0.5uMNMPP1 + 500nMOA	257	2.57
si_CA_CB + 0.5uM NMPP1	272	2.72
si_B55alphadelt + 0.5uMNMPP1	95	0.95

Figure 6.1 Analysing the effect of Okadaic acid and PP2A-B55 depletion on mitotic entry.

B) *HeLa-cdk1as* cells were treated with B55α and δ siRNA (20 nM each) for 72 h or PP2A-CA/CB (25 nm each) for 48 h. These cells were then arrested in G2 with 0.5 μM 1NMPP1 for 16–18 h. Samples were collected and the mitotic index was determined using phospho-H3 staining. Representative western blots show efficiency of depletion with the indicated antibodies. Histone H3 was used as a loading control.

I used recombinant thio-phosphorylated Ensa that I had already generated for the proteomic experiments in chapter 5.4. Initially, my aim was to optimise protein transfection and apply this method to G2 arrested *HeLa-cdk1as* or *U2OS-cdk1as* cells. Once the technique was established, I could test if premature inhibition of B55-PP2A by thio-Ensa would mimic the effects of OA and trigger mitotic entry.

Fig. 6.2 gives an overview of the reaction to generate constitutively active Ensa/Arpp19. Hyperactive truncated Gwl (E2) generated in the lab (Ocasio et al. 2016) was used to thio-phosphorylate purified recombinant Ensa and Arpp19 in the presence of ATP-γS. The thiol group in the phosphate moiety confers the non-hydrolysable property on these purified proteins. The aim of this work is to observe the effect of dominant active Ensa/Arpp19 on mitotic entry and exit, by transfecting the purified protein using MATERIchemical or physical transfection approaches in mammalian cells.

6.2 Affinity Purification and Transfection of Dominant-Active Ensa/Arpp19

From the previous work described in this thesis, a gateway entry clone with human Ensa and Arpp19 cDNA was available. These clones were used to generate His-tagged Ensa using Gateway cloning. His-Ensa plasmid was expressed and induced with IPTG overnight. The protein was purified using Nickel-NTA beads by batch purification as shown Fig. 6.3A workflow (Materials and Methods 2.2.5). Aliquots from different steps of purification are shown in Fig. 6.3B. Purified His-Ensa was thio-phosphorylated with E2 for varying time-points at 37°C to obtain maximum phosphorylation of the substrate. The phosphorylation was complete in 5 h of the reaction and these conditions was later used in this work to thio-phosphorylate recombinant Ensa and Arpp19. Thio-phosphorylation was also probed with the thio-ester antibody (Allen et al. 2007) following PNBM treatment (Fig 6.3C-D). However, when the protein was transfected into *HeLa* cells using a lipid-based Xfect protein transfectant, it was unsuccessful. This could be due to the positive charge of the 6X His that hinders its encapsulation into the plasma membrane and thus, the cytoplasm. Hence, GST-tagged Ensa and Arpp19 were cloned and purified, as GST-tag is neutral in charge.

GST-tagged Ensa and Arpp19 were expressed and purified as per the workflow shown in Fig. 6.3A and eluted with glutathione (Fig. 6.4A-B). The purified proteins were then thio-phosphorylated according to conditions optimized for His-Ensa in Fig. 6.2C-D

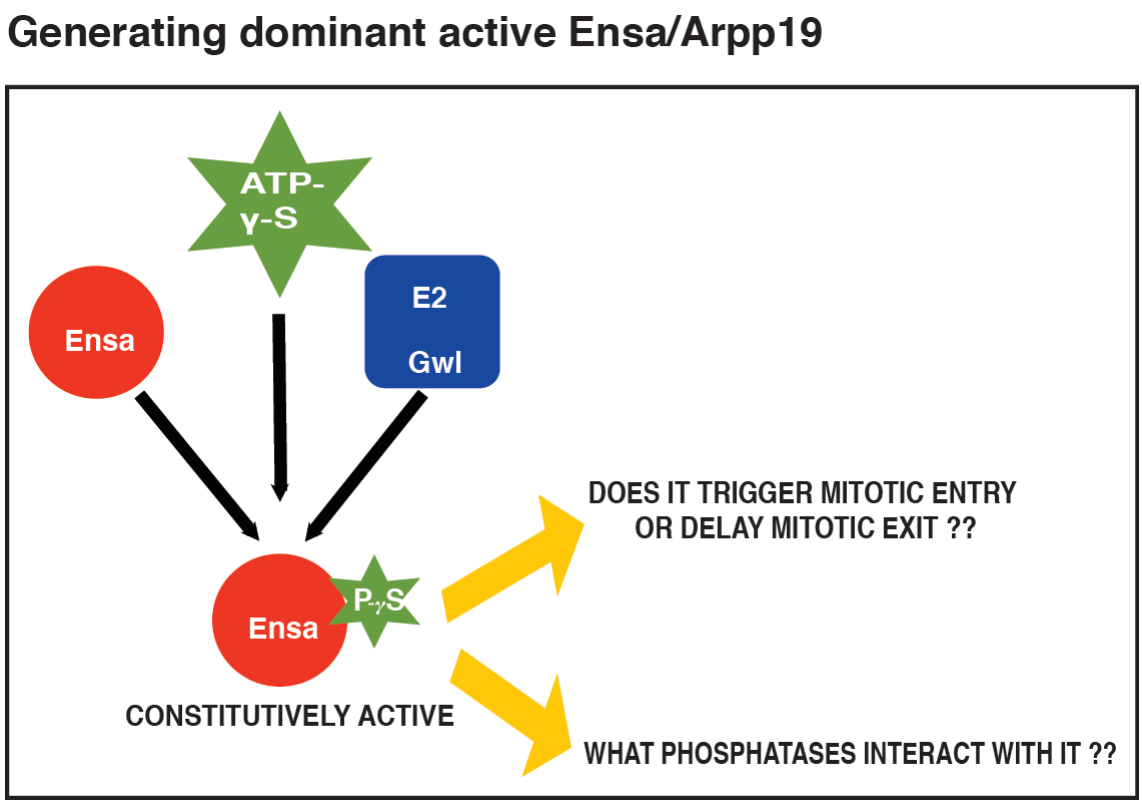

Figure 6.2 Schematic diagram for generating constitutively active Ensa/Arpp19 and the questions addressed using this system.

GST-tagged Ensa and Arpp19 were expressed and purified as per the workflow shown in Fig. 6.3A and eluted with glutathione (Fig. 6.4A-B). The purified proteins were then thio-phosphorylated according to conditions optimized for His-Ensa in Fig. 6.2C-D (Fig.6.4C). Auto-phosphorylation of E2 was also observed in the kinase assay. The purified proteins were then dialysed and concentrated into a neutral PBS/glycerol

GST-tagged Ensa and Arpp19 were expressed and purified as per the workflow shown in Fig. 6.3A and eluted with glutathione (Fig. 6.4A-B). The purified proteins were then thio-phosphorylated according to conditions optimized for His-Ensa in Fig. 6.2C-D (Fig.6.4C). Auto-phosphorylation of E2 was also observed in the kinase assay. The purified proteins were then dialysed and concentrated into a neutral PBS/glycerol solution. E2 was used as a positive control for Xfect transfections. I successfully transfected GST-tagged Ensa and thio-Ensa into asynchronous and mitotic *HeLa* cells.

The transfected proteins also retained their phosphorylation post-transfection. Although the amount of

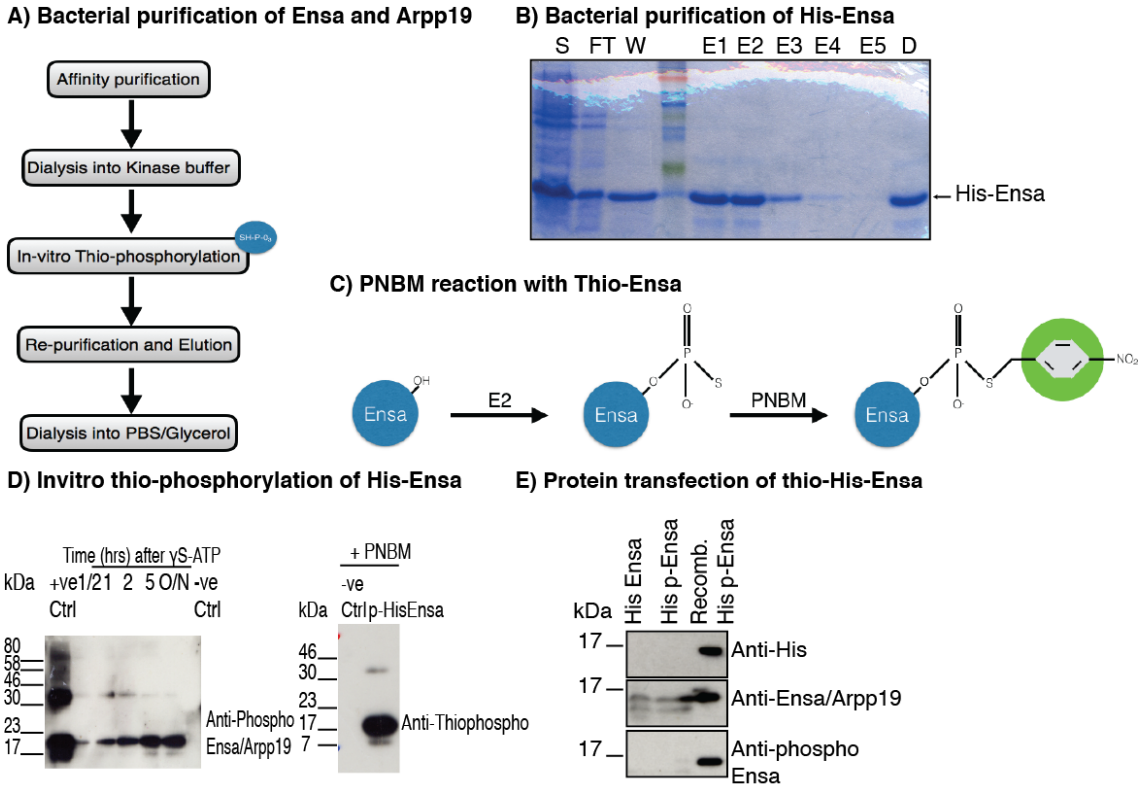

Figure6.3 Transfection of purified His-Ensa using Xfect transfection reagent

A) Schematic representation of generating dominant active Ensa and Arpp19 using bacterial purifications of recombinant proteins from *E. coli* and in vitro thiophosphorylation. B) Affinity purification of His-Ensa from *E. coli*. His-tagged hEnsa was expressed and induced using 1 mM IPTG overnight at 18°C. The over-expressed proteins were purified using Ni-NTA beads and eluted using imidazole. The eluted proteins were dialysed into kinase buffer overnight at 4°C. Aliquots of soluble fraction (S), flow-through (FT),
Washes (W1 and W2) and elutions (E1-5) were subjected to SDS-PAGE and Coomassie-staining. Arrow indicates the eluted His-Ensa protein. C) Schematic representation of In-vitro thio-phosphorylation and PMBM alkylation reaction. D) Purified His-Ensa was thio-phosphorylated by E2 (truncated Gwl) in the presence of ATP-γS at 37°C for varying periods. His-Ensa phosphorylated using cold ATP was used as a positive control and the reaction without ATP as the negative control. Samples were probed with the phospho-Ensa/Arpp19 antibody on a western blot. Samples after overnight incubation was treated with PNBM for 30 min at RT and probed with the thio-ester specific antibody. E) Thiophosphorylated His-Ensa was transfected using Xfect transfection reagent in
HeLa cells. Samples were collected 2 h post-transfection and probed with the indicated antibodies.

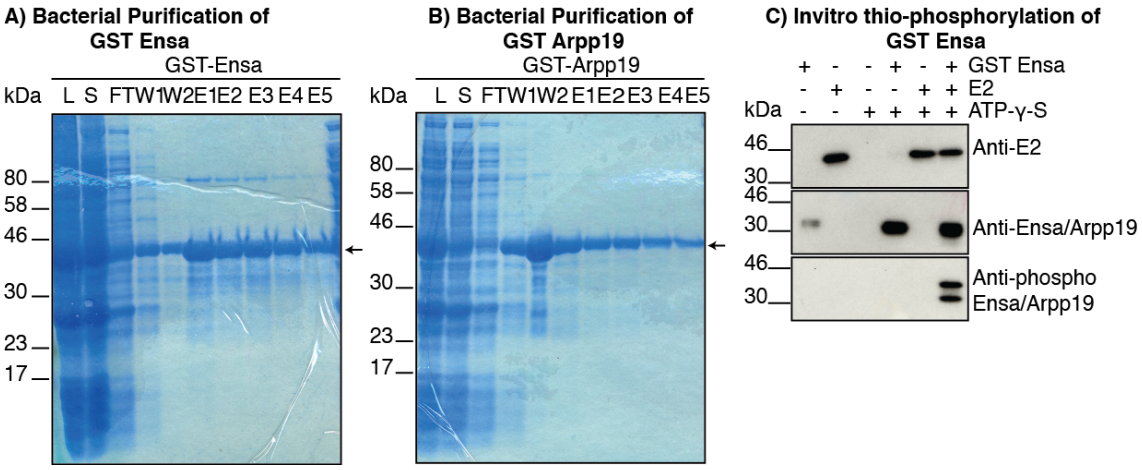

Figure 6.4 Transfection of purified GST Ensa using Xfect transfection reagent

A) and B) Affinity purification of GST-Ensa and GST Arpp19 respectively from *E. coli*. Each protein was expressed and induced with 1 mM IPTG individually for overnight at 18°C. The over-expressed proteins were purified using GST-Sepharose beads and then eluted from the beads using glutathione. Aliquots of Lysate (L), soluble fraction (S), flow-through (FT), Washes (W1 and W2) and elutions (E1–5) were subjected to SDS-PAGE and Coomassie-staining. Arrow indicates the eluted proteins. C) Purified GST-Ensa was thio-phosphorylated by E2 (truncated Gwl) in the presence of ATP-γS for 5 h at 37°C.

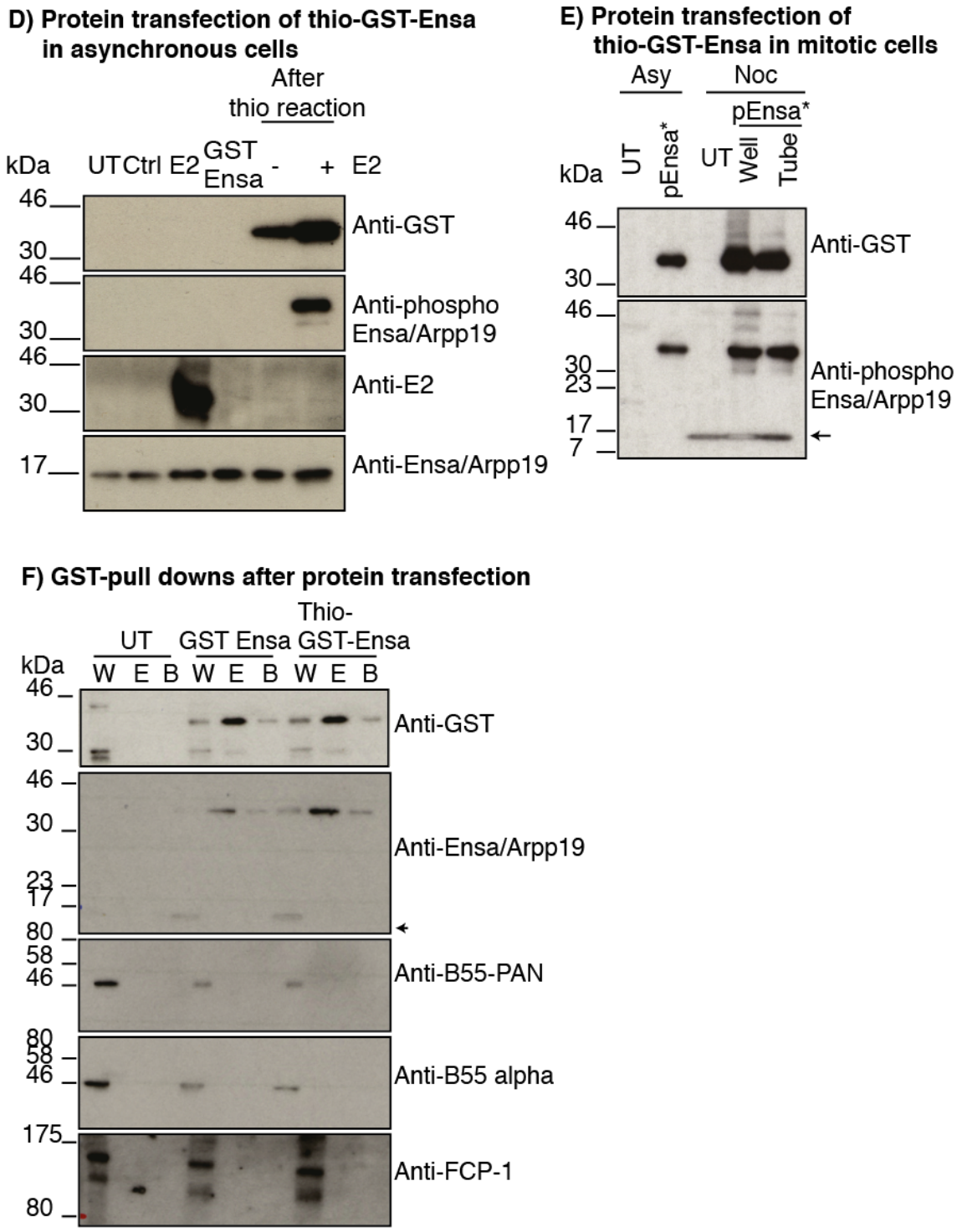

Figure 6.4 Transfection of purified GST Ensa using Xfect transfection reagent

D) Five micrograms of thio-phosphorylated and non-phosphorylated GST-Ensa was transfected into *HeLa* cells using the Xfect transfection reagent. Cells were collected after 2 h and analysed using the indicated antibodies on a western blot. Only GST-Ensa without the reagent was used as a negative control. Endogenous Ensa/Arpp19 is used as a loading control. E) Thio-GST Ensa was transfected into nocodazole-arrested *HeLa* cells using Xfect transfection reagent for 2 h. Transfection was carried out in 6-well dish and a universal tube. Cells were lysed and probed with the indicated antibodies on western blot. Arrow indicates phosphorylated endogenous Ensa/Arpp19. F) Co-immunoprecipitation assays performed with Xfect transfected GST-Ensa and GST-Thio-Ensa in *HeLa* cells. GST-sepharose beads were used to pull down the transiently transfected proteins. Arrow indicates endogenous Ensa/Arpp19 in the whole cell extracts (W). Aliquots of IP elution (E) and beads (B) were analysed using the indicated antibodies on a western blot.

protein transfected in asynchronous cells appears to exceed the endogenous expression, the efficiency of transfection was variable between experiments (Fig. 6.4D-E). To test the activity of the transfected protein, I performed GST-pull down assays 2 h post transfection and analysed its interaction with PP2A-B55. As seen in Fig. 6.4F, although GST-thio-Ensa is successfully transfected, it does not interact with PP2A in-vivo. This may be due to the misfolding of the transfected protein due to presence of GST-tag, which is larger than Ensa itself. It is also possible that although Ensa protein folding is unaffected, the large size of the tag interferes in its interaction with B55. This agrees with the previous studies by Williams et al., where the interaction with B55 was affected when a bulkier MBP (maltose-binding-protein) tag was used (Williams et al. 2014).

In previous experiments, I found that Flag-Ensa/Arpp19 successfully interacted with PP2A-B55 when expressed in mammalian cells. Thus, I decided to optimize protein transfection assays with Flag-tagged Ensa and Arpp19. My Flag-tagged Ensa and Arpp19 constructs were derived from Flag gateway destination vectors. These plasmids have a mammalian EFIa promoter and cannot be used for large-scale purification of the protein. To simplify the purification process, Flag Ensa and Arpp19 were cloned into p3E vectors designed and produced in Oliver Lab. The p3E vector is a GST- tagging vector with T7 promoter, ideal for expression in bacterial system. In addition, the presence of a prescission site enables the cleavage of GST tag following purification to obtain Flag-tagged Ensa and Arpp19 (Fig. 6.5A-C). The GST-Flag-tagged proteins were expressed and purified from *E.coli*. Aliquots from each step of the purification are shown in Fig. 6.5D-G. Un-phosphorylated and thio-phosphorylated Flag Arpp19 was successfully transfected in *HeLa* cells using the Xfect lipid-based reagent (Fig. 6.6A). The amount of protein transfected was approximately twice the amount of endogenous Ensa/Arpp19. Pull-down assays with recombinant transfected Flag Arpp19 show that the protein interacts with B55, thus showing that the protein is active in-vivo. The interaction is specific to thio-phosphorylated Arpp19, similar to that observed in previous studies (Gharbi-Ayachi et al. 2010) (Fig. 6.6B). Overall, I developed a new method to transfect recombinant thio-phosphorylated Ensa/Arpp19 into cells.

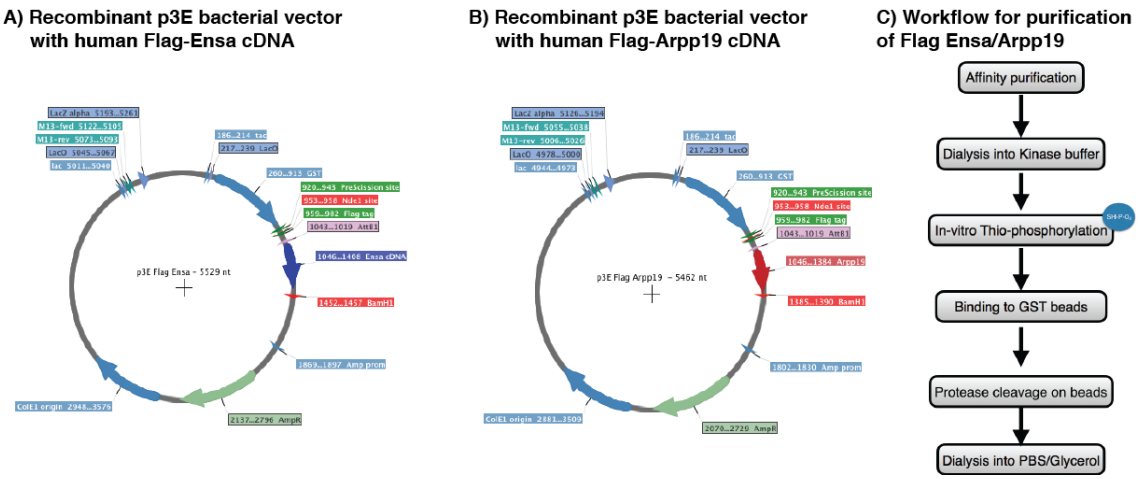

Figure 6.5 Bacterial purification of Flag-Ensa and Flag-Arpp19 using the p3E recombinant vector.

A) Map of the recombinant p3E GST-expression vector with human Flag-Ensa cDNA cloned using Nde1 and BamH1 restriction sites. B) Map of the recombinant p3E GST-expression vector with human Flag-Arpp19 cloned using the Nde1 and BamH1 restriction sites. C) Schematic representation of purifying and thio-phosphorylating Flag-tagged Ensa and Arpp19 from p3E GST vector.

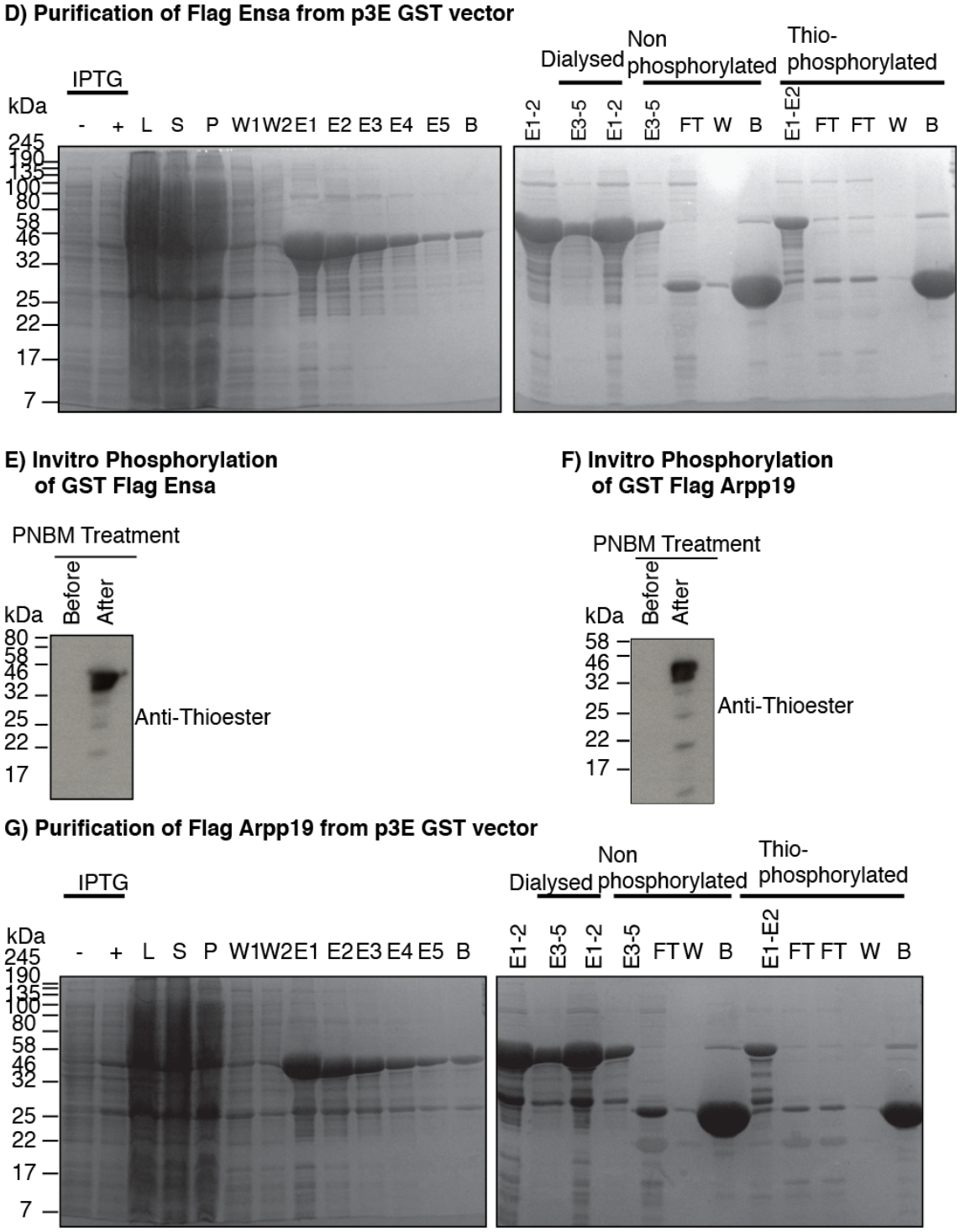

Figure 6.5 Bacterial purification of Flag-Ensa and Flag-Arpp19 using the p3E recombinant vector.

D) and E) Over-expression and purifications of GST-tagged Flag-Ensa and Flag-Arpp19 from E.coli respectively. Over-expression of the plasmid was induced with 1 M IPTG overnight at 18°C. Aliquots of cell lysate (L), soluble fraction (S), pellet (P), washes (W1–2), elutions (E1–5) before and after dialysis into kinase buffer and flow-through (FT) after treatment with precision protease were subjected to SDS-PAGE and Coomassie staining. F) and G) Purified GST-tagged Flag-Ensa and Flag-Arpp19 were thio-phosphorylated by hyperactive truncated Gwl (E2) in the presence of ATP-γS for 5 h at 37°C. Thio-phosphorylated proteins were treated with PNBM for 30 min at RT and probed with thio-ester specific antibody on a western blot.

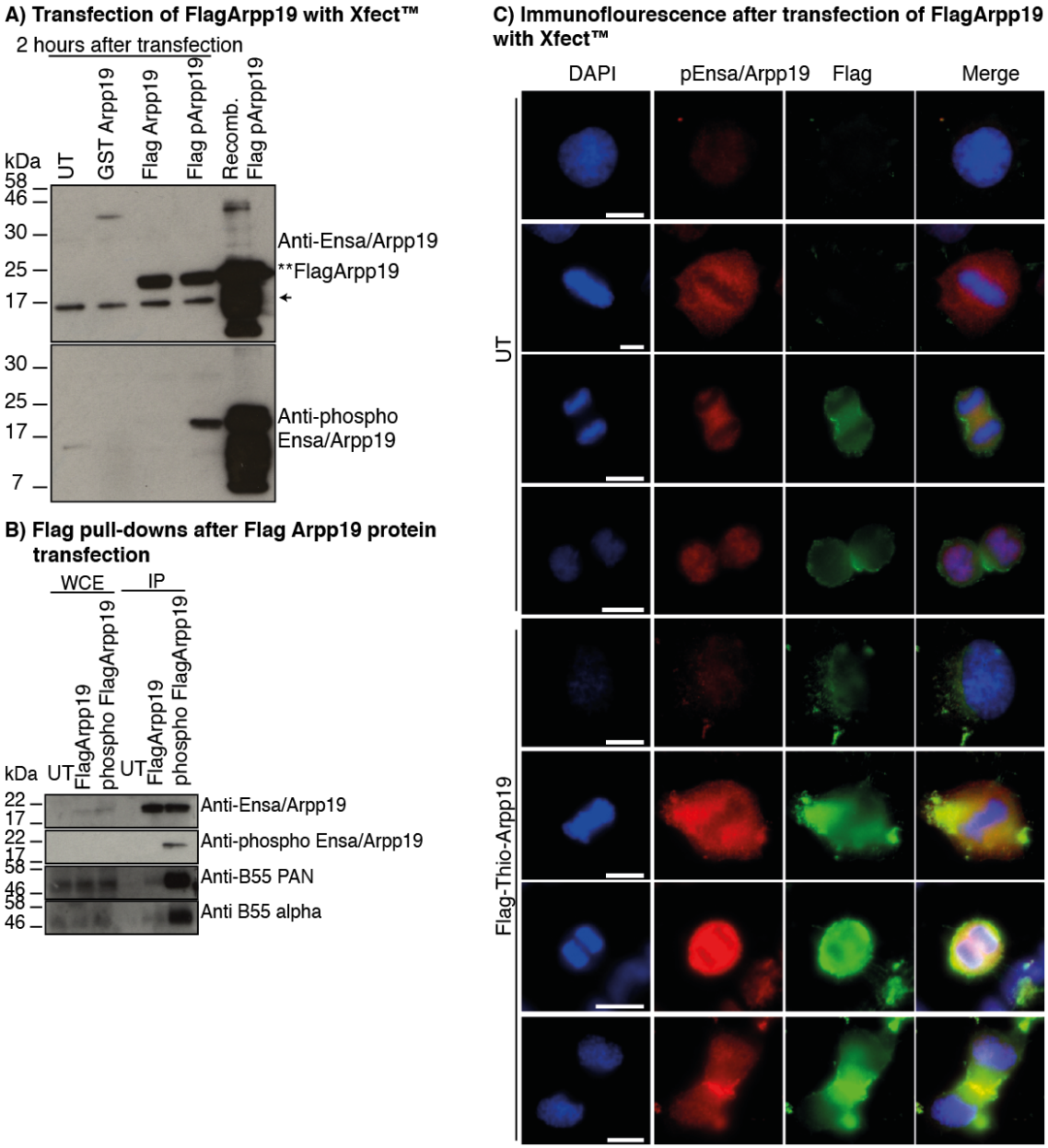

Figure 6.6 Transfection of Flag-Arpp19 using Xfect™ reagent and Co-immunoprecipitation to analyse the activity of the transfected protein

A) Transfection of 5 µg purified Flag-Arpp19 into *HeLa-cdk1as* cells using the Xfect transfection reagent. GST-Arpp19 was used as a positive control for the transfection. Flag-tagged proteins are indicated by ** and arrow indicates endogenous Ensa/Arpp19 used as a loading control. Samples were collected 2 h post-transfection and probed with the indicated antibodies. B) Co-immunoprecipitation of transfected Flag-Arpp19 protein with Flag-M2 magnetic beads. Cells were collected 2 h post-transfection for IP. Aliquots of whole cell lysate (WCE) and IP were analysed using the indicated antibodies.
C) Immunofluorescence of *HeLa-cdk1as* cells transfected with Flag-thio-Arpp19 using Xfect transfection reagent. Cells were fixed using PFA and visualised using Flag-FITC and phospho-Ensa/Arpp19-TRITC antibodies. DAPI (blue) was used to visualise the DNA. Images were taken on IX73_Olympus microscope using the oil immersion 100X lens N.A 1.40 oil, maximum intensity projections of variable z dimension slices. Scale bar 10 µm.

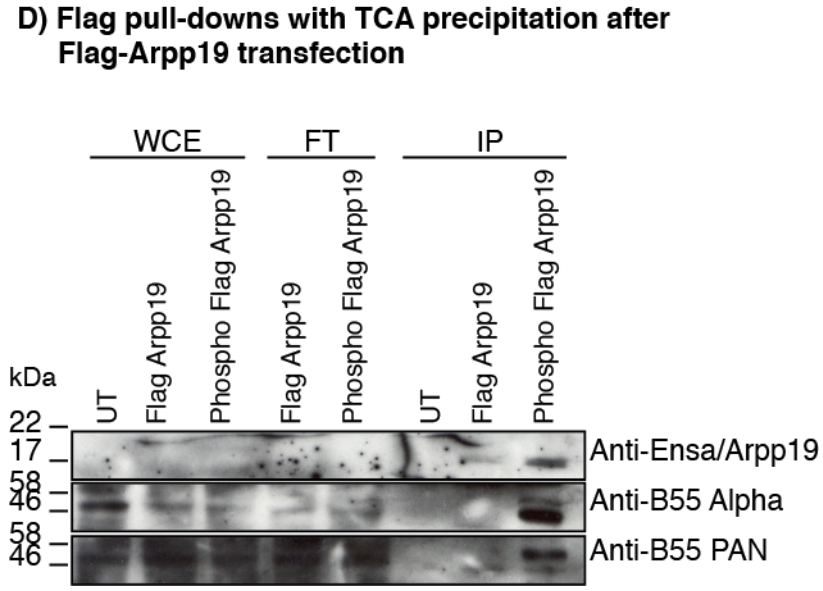

Figure 6.6 Transfection of Flag-Arpp19 using Xfect™ reagent and Co-immunoprecipitation to analyse the activity of the transfected protein

D) Transfected Flag-Arpp19 protein was subjected to co-immunoprecipitation on Flag-M2 magnetic beads using half the cell lysate. The other half of the whole cell extract (WCE) and the unbound fraction (FT) were precipitated with TCA. Equivalent volumes of WCE, FT and IP elution (IP) were analysed using western blot and indicated antibodies.

To study the effects of thio-phosphorylated Arpp19 and Ensa on cells I next performed immuno-fluorescence analysis using Flag antibodies. Thio-phosphorylated Arpp19 is seen to localize on the spindles and poles in metaphase. It localizes globally in anaphase and is seen in the midzone at telophase (Fig. 6.6C). In principle, this demonstrates that we have generated cells that maintain high phospho-Arpp19 during mitotic exit.

However, cells transfected with the constitutively active protein did not appear to show any evident phenotypes, i.e. premature mitotic entry and delayed mitotic exit. This may be due to residual B55 present in the cells even after binding the excess transfected protein. To test this hypothesis, whole cell lysates were split into two halves. One half was precipitated using trichloroacetic acid (TCA) and the other half was used for immunoprecipitation. The flow-through (unbound fraction) obtained after incubating the lysates with the Flag-beads was also precipitated with TCA. On comparing the TCA-precipitated whole cell extract and unbound fractions, residual B55 was observed in the unbound fraction with thio-Arpp19 (Fig. 6.6D). Surprisingly, although a significant reduction was not observed between the WCE and unbound fraction, distinct enrichment was observed in the B55 binding with thio-Arpp19. This is contradicting the observation that we transfect an excess of Arpp19, which should be more than enough to inhibit the endogenous B55-PP2A pool. One explanation to explain this apparent contradiction could be that a large proportion of the recombinant transfected protein is not biologically active in the cell either due to misfolding, or due to exclusion from the cytoplasm. Thus, the residual B55 needs to be inhibited either by increasing the amount of transfected protein or by reducing expression using the siRNA approach. As the amount of transfected protein in the cell is already twice the amount of endogenous, I decided to reduce the expression of PP2A-B55 optimally using siRNA to enable complete inhibition of the phosphatase. Therefore, RNAi depletion was integrated with protein transfection of its inhibitor for complete suppression of PP2A-B55 phosphatase.

HeLa-cdk1as cells treated with B55 siRNA for 72 h were synchronized in G2 with 1 µM or 0.5 µM 1NMPP1 and transfected with 5 µg Flag-thio-Arpp19. Samples were collected 2 h post-transfection, stained with PI staining and phospho-Ser10-Histone H3 antibodies for FACS analysis. Mitotic and G1 cells were gated and quantified using the BD Accuri software, FCS Express Flow.

A) Mitotic entry experiment with siB55 and purified thio-FlagArpp19 with 1μM 1NMPP1

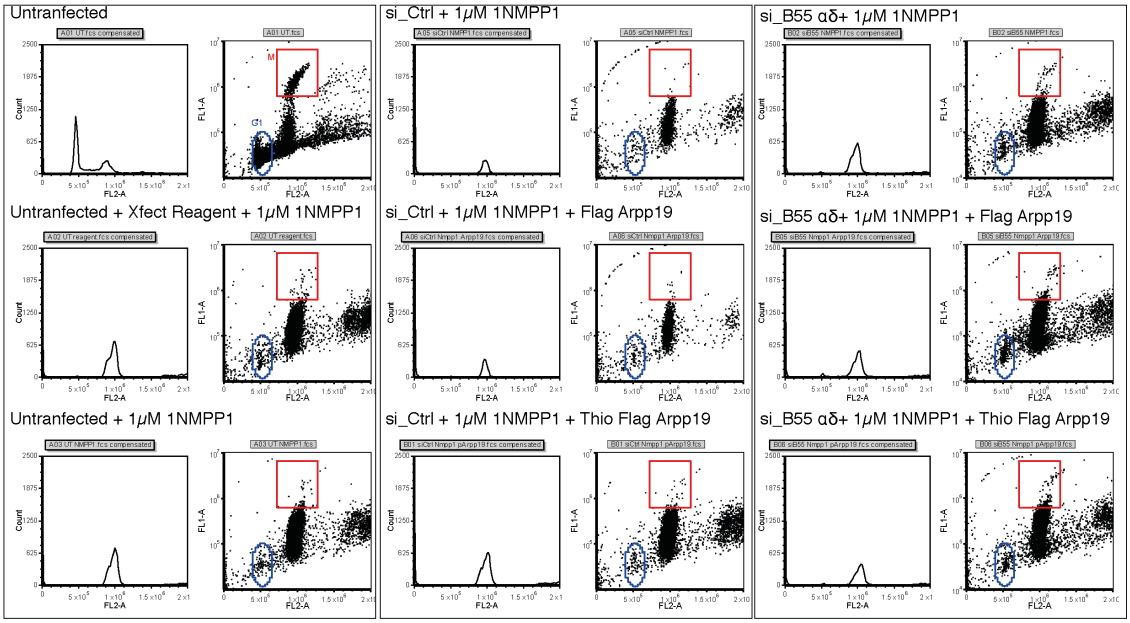

FCS Filename	Gate	# of Events	% of Gated Cells
UT	M	395	3.95
UT	G1	4584	45.84
UT 1μM 1NMPP1	M	51	0.51
UT 1μM 1NMPP1	G1	143	1.43
siCtrl 1μM 1NMPP1	M	9	0.09
siCtrl 1μM 1NMPP1	G1	85	0.85
siCtrl 1μM 1NMPP1 Arpp19	M	13	0.13
siCtrl 1μM 1NMPP1 Arpp19	G1	97	0.97
siCtrl 1μM 1NMPP1 pArpp19	M	35	0.35
siCtrl 1μM 1NMPP1 pArpp19	G1	111	1.11
siB55 1μM NMPP1	M	61	0.61
siB55 1μM NMPP1	G1	214	2.14
siB55 1μM NMPP1 Arpp19	M	114	1.14
siB55 1μM NMPP1 Arpp19	G1	328	3.28
siB55 1μM NMPP1 pArpp19	M	143	1.43
siB55 1μM NMPP1 pArpp19	G1	181	1.81

Figure 6.7 Mitotic entry experiment using purified constitutively active Flag-Arpp19

A) FACS analysis of *HeLa-cdk1as* cells depleted of B55α and δ subunit and transfected with 5 μg purified Thio-Flag-Arpp19. *HeLa-cdk1as* cells were synchronised in G2 with 1 μM 1NMPP1 for 20 h and then transfected using Xfect reagent. Samples were collected 2 h after transfection and mitotic index was determined using phospho-H3 staining.

B) Mitotic entry experiment with siB55 and purified thio-FlagArpp19 with 0.5 μM 1NMPP1

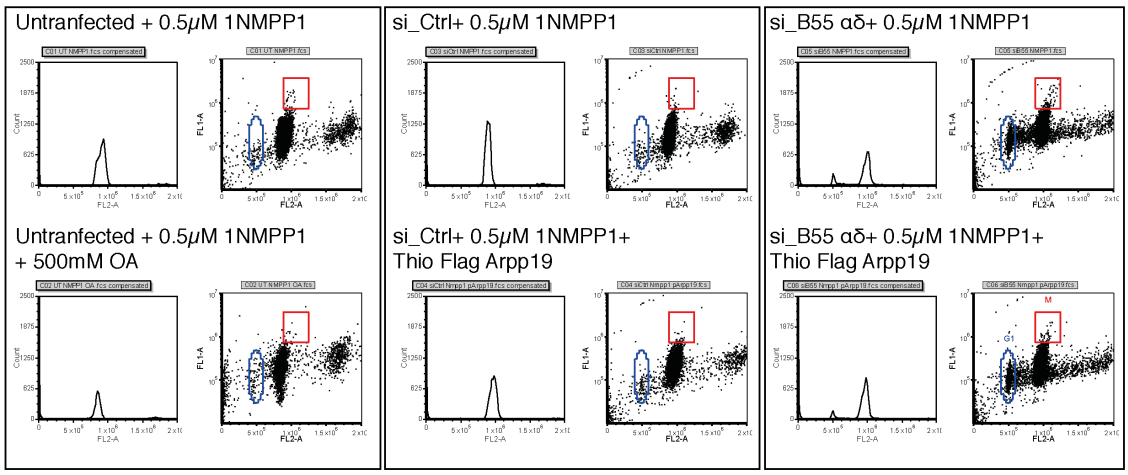

FCS Filename	Gate	# of Events	% of Gated Cells
UT 0.5μM 1NMPP1	G1	94	0.94
UT 0.5μM 1NMPP1	M	22	0.22
UT 0.5μM 1NMPP1 + OA	G1	109	1.09
UT 0.5μM 1NMPP1 + OA	M	18	0.18
siCtrl 0.5μM 1NMPP1	G1	106	1.06
siCtr l0.5μM 1NMPP1	M	16	0.16
siCtrl 0.5μM 1NMPP1 pArpp19	G1	108	1.08
siCtrl 0.5μM 1NMPP1 pArpp19	M	25	0.25
siB55 0.5μM 1NMPP1	G1	938	9.38
siB55 0.5μM 1NMPP1	M	83	0.83
siB55 0.5μM 1NMPP1 pArpp19	G1	735	7.35
siB55 0.5μM 1NMPP1 pArpp19	M	43	0.43

Figure 6.7 Mitotic entry experiment using purified constitutively active Flag-Arpp19

B) FACS analysis of *HeLa-cdk1as* cells depleted of B55α and δ subunit and transfected with 5 µg purified Thio-Flag-Arpp19. *HeLa-cdk1as* cells were synchronised in G2 with 0.5 µM 1NMPP1 for 20 h and then transfected using Xfect reagent. Samples were collected 2 h after transfection and mitotic index was determined using phospho-H3 staining.

As observed in the FACS profile in Fig. 6.7A, B55 depletion with 1 μM 1NMPP1 did not show any evident phenotypes. However, B55 depletion with 0.5 μM NMPP1 drove the cells into mitosis (M population increases 2-fold) and triggered exit (G1 increases 4-fold) (Fig. 6.7B). Surprisingly, transfection of Arpp19 has no expected additive effect of these cells despite complete inhibition of the phosphatase (Fig. 6.7A-B). It could not be determined if the G1 population difference occurred due to the protein transfection.

In addition, the slight decrease in the mitotic index and G1 population on Arpp19 transfection might be due to variability in B55 depletion among samples (Fig. 6.7B). Thus, preliminary experiments with B55-depletion and Flag-Arpp19 transfection showed no significant effect on the cell cycle profile. This was also true for cells treated with control siRNA. This could mean that B55-PP2A is not the phosphatase that is the major target of okadaic acid whose inhibition triggers mitotic entry. However, it is difficult to ultimately prove that we have completely inactivated B55-PP2A in the 1NMPP1-induced arrested cells. Moreover, the protein transfection itself could have had an inhibitory effect on mitotic entry over-riding the phosphatase inhibition.

Xfect is a peptide based transfection reagent. The Xfect peptide interacts with the protein of interest and transports it into the cells. The amino-acid composition of the Xfect reagent confers cell-penetrating properties to execute this function. Thus, the transfectant might interact with the cell membrane and inhibit mitosis. To test this I treated G2 cells with Xfect reagent and Xfect + Flag-thio-Arpp19. An untreated sample was used a control. When these cells were released from the 1NMPP1 block into STLC, only the untreated sample entered mitosis. Both the samples treated with Xfect reagent failed to enter mitosis even after 8 h of incubation (Data not shown). This result prompted us to further optimize the protein transfection procedure.

As an alternative to chemical transfection, I considered physical transfection methods of protein transfection. Bekei used Amaxa Nucleofection to transfect αSyn, a small (14.5 kDa) neuronal protein, for *in-cell* NMR studies in mammalian cells (Bekei 2013). In Bekei's thesis, the method was optimized to electroporate 2 x 10^6 *HeLa* cells with protein concentration of 1 mM. For this purpose, purified Flag-thio-Arpp19 was concentrated using Vivaspin centricon tubes and the buffer was exchanged to 20 mM Phosphate buffer with 150 mM NaCl. Four hundred micromoles of purified protein was

resuspended in electroporation buffer containing 2 mM ATP and 2 mM Glutathione. Both ATP and Glutathione were shown to improve cell recovery in *HeLa* cells (Bekei 2013). Trypsinised *HeLa* cells were resuspended in the protein-buffer mixture and electroporated with A#28 nucleofection program with 1 or 2 pulses. A 3-s gap between each pulse was maintained to reduce cell death by electroporation. Samples were allowed to recover in complete warm media for at least 5 h before analysing by western blot (Fig. 6.8A). Although, we see a band at the expected size, it was also observed in the un-transfected sample. An extra band around the same size was observed in the insoluble (pellet; P) fraction of the samples transfected with protein. Endogenous Ensa/Arpp19 is observed to be more concentrated in the cytosolic fraction that the pellet (marked by **). Thus, the transfected protein seems to be in the non-cytosolic fraction of the cell, if the transfection were successful. To optimize this technique further, I performed electroporation with two different programs with less cells (to increase the ratio of cells: protein) using A#28 and B#28 Amaxa program. Although the band around 22 kDA seems to be enriched in the Ensa cytosolic (S) fraction, it is also observed in the Buffer (S) fraction. A specific band around the expected size of 22 kDa was only observed in the insoluble (pellet, P) fraction with Ensa transfection (Fig. 6.8B). Thus, Amaxa Nucleofection proved unsuccessful in transfecting Flag-Arpp19 into the cytosol of mammalian cells.

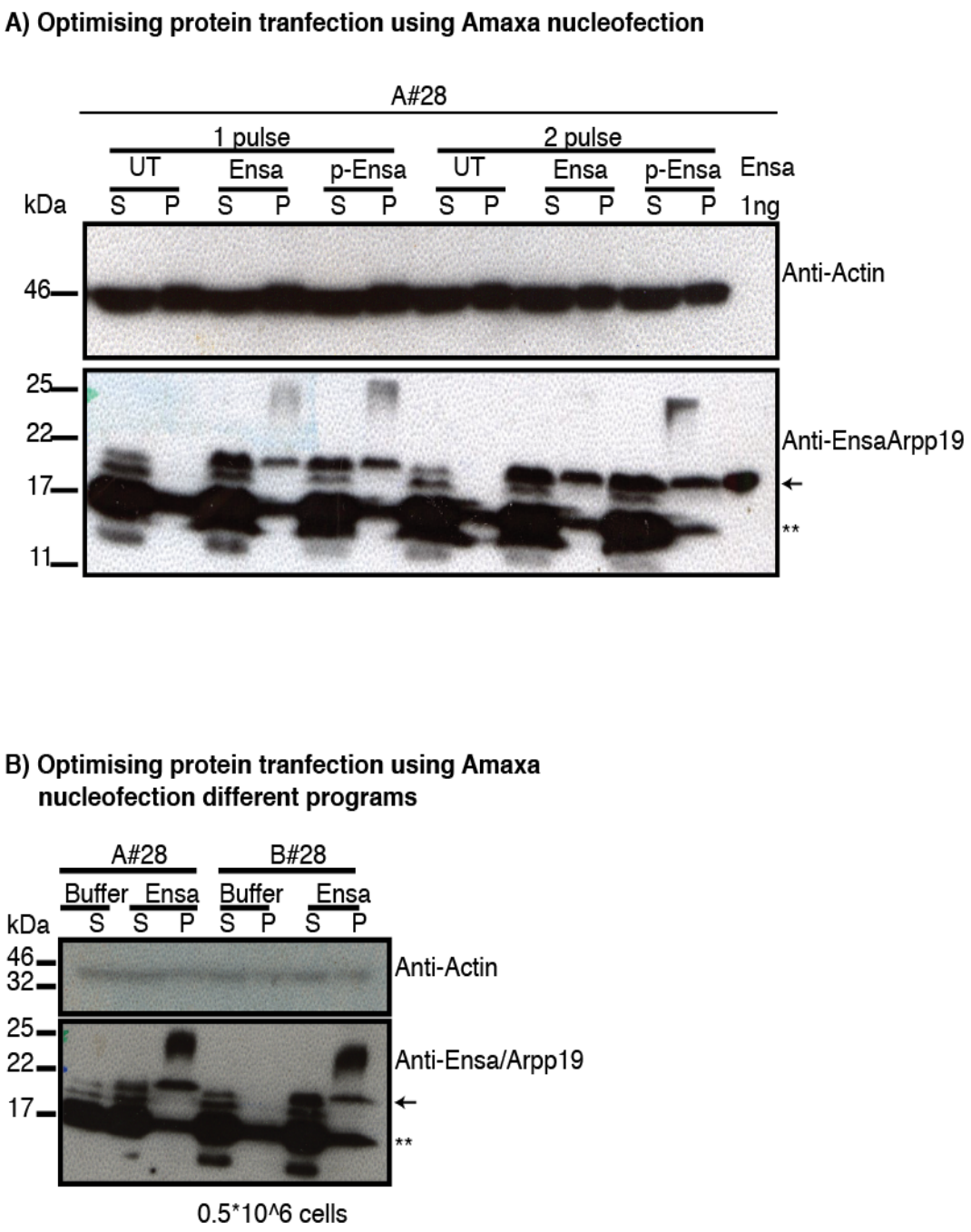

Figure 6.8 Optimisation of protein transfection using Amaxa Nucleofector Technology

A) Transfection of 5 µg of Flag Ensa and Flag-Thio-Ensa into 2 x 10^6 *HeLa*_as cells using the #A28 program optimised for *HeLa* cells on the Amaxa Nucleofector. Cells were fractionated following 1 or 2 pulses of electroporation and analysed using western blotting. Arrow indicates the expected size of Flag-tagged proteins and ** indicates expected size of endogenous Ensa/Arpp19. B) Five micrograms of Flag-Ensa was transfected into 0.5X 106 *HeLa-cdk1as* cells. Cells were then fractionated and analysed using shown antibodies on a western blot. The arrow indicates the expected size of Flag-Ensa and ** indicates the expected size of endogenous Ensa/Arpp19.

Another approach along the same lines was using the Neon Transfection Kit form Invitrogen to perform protein transfections. This approach was adapted from (Kim et al. 2014). They transfected the Cas protein into *U2OS* cells and observed its activity 24 h post-transfection. This was done to minimize off target-effects, as the protein cleaved DNA immediately after delivery and was itself is degraded within 24 h of transfection. Thus, this approach is ideal for our experiment, as the active protein can capture the residual B55 immediately after delivery and promote mitotic entry. As the protocol was optimized for *U2OS* cells in this paper, I used *U2OS-cdk1as* cells for this approach. As shown in Fig. 6.9A, preliminary experiments with 5 µg Flag-Arpp19 using the Neon Kit resulted in the successful transfection of the protein into the cytosolic fraction (S) (Fig. 6.9A). The amount of protein transfected is less than twice the amount of endogenous Ensa/Arpp19 (shown with an arrow). When 1 µg and 5 µg of Flag-Arpp19 were transfected and the cells were allowed to recover for 2 h post-transfection, the amount of transfected protein was almost equal to that of the endogenous protein (Fig. 6.9B). In addition, 1 µg of Flag Arpp19 seemed insufficient for transfection as no band was observed at the expected size. Thus, it seems increasing the amount of protein used and recovery time are important parameters to consider in Neon transfection. So I transfected 1 µg and 5 µg of Flag-Arpp19 using the Neon kit and allowed the cells to recover at 37°C for 24 h. When these cells were fractionated and blotted with Ensa/Arpp19 antibody, a band of the expected size appears in the soluble fraction, but the amount of transfected protein is almost half the amount of the endogenous (shown with an arrow) (Fig. 6.9C).

Thus, in all the transfection attempts, the ratio between endogenous and exogenous protein shows that we are not dramatically over-expressing thio-Arpp19.

As seen in Fig. 6.9C, the proteins stayed in the cytosol for at least 24 h post-transfection, unlike Cas9. To observe the effects of this stable and dominant active Arpp19 on *U2OS* cells, I imaged the transfected cells for 3 h, 1 h after transfection to observe effects of dominant active Flag-Arpp19. Although the electroporated cells recovered and adhered to the surface of the plate coated with Matrigel, very few mitotic divisions were observed in the transfected and control cells (Fig. 6.9D). More cell death was observed with protein-transfected samples as compared to the control. Thus, varying amounts of transfected protein despite using the same amount of recombinant

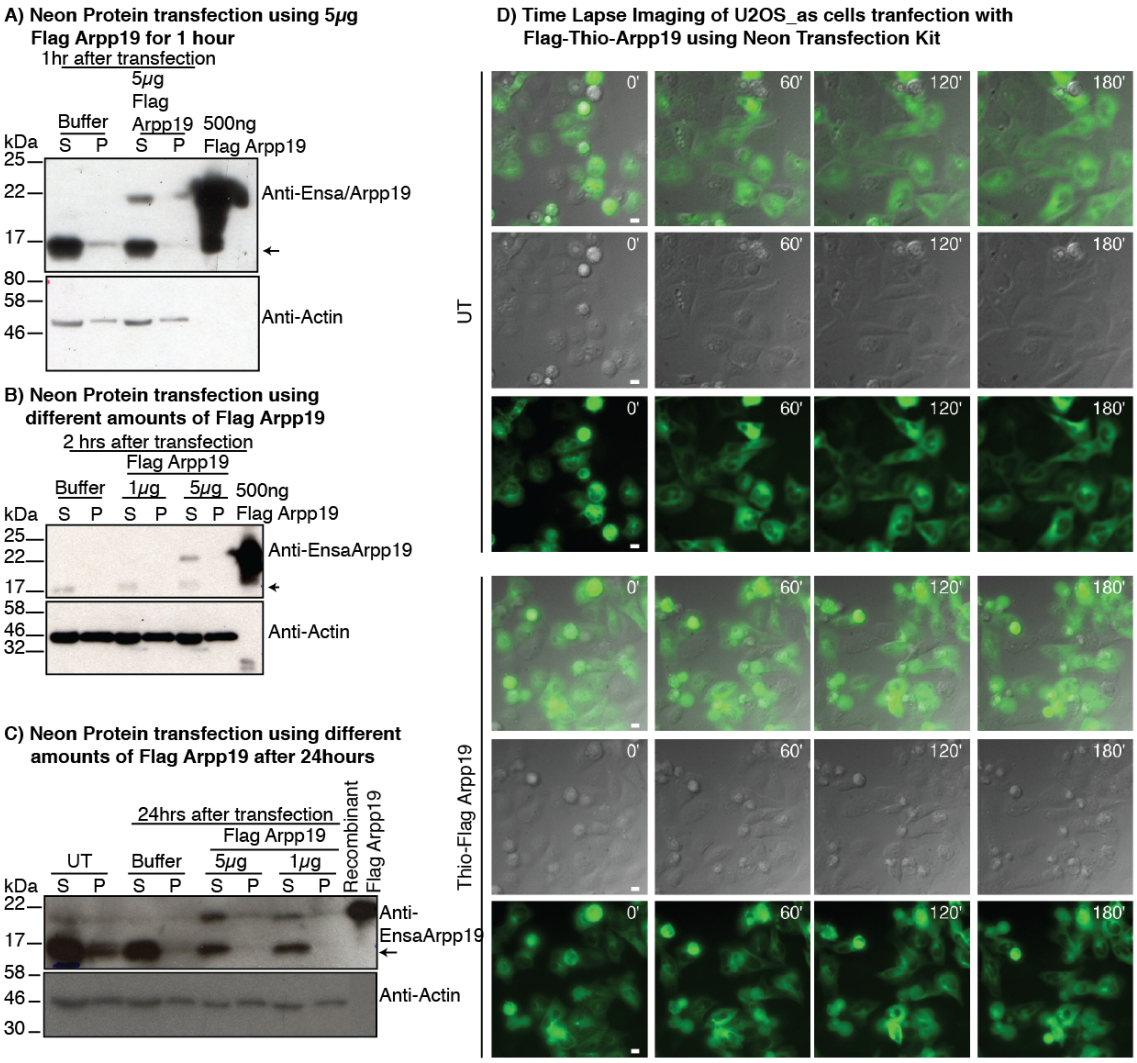

Figure 6.9 Optimisation of Neon Protein Transfection

A) Five micrograms of Flag-thio-Arpp19 were transfected into *U2OS-cdk1as* cells using the Neon Transfection Kit (#MPK1025). Cells were incubated at 37°C for 1 h and cell lysates were fractionated. The cellular fraction were analysed by western blotting. The arrow indicates endogenous Ensa/Arpp19. B) One and five micrograms of Flag-thio-Arpp19 was transfected into U2OS_as cells using the Neon Transfection Kit (#MPK1025). Cells were incubated at 37°C for 2 h and cell lysates were fractionated. The cellular fraction were analysed by western blotting. The arrow indicates endogenous Ensa/Arpp19. C) One and five micrograms of Flag-thio-Arpp19 was transfected into *U2OS-cdk1as* cells using the Neon Transfection Kit (#MPK1025). Cells were incubated at 37°C for 24 h and cell lysates were fractionated. The cellular fraction were analysed by western blotting. The arrow indicates endogenous Ensa/Arpp19. D) Time-lapse imaging of *U2OS-cdk1as* cells transfected with Flag-Thio-Arpp19 plated on matrigel-coated plates. Images were taken on the IX73_Olympus microscope using the 40X lens, N.A 0.60, for 3 h after transfection. Scale bar 10 µm.

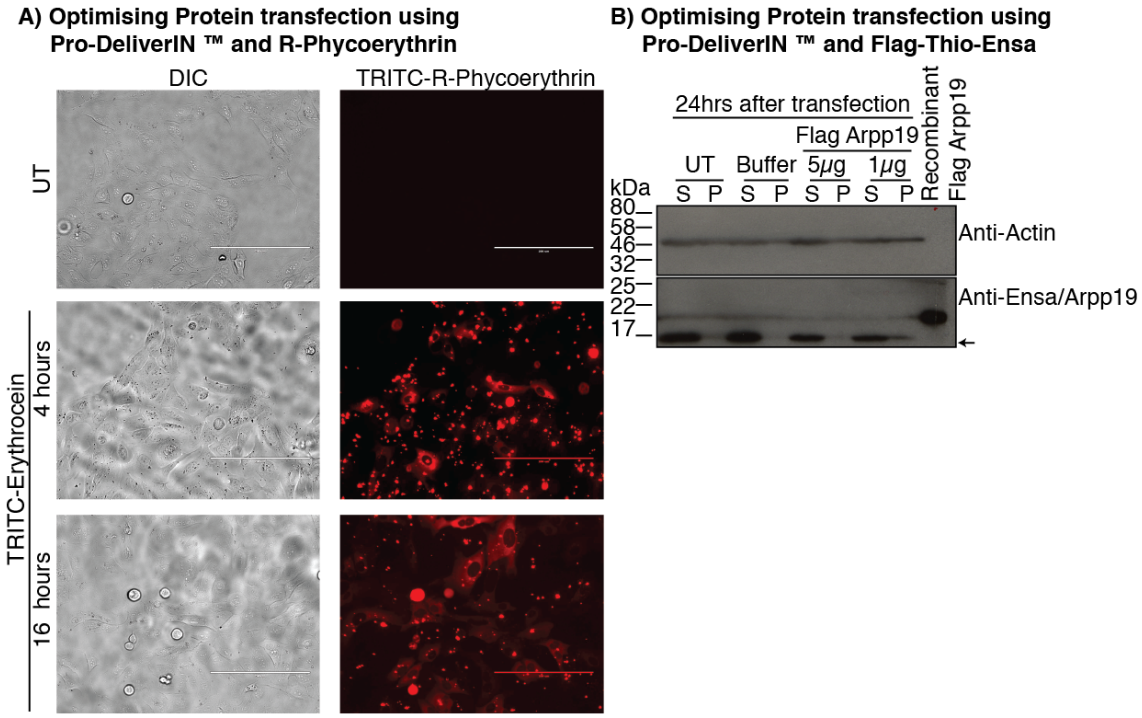

Figure 6.10 Protein Transfection using ProDeliverIN Reagent

A) Transfection of the positive control p-Erythrocein into *HeLa-cdk1as* cells using ProDeliverIN reagent. Images were taken using the 20X lens on the Axio Lab. A1 (Zeiss) microscope, 4 h and 16 h after transfection. Scale bar 10 μM B) Transfection of different amounts of purified Flag-thio-Arpp19 using the ProDeliverIN reagent. Samples were fractionated into soluble and insoluble components before analysing them using western blotting. The arrow indicates endogenous Ensa/Arpp19 in the cellular fractions.

protein shows inconsistency in the method. Additionally, the recovery of the cells from the physical transfection seems to be very slow to observe the switch-like G2/M transition.

As seen in Fig. 6.9C, the proteins stayed in the cytosol for at least 24 h post-transfection, unlike Cas9. To observe the effects of this stable and dominant active Arpp19 on *U2OS* cells, I imaged the transfected cells for 3 h, 1 h after transfection to observe effects of dominant active Flag-Arpp19. Although the electroporated cells recovered and adhered to the surface of the plate coated with Matrigel, very few mitotic divisions were observed in the transfected and control cells (Fig. 6.9D). More cell death was observed with protein-transfected samples as compared to the control. Thus, varying amounts of transfected protein despite using the same amount of recombinant protein shows inconsistency in the method. Additionally, the recovery of the cells from the physical transfection seems to be very slow to observe the switch-like G2/M transition.

Due to these reasons, another milder chemical transfectant called ProDeliverIN was tested to transfect Flag-Arpp19 into mammalian cells. ProDeliverIN is a lipid-based formulation that forms covalent bonds with the protein of interest. The cell internalizes this complex and the protein of interest is released into the cytosol. This product claims to be milder transfection reagent and to transfect biologically active molecules into the cell. I performed preliminary experiments with 1 x 10^5 *HeLa* cells in a 24-well plate. R-Phycoerythrin provided in the kit was used as a positive control. The transfection was done as per the manufacturer's recommended protocol. Transfected R-Phycoerythrin was observed under the microscope using epi-fluorescence and Flag Arpp19 was observed using western blot with Ensa/Arpp19 antibody. As seen in Fig. 6.10A, the transfection worked very well with the positive control. However, Flag Arpp19 transfection was unsuccessful, as no band of the expected size was observed in the cytosolic fraction (S). This could be due to a variety of reasons like the size of the protein, the buffer or the time of incubation. These parameters could not be tested due to the limitation of time.

In conclusion, both the chemical and electroporation methods were successful in delivering thio-phosphorylated Arpp19 into mammalian cells. Both methods proved to

have limitations with regards to cell viability and indirect effects on cell cycle progression. Hence, further optimization will be required to transfect biologically active thio-Ensa/Arpp19 into mammalian cells to study their effects on mitosis and investigate the Ensa/Arpp19-PP2A-B55 pathway in further detail. For single cell studies, microinjection will most likely be the preferential technique because the relatively mild treatment exerts less indirect effects that influence the outcome of the experiment.

CHAPTER7 DISCUSSION

In this thesis, I have performed an extensive genetic and biochemical analysis of mammalian Ensa and Arpp19. I have characterised the localisation and depletion phenotypes of these proteins, analysed the dynamics of complex formation with PP2A/B55 and have aimed at establishing a method to observe the consequences of dominant active Ensa/Arpp19 on mitotic entry and exit. The major findings of this work and its implication for our understanding of the G2/M transition are discussed below.

7.1 Ensa/Arpp19 Localisation Studies using Specific Antibodies and Fluorescent Markers

Although Greatwall kinase localisation and function has been described in various systems including mammalian cells, Ensa and Arpp19 have not been characterised equally well. In this thesis, I attempted to investigate the mitotic functions of Ensa and Arpp19. The first step towards mapping the functions of these highly similar proteins was to generate specific antibodies. I generated rabbit polyclonal antibodies against the dissimilar C-termini of *Gallus* proteins (homologous to humans) (Fig. 3.1A), which proved to be specific against recombinant (Fig. 3.1B) and exogenously expressed Ensa and Arpp19 respectively (Fig. 3.1D). However, these antibodies were unable to generate a distinctive signal to detect endogenous Ensa and Arpp19 by immuno-blotting, even though they could detect exogenously expressed protein (Fig. 3.1E-F). Thus, the specific antibodies could not be used in further investigation. This limits the scope of this thesis with regards to distinguishing the function of the individual paralogues Ensa and Arpp19. Hereafter, characterisation of endogenous Ensa and Arpp19 has been carried out by co-depletion, as it was easily detectable using commercial antibodies.

Localisation of Greatwall contributes to mitotic progression significantly. Greatwall is nuclear and is translocated to the cytoplasm in a phosphorylation-dependent manner just before nuclear envelope breakdown (NEBD). This enables PP2A inhibition via the Greatwall-Ensa/Arpp19 pathway and facilitates mitotic progression (P. Wang et al. 2013; Alvarez-Fernández et al. 2013; P. Wang et al. 2016). Whether Ensa and Arpp19 are spatially regulated in a similar way has not been investigated, although, it is likely

that Ensa/Arpp19 can diffuse easily through nuclear pores owing to their small size and are not spatially regulated (Alvarez-Fernández & Malumbres 2014). Localisation of yeast homologues of Ensa/Arpp19 (Igo1/2) is nuclear but has only moderate contribution in closed mitosis (Rossio et al. 2014). Thus, cellular localisation of Ensa and Arpp19 were investigated in mammalian cells using Pan Ensa/Arpp19 antibody and fluorescent markers.

Ensa/Arpp19 were found to be ubiquitously present in interphase cells with a slight enrichment in the nucleus. The cytoplasmic staining is granular but this is likely to be an artefact of fixation. Ensa/Arpp19 is evidently excluded from the chromosomes and appears to be dispersed evenly in mitosis (Fig. 3.2 A-B). The mitotic distribution of Ensa/Arpp19 is similar to Greatwall localisation in human cells, proposing an analogous spatial regulation of Ensa/Arpp19 in mammalian mitosis. Exogenously expressed Flag-tagged Ensa and Arpp19 reiterated these observations, as they localised ubiquitously in interphase and displayed mitotic chromosome exclusion (Fig. 3.3D and 3.4 A-B). Interestingly, Flag Arpp19 appeared to localise at the cortex, which could point to cortical functions of this protein (Fig. 3.4 A-B). This notion is further substantiated by the extensive blebbing phenotype observed upon Ensa/Arpp19 depletion. A major technical obstacle that was revealed during the course of this study is the disruption of Ensa/Arpp19 functions when larger fluorescent tags were used both on the N- and C-terminus (Fig. 3.3A-C). We dedicated a considerable effort to overcome this problem, but could not manage to find a suitable way to add GFP tags without disrupting the ability of these small proteins to bind to PP2A/B55. This is an important caveat that will influence future analysis of these proteins. Perhaps the use of smaller Halo or Snap-tags may be useful to overcome this problem in future.

However, examining GFP fusions of Ensa and Arpp19 showed mitotic exclusion from chromosomes similar to the endogenous proteins. Moreover, overexpression of GFP-Ensa delayed mitotic progression by delaying the cells in metaphase and causing mitotic exit with lagging chromosomes (Fig. 3.3D-E). This suggests that these proteins may still be functional as PP2A/B55 inhibitors even though the *in vitro* complex formation appears to be disrupted. Alternatively, a dominant negative effect involving other interacting proteins could be involved.

7.2 Genetic Analysis of Greatwall and Ensa/Arpp19 in Human Cell Lines

Using RNAi-mediated depletion, genetic analysis of Greatwall and Ensa/Arpp19 in human cells characterised their functions in mammalian mitosis. Depletion phenotypes of Greatwall kinase have been well characterised in mitotic entry and exit. Greatwall depletion leads to dramatic responses in *Drosophila*, *Xenopus* and starfish oocytes causing mitotic entry inhibition. This is indicated by Cdk inactivation and minimal mitotic substrate phosphorylation when Greatwall is depleted from interphase extracts (J. Yu et al. 2004; Zhao et al. 2008; Bettencourt-Dias et al. 2004; Glover 2012; Lorca & Castro 2012). However, these phenotypes were not recapitulated in mammalian cells. End-point assays such as immunofluorescences and 2D FACS in human cells showed chromosome congression and segregation defects accompanied by cytokinesis failure. Although endpoint assays showed a slower mitotic index in human cells, mouse cells failed to arrest in G2 on Greatwall depletion (Burgess et al. 2010; Voets & Wolthuis 2010; Alvarez-Fernández et al. 2013). I observed similar phenotypes (Fig. 4.1D-F) in Greatwall-depleted *HeLa* cells using live-cell imaging to measure the mitotic index dynamically in asynchronous population. Very little difference was observed in the mitotic index between control and Greatwall depleted cells (Fig. 4.1C), indicating the kinase does not affect mammalian mitotic entry as observed in *Xenopus* egg extracts. Using the *HeLa-cdk1as* cells that can be synchronised in late G2 phase, I found that G2-cells depleted of Greatwall entered mitosis when Cdk1 was activated, thus illustrating that mammalian cells can enter mitosis even in the presence of high phosphatase activity. However, minor inhibition of Cdk1 causes a G2 arrest in Greatwall-depleted cells, suggesting that these cells rely on high Cdk1 activity to counterbalance persistent PP2A/B55. Thus, Greatwall is not essential for mitotic entry but has a dramatic effect on the required Cdk1 threshold (Fig. 4.3A-B and 4.4A-B).

Ensa/Arpp19 mitotic phenotypes were characterised in human cells by depleting both individually and together. Similar to Greatwall, the single or double depletion of Ensa/Arpp19 did not affect mitotic entry dramatically. Although a slight decrease in mitotic index was observed with Ensa depletion as compared to Arpp19 and the double depletion, rescue experiments with Ensa-cDNA have to be performed to draw clear

conclusions (Fig. 4.2C). This is in contrast to the observations made by GharbiAyachi et al. (2010) where they observed a 50% reduction in the mitotic index with Arpp19 depletion but not Ensa. This difference in the function of the paralogues could be due to the high sequence homology between Ensa and Arpp19 (≈ 70%) making it difficult to differentiate between them. It could also be due to the unknown redundancy between these proteins and their varying concentrations in different cells lines. Stably expressing degron-tagged Ensa and Arpp19 followed by CrispR depletion of endogenous genes might be a viable approach to distinguish between these small proteins in addition to reducing off-target effects. This approach is however challenging given the number of isoforms reported for human Ensa, and the effect on tags on the function of the protein.

Interestingly, Ensa/Arpp19 depletion had a much less dramatic effect on the mitotic entry threshold than observed with Greatwall (Fig. 4.3C-D). This is an unexpected result, since Greatwall is a processive enzyme while Ensa/Arpp19 are stoichiometric inhibitors. Thus, even an incomplete depletion of Ensa/Arpp19 should result in release of active PP2A/B55 complexes, while small amounts of Greatwall may still be able to phosphorylate most of its substrates. Conversely, efficient depletion of both Ensa and Arpp19 was less effective in lowering the mitotic entry threshold for Cdk1 than Greatwall. This discrepancy could point to Ensa/Arpp19 independent functions of Greatwall and needs to be further investigated.

Characterisation of mitotic phenotypes of Greatwall and Ensa/Arpp19 also exhibit some surprising results. As observed with Greatwall, both these proteins displayed longer transit time in mitosis. Ensa and Arpp19 showed an additive effect in prolonging mitotic time due to metaphase delays when co-depleted as compared to single depletions (Fig. 4.2E). This implies redundancy between these proteins in their cell cycle functions. Greatwall depletion displayed chromosome segregation, condensation and cytokinesis defects congruent with previous studies. These defects point towards a major role of Greatwall kinase in mitotic maintenance and proper mitotic exit as previously stated (Burgess et al. 2010; Voets & Wolthuis 2010; Alvarez-Fernández et al. 2013). Ensa/Arpp19 depletion led to chromosome alignment defects like accumulation at the poles as well as lagging chromosomes indicative of premature mitotic exit defects (Fig. 4.2D-F). Surprisingly, the Greatwall hallmark cytokinesis defect was not observed upon depletion of Ensa/Arpp19, potentially indicating an Ensa/Arpp19 independent function

of Greatwall at mitotic exit. Additionally, mitotic entry in Ensa/Arpp19 depleted cells exhibit a significant blebbing phenotype that is absent on Greatwall-depletion (Fig. 4.3D). This implies a novel function of Ensa/Arpp19 in association with the cytoskeletal and cortical proteins, independent of Greatwall kinase. Although a few cytoskeletal proteins were identified in the proteomic screen with Ensa in metaphase and anaphase, these interactions were not significant as compared to the controls. Thus, further investigation is required to understand this function of Ensa/Arpp19 in maintaining the cell structure of mammalian cells at the G2/M transition. In summary, our siRNA results suggest some surprising differences between Greatwall and Ensa/Arpp19. However, off target effects of siRNA need to be taken into account, and more precise genetic tools such as chemical genetic inhibition of Greatwall and degron-tagged Ensa/Arpp19 will be required to come to firm conclusions.

7.3 Ensa/Arpp19 PP2A-B55 Complex Formation with PP2A-B55

Ensa/Arpp19-PP2A-B55 complex formation has been demonstrated in *Xenopus* extracts. The interaction is enriched in mitosis and is okadaic acid sensitive (Gharbi-Ayachi et al. 2010; Mochida et al. 2010). Cdk1 activates this pathway, inhibiting its counteracting phosphatase at the G2/M transition both via Greatwall activation and Ensa/Arpp19 phosphorylation independent of Greatwall (Blake-Hodek et al. 2012; Vigneron et al. 2011; Okumura et al. 2014). These interactions appeared to be okadaic acid sensitive, reducing the phosphatase activity towards Cdk substrates.

Although Greatwall was identified to be dephosphorylated by PP2A and later known to be a substrate of PP1 (Heim et al. 2015), Ensa/Arpp19 dephosphorylation remained unexplored. Two papers in 2014 proposed two different phosphatases executing Ensa/Arpp19 dephosphorylation. While Williams et al, (2014) proposed the ‘unfair competition model’ where PP2A itself dephosphorylates Ensa/Arpp19 while being inhibited by it (Williams et al. 2014) (Fig. 5.1A), our lab found FCP-1 to influence Ensa/Arpp19 dephosphorylation at mitotic exit (Hégarat, Vesely, Vinod, Ocasio, Peter, Gannon, Oliver, Novák & Hochegger 2014b). The ‘unfair competition’ model will only work when Greatwall is completely inactivated in response to okadaic acid. However, in the presence of Okadaic acid 50% of Ensa/Arpp19 inhibitory activity is retained,

suggesting residual Greatwall kinase activity. Thus, I attempted to test the 'unfair competition' model with a view to identify the unknown phosphatases contributing to Ensa/Arpp19 dephosphorylation at the metaphase-anaphase transition.

In agreement with the Goldberg model, Greatwall was dephosphorylated before Ensa/Arpp19 (Fig. 5.1C-D). Moreover Ensa/Arpp19-PP2A B55 interaction in the presence of okadaic acid causes the complex to fall apart in both *Hek293* and *HeLa* cells, as proposed by the Goldberg lab (Fig. 5.2B) (Williams et al. 2014). However, overexpression of Flag tagged Ensa and Arpp19 seemed to cause deregulated phosphorylation of the Greatwall site of these exogenous proteins. This appeared to occur both in intact 293T cells (Fig. 5.2A and C) but also during extract preparation for immunoprecipitation in *HeLa* cells (Fig. 5.3D). Thus, the balance of Greatwall, Ensa/Arpp19 and PP2A/B55 appears to be highly interdependent and sensitive to disturbance in the stoichiometric balance between these proteins. We finally resorted to recombinant thiophosphorylated Ensa and Arpp19 to examine its mitotic specific interactions. In this case, PP2A-B55 was significantly enriched in Flag Ensa/Arpp19 immunoprecipitates only in the presence of Greatwall phosphorylation.

Our analysis of Flag-Ensa and Arpp19 immunoprecipitates revealed the presence of a smaller protein around the same size of endogenous Ensa/Arpp19 that co-purifies with Flag-tagged proteins (Fig. 5.2A and Fig. 5.3C and D). The interaction of the 17-kDa protein was sensitive to okadaic acid, suggesting that it is a part of the inhibitor-phosphatase complex (Fig. 5.2B). Size exclusion chromatography confirmed that the presence of this peptide was not due to dimerization of the phosphatase complex, where each phosphatase monomer in the dimer, would interact with either an exogenous or an endogenous Ensa/Arpp19 (Fig. 5.4A). It is tempting to believe that Ensa/Arpp19 dimerises/polymerises with endogenous Ensa/Arpp19 in the complex with PP2A-B55. However, this interaction was not observed with recombinant Greatwall-thiophosphorylated Ensa/Arpp19 when incubated with cell lysates (Fig. 5.5B and D). This could be either due to the dimerization/polymerisation of the recombinant protein beforehand, thus occupying the sites of interaction with its endogenous counterparts. In addition, as the recombinant protein is only phosphorylated at the Greatwall site, this polymerisation of Ensa/Arpp19 can be dependent on other post-translational modifications (PTMs) such as Cdk1 or PKA phosphorylations. The cell lysates do not

appear to phosphorylate unphosphorylated Ensa/Arpp19 when incubated at physiological conditions, suggesting that the other post-translational modifications of these proteins are unlikely in lysates. Moreover, this small peptide could also be an N-terminal truncation of the Flag fusion proteins or one of the many isoforms of Ensa/Arpp19 that differ at their N-termini (Fig. 5.4E and F). This idea is based on the observation that the 17-kDa peptide is not identified by Flag or the antisera raised against the differing N-termini between Ensa and Arpp19. Only the commercial Pan Ensa/Arpp19 antibody that spans the C-termini identifies it (Fig. 5.4C and D). Therefore, careful analysis of interactions between these isoforms using different fusion tags such as Myc or HA is required to further address this question.

7.4 Identifying Novel Interactors of Ensa/Arpp19 at Metaphase-Anaphase Transition

As previously discussed, Hegarat et al. (2014) demonstrated that okadaic or tautomycetin phosphatase inhibition individually are not sufficient to supress Ensa/Arpp19 dephosphorylation during mitotic exit. A recent paper from the Mayer lab, demonstrated that Greatwall inhibition is a two-step process in *Xenopus* extracts - initiated by PP1 and majorly executed by PP2A (Heim et al. 2015). Moreover, FCP1 was also shown to be a major Greatwall phosphatase (Monica et al. 2015). These observations could reconcile the ‘unfair competition’ model with the Hegarat study, as complete inactivation of Greatwall can be achieved in a stepwise manner. Once Greatwall is dephosphorylated partially by PP1, the slow dephosphorylation of Ensa/Arpp19 can lead to its release and subsequent complete dephosphorylation of Greatwall by PP2A. However, a major finding in the Hegarat paper was that Ensa dephosphorylation could proceed even in the presence of high Greatwall activity. This finding directly contradicts the unfair completion model, where the slow dephosphorylation activity of PP2A/B55 will act on Ensa/Arp only when Greatwall is completely inactivated. This suggests the presence of an additional anaphase phosphatase that dephosphorylates Ensa/Arpp19 presumably when it is not bound to PP2A/B55.

I attempted to purify phosphatases acting on Greatwall thio-phosphorylated recombinant Ensa using mitotic and mitotic exit extracts from *HeLa-cdk1as* to specifically inhibit Cdk1 activity using 1NMPP1. PP2A-B55 was enriched with only thio-phosphorylated Ensa immunoprecipitates as observed in previous studies (Fig. 5.5B) (Gharbi-Ayachi et al. 2010; Mochida et al. 2010), while interaction was observed in both metaphase and anaphase due to the non-hydrolysable nature of the thio-phospho group (Fig. 5.5D).

A proteomic screen using these immunoprecipitates displayed significant enrichment in the PP2A subunits specifically in thio-phosphorylated Ensa samples (Fig. 5.6D and E). A few membrane and cytoskeletal proteins such as lamin B1 were enriched with unphosphorylated Ensa (Fig. 5.6A and D). Moreover, reanalysing the data obtained from the LC-MS using a relaxed False Discovery Rate (5%) might lead to the enrichment of interactors with low molar concentrations in cellular extracts. However, the bait itself was not significantly enriched as compared to the negative controls. The beads only control displayed large amount of non-specific bands in the Flag elutions on the silver stained gel. It is therefore possible that biologically significant interactions of thio-Ensa and Ensa are masked by the unspecific interactions of the negative control. Further optimisations of the purification protocol will be required to clarify this and detect further Ensa/Arpp19 interactors.

7.5 Protein Transfection of Thiophosphorylated Recombinant Proteins to Generate Dominant Active Effects

It has been long known that the Cdk-counteracting phosphatase is okadaic acid-sensitive. In *Xenopus*, PP2A-B55 was found to contribute to majority of Cdk substrate dephosphorylation at mitotic exit (Mochida et al. 2009; Vigneron et al. 2009; Castilho et al. 2009). Although okadaic acid promotes mitotic entry in mammalian cells (Gowdy et al. 1998), this phenotype is not reiterated by B55α depletion or the depletion of all four paralogues of PP2A-B55 (Schmitz et al. 2010; Cundell et al. 2013). These observations were made using the RNAi-mediated approach, which might result in incomplete inhibition of the phosphatase and hence their effects on global mitotic exit

are not visible. Therefore, whether PP2A-B55 is the okadaic acid sensitive phosphatase contributing towards mammalian mitosis is still an open question.

To begin addressing this hypothesis, I analysed the effects of B55 inhibition on mitotic entry in the absence of Cdk1 activity. Although okadaic acid triggered mitosis even in the absence of Cdk1 activity, B55αδ subunits did not appear to have a significant effect (Fig. 6.1A and B). Conversely, depletion of the catalytic subunits A/C caused a minor two-fold increase in mitotic cells. Additionally, a fraction of these cells also progressed into G1 despite the absence of Cdk1 activity. Thus, phosphatase inhibition promotes mitotic progression even in the absence of Cdk1 activity, but it remains unclear if this phosphatase constitutes PP2A-B55, the target of the Greatwall/Ensa pathway.

As complete depletion of the regulatory subunits of the phosphatase could not be achieved using RNAi-mediated approach similar to previous studies (Fig. 6.1C), I attempted to generate and transfect constitutively phosphorylated Ensa and Arpp19 to achieve more efficient and rapid inhibition of PP2A-B55 (Fig. 6.2). Recombinant Ensa was thio-phosphorylated *in-vitro* at the Greatwall phosphosites by recombinant truncated version of Greatwall (E2) (Ocasio et al. 2016) (Fig. 6.3D and Fig.6.5E and G). Bacterial purification of human Ensa using various expression vectors was attempted. Highly charged tags such as 6X-His failed to enter the cell (Fig. 6.3E) while bulkier tags such as GST interfered with the PP2A-B55 interaction of transfected Ensa (Fig. 6.4F) (also reported by Williams et al. (2014)). Finally, based on the successful interaction of Flag-tagged Ensa and Arpp19 with PP2A-B55 in the earlier experiments in this thesis, Flag-tagged Ensa and Arpp19 were purified using the GST vector after which the GST-tag was cleaved off using a prescission protease (Fig. 6.5A-G).

Various protein transfection techniques were applied to deliver this dominant active Ensa into live cells. Chemical methods of transfection were more successful than the physical methods for transfecting the protein in the cytosolic fraction. Physical methods such as Amaxa were completely unsuccessful (Fig. 6.8), and the Neon transfection displayed inconsistency in the amount of transfected protein in the cytosolic fraction in comparison to endogenous Ensa/Arpp19 (Fig. 6.9A-C). Additionally, the physical methods also appeared to take longer to recover from the impact of transfection and

undergo mitosis, and thus were not suitable to study a switch-like response such as mitotic entry (Fig. 6.9D).

Among the chemical methods Xfect, a lipid-based transfection reagent proved to be most successful in transfecting dominant active Flag-Ensa and Arpp19 (Fig. 6.6A and C). The amount of transfected protein almost twice the amount as endogenous Ensa/Arpp19. The transfected protein successfully interacted with PP2A-B55 and was significantly enriched in the Flag immunoprecipitates (Fig. 6.6B). Thus, Xfect transfection generated pool of dominant active Flag-Arpp19 *in-vivo*. However, this extensive amount of thio-phosphorylated Arpp19 failed to cause an increase in mitotic index. Examining the unbound fraction of PP2A-B55 after the Flag immunoprecipitation experiment suggested that the recombinant protein was not sufficient to inhibit all free phosphatase (Fig. 6.6D). The molar concentrations of the phosphatase in these cells are not known. However, it is highly unlikely that the cellular phosphatase concentrations are more than the amount of endogenous and transfected Ensa/Arpp19 put together. One possibility is that the excess amount of transfected protein is misfolded which renders it biologically inactive. Therefore, to enable saturation of the active inhibitor molecules *in-vivo*, PP2A-B55αδ subunits were depleted using siRNA oligos.

Combining Xfect transfection with siRNA depletion of B55αδ were analysed for mitotic cells using Ser10-phospho- Histone H3 staining in G2-arrested *HeLa-cdk1as* cells (Fig. 6.7). Though the mitotic index was increased slightly on B55αδ depletion as observed earlier, no additive effect was observed on transfecting dominant active Flag-Arpp19. One possibility for this observation is that PP2A-B55 is not the only Cdk-counteracting phosphatase functioning in mammalian mitotic entry. However, even control G2-arrested cells treated with the Xfect reagent did not initiate mitotic entry after washing off the Cdk-1 inhibitor as compared to the untransfected sample. This further complicated the interpretation of the results from the protein transection since the experimental manipulation itself appears to block mitotic entry.

Thus, both physical and chemical methods of protein transfection proved unsuccessful due to their indirect effects on cell viability and progression through cell cycle. Further optimisation of the protein transfection techniques is required to analyse the dominant

active effects of Ensa/Arpp19 in mammalian mitosis. Alternative approaches such as microinjection could be applied to transfect biologically active proteins and subsequent single cell analysis can be carried out.

CHAPTER8 FINAL CONCLUSION

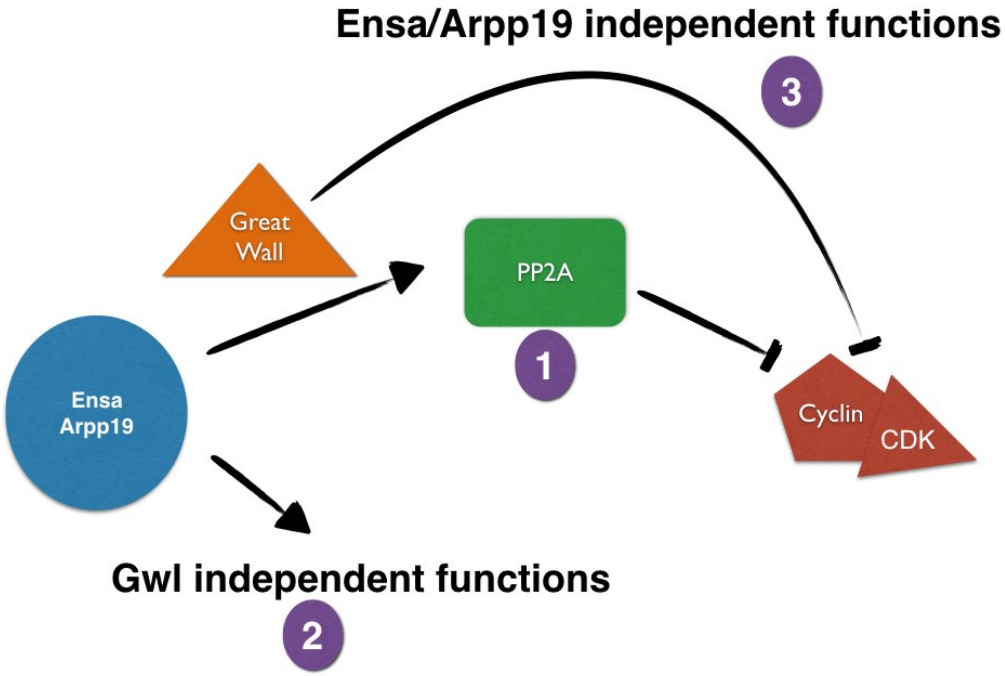

Figure 8: Schematic representation of future work proposed in this thesis

The model in figure 8.1 summarizes the findings in this thesis and the subsequent possibilities these might lead to.

1. In this work, we re-established the complex formation of Ensa/arpp19 with PP2A-B55 phosphatase in mammalian mitosis. However, the dynamics of this interaction need to be studied in greater detail. Interaction studies in this thesis indicated the potential dimerization of the small proteins Ensa/Arpp19 while binding the active site of the phosphatase. If such an interaction exists, it would be interesting to analyse if they form a homo- or hetero-dimer. This in turn could shed light on the individual functions of these proteins. Additionally, it might be worth addressing this question with bioinformatics tools to understand the structure of the active site of the phosphatase with the help of the available structure of B56 subunit (J. Wang et al. 2016). This would help in gauging the spatial arrangement of the amino acid residues in the active site of the

phosphatase and the hypothetical binding area available for the Ensa/Arpp19 dimer.

2. Ensa/Arpp19 might have functions at the cell cortex that are independent of Greatwall. As explained in Chapter 4, Ensa/Arpp19 depletion led to a blebbing phenotype, which was not observed, with Greatwall depletion. This suggests Greatwall -independent functions of these small proteins at the cell cortex. Ensa/Arpp19 resembles ECT2 overexpression phenotypes documented in (Niiya et al. 2006) where phosphorylation of Ect2 at the CDK1 phosphorylation site led to excessive blebbing at the cortex in dividing cells. As Rho is required for mitotic cortical retraction and rigidity during cell rounding (Maddox & Burridge 2003) and Ect2 phosphorylation influences its accumulation (Niiya et al. 2006), it is possible that Ensa/Arpp19 might contribute to the cortical actin rearrangements during mitotic entry via this pathway. Further interaction studies and phenotypic analysis is required to uncover these cortical functions of Ensa/Arpp19.

3. Similarly, Greatwall depletion leads to defective cytokinesis in 15% of the total cell population (Fig 4.1). This is not the case in Ensa/Arpp19-depleted cells. These observations point to an Ensa/Arpp19-independent function of the kinases in cytokinesis. This points to the presence of additional substrates of Greatwall that might contribute to the cytokinesis pathway. This can be investigated by a proteomic analysis using wild type and mutant Greatwall, to identify cytoskeletal proteins interacting with the kinase. Another striking observation from this thesis is that Greatwall depletion cause a significantly more dramatic phenotype in the Cdk1 inhibitor titration experiments when compared to Ensa/Arpp19 depletion. This indicates a potential function of Greatwall in the Cdk1 activation loop that is independent of Ensa/Arpp19 phosphorylation.

Overall, this work identifies the phenotypes of Ensa/Arpp19 and reinstates the dynamics of complex formation with PP2A-B55 phosphatase in mammalian mitosis. Further investigation will be required to understand the regulation of mitotic entry by fine-tuning the kinase-phosphatase equilibrium.

CHAPTER9 BIBLIOGRAPHY

Abal, M. et al., 2002. Microtubule release from the centrosome in migrating cells. *Journal of Cell Biology*, 159(5), pp.731–737.

Acquaviva, C. & Pines, J., 2006. The anaphase-promoting complex/cyclosome: APC/C. *Journal of Cell Science*, 119(Pt 12), pp.2401–2404.

Adhikari, D. et al., 2014. Mastl is required for timely activation of APC/C in meiosis I and Cdk1 reactivation in meiosis II. *The Journal of Cell Biology*, 206(7), pp.843–853.

Agius, L., 2008. Glucokinase and molecular aspects of liver glycogen metabolism. *The Biochemical journal*, 414(1), pp.1–18.

Agostinis, P. et al., 1992. Specificity of the polycation-stimulated (type-2A) and ATP,Mg-dependent (type-1) protein phosphatases toward substrates phosphorylated by P34cdc2 kinase. *European journal of biochemistry / FEBS*, 205(1), pp.241–248.

Alberts, B. et al., 2010. *Essential Cell Biology* 3rd ed., New York: Garland Science. Available at: http://ftp.dsma.dp.ua/211/ENG/Other/Alberts%20-%20Essential%20Cell%20Biology%203rd%20ed.pdf.

Alberts, B. et al., 2014. *Molecular Biology of the Cell* 6 ed., New York: Garland Science.

Allen, J.J. et al., 2007. A semisynthetic epitope for kinase substrates. *Nature Methods*, 4(6), pp.511–516.

Alonso, A. et al., 2004. Protein tyrosine phosphatases in the human genome. *Cell*, 117(6), pp.699–711.

Alvarez-Fernández, M. & Malumbres, M., 2014. Preparing a cell for nuclear envelope breakdown: Spatio-temporal control of phosphorylation during mitotic entry. *BioEssays : news and reviews in molecular, cellular and developmental biology*, 36(8), pp.757–765.

Alvarez-Fernández, M. et al., 2013. Greatwall is essential to prevent mitotic collapse after nuclear envelope breakdown in mammals. *Proceedings of the National Academy of Sciences*, 110(43), pp.17374–17379.

Andrews, P.D. et al., 2004. Aurora B regulates MCAK at the mitotic centromere. *Developmental Cell*, 6(2), pp.253–268.

Angrisani, A. et al., 2011. A new human dyskerin isoform with cytoplasmic localization. *Biochimica et Biophysica Acta (BBA) - General Subjects*, 1810(12), pp.1361–1368. Available at: http://www.diss.fu-berlin.de/diss/servlets/MCRFileNodeServlet/FUDISS_derivate_000000014186/Beata_Bekei_Dissertation_26Sept2013.pdf.

Archambault, J. et al., 1998. FCP1, the RAP74-interacting subunit of a human protein phosphatase that dephosphorylates the carboxyl-terminal domain of RNA polymerase IIO. *The Journal of biological chemistry*, 273(42), pp.27593–27601.

Archambault, V. et al., 2007. Mutations in drosophila Greatwall/Scant reveal its roles in mitosis and meiosis and interdependence with polo kinase. *PLoS Genetics*, 3(11), pp.2163–2179.

Ayad, N.G. et al., 2003. Tome-1, a trigger of mitotic entry, is degraded during G1 via the APC. *Cell*, 113(1), pp.101–113.

Baldin, V. & Ducommun, B., 1995. Subcellular localisation of human wee1 kinase is regulated during the cell cycle. *Journal of Cell Science*, 108 (Pt 6), pp.2425–2432.

Bantscheff, M. et al., 2007. Quantitative mass spectrometry in proteomics: a critical review. *Analytical and Bioanalytical Chemistry*, 389(4), pp.1017–1031.

Barnum, K.J. & O'Connell, M.J., 2014. Cell Cycle Regulation by Checkpoints. In *Cell Cycle Control*. Methods in Molecular Biology. New York, NY: Springer New York, pp. 29–40.

Barr, F.A., Elliott, P.R. & Gruneberg, U., 2011. Protein phosphatases and the regulation of mitosis. *Journal of Cell Science*, 124(Pt 14), pp.2323–2334.

Bartholomew, C.R. et al., 2001. Cdc5 interacts with the Wee1 kinase in budding yeast. *Molecular and Cellular Biology*, 21(15), pp.4949–4959.

Bassermann, F. et al., 2008. The Cdc14B-Cdh1-Plk1 axis controls the G2 DNA-damage-response checkpoint. *Cell*, 134(2), pp.256–267.

Bekei, B., 2013. *In-cell NMR Spectroscopy in Mammalian*

Cells. Budapest,Hungary. Available at: http://www.diss.fu-berlin.de/diss/servlets/MCRFileNodeServlet/FUDISS_derivate_000000014186/Beata_Bekei_Dissertation_26Sept2013.pdf.

Bettencourt-Dias, M. et al., 2004. Genome-wide survey of protein kinases required for cell cycle progression. *Nature*, 432(7020), pp.980–987.

Biondi, R.M. et al., 2000. Identification of a pocket in the PDK1 kinase domain that interacts with PIF and the C-terminal residues of PKA. *The EMBO Journal*, 19(5), pp.979–988.

Blagden, S.P. & Glover, D.M., 2003. Polar expeditions--provisioning the centrosome for mitosis. *Nature Publishing Group*, 5(6), pp.505–511.

Blake-Hodek, K.A. et al., 2012. Determinants for activation of the atypical AGC kinase Greatwall during M phase entry. *Molecular and Cellular Biology*, 32(8), pp.1337–1353.

Blomberg, I. & Hoffmann, I., 1999. Ectopic Expression of Cdc25A Accelerates the G1/S Transition and Leads to Premature Activation of Cyclin E- and Cyclin A-

Dependent Kinases. *Molecular and Cellular Biology*, 19(9), pp.6183–6194.

Boettcher, J.M. et al., 2008. Membrane-Induced Folding of the cAMP-Regulated Phosphoprotein Endosulfine-α†. *Biochemistry*, 47(47), pp.12357–12364.

Boldogh, I.R., Yang, H.C. & Pon, L.A., 2001. Mitochondrial inheritance in budding yeast. *Traffic*, 2(6), pp.368–374.

Bollen, M. et al., 2010. The extended PP1 toolkit: designed to create specificity. *Trends in Biochemical Sciences*, 35(8), pp.450–458.

Bollen, M., Gerlich, D.W. & Lesage, B., 2009. Mitotic phosphatases: from entry guards to exit guides. *Trends in Cell Biology*, 19(10), pp.531–541.

Bolognese, F. et al., 1999. The cyclin B2 promoter depends on NF-Y, a trimer whose CCAAT-binding activity is cell-cycle regulated. *Oncogene*, 18(10), pp.1845–1853.

Bontron, S. et al., 2013. Yeast Endosulfines Control Entry into Quiescence and Chronological Life Span by Inhibiting Protein Phosphatase 2A. *Cell reports*.

Booher, R.N., Holman, P.S. & Fattaey, A., 1997. Human Myt1 is a cell cycle-regulated kinase that inhibits Cdc2 but not Cdk2 activity. *The Journal of biological chemistry*, 272(35), pp.22300–22306.

Boutros, R., Dozier, C. & Ducommun, B., 2006. The when and wheres of CDC25 phosphatases. *Current Opinion in Cell Biology*, 18(2), pp.185–191.

Brown, Nicholas R et al., 2015. CDK1 structures reveal conserved and unique features of the essential cell cycle CDK. *Nature Communications*, 6, p.6769.

Brown, Nick R et al., 1999. The structural basis for specificity of substrate and recruitment peptides for cyclin-dependent kinases. *Nature Publishing Group*, 1(7), pp.438–443.

Brust-Mascher, I. et al., 2004. Model for anaphase B: role of three mitotic motors in a switch from poleward flux to spindle elongation. *Proceedings of the National Academy of Sciences of the United States of America*, 101(45), pp.15938–15943.

Bulavin, D.V. et al., 2001. Initiation of a G2/M checkpoint after ultraviolet radiation requires p38 kinase. *Nature*, 411(6833), pp.102–107.

Burgess, A. et al., 2010. Loss of human Greatwall results in G2 arrest and multiple mitotic defects due to deregulation of the cyclin B-Cdc2/PP2A balance. *Proceedings of the National Academy of Sciences*, 107(28), pp.12564–12569.

Busino, L. et al., 2003. Degradation of Cdc25A by beta-TrCP during S phase and in response to DNA damage. *Nature*, 426(6962), pp.87–91.

Cancer Research UK, 2014. Worldwide cancer statistics. *cancerresearchuk.org*. Available at: http://www.cancerresearchuk.org/health-professional/cancer-statistics/worldwide-cancer/mortality#heading-Zero [Accessed August 23, 2016].

Castilho, P.V. et al., 2009. The M phase kinase Greatwall (Gwl) promotes inactivation of PP2A/B55delta, a phosphatase directed against CDK phosphosites. *Molecular biology of the cell*, 20(22), pp.4777–4789.

Castro, A. et al., 2005. The anaphase-promoting complex: a key factor in the regulation of cell cycle. *Oncogene*, 24(3), pp.314–325.

Cazales, M. et al., 2005. CDC25B phosphorylation by Aurora-A occurs at the G2/M transition and is inhibited by DNA damage. *Cell cycle (Georgetown, Tex)*, 4(9), pp.1233–1238.

Chambers, R.S. & Dahmus, M.E., 1994. Purification and characterization of a phosphatase from HeLa cells which dephosphorylates the C-terminal domain of RNA polymerase II. *The Journal of biological chemistry*, 269(42), pp.26243–26248.

Chambers, R.S. & Kane, C.M., 1996. Purification and Characterization of an RNA Polymerase II Phosphatase from Yeast. *The Journal of biological chemistry*, 271(40), pp.24498–24504.

Chan, T.A. et al., 2000. Cooperative effects of genes controlling the G(2)/M checkpoint. *Genes & development*, 14(13), pp.1584–1588.

Chapman, D.L. & Wolgemuth, D.J., 1992. Identification of a mouse B-type cyclin which exhibits developmentally regulated expression in the germ line. *Molecular reproduction and development*, 33(3), pp.259–269.

Charrier-Savournin, F.B. et al., 2004. p21-Mediated Nuclear Retention of Cyclin B1-Cdk1 in Response to Genotoxic Stress. *Molecular biology of the cell*, 15(9), pp.3965–3976.

Cheeseman, I.M. & Desai, A., 2008. Molecular architecture of the kinetochore-microtubule interface. *Nature Reviews Molecular Cell Biology*, 9(1), pp.33–46.

Cheeseman, I.M. et al., 2002. Phospho-Regulation of Kinetochore-Microtubule Attachments by the Aurora Kinase Ipl1p. *Cell*, 111(2), pp.163–172.

Cheeseman, I.M. et al., 2006. The conserved KMN network constitutes the core microtubule-binding site of the kinetochore. *Cell*, 127(5), pp.983–997.

Chen, J., 1996. Cyclin-binding motifs are essential for the function of p21(CIP1). *Molecular and Cellular Biology*, 16(9), pp.4673–4682.

Chen, M.-S., Ryan, C.E. & Piwnica-Worms, H., 2003. Chk1 kinase negatively regulates mitotic function of Cdc25A phosphatase through 14-3-3 binding. *Molecular and Cellular Biology*, 23(21), pp.7488–7497.

Chen, M.S. et al., 2001. Absence of apparent phenotype in mice lacking Cdc25C protein phosphatase. *Molecular and Cellular Biology*, 21(12), pp.3853–3861.

Chen, R.-H. et al., 1999. The Spindle Checkpoint of Budding Yeast Depends on a Tight Complex between the Mad1 and Mad2 Proteins. *Molecular biology of the cell*,

10(8), pp.2607–2618.

Chevrier, V. et al., 2002. The Rho-associated protein kinase p160ROCK is required for centrosome positioning. *The Journal of Cell Biology*, 157(5), pp.807–817.

Chica, N. et al., 2016. Nutritional Control of Cell Size by the Greatwall-Endosulfine-PP2A·B55 Pathway. *Current Biology*, 26(3), pp.319–330.

Cho, E.J. et al., 2001. Opposing effects of Ctk1 kinase and FCP1 phosphatase at Ser 2 of the RNA polymerase II C-terminal domain. *Genes & development*, 15(24), pp.3319–3329.

Cho, H.P. et al., 2005. The dual-specificity phosphatase CDC14B bundles and stabilizes microtubules. *Molecular and Cellular Biology*, 25(11), pp.4541–4551.

Chow, J.P.H. & Poon, R.Y.C., 2013. The CDK1 inhibitory kinase MYT1 in DNA damage checkpoint recovery. *Oncogene*, 32(40), pp.4778–4788.

Cimini, D., 2007. Detection and correction of merotelic kinetochore orientation by Aurora B and its partners. *Cell cycle (Georgetown, Tex)*, 6(13), pp.1558–1564.

Clemente-Blanco, A. et al., 2009. Cdc14 inhibits transcription by RNA polymerase I during anaphase. *Nature*, 458(7235), pp.219–222.

Conklin, D.S., Galaktionov, K. & Beach, D., 1995. 14-3-3-Proteins Associate with Cdc25-Phosphatases. *Proceedings of the National Academy of Sciences of the United States of America*, 92(17), pp.7892–7896.

Crenshaw, D.G. et al., 1998. The mitotic peptidyl-prolyl isomerase, Pin1, interacts with Cdc25 and Plx1. *The EMBO Journal*, 17(5), pp.1315–1327.

Cueille, N. et al., 2001. Flp1, a fission yeast orthologue of the S-cerevisiae CDC14 gene, is not required for cyclin degradation or rum1p stabilisation at the end of mitosis. *J Cell Sci*, 114(14), pp.2649–2664.

Cundell, M.J. et al., 2013. The BEG (PP2A-B55/ENSA/Greatwall) pathway ensures cytokinesis follows chromosome separation. *Molecular Cell*, 52(3), pp.393–405.

Cyert, M.S. & Kirschner, M.W., 1988. Regulation of MPF activity in vitro. *Cell*, 53(2), pp.185–195.

D'Amours, D. & Amon, A., 2004. At the interface between signaling and executing anaphase--Cdc14 and the FEAR network. *Genes & development*, 18(21), pp.2581–2595.

Dalal, S.N. et al., 1999. Cytoplasmic localization of human cdc25C during interphase requires an intact 14-3-3 binding site. *Molecular and Cellular Biology*, 19(6), pp.4465–4479.

De Antoni, A. et al., 2005. The Mad1/Mad2 Complex as a Template for Mad2 Activation in the Spindle Assembly Checkpoint. *Current Biology*, 15(3), pp.214–225.

De Bondt, H.L. et al., 1993. Crystal structure of cyclin-dependent kinase 2. *Nature*, 363(6430), pp.595–602.

De Virgilio, C., 2012. The essence of yeast quiescence. *FEMS microbiology reviews*, 36(2), pp.306–339.

De Wulf, P., Montani, F. & Visintin, R., 2009. Protein phosphatases take the mitotic stage. *Current Opinion in Cell Biology*, 21(6), pp.806–815.

DeLange, R.J. et al., 1968. Activation of Skeletal Muscle Phosphorylase Kinase by Adenosine Triphosphate and Adenosine 3“,5-”Monophosphate. *The Journal of biological chemistry*, 243(9), pp.2200–2208.

Deluca, J.G. et al., 2006. Kinetochore microtubule dynamics and attachment stability are regulated by Hec1. *Cell*, 127(5), pp.969–982.

Dephoure, N. et al., 2008. A quantitative atlas of mitotic phosphorylation. *Proceedings of the National Academy of Sciences*, 105(31), pp.10762–10767.

Depreux, F.F. et al., 2015. Disruption of the lamin A and matrin-3 interaction by myopathic LMNA mutations. *Human molecular genetics*, 24(15), pp.4284–4295.

Dohadwala, M. et al., 1994. Phosphorylation and inactivation of protein phosphatase 1 by cyclin-dependent kinases. *Proceedings of the National Academy of Sciences of the United States of America*, 91(14), pp.6408–6412.

Domingo-Sananes, M.R. et al., 2011. Switches and latches: a biochemical tug-of-war between the kinases and phosphatases that control mitosis. *Philosophical Transactions of the Royal Society B: Biological Sciences*, 366(1584), pp.3584–3594.

Dorée, M. & Hunt, T., 2002. From Cdc2 to Cdk1: when did the cell cycle kinase join its cyclin partner? *Journal of Cell Science*, 115(12), pp.2461–2464.

Draetta, G., 1993. Cdc2 activation: the interplay of cyclin binding and Thr161 phosphorylation. *Trends in Cell Biology*, 3(9), pp.287–289.

Draetta, G. & Eckstein, J., 1997. Cdc25 protein phosphatases in cell proliferation. *Biochimica et biophysica acta*, 1332(2), pp.M53–63.

Draetta, G. et al., 1989. Cdc2 protein kinase is complexed with both cyclin A and B: evidence for proteolytic inactivation of MPF. *Cell*, 56(5), pp.829–838.

Dryden, S.C. et al., 2003. Role for human SIRT2 NAD-dependent deacetylase activity in control of mitotic exit in the cell cycle. *Molecular and Cellular Biology*, 23(9), pp.3173–3185.

Dulubova, I. et al., 2001. ARPP-16/ARPP-19: a highly conserved family of cAMP-regulated phosphoproteins. *Journal of neurochemistry*, 77(1), pp.229–238. Available at: http://onlinelibrary.wiley.com/doi/10.1046/j.1471-4159.2001.00191.x/abstract;jsessionid=471C54322A076079E9FD477F67E74120.f03t02.

Dunphy, W.G. & Kumagai, A., 1991. The cdc25 protein contains an intrinsic phosphatase activity. *Cell*, 67(1), pp.189–196.

Dupré, A. et al., 2013. The phosphorylation of ARPP19 by Greatwall renders the auto-amplification of MPF independently of PKA in Xenopus oocytes. *Journal of Cell Science*, 126(Pt 17), pp.3916–3926.

Dutertre, S. et al., 2004. Phosphorylation of CDC25B by Aurora-A at the centrosome contributes to the G2-M transition. *Journal of Cell Science*, 117(12), pp.2523–2531.

Elia, A.E.H. et al., 2003. The molecular basis for phosphodependent substrate targeting and regulation of Plks by the Polo-box domain. *Cell*, 115(1), pp.83–95.

Elzen, Den, N. & Pines, J., 2001. Cyclin a Is Destroyed in Prometaphase and Can Delay Chromosome Alignment and Anaphase. *The Journal of Cell Biology*, 153(1), pp.121–136.

Endicott, J.A. & Noble, M.E.M., 2013. Structural characterization of the cyclin-dependent protein kinase family. *Biochemical Society Transactions*, 41(4), pp.1008–1016.

Erlandsson, F. et al., 2000. A detailed analysis of cyclin A accumulation at the G(1)/S border in normal and transformed cells. *Experimental cell research*, 259(1), pp.86–95.

Etemad, B. & Kops, G.J., 2016. Attachment issues: kinetochore transformations and spindle checkpoint silencing. *Current Opinion in Cell Biology*, 39, pp.101–108.

Evans, T. et al., 1983. Cyclin - a Protein Specified by Maternal Messenger-Rna in Sea-Urchin Eggs That Is Destroyed at Each Cleavage Division. *Cell*, 33(2), pp.389–396.

Fattaey, A. & Booher, R.N., 1997. Myt1: a Wee1-type kinase that phosphorylates Cdc2 on residue Thr14. *Progress in cell cycle research*, 3, pp.233–240.

Fava, L.L. et al., 2011. Probing the in vivo function of Mad1:C‐Mad2 in the spindle assembly checkpoint. *The EMBO Journal*, 30(16), pp.3322–3336.

Favre, B., Turowski, P. & Hemmings, B.A., 1997. Differential inhibition and posttranslational modification of protein phosphatase 1 and 2A in MCF7 cells treated with calyculin-A, okadaic acid, and tautomycin. *The Journal of biological chemistry*, 272(21), pp.13856–13863.

Ferguson, A.M. et al., 2005. Normal cell cycle and checkpoint responses in mice and cells lacking Cdc25B and Cdc25C protein phosphatases. *Molecular and Cellular Biology*, 25(7), pp.2853–2860.

Ferrigno, P., Langan, T.A. & Cohen, P., 1993. Protein phosphatase 2A1 is the major enzyme in vertebrate cell extracts that dephosphorylates several physiological substrates for cyclin-dependent protein kinases. *Molecular biology of the cell*, 4(7), pp.669–677. Available at: https://www.ncbi.nlm.nih.gov/pmc/articles/PMC300977/?page=1.

Félix, M.A., Cohen, P. & Karsenti, E., 1990. Cdc2 H1 kinase is negatively regulated by a type 2A phosphatase in the Xenopus early embryonic cell cycle: evidence from the effects of okadaic acid. *The EMBO Journal*, 9(3), pp.675–683.

Fisher, R.P. & Morgan, D.O., 1994. A novel cyclin associates with MO15/CDK7 to form the CDK-activating kinase. *Cell*, 78(4), pp.713–724.

Flemming, W., 1882. Zellsubstanz, Kern und Zelltheilung. pp.1–482.

Flint, A.J. et al., 1997. Development of "substrate-trapping" mutants to identify physiological substrates of protein tyrosine phosphatases. *Proceedings of the National Academy of Sciences of the United States of America*, 94(5), pp.1680–1685.

Frank-Vaillant, M. et al., 1999. Two Distinct Mechanisms Control the Accumulation of Cyclin B1 and Mos in Xenopus Oocytes in Response to Progesterone. *Molecular biology of the cell*, 10(10), pp.3279–3288.

Fung, T.K. & Poon, R.Y.C., 2005. A roller coaster ride with the mitotic cyclins. *Seminars in cell & developmental biology*, 16(3), pp.335–342.

Fung, T.K., Ma, H.T. & Poon, R.Y.C., 2007. Specialized roles of the two mitotic cyclins in somatic cells: cyclin A as an activator of M phase-promoting factor. *Molecular biology of the cell*, 18(5), pp.1861–1873.

Gabrielli, B.G. et al., 1996. Cytoplasmic accumulation of cdc25B phosphatase in mitosis triggers centrosomal microtubule nucleation in HeLa cells. *Journal of Cell Science*, 109 (Pt 5), pp.1081–1093.

Galaktionov, K. & Beach, D., 1991. Specific activation of cdc25 tyrosine phosphatases by B-type cyclins: evidence for multiple roles of mitotic cyclins. *Cell*, 67(6), pp.1181–1194.

Gallant, P. & Nigg, E.A., 1992. Cyclin B2 undergoes cell cycle-dependent nuclear translocation and, when expressed as a non-destructible mutant, causes mitotic arrest in HeLa cells. *The Journal of Cell Biology*, 117(1), pp.213–224.

Garcia, B.A. et al., 2005. Modifications of human histone H3 variants during mitosis. *Biochemistry*, 44(39), pp.13202–13213.

Gassmann, R. et al., 2010. Removal of Spindly from microtubule-attached kinetochores controls spindle checkpoint silencing in human cells. *Genes & development*, 24(9), pp.957–971.

Gautier, J. et al., 1991. cdc25 is a specific tyrosine phosphatase that directly activates p34cdc2. *Cell*, 67(1), pp.197–211.

Gautier, J. et al., 1990. Cyclin Is a Component of Maturation-Promoting Factor From Xenopus. *Cell*, 60(3), pp.487–494.

Gautier, J. et al., 1988. Purified Maturation-Promoting Factor Contains the Product of a Xenopus Homolog of the Fission Yeast-Cell Cycle Control Gene Cdc2. *Cell*, 54(3),

pp.433–439.

Gavet, O. & Pines, J., 2010. Progressive Activation of CyclinB1-Cdk1 Coordinates Entry to Mitosis. *Developmental Cell*, 18(4), pp.533–543.

Geley, S. et al., 2001. Anaphase-promoting complex/cyclosome-dependent proteolysis of human cyclin A starts at the beginning of mitosis and is not subject to the spindle assembly checkpoint. *The Journal of Cell Biology*, 153(1), pp.137–148.

Gharbi-Ayachi, A. et al., 2010. The substrate of Greatwall kinase, Arpp19, controls mitosis by inhibiting protein phosphatase 2A. *Science (New York, NY)*, 330(6011), pp.1673–1677.

Girard, F. et al., 1991. Cyclin A is required for the onset of DNA replication in mammalian fibroblasts. *Cell*, 67(6), pp.1169–1179.

Girault, J.A. et al., 1990. Differential expression of ARPP-16 and ARPP-19, two highly related cAMP-regulated phosphoproteins, one of which is specifically associated with dopamine-innervated brain regions. *The Journal of Neuroscience*, 10(4), pp.1124–1133.

Glover, D.M., 2012. The overlooked greatwall: a new perspective on mitotic control. *Open Biology*, 2(3), pp.120023–120023.

Gong, D. & Ferrell, J.E., 2010. The roles of cyclin A2, B1, and B2 in early and late mitotic events. *Molecular biology of the cell*, 21(18), pp.3149–3161.

Gong, D. et al., 2007. Cyclin A2 regulates nuclear-envelope breakdown and the nuclear accumulation of cyclin B1. *Current biology : CB*, 17(1), pp.85–91.

Goris, J. et al., 1989. Okadaic acid, a specific protein phosphatase inhibitor, induces maturation and MPF formation in Xenopus laevis oocytes. *FEBS letters*, 245(1-2), pp.91–94.

Gowdy, P.M., Anderson, H.J. & Roberge, M., 1998. Entry into mitosis without Cdc2 kinase activation. *Journal of Cell Science*, 111 (Pt 22), pp.3401–3410.

Grallert, A. et al., 2015. A PP1-PP2A phosphatase relay controls mitotic progression. *Nature*, 517(7532), pp.94–98.

Gray, J.V. et al., 2004. “Sleeping beauty”: quiescence in Saccharomyces cerevisiae. *Microbiology and Molecular Biology Reviews*, 68(2), pp.187–206.

Gu, Y., Rosenblatt, J. & Morgan, D.O., 1992. Cell cycle regulation of CDK2 activity by phosphorylation of Thr160 and Tyr15. *The EMBO Journal*, 11(11), pp.3995–4005.

Hagan, I.M., 2008. The spindle pole body plays a key role in controlling mitotic commitment in the fission yeast Schizosaccharomyces pombe. *Biochemical Society Transactions*, 36(Pt 5), pp.1097–1101.

Hagting, A. et al., 2002. Human securin proteolysis is controlled by the spindle checkpoint and reveals when the APC/C switches from activation by Cdc20 to

Cdh1. *The Journal of Cell Biology*, 157(7), pp.1125–1137.

Hagting, A. et al., 1999. Translocation of cyclin B1 to the nucleus at prophase requires a phosphorylation-dependent nuclear import signal. *Current biology : CB*, 9(13), pp.680–689.

Hanks, S.K. & Hunter, T., 1995. The Eukaryotic protein kinase superfamily: kinase catalytic domain structure and classification. *FASEB*, 9, p.578.

Hanks, S.K. & Quinn, A.M., 1991. [2] Protein kinase catalytic domain sequence database: Identification of conserved features of primary structure and classification of family members. In *Protein Phosphorylation Part A: Protein Kinases: Assays, Purification, Antibodies, Functional Analysis, Cloning, and Expression*. Methods in Enzymology. Elsevier, pp. 38–62.

Hansen, D.V. et al., 2004. Plk1 regulates activation of the anaphase promoting complex by phosphorylating and triggering SCFbetaTrCP-dependent destruction of the APC Inhibitor Emi1. *Molecular biology of the cell*, 15(12), pp.5623–5634.

Hara, K., Tydeman, P. & Kirschner, M., 1980. A cytoplasmic clock with the same period as the division cycle in Xenopus eggs. *Proceedings of the National Academy of Sciences of the United States of America*, 77(1), pp.462–466.

Hara, M. et al., 2012. Greatwall kinase and cyclin B-Cdk1 are both critical constituents of M-phase-promoting factor. *Nature Communications*, 3, p.1059.

Harper, J.W., Burton, J.L. & Solomon, M.J., 2002. The anaphase-promoting complex: it's not just for mitosis any more. *Genes & development*, 16(17), pp.2179–2206.

Hartwell, L.H., 1978. Cell division from a genetic perspective. *The Journal of Cell Biology*, 77(3), pp.627–637.

Hartwell, L.H. et al., 1974. Genetic controlof the cell division cycle in yeast. *Science (Wash DC)*.

Hatano, Y. et al., 2016. Positive feedback promotes mitotic exit via the APC/C-Cdh1-separase-Cdc14 axis in budding yeast. *Cellular signalling*, 28(10), pp.1545–1554.

Hauf, S., Waizenegger, I.C. & Peters, J.M., 2001. Cohesin cleavage by separase required for anaphase and cytokinesis in human cells. *Science (New York, NY)*, 293(5533), pp.1320–1323.

Heim, A., Konietzny, A. & Mayer, T.U., 2015. Protein phosphatase 1 is essential for Greatwall inactivation at mitotic exit. *EMBO reports*, 16(11), pp.e201540876–1510.

Henglein, B. et al., 1994. Structure and cell cycle-regulated transcription of the human cyclin A gene. *Proceedings of the National Academy of Sciences of the United States of America*, 91(12), pp.5490–5494.

Hermeking, H. et al., 1997. 14-3-3 sigma is a p53-regulated inhibitor of G2/M progression. *Molecular Cell*, 1(1), pp.3–11.

Heron, L. et al., 1998. Human alpha-endosulfine, a possible regulator of sulfonylurea-sensitive K-ATP channel: Molecular cloning, expression and biological properties. *Proceedings of the National Academy of Sciences of the United States of America*, 95(14), pp.8387–8391.

Hershko, A. & Ciechanover, A., 1998. The ubiquitin system. *Annual review of biochemistry*, 67(1), pp.425–479.

Hégarat, N. et al., 2011. Aurora A and Aurora B jointly coordinate chromosome segregation and anaphase microtubule dynamics. *The Journal of Cell Biology*, 195(7), pp.1103–1113.

Hégarat, N., Rata, S. & Hochegger, H., 2016. Bistability of mitotic entry and exit switches during open mitosis in mammalian cells. *BioEssays : news and reviews in molecular, cellular and developmental biology*, 38(7), pp.627–643.

Hégarat, N., Vesely, C., Vinod, P.K., Ocasio, C., Peter, N., Gannon, J., Oliver, A.W., Novák, B. & Hochegger, H., 2014a. PP2A/B55 and FCP1 Regulate Greatwall and Ensa Dephosphorylation during Mitotic Exit G. P. Copenhaver, ed. *PLoS Genetics*, 10(1), p.e1004004.

Hégarat, N., Vesely, C., Vinod, P.K., Ocasio, C., Peter, N., Gannon, J., Oliver, A.W., Novák, B. & Hochegger, H., 2014b. PP2A/B55 and FCP1 Regulate Greatwall and Ensa Dephosphorylation during Mitotic Exit G. P. Copenhaver, ed. *PLoS Genetics*, 10(1), p.e1004004.

Hochegger, H. et al., 2007. An essential role for Cdk1 in S phase control is revealed via chemical genetics in vertebrate cells. *The Journal of Cell Biology*, 178(2), pp.257–268.

Hochegger, H., Takeda, S. & Hunt, T., 2008. Cyclin-dependent kinases and cell-cycle transitions: does one fit all? *Nature Reviews Molecular Cell Biology*, 9(11), pp.910–916.

Hoffmann, I. et al., 1993. Phosphorylation and activation of human cdc25-C by cdc2--cyclin B and its involvement in the self-amplification of MPF at mitosis. *The EMBO Journal*, 12(1), pp.53–63.

Hoffmann, I., Draetta, G. & Karsenti, E., 1994. Activation of the phosphatase activity of human cdc25A by a cdk2-cyclin E dependent phosphorylation at the G1/S transition. *The EMBO Journal*, 13(18), pp.4302–4310.

Howard, A. & Pelc, S.R., 1953. Synthesis of Desoxyribonucleic Acid in Normal and Irradiated Cells and Its Relation to Chromosome Breakage. *Heredity Suppl.*, 6, pp.216–273. Available at: https://inis.iaea.org/search/search.aspx?orig_q=RN:17031504.

Howell, B.J. et al., 2001. Cytoplasmic dynein/dynactin drives kinetochore protein transport to the spindle poles and has a role in mitotic spindle checkpoint inactivation. *The Journal of Cell Biology*, 155(7), pp.1159–1172.

Hoyt, M.A., Totis, L. & Roberts, B.T., 2016. S. cerevisiae genes required for cell cycle

arrest in response to loss of microtubule function. *Cell*, 66(3), pp.507–517.

Huet, X. et al., 1996. Cyclin A expression is under negative transcriptional control during the cell cycle. *Molecular and Cellular Biology*, 16(7), pp.3789–3798.

Hutterer, A. et al., 2006. Mitotic activation of the kinase Aurora-A requires its binding partner Bora. *Developmental Cell*, 11(2), pp.147–157.

Hwang, L.H. et al., 1998. Budding yeast Cdc20: a target of the spindle checkpoint. *Science (New York, NY)*, 279(5353), pp.1041–1044. Available at: http://www.jstor.org.ezproxy.sussex.ac.uk/stable/2894630?seq=1#page_scan_tab_contents.

Ivar Walaas, S., Aswad, D.W. & Greengard, P., 1983. A dopamine- and cyclic AMP-regulated phosphoprotein enriched in dopamine-innervated brain regions. *Nature*, 301(5895), pp.69–71. Available at: http://www.nature.com/nature/journal/v301/n5895/abs/301069a0.html.

Izumi, T. & Maller, J.L., 1993. Elimination of cdc2 phosphorylation sites in the cdc25 phosphatase blocks initiation of M-phase. *Molecular biology of the cell*, 4(12), pp.1337–1350.

Jackman, M. et al., 2003. Active cyclin B1-Cdk1 first appears on centrosomes in prophase. *Nature Publishing Group*, 5(2), pp.143–148.

Jeffrey, P.D. et al., 1995. Mechanism of CDK activation revealed by the structure of a cyclinA-CDK2 complex. *Nature*.

Jeffrey, P.D., Tong, L. & Pavletich, N.P., 2000. Structural basis of inhibition of CDK-cyclin complexes by INK4 inhibitors. *Genes & development*, 14(24), pp.3115–3125.

Jiang, Z.-X. & Zhang, Z.-Y., 2008. Targeting PTPs with small molecule inhibitors in cancer treatment. *Cancer and Metastasis Reviews*, 27(2), pp.263–272.

Jinno, S. et al., 1994. Cdc25A is a novel phosphatase functioning early in the cell cycle. *The EMBO Journal*, 13(7), pp.1549–1556.

Joaquin, M. & Watson, R.J., 2003. Cell cycle regulation by the B-Myb transcription factor. *CMLS Cellular and Molecular Life Sciences*, 60(11), pp.2389–2401.

Johnson, H.J. et al., 2009. In vivo inactivation of MASTL kinase results in thrombocytopenia. *Experimental hematology*, 37(8), pp.901–908.

Johnson, L.N. et al., 1998. The structural basis for substrate recognition and control by protein kinases. *FEBS letters*, 430(1-2), pp.1–11.

Juanes, M.A. et al., 2013. Budding Yeast Greatwall and Endosulfines Control Activity and Spatial Regulation of PP2A(Cdc55) for Timely Mitotic Progression F. Uhlmann, ed. *PLoS Genetics*, 9(7).

Kaiser, B.K. et al., 2002. Disruption of centrosome structure, chromosome segregation,

and cytokinesis by misexpression of human Cdc14A phosphatase. *Molecular biology of the cell*, 13(7), pp.2289–2300.

Kaldis, P., 1999. The cdk-activating kinase (CAK): from yeast to mammals. *CMLS Cellular and Molecular Life Sciences*, 55(2), pp.284–296.

Kaldis, P. et al., 1998. Localization and regulation of the cdk-activating kinase (Cak1p) from budding yeast. *Journal of Cell Science*, 111 (Pt 24), pp.3585–3596.

Katula, K.S. et al., 1997. Cyclin-dependent kinase activation and S-phase induction of the cyclin B1 gene are linked through the CCAAT elements. *Cell growth & differentiation : the molecular biology journal of the American Association for Cancer Research*, 8(7), pp.811–820.

Kelly, A.E. & Funabiki, H., 2009. Correcting aberrant kinetochore microtubule attachments: an Aurora B-centric view. *Current Opinion in Cell Biology*, 21(1), pp.51–58.

Khadaroo, B. et al., 2004. The first green lineage cdc25 dual-specificity phosphatase. *Cell cycle (Georgetown, Tex)*, 3(4), pp.513–518.

Kim, S. et al., 2014. Highly efficient RNA-guided genome editing in human cells via delivery of purified Cas9 ribonucleoproteins. *Genome Research*, 24(6), pp.1012–1019.

Kim, S.H. et al., 1998. Fission yeast Slp1: an effector of the Mad2-dependent spindle checkpoint. *Science (New York, NY)*, 279(5353), pp.1045–1047.

Knighton, D.R., Zheng, J.H., Teneyck, L.F., Ashford, V.A., et al., 1991. Crystal-Structure of the Catalytic Subunit of Cyclic Adenosine-Monophosphate Dependent Protein-Kinase. *Science (New York, NY)*, 253(5018), pp.407–414.

Knighton, D.R., Zheng, J.H., Teneyck, L.F., Xuong, N.H., et al., 1991. Structure of a Peptide Inhibitor Bound to the Catalytic Subunit of Cyclic Adenosine-Monophosphate Dependent Protein-Kinase. *Science (New York, NY)*, 253(5018), pp.414–420.

Knudsen, K.E. et al., 1999. Cyclin A Is a Functional Target of Retinoblastoma Tumor Suppressor Protein-mediated Cell Cycle Arrest. *The Journal of biological chemistry*, 274(39), pp.27632–27641.

Kobayashi, H. et al., 1992. Identification of the domains in cyclin A required for binding to, and activation of, p34cdc2 and p32cdk2 protein kinase subunits. *Molecular biology of the cell*, 3(11), pp.1279–1294.

Koff, A. et al., 1992. Formation and activation of a cyclin E-cdk2 complex during the G1 phase of the human cell cycle. *Science (New York, NY)*, 257(5077), pp.1689–1694.

Kops, G.J.P.L., Weaver, B.A.A. & Cleveland, D.W., 2005. On the road to cancer: aneuploidy and the mitotic checkpoint. *Nature Reviews Cancer*, 5(10), pp.773–785.

Kornbluth, S. et al., 1994. Membrane localization of the kinase which phosphorylates p34cdc2 on threonine 14. *Molecular biology of the cell*, 5(3), pp.273–282.

Kostich, M. et al., 2002. Human members of the eukaryotic protein kinase family. *Genome Biology*, 3(9), p.research0043.1.

Kramer, E.R. et al., 2000. Mitotic regulation of the APC activator proteins CDC20 and CDH1. *Molecular biology of the cell*, 11(5), pp.1555–1569.

Krasinska, L. et al., 2007. Regulation of multiple cell cycle events by Cdc14 homologues in vertebrates. *Experimental cell research*, 313(6), pp.1225–1239.

Krämer, A. et al., 1997. CBP/cycA, a CCAAT-binding protein necessary for adhesion-dependent cyclin A transcription, consists of NF-Y and a novel Mr 115,000 subunit. *Cancer Research*, 57(22), pp.5117–5121.

Kumagai, A. & Dunphy, W.G., 1999. Binding of 14-3-3 proteins and nuclear export control the intracellular localization of the mitotic inducer Cdc25. *Genes & development*, 13(9), pp.1067–1072.

Kumagai, A. & Dunphy, W.G., 1992. Regulation of the cdc25 protein during the cell cycle in Xenopus extracts. *Cell*, 70(1), pp.139–151.

Kumagai, A. & Dunphy, W.G., 1991. The cdc25 protein controls tyrosine dephosphorylation of the cdc2 protein in a cell-free system. *Cell*, 64(5), pp.903–914.

Kwon, Y.G. et al., 1997. Cell cycle-dependent phosphorylation of mammalian protein phosphatase 1 by cdc2 kinase. *Proceedings of the National Academy of Sciences of the United States of America*, 94(6), pp.2168–2173.

LaBaer, J. et al., 1997. New functional activities for the p21 family of CDK inhibitors. *Genes & development*, 11(7), pp.847–862.

Labandera, A.-M. et al., 2015. The mitotic PP2A regulator ENSA/ARPP-19 is remarkably conserved across plants and most eukaryotes. *Biochemical and biophysical research communications*, 458(4), pp.739–744. Available at: http://www.ncbi.nlm.nih.gov/pubmed/25666948.

Lan, W. et al., 2004. Aurora B phosphorylates centromeric MCAK and regulates its localization and microtubule depolymerization activity. *Current biology : CB*, 14(4), pp.273–286.

Laoukili, J. et al., 2005. FoxM1 is required for execution of the mitotic programme and chromosome stability. *Nature Publishing Group*, 7(2), pp.126–136.

Lee, J., Kumagai, A. & Dunphy, W.G., 2001. Positive regulation of Wee1 by Chk1 and 14-3-3 proteins. *Molecular biology of the cell*, 12(3), pp.551–563.

Lee, M.G. & Nurse, P., 1987. Complementation used to clone a human homologue of the fission yeast cell cycle control gene cdc2. *Nature*, 327(6117), pp.31–35. Available at:

http://www.nature.com/nature/journal/v327/n6117/abs/327031a0.html.

Lee, P. et al., 2013. Rim15 ‐ dependent activation of Hsf1 and Msn2/4 transcription factors by direct phosphorylation in Saccharomyces cerevisiae. *FEBS letters*, 587(22), pp.3648–3655.

Li, R. & Murray, A.W., 1991. Feedback control of mitosis in budding yeast. *Cell*, 66(3), pp.519–531.

Lincoln, A.J. et al., 2002. Cdc25b phosphatase is required for resumption of meiosis during oocyte maturation. *Nature genetics*, 30(4), pp.446–449.

Lindqvist, A. et al., 2005. Cdc25B cooperates with Cdc25A to induce mitosis but has a unique role in activating cyclin B1-Cdk1 at the centrosome. *The Journal of Cell Biology*, 171(1), pp.35–45.

Lindqvist, A. et al., 2007. Cyclin B1-Cdk1 activation continues after centrosome separation to control mitotic progression. *PLoS biology*, 5(5), p.e123.

Lindqvist, A., Rodríguez-Bravo, V. & Medema, R., 2009. The decision to enter mitosis: feedback and redundancy in the mitotic entry network. *The Journal of Cell Biology*.

Liu, D. et al., 2009. Sensing chromosome bi-orientation by spatial separation of aurora B kinase from kinetochore substrates. *Science (New York, NY)*, 323(5919), pp.1350–1353.

Liu, F., 1997. The human Myt1 kinase preferentially phosphorylates Cdc2 on threonine 14 and localizes to the endoplasmic reticulum and Golgi complex. *Molecular and Cellular Biology*, 17(2), pp.571–583.

Liu, N. et al., 1998. A new model of cell cycle-regulated transcription: repression of the cyclin A promoter by CDF-1 and anti-repression by E2F. *Oncogene*, 16(23), pp.2957–2963.

Liu, Q.H. et al., 2000. Chk1 is an essential kinase that is regulated by Atr and required for the G(2)/M DNA damage checkpoint. *Genes & development*, 14(12), pp.1448–1459.

Lohka, M.J., Hayes, M.K. & Maller, J.L., 1988. Purification of maturation-promoting factor, an intracellular regulator of early mitotic events. *Proceedings of the National Academy of Sciences of the United States of America*, 85(9), pp.3009–3013.

Lolli, G. & Johnson, L.N., 2005. CAK-Cyclin-dependent Activating Kinase: a key kinase in cell cycle control and a target for drugs? *Cell cycle (Georgetown, Tex)*, 4(4), pp.572–577.

London, N. et al., 2012. Phosphoregulation of Spc105 by Mps1 and PP1 Regulates Bub1 Localization to Kinetochores. *Current Biology*, 22(10), pp.900–906.

Lorca, T. & Castro, A., 2012. Deciphering the New Role of the Greatwall/PP2A Pathway in Cell Cycle Control. *Genes & Cancer*, 3(11-12), pp.712–720.

Lorca, T. & Castro, A., 2013. The Greatwall kinase: a new pathway in the control of the cell cycle. *Oncogene*, 32(5), pp.537–543.

Lorca, T. et al., 2010. Constant regulation of both the MPF amplification loop and the Greatwall-PP2A pathway is required for metaphase II arrest and correct entry into the first embryonic cell cycle. *Journal of Cell Science*, 123(Pt 13), pp.2281–2291.

Lozano, J.-C. et al., 2002. Molecular cloning, gene localization, and structure of human cyclin B3. *Biochemical and biophysical research communications*, 291(2), pp.406–413.

Lu, X. et al., 2008. The type 2C phosphatase Wip1: An oncogenic regulator of tumor suppressor and DNA damage response pathways. *Cancer and Metastasis Reviews*, 27(2), pp.123–135.

Luo, Y., Hurwitz, J. & Massagué, J., 1995. Cell-cycle inhibition by independent CDK and PCNA binding domains in p21Cip1. *Nature*, 375(6527), pp.159–161.

Ma, S. et al., 2016. Greatwall dephosphorylation and inactivation upon mitotic exit is triggered by PP1. *Journal of Cell Science*, 129(7), pp.1329–1339.

MacKeigan, J.P., Murphy, L.O. & Blenis, J., 2005. Sensitized RNAi screen of human kinases and phosphatases identifies new regulators of apoptosis and chemoresistance. *Nature Publishing Group*, 7(6), pp.591–600.

Macůrek, L. et al., 2008. Polo-like kinase-1 is activated by aurora A to promote checkpoint recovery. *Nature*, 455(7209), pp.119–U88.

Maddox, A.S. & Burridge, K., 2003. RhoA is required for cortical retraction and rigidity during mitotic cell rounding. *The Journal of Cell Biology*, 160(2), pp.255–265.

Mailand, N. et al., 2002. Deregulated human Cdc14A phosphatase disrupts centrosome separation and chromosome segregation. *Nature Publishing Group*, 4(4), pp.317–322.

Mailand, N. et al., 2006. Destruction of Claspin by SCFbetaTrCP restrains Chk1 activation and facilitates recovery from genotoxic stress. *Molecular Cell*, 23(3), pp.307–318.

Malumbres, M. & Barbacid, M., 2005. Mammalian cyclin-dependent kinases. *Trends in Biochemical Sciences*, 30(11), pp.630–641.

Mamely, I. et al., 2006. Polo-like kinase-1 controls proteasome-dependent degradation of Claspin during checkpoint recovery. *Current biology : CB*, 16(19), pp.1950–1955.

Manni, I. et al., 2001. NF-Y mediates the transcriptional inhibition of the cyclin B1, cyclin B2, and cdc25C promoters upon induced G2 arrest. *The Journal of biological chemistry*, 276(8), pp.5570–5576.

Manning, G. et al., 2002. The Protein Kinase Complement of the Human Genome.

Science (New York, NY), 298(5600), pp.1912–1934.

Mansfeld, J. et al., 2011. APC15 drives the turnover of MCC-CDC20 to make the spindle assembly checkpoint responsive to kinetochore attachment. *Nature Cell Biology*, 13(10), pp.1234–1243.

Mapelli, M. et al., 2006. Determinants of conformational dimerization of Mad2 and its inhibition by p31comet. *The EMBO Journal*, 25(6), pp.1273–1284.

Maresca, T.J. & Salmon, E.D., 2009. Intrakinetochore stretch is associated with changes in kinetochore phosphorylation and spindle assembly checkpoint activity. *The Journal of Cell Biology*, 184(3), pp.373–381.

Margolis, S.S. et al., 2006. A role for PP1 in the Cdc2/Cyclin B-mediated positive feedback activation of Cdc25. *Molecular biology of the cell*, 17(4), pp.1779–1789.

Margolis, S.S. et al., 2003. PP1 control of M phase entry exerted through 14-3-3-regulated Cdc25 dephosphorylation. *The EMBO Journal*, 22(21), pp.5734–5745.

Matsushime, H. et al., 1992. Identification and properties of an atypical catalytic subunit (p34PSK-J3/cdk4) for mammalian D type G1 cyclins. *Cell*, 71(2), pp.323–334.

Mayer-Jaekel, R.E. et al., 1994. Drosophila mutants in the 55 kDa regulatory subunit of protein phosphatase 2A show strongly reduced ability to dephosphorylate substrates of p34cdc2. *Journal of Cell Science*, 107 (Pt 9), pp.2609–2616.

Mäkelä, T.P. et al., 1994. A cyclin associated with the CDK-activating kinase MO15. *Nature*, 371(6494), pp.254–257.

McCloy, R.A. et al., 2014. Partial inhibition of Cdk1 in G2 phase overrides the SAC and decouples mitotic events. *Cell cycle (Georgetown, Tex)*, 13(9), pp.1400–1412.

McGowan, C.H. & Russell, P., 1993. Human Wee1 kinase inhibits cell division by phosphorylating p34cdc2 exclusively on Tyr15. *The EMBO Journal*, 12(1), pp.75–85.

McIntosh, J.R., Grishchuk, E.L. & West, R.R., 2002. Chromosome-microtubule interactions during mitosis. *Annual review of cell and developmental biology*, 18(1), pp.193–219.

Mei, L. & Huganir, R.L., 1991. Purification and Characterization of a Protein Tyrosine Phosphatase Which Dephosphorylates the Nicotinic Acetylcholine-Receptor. *The Journal of biological chemistry*, 266(24), pp.16063–16072.

Meinhart, A. et al., 2005. A structural perspective of CTD function. *Genes & development*, 19(12), pp.1401–1415.

Meselson, M. & Stahl, F.W., 1958. THE REPLICATION OF DNA IN ESCHERICHIA COLI. *Proceedings of the National Academy of Sciences of the United States of America*, 44(7), pp.671–682.

Meyerson, M. & Harlow, E., 1994. Identification of G1 kinase activity for cdk6, a novel

cyclin D partner. *Molecular and Cellular Biology*, 14(3), pp.2077–2086.

Michael, W.M. & Newport, J., 1998. Coupling of mitosis to the completion of S phase through Cdc34-mediated degradation of Wee1. *Science (New York, NY)*, 282(5395), pp.1886–1889.

Minshull, J., Blow, J.J. & Hunt, T., 1989. Translation of Cyclin Messenger-Rna Is Necessary for Extracts of Activated Xenopus Eggs to Enter Mitosis. *Cell*, 56(6), pp.947–956.

Miyazaki, W.Y. & Orr-Weaver, T.L., 1994. Sister-chromatid cohesion in mitosis and meiosis. *Annual review of genetics*.

Mocciaro, A. & Schiebel, E., 2010. Cdc14: a highly conserved family of phosphatases with non-conserved functions? *Journal of Cell Science*, 123(Pt 17), pp.2867–2876.

Mochida, S., 2014. Regulation of α-endosulfine, an inhibitor of protein phosphatase 2A, by multisite phosphorylation. *FEBS Journal*, 281(4), pp.1159–1169.

Mochida, S. & Hunt, T., 2007. Calcineurin is required to release Xenopus egg extracts from meiotic M phase. *Nature*, 449(7160), pp.336–340.

Mochida, S. et al., 2010. Greatwall phosphorylates an inhibitor of protein phosphatase 2A that is essential for mitosis. *Science (New York, NY)*, 330(6011), pp.1670–1673.

Mochida, S. et al., 2009. Regulated activity of PP2A-B55 delta is crucial for controlling entry into and exit from mitosis in Xenopus egg extracts. *The EMBO Journal*, 28(18), pp.2777–2785.

Monica, Della, R. et al., 2015. FCP1 phosphatase controls Greatwall kinase to promote PP2A-B55 activation and mitotic progression. *eLife*, 4, p.e10399.

Morgan, D.O., 2007. *The Cell Cycle*, New Science Press. Available at: https://books.google.co.uk/books?id=ScEuiD2V6GoC&printsec=frontcover#v=onepage&q&f=false.

Mueller, P.R. et al., 1995. Myt1: a membrane-associated inhibitory kinase that phosphorylates Cdc2 on both threonine-14 and tyrosine-15. *Science (New York, NY)*, 270(5233), pp.86–90.

Murray, A.W. & Kirschner, M.W., 1989a. Cyclin synthesis drives the early embryonic cell cycle. *Nature*, 339(6222), pp.275–280.

Murray, A.W. & Kirschner, M.W., 1989b. Dominoes and clocks: the union of two views of the cell cycle. *Science (New York, NY)*, 246(4930), pp.614–621. Available at: http://www.ncbi.nlm.nih.gov/pubmed/2683077.

Musacchio, A. & Salmon, E.D., 2007. The spindle-assembly checkpoint in space and time. *Nature Reviews Molecular Cell Biology*, 8(5), pp.379–393.

Nakajima, H. et al., 2003. Identification of a consensus motif for Plk (Polo-like kinase) phosphorylation reveals Myt1 as a Plk1 substrate. *The Journal of biological*

chemistry, 278(28), pp.25277–25280.

Nakanishi, M. et al., 1995. Identification of the active region of the DNA synthesis inhibitory gene p21Sdi1/CIP1/WAF1. *The EMBO Journal*, 14(3), pp.555–563.

Neumann, B. et al., 2010. Phenotypic profiling of the human genome by time-lapse microscopy reveals cell division genes. *Nature*, 464(7289), pp.721–727.

Nguyen, T.B. et al., 2002. Characterization and expression of mammalian cyclin b3, a prepachytene meiotic cyclin. *The Journal of biological chemistry*, 277(44), pp.41960–41969.

Nicklas, R.B., 1997. How cells get the right chromosomes. *Science (New York, NY)*, 275(5300), pp.632–637.

Niiya, F. et al., 2005. Inhibition of cyclin-dependent kinase 1 induces cytokinesis without chromosome segregation in an ECT2 and MgcRacGAP-dependent manner. *The Journal of biological chemistry*, 280(43), pp.36502–36509.

Niiya, F. et al., 2006. Phosphorylation of the cytokinesis regulator ECT2 at G2/M phase stimulates association of the mitotic kinase Plk1 and accumulation of GTP-bound RhoA. *Oncogene*, 25(6), pp.827–837.

Nishimoto, T., 1992. Mitotic checkpoints. *Current Opinion in Cell Biology*, 4(2), pp.174–179.

Norbury, C. & Nurse, P., 1992. Animal cell cycles and their control. *Annual review of biochemistry*, 61, pp.441–470.

Nurse, P. & Thuriaux, P., 1980. Regulatory genes controlling mitosis in the fission yeast Schizosaccharomyces pombe. *Genetics*, 96(3), pp.627–637.

Nurse, P., Thuriaux, P. & Nasmyth, K., 1976. Genetic control of the cell division cycle in the fission yeast Schizosaccharomyces pombe. *Molecular and General Genetics MGG*, 146(2), pp.167–178.

O'Farrell, P.H., 2001. Triggering the all-or-nothing switch into mitosis. *Trends in Cell Biology*, 11(12), pp.512–519.

Obsil, T. & Obsilova, V., 2008. Structure/function relationships underlying regulation of FOXO transcription factors. *Oncogene*, 27(16), pp.2263–2275.

Ocasio, C.A. et al., 2016. A first generation inhibitor of human Greatwall kinase, enabled by structural and functional characterisation of a minimal kinase domain construct. *Oncotarget*, 5(0).

Okamoto, K. & Sagata, N., 2007. Mechanism for inactivation of the mitotic inhibitory kinase Wee1 at M phase. *Proceedings of the National Academy of Sciences of the United States of America*, 104(10), pp.3753–3758.

Okumura, E. et al., 2014. Cyclin B-Cdk1 inhibits protein phosphatase PP2A-B55 via a Greatwall kinase-independent mechanism. *The Journal of Cell Biology*, 204(6),

pp.881–889.

Parker, L.L. & Piwnica-Worms, H., 1992. Inactivation of the p34cdc2-cyclin B complex by the human WEE1 tyrosine kinase. *Science (New York, NY)*, 257(5078), pp.1955–1957.

Parker, L.L., Atherton-Fessler, S. & Piwnica-Worms, H., 1992. p107wee1 is a dual-specificity kinase that phosphorylates p34cdc2 on tyrosine 15. *Proceedings of the National Academy of Sciences of the United States of America*, 89(7), pp.2917–2921.

Paweletz, N., 2001. *Walther Flemming: pioneer of mitosis research*,

Pedruzzi, I. et al., 2003. TOR and PKA Signaling Pathways Converge on the Protein Kinase Rim15 to Control Entry into G0. *Molecular Cell*, 12(6), pp.1607–1613.

Peng, A. et al., 2010. A novel role for greatwall kinase in recovery from DNA damage. *Cell cycle (Georgetown, Tex)*, 9(21), pp.4364–4369.

Peng, A., Wang, L. & Fisher, L.A., 2011. Greatwall and Polo-like kinase 1 coordinate to promote checkpoint recovery. *Journal of Biological Chemistry*, 286(33), pp.28996–29004.

Peng, C.Y. et al., 1998. C-TAK1 protein kinase phosphorylates human Cdc25C on serine 216 and promotes 14-3-3 protein binding. *Cell growth & differentiation : the molecular biology journal of the American Association for Cancer Research*, 9(3), pp.197–208.

Perry, J.A. & Kornbluth, S., 2007. Cdc25 and Wee1: analogous opposites? *Cell Division*, 2(1), p.12.

Peschiaroli, A. et al., 2006. SCFβTrCP-Mediated Degradation of Claspin Regulates Recovery from the DNA Replication Checkpoint Response. *Molecular Cell*, 23(3), pp.319–329.

Peters, J.-M., 2006. The anaphase promoting complex/cyclosome: a machine designed to destroy. *Nature Reviews Molecular Cell Biology*, 7(9), pp.644–656.

Peters, J.-M., 2002. The anaphase-promoting complex: proteolysis in mitosis and beyond. *Molecular Cell*, 9(5), pp.931–943.

Petri, E.T. et al., 2007. The crystal structure of human cyclin B. *Cell cycle (Georgetown, Tex)*, 6(11), pp.1342–1349. Available at: http://www.ncbi.nlm.nih.gov/pubmed/17495533.

Peyrollier, K. et al., 1996. α Endosulfine Is a Novel Molecule, Structually Related to a Family of Phosphoproteins. *Biochemical and biophysical research communications*, 223(3), pp.583–586.

Pérez-Hidalgo, L. & Moreno, S., 2016. Nutrients control cell size. *Cell cycle (Georgetown, Tex)*.

Pfender, S. et al., 2015. Live imaging RNAi screen reveals genes essential for meiosis in mammalian oocytes. *Nature*, 524(7564), pp.239–242. Available at: http://www.ncbi.nlm.nih.gov/pubmed/26147080nature14568.

Pfleger, C.M. & Kirschner, M.W., 2000. The KEN box: an APC recognition signal distinct from the D box targeted by Cdh1. *Genes & development*, 14(6), pp.655–665.

Philips, A. et al., 1999. CHF: a novel factor binding to cyclin A CHR corepressor element. *Oncogene*, 18(46), pp.6222–6232.

Picard, A. et al., 1989. Involvement of protein phosphatases 1 and 2A in the control of M phase-promoting factor activity in starfish. *The Journal of Cell Biology*, 109(6 Pt 2), pp.3347–3354.

Picard, A. et al., 1991. Okadaic acid mimics a nuclear component required for cyclin B-cdc2 kinase microinjection to drive starfish oocytes into M phase. *The Journal of Cell Biology*, 115(2), pp.337–344.

Pieroni, E. et al., 2008. Protein networking: insights into global functional organization of proteomes. *Proteomics*, 8(4), pp.799–816.

Pines, J., 2011. Cubism and the cell cycle: the many faces of the APC/C. *Nature Reviews Molecular Cell Biology*, 12(7), pp.427–438.

Pines, J. & Hunt, T., 1987a. Molecular cloning and characterization of the mRNA for cyclin from sea urchin eggs. *The EMBO Journal*, 6(10), pp.2987–2995.

Pines, J. & Hunt, T., 1987b. Molecular-Cloning and Characterization of the Messenger-Rna for Cyclin From Sea-Urchin Eggs. *The EMBO Journal*, 6(10), pp.2987–2995. Available at: http://www.ncbi.nlm.nih.gov/pubmed/?term=Molecular-Cloning+and+Characterization+of+the+Messenger-Rna+for+Cyclin+From+Sea-Urchin+Eggs.

Pines, J. & Hunter, T., 1989. Isolation of a human cyclin cDNA: Evidence for cyclin mRNA and protein regulation in the cell cycle and for interaction with p34cdc2. *Cell*, 58(5), pp.833–846.

Pinsky, B.A. et al., 2006. Glc7/protein phosphatase 1 regulatory subunits can oppose the Ipl1/aurora protein kinase by redistributing Glc7. *Molecular and Cellular Biology*, 26(7), pp.2648–2660.

Pomerening, J.R., Sontag, E.D. & Ferrell, J.E., 2003. Building a cell cycle oscillator: hysteresis and bistability in the activation of Cdc2. *Nature Publishing Group*, 5(4), pp.346–351.

Pomerening, J.R., Ubersax, J.A. & Ferrell, J.E., 2008a. Rapid cycling and precocious termination of G1 phase in cells expressing CDK1AF. *Molecular biology of the cell*, 19(8), pp.3426–3441.

Pomerening, J.R., Ubersax, J.A. & Ferrell, J.E., 2008b. Rapid cycling and precocious termination of G1 phase in cells expressing CDK1AF. *Molecular biology of the*

cell, 19(8), pp.3426–3441.

Potapova, T.A. et al., 2011. Mitotic progression becomes irreversible in prometaphase and collapses when Wee1 and Cdc25 are inhibited. *Molecular biology of the cell*, 22(8), pp.1191–1206.

Qian, J. et al., 2011. PP1/Repo-Man Dephosphorylates Mitotic Histone H3 at T3 and Regulates Chromosomal Aurora B Targeting. *Current Biology*, 21(9), pp.766–773.

Queralt, E. et al., 2006. Downregulation of PP2A(Cdc55) phosphatase by separase initiates mitotic exit in budding yeast. *Cell*, 125(4), pp.719–732.

Rangone, H. et al., 2011. Suppression of Scant Identifies Endos as a Substrate of Greatwall Kinase and a Negative Regulator of Protein Phosphatase 2A in Mitosis O. Cohen-Fix, ed. *PLoS Genetics*, 7(8), p.e1002225.

Ravnik, S.E. & Wolgemuth, D.J., 1999. Regulation of meiosis during mammalian spermatogenesis: the A-type cyclins and their associated cyclin-dependent kinases are differentially expressed in the germ-cell lineage. *Developmental biology*, 207(2), pp.408–418.

Reed, S.I., Hadwiger, J.A. & Lörincz, A.T., 1985. Protein kinase activity associated with the product of the yeast cell division cycle gene CDC28. *Proceedings of the National Academy of Sciences of the United States of America*, 82(12), pp.4055–4059.

Rodier, G. et al., 2008. Phosphorylation of Skp2 regulated by CDK2 and Cdc14B protects it from degradation by APCCdh1 in G1 phase. *The EMBO Journal*, 27(4), pp.679–691.

Rogers, S. et al., 2016. PP1 initiates the dephosphorylation of MASTL, triggering mitotic exit and bistability in human cells. *Journal of Cell Science*, 129(7), pp.1340–1354.

Rosenberg, J.S., Cross, F.R. & Funabiki, H., 2011. KNL1/Spc105 recruits PP1 to silence the spindle assembly checkpoint. *Current biology : CB*, 21(11), pp.942–947.

Rosenblatt, J., Gu, Y. & Morgan, D.O., 1992. Human cyclin-dependent kinase 2 is activated during the S and G2 phases of the cell cycle and associates with cyclin A. *Proceedings of the National Academy of Sciences of the United States of America*, 89(7), pp.2824–2828.

Rossio, V. & Yoshida, S., 2011. Spatial regulation of Cdc55-PP2A by Zds1/Zds2 controls mitotic entry and mitotic exit in budding yeast. *The Journal of Cell Biology*, 193(3), pp.445–454.

Rossio, V. et al., 2014. Comparative genetic analysis of PP2A-Cdc55 regulators in budding yeast. *Cell cycle (Georgetown, Tex)*, 13(13), pp.2073–2083.

Rothblum-Oviatt, C.J., Ryan, C.E. & Piwnica-Worms, H., 2001. 14-3-3 binding regulates catalytic activity of human Wee1 kinase. *Cell growth & differentiation : the molecular biology journal of the American Association for Cancer Research*,

12(12), pp.581–589.

Roy, S.H. et al., 2011. Control of Cdc14 activity coordinates cell cycle and development in Caenorhabditis elegans. *Mechanisms of Development*, 128(7-10), pp.317–326.

Ruas, M. & Peters, G., 1998. The p16INK4a/CDKN2A tumor suppressor and its relatives. *Biochimica et biophysica acta*, 1378(2), pp.F115–77. Available at: http://www.ncbi.nlm.nih.gov/pubmed/?term=The+p16INK4a%2FCDKN2A+tumor+suppressor+and+its+relatives.

Ruchaud, S., Carmena, M. & Earnshaw, W.C., 2007. Chromosomal passengers: conducting cell division. *Nature Reviews Molecular Cell Biology*, 8(10), pp.798–812.

Rudolph, J., 2007. Inhibiting transient protein-protein interactions: lessons from the Cdc25 protein tyrosine phosphatases. *Nature Reviews Cancer*, 7(3), pp.202–211.

Rupes, I., 2002. Checking cell size in yeast. *Trends in Genetics*, 18(9), pp.479–485.

Russell, P. & Nurse, P., 1986. cdc25+ functions as an inducer in the mitotic control of fission yeast. *Cell*, 45(1), pp.145–153.

Russo, A.A., Jeffrey, P.D. & Pavletich, N.P., 1996. Structural basis of cyclin-dependent kinase activation by phosphorylation. *Nature structural biology*, 3(8), pp.696–700.

Sadhu, K. et al., 1990. Human homolog of fission yeast cdc25 mitotic inducer is predominantly expressed in G2. *Proceedings of the National Academy of Sciences of the United States of America*, 87(13), pp.5139–5143.

Salsi, V. et al., 2003. Interactions between p300 and multiple NF-Y trimers govern cyclin B2 promoter function. *The Journal of biological chemistry*, 278(9), pp.6642–6650.

Santos, S.D.M. et al., 2012. Spatial positive feedback at the onset of mitosis. *Cell*, 149(7), pp.1500–1513.

Sarkar, S. et al., 2014. The Rim15-endosulfine-PP2ACdc55 signalling module regulates entry into gametogenesis and quiescence via distinct mechanisms in budding yeast. G. P. Copenhaver, ed. *PLoS Genetics*, 10(6), p.e1004456.

Schmitz, M.H.A. et al., 2010. Live-cell imaging RNAi screen identifies PP2A-B55alpha and importin-beta1 as key mitotic exit regulators in human cells. *Nature Cell Biology*, 12(9), pp.886–893.

Schreiber, A. et al., 2011. Structural basis for the subunit assembly of the anaphase-promoting complex. *Nature*, 470(7333), pp.227–232.

Schulze, A. et al., 1995. Cell cycle regulation of the cyclin A gene promoter is mediated by a variant E2F site. *Proceedings of the National Academy of Sciences of the United States of America*, 92(24), pp.11264–11268.

Sciortino, S. et al., 2001. The cyclin B1 gene is actively transcribed during mitosis in HeLa cells. *EMBO reports*, 2(11), pp.1018–1023.

Sedgwick, G.G. et al., 2013. Mechanisms controlling the temporal degradation of Nek2A and Kif18A by the APC/C-Cdc20 complex. *The EMBO Journal*, 32(2), pp.303–314.

Seki, A. et al., 2008. Bora and the kinase Aurora A cooperatively activate the kinase Plk1 and control mitotic entry. *Science (New York, NY)*, 320(5883), pp.1655–1658.

Seshacharyulu, P. et al., 2013. Phosphatase: PP2A structural importance, regulation and its aberrant expression in cancer. *Cancer Letters*, 335(1), pp.9–18.

Sha, W. et al., 2003. Hysteresis drives cell-cycle transitions in Xenopus laevis egg extracts. *Proceedings of the National Academy of Sciences of the United States of America*, 100(3), pp.975–980.

Shaltiel, I.A. et al., 2015. The same, only different - DNA damage checkpoints and their reversal throughout the cell cycle. *Journal of Cell Science*, 128(4), pp.607–620.

Shepperd, L.A. et al., 2012. Phosphodependent recruitment of Bub1 and Bub3 to Spc7/KNL1 by Mph1 kinase maintains the spindle checkpoint. *Current biology : CB*, 22(10), pp.891–899.

Sherr, C.J., 2001. The INK4a/ARF network in tumour suppression. *Nature Reviews Molecular Cell Biology*, 2(10), pp.731–737.

Sherr, C.J. & Roberts, J.M., 1999. CDK inhibitors: positive and negative regulators of G1-phase progression. *Genes & development*, 13(12), pp.1501–1512.

Shima, D.T. et al., 1998. An Ordered Inheritance Strategy for the Golgi Apparatus: Visualization of Mitotic Disassembly Reveals a Role for the Mitotic Spindle. *The Journal of Cell Biology*, 141(4), pp.955–966.

Shimizu, T. et al., 2002. Adenosine 5'-O-(3-thiotriphosphate) hydrolysis by dynein. *Biochemistry*, 28(17), pp.7022–7027.

Shteinberg, M. et al., 1999. Phosphorylation of the cyclosome is required for its stimulation by Fizzy/cdc20. *Biochemical and biophysical research communications*, 260(1), pp.193–198.

Sigl, R. et al., 2009. Loss of the mammalian APC/C activator FZR1 shortens G1 and lengthens S phase but has little effect on exit from mitosis. *Journal of Cell Science*, 122(Pt 22), pp.4208–4217.

Simanis, V. & Nurse, P., 1986. The cell cycle control gene cdc2+ of fission yeast encodes a protein kinase potentially regulated by phosphorylation. *Cell*, 45(2), pp.261–268.

Smoyer, C.J. & Jaspersen, S.L., 2014. Breaking down the wall: the nuclear envelope during mitosis. *Current Opinion in Cell Biology*, 26, pp.1–9.

Solomon, M.J. et al., 1990. Cyclin activation of p34cdc2. *Cell*, 63(5), pp.1013–1024.

Soucek, T. et al., 1997. Deregulated expression of E2F-1 induces cyclin A- and E-associated kinase activities independently from cell cycle position. *Oncogene*, 14(19), pp.2251–2257.

Stegmeier, F. & Amon, A., 2004. Closing mitosis: the functions of the Cdc14 phosphatase and its regulation. *Annual review of genetics*, 38, pp.203–232.

Stetina, Von, J.R. et al., 2008. alpha-Endosulfine is a conserved protein required for oocyte meiotic maturation in Drosophila. *Development (Cambridge, England)*, 135(22), pp.3697–3706.

Stewart, Z.A. & Pietenpol, J.A., 2001. p53 Signaling and cell cycle checkpoints. *Chemical Research in Toxicology*, 14(3), pp.243–263.

Stukenberg, P.T. & Kirschner, M.W., 2001. Pin1 acts catalytically to promote a conformational change in Cdc25. *Molecular Cell*, 7(5), pp.1071–1083.

Subbarayalu, P. et al., 2016. Abstract 3658: A novel microtubule associated RNA binding protein matrin 3 act as a tumor suppressor by regulating mitotic spindle organizing proteins in triple negative breast cancers. *Cancer Research*, 76(14 Supplement), pp.3658–3658.

Sudakin, V., Chan, G.K. & Yen, T.J., 2001. Checkpoint inhibition of the APC/C in HeLa cells is mediated by a complex of BUBR1, BUB3, CDC20, and MAD2. *The Journal of Cell Biology*, 154(5), pp.925–936.

Sunkara, P.S., Wright, D.A. & Rao, P.N., 1979. Mitotic factors from mammalian cells induce germinal vesicle breakdown and chromosome condensation in amphibian oocytes. *Proceedings of the National Academy of Sciences of the United States of America*, 76(6), pp.2799–2802.

Sweeney, C. et al., 1996. A distinct cyclin A is expressed in germ cells in the mouse. *Development (Cambridge, England)*, 122(1), pp.53–64.

Swenson, K.I., Farrell, K.M. & Ruderman, J.V., 1986. The clam embryo protein cyclin A induces entry into M phase and the resumption of meiosis in Xenopus oocytes. *Cell*, 47(6), pp.861–870.

Swinnen, E. et al., 2006. Rim15 and the crossroads of nutrient signalling pathways in Saccharomyces cerevisiae. *Cell Division*, 1(1), p.3.

Takaki, T. et al., 2008. Polo-like kinase 1 reaches beyond mitosis-cytokinesis, DNA damage response, and development. *Current Opinion in Cell Biology*, 20(6), pp.650–660.

Talarek, N. et al., 2010. Initiation of the TORC1-regulated G0 program requires Igo1/2, which license specific mRNAs to evade degradation via the 5“-3” mRNA decay pathway. *Molecular Cell*, 38(3), pp.345–355.

Tamaskovic, R., Bichsel, S.J. & Hemmings, B.A., 2003. NDR family of AGC kinases--

essential regulators of the cell cycle and morphogenesis. *FEBS letters*, 546(1), pp.73–80.

Tanaka, T.U. et al., 2002. Evidence that the Ipl1-Sli15 (Aurora kinase-INCENP) complex promotes chromosome bi-orientation by altering kinetochore-spindle pole connections. *Cell*, 108(3), pp.317–329.

Taylor, S.S., Radzio-Andzelm, E. & Hunter, T., 1995. How do protein kinases discriminate between serine/threonine and tyrosine? Structural insights from the insulin receptor protein-tyrosine kinase. *The FASEB journal : official publication of the Federation of American Societies for Experimental Biology*, 9(13), pp.1255–1266.

Thompson, L.J., Bollen, M. & Fields, A.P., 1997. Identification of protein phosphatase 1 as a mitotic lamin phosphatase. *The Journal of biological chemistry*, 272(47), pp.29693–29697.

Thornton, B.R. & Toczyski, D.P., 2003. Securin and B-cyclin/CDK are the only essential targets of the APC. *Nature Publishing Group*, 5(12), pp.1090–1094.

Tominaga, Y. et al., 2006. Murine Wee1 plays a critical role in cell cycle regulation and pre-implantation stages of embryonic development. *International Journal of Biological Sciences*, 2(4), pp.161–170.

Toyoshima-Morimoto, F. et al., 2001. Polo-like kinase 1 phosphorylates cyclin B1 and targets it to the nucleus during prophase. *Nature*, 410(6825), pp.215–220.

Toyoshima-Morimoto, F., Taniguchi, E. & Nishida, E., 2002. Plk1 promotes nuclear translocation of human Cdc25C during prophase. *EMBO reports*, 3(4), pp.341–348.

Trautmann, S. et al., 2001. Fission yeast Clp1p phosphatase regulates G2/M transition and coordination of cytokinesis with cell cycle progression. *Current biology : CB*, 11(12), pp.931–940.

Trinkle-Mulcahy, L. & Lamond, A.I., 2006. Mitotic phosphatases: no longer silent partners. *Current Opinion in Cell Biology*, 18(6), pp.623–631.

Trinkle-Mulcahy, L. et al., 2003. Time-lapse imaging reveals dynamic relocalization of PP1gamma throughout the mammalian cell cycle. *Molecular biology of the cell*, 14(1), pp.107–117.

Tsai, L.H., Harlow, E. & Meyerson, M., 1991. Isolation of the human cdk2 gene that encodes the cyclin A- and adenovirus E1A-associated p33 kinase. *Nature*, 353(6340), pp.174–177.

Tumurbaatar, I. et al., 2011. Human Cdc14B promotes progression through mitosis by dephosphorylating Cdc25 and regulating Cdk1/cyclin B activity. *PloS one*, 6(2), p.e14711.

Turner, W., 1890. The Cell Theory, Past and Present. *Nature*, 43(1097), pp.10–15. Available at: http://www.ncbi.nlm.nih.gov/pubmed/17231856.

Uchida, S. et al., 2004. Nuclear export signal in CDC25B. *Biochemical and biophysical research communications*, 316(1), pp.226–232.

Vader, G., Medema, R.H. & Lens, S.M.A., 2006. The chromosomal passenger complex: guiding Aurora-B through mitosis. *The Journal of Cell Biology*, 173(6), pp.833–837.

Vagnarelli, P. et al., 2006. Condensin and Repo-Man-PP1 co-operate in the regulation of chromosome architecture during mitosis. *Nature Publishing Group*, 8(10), pp.1133–1142.

Vairapandi, M. et al., 2002. GADD45b and GADD45g are cdc2/cyclinB1 kinase inhibitors with a role in S and G2/M cell cycle checkpoints induced by genotoxic stress. *Journal of Cellular Physiology*, 192(3), pp.327–338.

van Vugt, M.A.T.M. & Medema, R.H., 2004. Checkpoint Adaptation and Recovery: Back with Polo after the Break. *Cell cycle (Georgetown, Tex)*.

van Vugt, M.A.T.M. & Medema, R.H., 2005. Getting in and out of mitosis with Polo-like kinase-1. *Oncogene*, 24(17), pp.2844–2859.

van Vugt, M.A.T.M., Brás, A. & Medema, R.H., 2004. Polo-like kinase-1 controls recovery from a G2 DNA damage-induced arrest in mammalian cells. *Molecular Cell*, 15(5), pp.799–811.

Varela, E. et al., 2009. Lte1, Cdc14 and MEN-controlled Cdk inactivation in yeast coordinate rDNA decompaction with late telophase progression. *The EMBO Journal*, 28(11), pp.1562–1575.

Vázquez-Novelle, M.D. et al., 2010. Human Cdc14A phosphatase modulates the G2/M transition through Cdc25A and Cdc25B. *Journal of Biological Chemistry*, 285(52), pp.40544–40553.

Vesely, C., 2013. Investigation of the mechanisms of the G2/M phase transition in human cells : the role of Greatwall kinase.

Vigneron, S. et al., 2011. Characterization of the mechanisms controlling Greatwall activity. *Molecular and Cellular Biology*, 31(11), pp.2262–2275.

Vigneron, S. et al., 2009. Greatwall maintains mitosis through regulation of PP2A. *The EMBO Journal*, 28(18), pp.2786–2793.

Vinod, P.K. & Novák, B., 2015. Model scenarios for switch-like mitotic transitions. *FEBS letters*, 589(6), pp.667–671.

Virshup, D.M. & Shenolikar, S., 2009. From Promiscuity to Precision: Protein Phosphatases Get a Makeover. *Molecular Cell*, 33(5), pp.537–545.

Virsolvy-Vergine, A. et al., 1992. Endosulfine, an endogenous peptidic ligand for the sulfonylurea receptor: purification and partial characterization from ovine brain. *Proceedings of the National Academy of Sciences of the United States of America*, 89(14), pp.6629–6633.

Visconti, R. et al., 2012. FCP1-dependent dephosphorylation is required for M-phase-promoting factor inactivation at mitosis exit. *Nature Communications*, 3, pp.894–810.

Visintin, R. et al., 1998. The phosphatase Cdc14 triggers mitotic exit by reversal of Cdk-dependent phosphorylation. *Molecular Cell*, 2(6), pp.709–718.

Voets, E. & Wolthuis, R., 2015. MASTL promotes cyclin B1 destruction by enforcing Cdc20-independent binding of cyclin B1 to the APC/C. *Biology Open*, 4(4), pp.484–495.

Voets, E. & Wolthuis, R.M.F., 2010. MASTL is the human orthologue of Greatwall kinase that facilitates mitotic entry, anaphase and cytokinesis. *Cell cycle (Georgetown, Tex)*, 9(17), pp.3591–3601.

Wang, J. et al., 2016. Crystal structure of a PP2A B56-BubR1 complex and its implications for PP2A substrate recruitment and localization. *Protein & cell*, 7(7), pp.516–526.

Wang, M. et al., 2015. Version 4.0 of PaxDb: Protein abundance data, integrated across model organisms, tissues, and cell-lines. K. S. Lilley et al., eds. *Proteomics*, 15(18), pp.3163–3168. Available at: http://www.ncbi.nlm.nih.gov/pubmed/25656970.

Wang, P. et al., 2013. Cell cycle regulation of Greatwall kinase nuclear localization facilitates mitotic progression. *The Journal of Cell Biology*, 202(2), pp.277–293.

Wang, P. et al., 2016. Spatial regulation of greatwall by Cdk1 and PP2A-Tws in the cell cycle. *Cell cycle (Georgetown, Tex)*, 15(4), pp.528–539.

Wang, P., Pinson, X. & Archambault, V., 2011. PP2A-twins is antagonized by greatwall and collaborates with polo for cell cycle progression and centrosome attachment to nuclei in drosophila embryos. *PLoS Genetics*, 7(8), p.e1002227.

Wang, X.W. et al., 1999. GADD45 induction of a G(2)/M cell cycle checkpoint. *Proceedings of the National Academy of Sciences of the United States of America*, 96(7), pp.3706–3711.

Wasner, M., Haugwitz, U., et al., 2003. Three CCAAT-boxes and a single cell cycle genes homology region (CHR) are the major regulating sites for transcription from the human cyclin B2 promoter. *Gene*, 312, pp.225–237.

Wasner, M., Tschöp, K., et al., 2003. Cyclin B1 transcription is enhanced by the p300 coactivator and regulated during the cell cycle by a CHR-dependent repression mechanism. *FEBS letters*, 536(1-3), pp.66–70.

Wassmann, K. & Benezra, R., 2001. Mitotic checkpoints: from yeast to cancer. *Current Opinion in Genetics & Development*, 11(1), pp.83–90.

Watanabe, N. et al., 2005. Cyclin-dependent kinase (CDK) phosphorylation destabilizes somatic Wee1 via multiple pathways. *Proceedings of the National Academy of Sciences of the United States of America*, 102(33), pp.11663–11668.

Watanabe, N. et al., 2004. M-phase kinases induce phospho-dependent ubiquitination of somatic Wee1 by SCFbeta-TrCP. *Proceedings of the National Academy of Sciences of the United States of America*, 101(13), pp.4419–4424.

Weinert, T. & Hartwell, L., 1989. Control of G2 delay by the rad9 gene of Saccharomyces cerevisiae. *Journal of cell science. Supplement*, 12, pp.145–148.

Weiss, E. & Winey, M., 1996. The Saccharomyces cerevisiae spindle pole body duplication gene MPS1 is part of a mitotic checkpoint. *The Journal of Cell Biology*, 132(1-2), pp.111–123.

Welburn, J.P.I. et al., 2007. How tyrosine 15 phosphorylation inhibits the activity of cyclin-dependent kinase 2-cyclin A. *The Journal of biological chemistry*, 282(5), pp.3173–3181.

White-Cooper, H. et al., 1996. Mutations in new cell cycle genes that fail to complement a multiply mutant third chromosome of Drosophila. *Genetics*, 144(3), pp.1097–1111.

Wicky, S. et al., 2011. The Zds proteins control entry into mitosis and target protein phosphatase 2A to the Cdc25 phosphatase. *Molecular biology of the cell*, 22(1), pp.20–32.

Williams, B.C. et al., 2014. Greatwall-phosphorylated Endosulfine is both an inhibitor and a substrate of PP2A-B55 heterotrimers. J. Pines, ed. *eLife*, 3, p.e01695.

Winkler, C. et al., 2015. The selective inhibition of protein phosphatase-1 results in mitotic catastrophe and impaired tumor growth. *J Cell Sci*, 128(24), pp.4526–4537.

Wong, P.Y. et al., 2016. MASTL(Greatwall) regulates DNA damage responses by coordinating mitotic entry after checkpoint recovery and APC/C activation. *Scientific reports*, 6, p.22230.

Wu, J.Q. et al., 2009. PP1-mediated dephosphorylation of phosphoproteins at mitotic exit is controlled by inhibitor-1 and PP1 phosphorylation. *Nature Cell Biology*, 11(5), pp.644–651.

Xia, G. et al., 2004. Conformation‐specific binding of p31comet antagonizes the function of Mad2 in the spindle checkpoint. *The EMBO Journal*, 23(15), pp.3133–3143.

Xiao, Z. et al., 2003. Chk1 mediates S and G2 arrests through Cdc25A degradation in response to DNA-damaging agents. *The Journal of biological chemistry*, 278(24), pp.21767–21773.

Yamamoto, T.M. et al., 2014. Regulation of Greatwall kinase by protein stabilization and nuclear localization. *Cell cycle (Georgetown, Tex)*, 13(22), pp.3565–3575.

Yamamoto, T.M. et al., 2011. Regulation of Greatwall kinase during Xenopus oocyte maturation. *Molecular biology of the cell*, 22(13), pp.2157–2164. Available at: https://www.ncbi.nlm.nih.gov/pubmed/21551066.

Yang, J. & Kornbluth, S., 1999. All aboard the cyclin train: subcellular trafficking of cyclins and their CDK partners. *Trends in Cell Biology*, 9(6), pp.207–210.

Yang, M. et al., 2007. p31comet Blocks Mad2 Activation through Structural Mimicry. *Cell*, 131(4), pp.744–755.

Yeo, M. et al., 2003. A novel RNA polymerase II C-terminal domain phosphatase that preferentially dephosphorylates serine 5. *The Journal of biological chemistry*, 278(28), pp.26078–26085.

Yu, H., 2002. Regulation of APC–Cdc20 by the spindle checkpoint. *Current Opinion in Cell Biology*, 14(6), pp.706–714.

Yu, J. et al., 2006. Greatwall kinase participates in the Cdc2 autoregulatory loop in Xenopus egg extracts. *Molecular Cell*, 22(1), pp.83–91.

Yu, J. et al., 2004. Greatwall kinase: a nuclear protein required for proper chromosome condensation and mitotic progression in Drosophila. *The Journal of Cell Biology*, 164(4), pp.487–492.

Yu, X. et al., 2003. The BRCT domain is a phospho-protein binding domain. *Science (New York, NY)*, 302(5645), pp.639–642.

Yuan, J. et al., 2002. Cooperative phosphorylation including the activity of polo-like kinase 1 regulates the subcellular localization of cyclin B1. *Oncogene*, 21(54), pp.8282–8292.

Zetterberg, A., Engström, W. & Dafgård, E., 1984. The relative effects of different types of growth factors on DNA replication, mitosis, and cellular enlargement. *Cytometry*, 5(4), pp.368–375.

Zhan, Q.M. et al., 1999. Association with Cdc2 and inhibition of Cdc2/cyclin B1 kinase activity by the p53-regulated protein Gadd45. *Oncogene*, 18(18), pp.2892–2900.

Zhang, Y. et al., 2006. Determinants for dephosphorylation of the RNA polymerase II C-terminal domain by Scp1. *Molecular Cell*, 24(5), pp.759–770.

Zhao, Y. et al., 2008. Roles of Greatwall kinase in the regulation of cdc25 phosphatase. *Molecular biology of the cell*, 19(4), pp.1317–1327.

Zhou, J. et al., 2002. Minor alteration of microtubule dynamics causes loss of tension across kinetochore pairs and activates the spindle checkpoint. *The Journal of biological chemistry*, 277(19), pp.17200–17208.

Zhu, W., Giangrande, P.H. & Nevins, J.R., 2004. E2Fs link the control of G1/S and G2/M transcription. *The EMBO Journal*, 23(23), pp.4615–4626.

Zindy, F. et al., 1992. Cyclin A is required in S phase in normal epithelial cells. *Biochemical and biophysical research communications*, 182(3), pp.1144–1154.

Zwicker, J. et al., 1995. Cell cycle regulation of the cyclin A, cdc25C and cdc2 genes is based on a common mechanism of transcriptional repression. *The EMBO Journal*,

14(18), pp.4514–4522.